Mechanics of Tissue Renewal: Stem Cell Dynamics, Self-Organisation, and Response

Dissertation

zur
Erlangung des

Doktorgrades

der Mathematisch-Naturwissenschaftlichen Fakultät

der Universität zu Köln

vorgelegt von

Johannes Caspar KRÄMER

geboren in Pforzheim.

Köln
2026

Begutachtung: Prof. Dr. J. Elgeti

Prof. Dr. J. Krug

Tag der mündlichen Prüfung: 13. JULY 2026

Abstract

Epithelial tissues experience constant wear and tear, which requires a well orchestrated renewal mechanism to preserve structural integrity and functional homeostasis. Lost cells are replaced by a finely tuned cascade of cell division and differentiation. Stem cells are at the top of this cascade and give rise to differentiated progeny. Yet, it remains unclear how cell division and differentiation are regulated and what controls cellular organisation in tissues. Mechanical feedback on growth is a possible control mechanism for cell divisions. In this work we investigate how the interplay of intercellular mechanical interactions and its feedback on growth influence stem cell dynamics and self-organisation in two distinct cell-fate models.

We employ a particle-based simulation framework in which each cell is represented by two particles subject to active growth forces. Division is triggered when their separation exceeds a threshold, while apoptosis occurs stochastically. Cells interact as soft adhesive spheres, and dissipative particle dynamics account for fluctuations and energy dissipation. Cell–cell interactions, in conjunction with active growth, establish an explicit mechanical feedback mechanism on cellular growth, thereby implicitly regulating the rate of cell division.

First, we study the textbook picture of epithelial tissue renewal in which stem cells divide asymmetrically to produce one stem cell and one transient amplifying cell. The latter undergo a finite number of symmetric divisions–increasing the total cell mass–prior to terminal differentiation and loss. We observe emergent superdiffusive motion of stem cells driven by the proliferation of their progeny. Further, stem cells are spatially separated, surrounded by offspring in small confined proliferating units. Stem cell separation is caused by an effective stem cell repulsion, mediated by proliferating daughter cells. The static structure is quantitatively described by an effective equilibrium analogy in which stem cell pairs interact via a repulsive exponentially decaying potential, with a characteristic length scale determined by the number of amplifying division cycles.

In a second cell fate model we allow for symmetric stem cell self-renewal, which enables dynamic adaption of the stem cell number. The combination of constant differentiation rates and implicit control of division rates by mechanical feedback leads to a well-defined tissue composition. We develop an analytical theory that predicts population stability and global composition across a broad parameter range, including transitions between stem-cell-rich, stem-cell-rare, and stem-cell-depleted regimes. We focus on the biologically relevant regime for most epithelial tissues: a rare, slowly cycling stem cell population. In this regime, simulations reveal that stem cells organize into stable, spatially confined niches, with a small but finite number of cells. Transit-amplifying cells replenish depleted regions but cannot sustain indefinite clonal

expansion, preserving stem cells as the long-term source of tissue maintenance.

To measure the response in self-renewed tissues, we develop a novel framework to quantify the mechanical response coefficient from number fluctuations. From mechanical feedback we map the growth equation onto an Ornstein–Uhlenbeck-like process governing the fluctuation dynamics of a cell population, from which we derive a set of static and dynamic observables to characterize the fluctuation–response properties of the tissue. Analysis of two-particle growth (2PG) simulations demonstrates that this approach is well-suited to measure tissue response from steady-state fluctuations. Furthermore, we demonstrate that this analysis allows to identify additional complexity, like memory in the growth feedback. In another multi-scale simulation model of cellular growth, our analysis enables one to measure the response coefficients, which was previously unfeasible. Compared to the 2PG model, we find even stronger memory effects that may also be present in real biological tissue.

In conclusion, we show how the microscopic details of cell fate and mechanical cell-cell interactions shape the stem cell organisation. We introduce novel analysis methods to quantify the spatio-temporal pattern and dynamics in tissues. Our results indicate that these tools can support future experiments and provide more detailed insights in the underlying mechanisms of multi-cellular tissues.

Zusammenfassung

Epithelgewebe sind ständiger Abnutzung ausgesetzt, was einen gut abgestimmten Mechanismus zur Erneuerung erfordert, um die strukturelle Integrität und funktionelle Homöostase aufrechtzuerhalten. Zellverlust wird durch eine genau abgestimmten Kaskade von Zellteilung und Differenzierung ausgeglichen. Stammzellen stehen am Beginn dieser Kaskade und bringen differenzierte Nachkommen hervor. Jedoch bleibt unklar, wie Zellteilung und Differenzierung reguliert werden und was die Organisation von Zellen in Geweben beeinflusst. Mechanische Rückkopplung auf das Wachstum ist ein möglicher Kontrollmechanismus der Zellteilung. In dieser Arbeit untersuchen wir in zwei unterschiedlichen Differenzierungsmodellen, wie das Zusammenspiel interzellulärer mechanischer Wechselwirkungen und deren Rückkopplung auf das Zellwachstum die Dynamik und Selbstorganisation von Stammzellen in Geweben beeinflusst.

Wir verwenden ein teilchenbasiertes Simulationsmodell, in dem jede Zelle durch zwei Punktteilchen dargestellt wird, auf die eine aktive Wachstumskraft einwirkt. Die Zellteilung wird durchgeführt, wenn der Teilchenabstand einen Grenzwert überschreitet, während die Apoptose stochastisch abläuft. Zellen wechselwirken durch ein Lennard-Jones ähnliches Potential miteinander wie weiche, aneinander haftende Kugeln, und die dissipative Teilchendynamik berücksichtigt Fluktuationen und Energieverlust. Zell-Zell-Wechselwirkungen bilden in Verbindung mit dem aktiven Wachstum einen expliziten mechanischen Rückkopplungsmechanismus für das Zellwachstum und regulieren dadurch implizit die Rate der Zellteilung.

Zunächst untersuchen wir das Lehrbuchmodell zur Erneuerung von Epithelgeweben, in dem sich Stammzellen asymmetrisch teilen und dabei je eine Stammzelle sowie eine kurzlebige (transiente) proliferierende Zelle hervorbringen. Letztere durchläuft eine endliche Anzahl symmetrischer Teilungen, wodurch die Gesamtzellmasse zunimmt, bevor sie abschließend differenziert und verloren geht. Wir beobachten eine superdiffusive Bewegung der Stammzellen, die durch die Vervielfältigung ihrer Nachkommen angetrieben wird. Darüber hinaus sind Stammzellen räumlich voneinander getrennt und von ihren Nachkommen in kleinen, begrenzten Wachstums-Einheiten umgeben. Die räumliche Trennung der Stammzellen wird durch eine effektive Abstoßung der Stammzellen verursacht, welche von den sich teilenden Tochterzellen erzeugt wird. Die statische Struktur kann quantitativ mithilfe einer Analogie des effektiven Gleichgewichts beschrieben werden, in der Stammzellpaare über ein repulsives exponentiell abfallendes Potential wechselwirken, wobei die charakteristische Längenskala durch die Anzahl der Teilungszyklen von transienten Zellen bestimmt wird.

In einem zweiten Differenzierungsmodell betrachten wir die symmetrische Selbsterneuerung von Stammzellen, was eine dynamische Anpassung der Stammzellzahl

ermöglicht. Die Kombination von konstanten Differenzierungsraten und implizit durch mechanische Rückkopplung gesteuerten Teilungsraten führt zu einer klar festgelegten Zusammensetzung des Gewebes. Wir entwickeln eine analytische Theorie, die die Stabilität der Population und deren globale Zusammensetzung über einen weiten Parameterbereich hinweg beschreibt, einschließlich Übergängen zwischen Zustanden, in denen Stammzellen überwiegen, spärlich vorkommen, oder ihr Vorkommen erschöpft ist. Wir konzentrieren uns weiter auf den für die meisten Epithelgewebe biologisch relevanten Zustand: eine geringe, sich langsam teilende Stammzellpopulation. In diesem Zustand zeigen Simulationen, dass sich Stammzellen in stabilen, räumlich begrenzten Nischen mit einer kleinen, aber endlichen Anzahl organisieren. Transiente Zellen füllen stammzellfreie Regionen wieder auf, können jedoch keine unbegrenzte Klon-Ausbreitung erreichen, während Stammzellen als langfristige Quelle für die Erneuerung des Gewebes erhalten bleiben.

Um die Anpassungsreaktion von sich selbst erneuernden Geweben zu messen, entwickeln wir einen neuartigen Ansatz zur Messung der mechanischen Reaktion anhand von Fluktuationen in der Zellzahl. Ausgehend von mechanischer Rückkopplung bilden wir die Wachstumsdynamik eines zellulären Gewebes auf einen Ornstein-Uhlenbeck-ähnlichen Prozess ab, um die Fluktuationsdynamik der Zellpopulation zu beschreiben. Daraus leiten wir eine Reihe statischer und dynamischer Observablen ab, um die Fluktuations-Antwort-Eigenschaften des Gewebes zu bestimmen. Die Analyse von Simulationen des Zwei-Teilchen-Wachstums (2PG) zeigt, dass dieser Ansatz gut geeignet ist, um die Anpassungsreaktion des Gewebes mittels Fluktuationen um den stationären Gleichgewichtszustand zu messen. Darüber hinaus zeigen wir, dass diese Analyse es ermöglicht, zusätzliche Komplexität eines Systems zu identifizieren, wie beispielsweise einen Gedächtniseffekt, der dem Kontrollmechanismus des Zellwachstums zugrunde liegt. In einem weiteren Simulationsmodell, das verschiedene Aspekte des Zellwachstums vereint, ermöglicht unsere Analyse die Messung der Anpassungsreaktion, was zuvor nicht möglich war. Im Vergleich zum 2PG-Modell finden wir noch stärkere Gedächtniseffekte, die möglicherweise auch in realen biologischen Geweben vorhanden sind.

Zusammenfassend zeigen wir, wie die mikroskopischen Details des Zellschicksals und die mechanischen Zell-Zell-Wechselwirkungen die Organisation von Stammzellen prägen. Wir stellen neuartige Analysemethoden vor, mit denen sich die räumlichen und zeitlichen Muster und Dynamik in Geweben quantifizieren lassen. Unsere Ergebnisse lassen erkennen, dass diese Methoden zukünftige Experimente unterstützen und detailliertere Einblicke in die zugrunde liegenden Mechanismen mehrzelliger Gewebe liefern können.

Contents

Abstract v

Zusammenfassung vii

1 Introduction 1
1.1 Dead or Alive or Fluctuating? . . . 1
1.1.1 From hard to soft to fluctuating . . . 2
1.1.2 Proliferating active matter . . . 4
1.2 Tissue mechanics and cell cycle regulation in growing tissues. . . . 5
1.2.1 The homeostatic pressure theory . . . 6
1.3 Stem Cell Biology and Self-organisation . . . 10
1.3.1 Tissue renewal by stem cells . . . 10
1.3.2 Stem cell dynamics and structure formation in epithelial tissues 14
1.4 Computational modelling of cells and tissues . . . 16
1.4.1 Rule based models: Cellular automata . . . 17
1.4.2 Energy-functional, foam-like models . . . 18
1.4.3 Particle based models . . . 20
1.4.4 Multiscale and hybrid models and data driven modelling . . . 21
1.5 Outlook on the thesis . . . 21
References . . . 23

2 Mechanically driven stem cell separation via proliferating daughter cells 35
2.1 Introduction . . . 35
2.2 Simulation model . . . 37
2.3 Isolated stem cell . . . 38
2.4 Stem cell interaction . . . 39
2.5 Confluent tissue maintained by stem cells . . . 41
2.6 Stem cell repulsion in three dimensions . . . 44
2.7 Independence of homeostatic pressure controlled divisions . . . 44
2.8 Discussion and conclusion . . . 45

Supplementary Information - Chapter 2 48
2.A Supplementary animations of tissue simulations . . . 48
2.B Simulation model . . . 48
2.C Division rate of isolated SC . . . 50
2.D Stem cell motion . . . 50
2.D.1 MSD of isolated stem cells and stem cells in tissues . . . 51
2.D.2 Displacement distribution . . . 53

2.D.3 Overdamped dynamics . . . 54
2.E Additional results for simulations of stem cells in tissues . . . 54
2.E.1 Cell densities in confluent tissues . . . 54
2.E.2 Cluster analysis . . . 55
2.E.3 Effective diffusion coefficient and relaxation . . . 56
2.F Stochastic division rate model . . . 57
References . . . 59

3 Mechanics and fate stochasticity shape stem cell distribution in tissues 65
3.1 Introduction . . . 65
3.2 Mechanical control of fate proportions in stem-cell derived tissues . . . 67
3.3 Agent-based simulations of stem cell derived tissues . . . 70
3.4 Self-organized formation of stem cell clusters in stem cell derived tissues 71
3.5 Long-term temporal dynamics of stem cell clusters . . . 73
3.6 Discussion . . . 76

Supplementary Information - Chapter 3 78
3.A Data availability . . . 78
3.B Auxiliary information for continuum theory . . . 78
3.C Two particle growth model (2PG) and simulation setup . . . 79
3.C.1 Brownian dynamics simulations . . . 80
3.D Parameter selection: Growth rate variation . . . 81
3.E Additional tissue configurations to show robustness of main text results 82
3.E.1 Static properties . . . 83
3.E.2 Dynamic properties . . . 86
References . . . 87

4 Measuring the dynamic response coefficient of cellular tissues from steady state fluctuations reveals growth induced division rate memory 93
4.1 Introduction . . . 93
4.2 Fluctuation response in systems with crowding feedback . . . 94
4.3 Application to growing tissue systems . . . 98
4.3.1 Stochastic Model . . . 98
4.3.2 Agent based tissue simulations with mechanical feedback–2PG 99
4.3.3 Membrane potential dependent growth–VMPG simulations . . 102
4.3.4 Memory in Division control . . . 103
4.4 Discussion . . . 105

Supplementary Information - Chapter 4 107
4.A Details on density fluctuations due to noise . . . 107
4.B Simulation details and additional results . . . 110
4.B.1 sODE model . . . 110
4.B.2 Two particle growth model . . . 111
4.B.3 Voronoi membrane potential growth (VMPG) model . . . 114

4.B.4 Stretch Response 114
4.B.5 Mean back relaxation 115
References 116

5 Discussion and Outlook **121**
5.1 Summary 121
5.2 Discussion 124
5.3 Outlook 126
References 130

6 Eidesstattliche Erklärung — Declaration for the doctoral thesis **133**

7 Declaration of individual contributions **135**

8 Acknowledgments **137**

List of Figures

1.1 Non-equilibrium fluctuations in RBCs. 3
1.2 Mechanotransduction controls cell fate via biochemical and biomechanical signals. 5
1.3 Schematic representation of the homeostatic pressure Gedankenexperiment. 7
1.4 Anisotropic growth at surfaces. 8
1.5 Tensile tissue growth. 9
1.6 Epithelial renewal by stem cells 11
1.7 Definition of stemness. 13
1.8 Stem cells as diffusing many-particle system. 15
1.9 The role of computer simulations. 16
1.10 Discrete computational models. 17
1.11 Schematic representation of two-particle growth (2PG) model. 20

2.1 Stem cell (SC) division and differentiation scheme leads to well-separated SC arrangement. 37
2.2 Interaction parameter determination. 40
2.3 SC separation in bulk tissue is explained by equilibrium model with simple repulsive interaction. 42
2.4 Dynamics of SC and BD simulations. 43
2.5 Stem Cell repulsion qualitatively remains in three dimensions. 44
2.6 Relevance of homeostatic pressure growth control. 45
2.C.1 Division rate of isolated SCs. 51
2.D.1 Single stem cell trajectory shows long persistent segments. 51
2.D.2 Mean squared displacement for isolated SCs. 52
2.D.3 Mean squared displacement for SCs in tissues. 53
2.D.4 Displacement distribution function of isolated SCs. 54
2.D.5 MSD for isolated SCs as function of cell mass. 55
2.E.1 Progenitor cell density around isolated SCs. 55
2.E.2 Cluster size distribution function for SCs in tissues 56
2.E.3 Effective diffusion coefficient. 56
2.F.1 Complementary cumulative distribution function (cCDF) for cell fate events in stochastic model and cell size distribution function. 57
2.F.2 Quantitative results for stochastic division model 58

3.2.1 Homeostasis of stem-cell derived tissues via mechanical control. . . . 68
3.3.1 Details of selected tissues chosen for detailed analysis 70

3.4.1 Spatial structure and niche formation 72
3.5.1 Temporal stability of stem-cell clusters 74
3.5.2 Lineage tracing in mechanical simulations. 75
3.D.1 Parameter sweep division rate and growth coefficient 82
3.E.1 Additional tissue configuration to show robustness of results. 83
3.E.2 Niche formation and static structure. 84
3.E.3 MSD and Density fluctuations. 86

4.3.1 Analysis of stochastic model trajectories against ground truth. 99
4.3.2 Fluctuation-response in agent based simulations 100
4.3.3 Comparison of fluctuation-response and perturbation response parameters. 101
4.3.4 Membrane potential controlled cell cycle dynamics. 102
4.3.5 Division memory effects on fluctuation response. 104
4.B.1 Perturbation-response in agent based simulations. 113
4.B.2 Stretch response rate dependence. 114
4.B.3 Mean back relaxation. 115

5.3.1 Mechanoresponse in stem cell generated tissues. 128

List of Tables

2.B.1 Simulation parameters of the standard tissue. 50

3.C.1 Standard parameter set of agent based tissue simulations. 81

4.B.1 2PG tissue simulation parameters (standard parameter set). 112

1 Introduction

What is the role of mechanical forces in cell-cell interactions in multi-cellular tissues with complex hierarchies?

In this thesis we aim to puzzle out some aspects to answer this overarching question. The goal is to understand how microscopic, mechanical cell-cell interactions contribute to stem cell dynamics and self-organisation at the tissue scale. In particular multi-cellular systems with distinct connected cell lineage hierarchies are investigated, but also how cell fate is mechanistically controlled and facilitates agile adaptation in noisy environments and in response to perturbations.

In this introduction chapter, some basic concepts and recent literature are discussed in order to work out the substance of the overarching questions. First, the field of active and living matter is introduced, emphasizing the importance of fluctuations for life. Then, the potential role of mechanical interactions in growing tissues is reviewed, followed by an introduction of the biological and physical aspects of growing tissues self-renewed by stem cells. Last, a brief discussion of present simulation models for cellular tissues is given and we select a suitable method to tackle our objectives.

1.1 Dead or Alive or Fluctuating?

How can we decide that matter is alive? While some forms of matter are clearly *dead*, like a piece of metal or plastic, and some are very *alive*, like mammals, insects, or plants, defining the transition from dead to living matter is far from trivial. Neglecting the philosophical depth of the question of what life is, here, we want to focus on a physics inspired definition and some basic phenomena that allow us to distinguish dead (passive), active (not living yet), and living matter. Consider the fundamental building block of every complex or complicated form of life: cells. Animal cells are enclosed by a lipid bilayer membrane surrounding the cytoplasm, and contain genetic information in form of DNA and RNA. Altogether this forms a complex structure of proteins, polymers, and filaments. But how does an assembly of these passive building blocks come to life? One key requirement is motion beyond thermal fluctuations. For cells to be alive it requires them do actively move or exert forces on their surrounding by internal energy consumption!

In this opening section, a brief discussion of the difference between passive and active matter is given. Focusing on the difference between classical, i.e. hard and soft, condensed matter physics and active matter physics. Using the example of red blood cells (RBCs), we highlight the role of *fluctuations* for active matter. Eventually, we conclude with a special form of active matter: *proliferating*, or growing and dividing, or *living* matter. Here, in addition to active forces, number balance is no longer

conserved due to processes like cell loss or division. Higher forms of life additionally require even more subtle characteristics, like maintaining genome integrity, signaling pathways, or response to external cues, which go beyond the scope of this work.

1.1.1 From hard to soft to fluctuating

Classical condensed matter physics consists of the study of ordered matter [43]. Electromagnetic forces between atoms result in well defined structures, short range order in well defined grids. From their microscopic interaction, macroscopic order and properties of materials arise. These systems can show a variety of interesting physical phenomena, ranging from quantum effects, like superconductivity, to other forms of (classical) magnetism. When interaction between atoms or molecules are reduced, e.g. in the regime of Van der Waals forces, structures become much easier to deform, and need to be described on scales much larger than the constituting atoms [118]. Thermal fluctuations result in (static) self assembly of matter [121]. This marks the regime of soft matter, which covers typical forms of matter like liquids, polymers, gels, or foams. Due to the weaker interactions between molecules, thermal fluctuations play a role and shape their structure. Yet, such molecular systems, which are the building blocks of the cells, are still passive.

A central property of these passively fluctuating systems is, that they obey detailed balance and fulfill the fluctuation-dissipation theorem, i.e. their thermal fluctuation, which are usually identified with Brownian motion, comes from interactions with surrounding gas or fluid particles, and that motion due to an external force results in dissipation of energy. Fluctuations of a time dependent observable $x(t)$, e.g. position of a particle, can be used to calculate the power spectral density $S(\omega) = \langle \tilde{x}(\omega)\tilde{x}^*(\omega)\rangle$ for frequencies ω, where $\tilde{x}$ is the Fourier-transform of x. On the other hand, when perturbing the system by an external force $f(t)$, in first order the response depends linearly on the force and is weighted by the susceptibility $\chi(t)$. This results in a shift of the observable $\langle x(t)\rangle = \langle x\rangle_{eq} + \int_{-\infty}^{t} dt' f(t')\chi(t-t')$ away from its equilibrium position $\langle x\rangle_{eq}$. Now, the fluctuation-dissipation theorem states that the power spectral density and susceptibility are connected by the relation $S(\omega) = \mathrm{Im}\{\chi\} \cdot 2k_B T/\omega$. This means, in equilibrium, the response to a small external force is completely determined by the statistics of spontaneous fluctuations.

In active systems, the fluctuation dissipation theorem is no longer valid as a consequence of broken detail balance due to continuous internal energy consumption [79, 98]. Violation of this theorem is a strong signature of non-equilibrium physics and generalizations of the theorem further improve the understanding of active systems [96]. This form of non-equilibrium physics has attracted a lot of interest in the physical community, as one can see from the vast increase just in review article over the last decades [111]. However, such a strongly growing field tends to lack a clear, unified definition and many sub-disciplines are evolving in parallel, yet, coexist unattached. The central interest in this thesis are actively growing cellular systems, yet, we want to illustrate the consequences and richness of information encoded in fluctuations with an illustrative example of red blood cells.

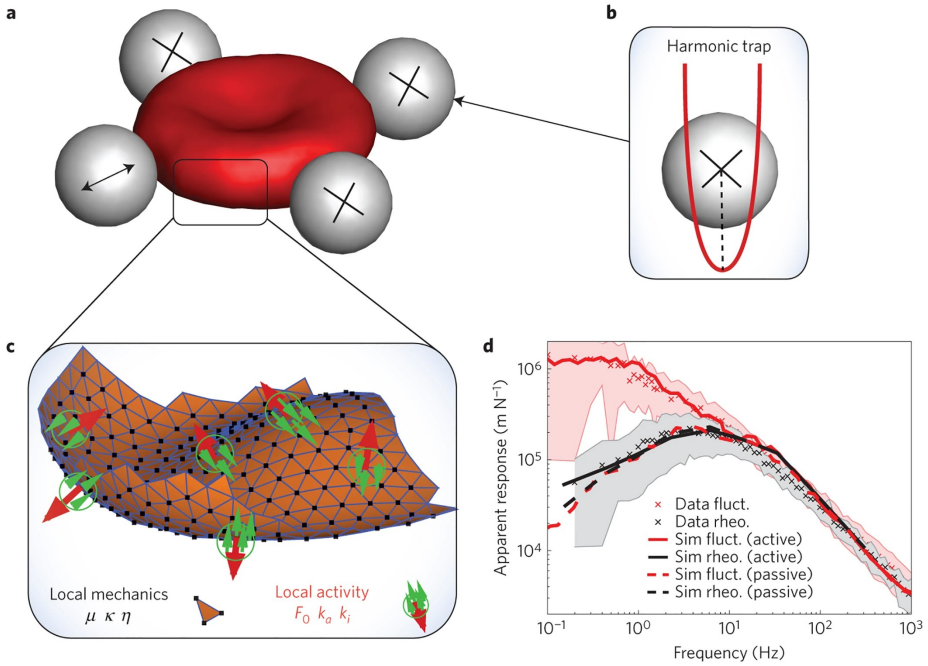

Figure 1.1: Fluctuations reveal active nature of RBCs. (A) schematic of the experimental setup, mimicked in simulations, and (B) sketch of optical tweezer controlling bead position through confining potential. (C) Combination of local mechanics and local activity for cell membrane describes nature of non-equilibrium fluctuations observed in (D) the power spectrum at frequencies below 10 Hz. Data points were measured for fresh RBCs in active and passive rheology. Figure taken from [116] by permission of the publisher.

1.1.1.1 Red blood cells: The power of fluctuations for active matter

To illustrate the difference between passive and active matter, we begin with a condensed discussion of the surprising activity pattern found in red blood cells (RBCs). These cells are an interesting case as they exist close to the boundary between dead and alive. RBCs in mammals are biconcave discs, and lack a nucleus. They are generated in the bone marrow and cannot self-renew, which disqualifies them from being a truly living organism. Yet, their fluctuation spectrum hints non-passive characteristics.

Experimentally, Turlier et al. [116] have studied RBCs using a trap constructed by four magnetic beads, where each bead is controlled by optical tweezers (see Fig. 1.1). Three of them are tightly coupled to keep the cell in place, while the fourth, probe bead is used to measure the dynamics of the cell. This allows to detect free membrane fluctuations of the cell in a passive rheology measurement. From the displacement of the probe bead, one can calculate the power spectral density of fluctuations. Active measurements are realized by exerting an oscillating force over a broad frequency range on the cell by the fourth bead and calculating the elastic and dissipative contribution from the response function.

The fluctuation dissipation theorem, which holds true for thermal fluctuations, provides a connection between power spectral density and the dissipative part of the response function, as discussed above. However, a significant deviation in the low frequency regime between 0.1 to 10 Hertz of the power spectral density is found between active and passive rheology of membrane fluctuation, when probing fresh RBCs (see Fig. 1.1). For old, ATP-depleted, RBCs on the other hand, no such difference between the two measurement protocols can be observed. Such a difference between active and passive measurement in "living" systems indicates, that energy consumption in the cell does break detailed balance. Computer simulations, which recreate the experimental setup could confirm the hypothesis, that ATP hydrolysis in the cells could be a possible mechanism that causes the observed differences and drives the cell out of equilibrium.

The illustrative example of RBCs nicely shows, how fluctuations teaches relevant information about the active nature of a system and non-equilibrium in general [107]. We will employ this feature later in the thesis, when studying density fluctuations in growing cell populations in chapter 4. More generally, this example shows us again how active matter is different to equilibrium soft matter and how novel features emerge form deviations of equilibrium theorems.

1.1.2 Proliferating active matter

Multi-cellular, living systems are non-equilibrium systems as their components constantly consume energy. In addition, cell number conservation is locally broken by replication and loss [52]. This results in a non-vanishing source term in the continuity equation

$$\partial_t \rho(\boldsymbol{r}, t) + \nabla \boldsymbol{j}(\boldsymbol{r}, t) = k\rho(\boldsymbol{r}, t), \tag{1.1}$$

where $\partial_t \rho(\boldsymbol{r}, t)$ is the temporal change of cell number or cell mass density at position $\boldsymbol{r}$ and time t, and $\boldsymbol{j} = \rho \boldsymbol{v}$ is the cell flux with velocity $\boldsymbol{v}$. The net growth rate $k = k_d - k_a$ describes the change in cell number as difference of creation rate k_d, e.g. by division, and loss rate k_a, e.g. due to programmed cell death, so called apoptosis. Homeostasis, i.e. a steady state in which globally cell number is conserved, is achieved for $k = 0$, and for $k > 0$ or $k < 0$ the system grows or shrinks, respectively.

Generally, stable growth requires a feedback mechanism [105]. How exactly this feedback is implemented can vary, yet, mechanotransduction, i.e. the interplay between subcellular chemical pathways and inter-cellular physical forces, has been found to be a well-established mechanism [1]. Yet, purely mechanical arguments have been found to have great predictive power, as we will discuss in the following section by introducing the concept of mechanically regulated cell cycle dynamic.

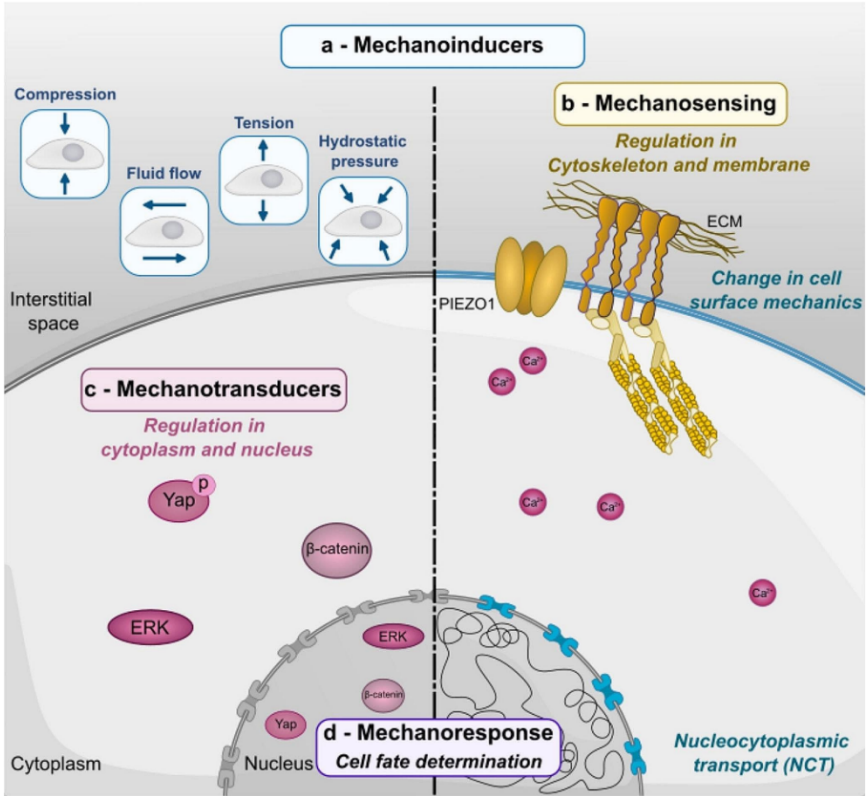

Figure 1.2: Mechanotransduction controls cell fate via biochemical and biomechanical signals. (a) Mechanical forces, like compression, tension, or shear (extrinsic forces) and intrinsic changes to cell membrane trigger response in (b) mechano-sensing elements, like ion-channels. (c) Response can trigger cascades in ion or protein pathways, which (d) eventually initiate cell fate decision, like entering a growth phase, or initiating division, differentiation, or apoptosis. Taken from [1] with permission under open access license CC-BY-4.0.

1.2 Tissue mechanics and cell cycle regulation in growing tissues.

Tissues are assembled bottom-up from individual cells. Yet, on larger length scales, continuum descriptions can be used to approximate their dynamics. Coarse grained models explain effects like fluidization of tissues, tissue folding and cellular flows based on elastic properties and geometrical arguments [49, 51, 99]. Complex folding patterns result from the elastic properties and geometrical details of thin cellular sheets with differential growth [26]. Growth induced stress can result in buckling instabilities of elastic substrates [53], compartment formation due to pressure driven cellular flows [54], or formation of villi in the intestine and shows high sensitivity to the details of the underlying process, like growth inhomogeneities, geometrical constraints, and compressibility [11, 103, 106].

In confinement, cellular divisions cause an increasing tissue pressure, which in-

hibits cell division, a process controlled on a sub-cellular level by mechano-chemical pathways and membrane potentials [32, 85]. Physical forces, cell fate, and elastic properties of mesoscopic tissues are linked by mechano-chemical coupling, so called *mechanotransduction* (see Fig. 1.2). These cues play a fundamental role in shaping an organism, but can also provide regulatory feedback onto growth [63]. But not only mechanical stresses but also mechano-chemical interactions add to the complexity of shape formation in biological systems [48]. Cellular tension is mediated by adhesion-proteins, like cadherin, catenin, or integrin, thus, already small local changes in adhesion can result in changes of cell shape and fate [122]. How mechano-chemical coupling facilitates tissue regulation and contributes to cell decision making has received much attention, but is still not fully understood [1, 39].

Experiments show, that compression suppresses growth [57], and can even induce apoptosis [22]. This supports the minimal theory, that the cell cycle dynamics are subject to mechanical feedback [105]. After introducing how this hypothesis results in the *homeostatic pressure* theory, we further discuss how a mechanically based framework can explain complex multi-cellular dynamics as a consequence of differential growth. This illustrates the relevance of mechanical contributions in growing systems, and how complex effects, like stabilization of growing cell spheroids or tensile states of growth, can be reasoned.

1.2.1 Continuum mechanics of growing tissues: The homeostatic pressure theory

To introduce the concept of *homeostatic pressure* the *Gedankenexperiment* originally presented by Basan et al. [7] is revisited. Consider a finite, closed volume in which cells have infinite access to nutrients and dying cells are efficiently removed (see Fig. 1.3). In the first case, the volume is separated into two chambers by a movable wall. One, in which the cells grow, and a second, in which a spring exerts a force according to Hooke's law. When cells grow and divide the colony will expand, until the force exerted on the wall by the cells cannot overcome the force of the spring. At this point, cell division and apoptosis, with rates k_d and k_a, respectively, are balanced and the net growth of the tissue stops. The system pressure P at this point is called the homeostatic pressure P^H. We expend the net growth rate around the homeostatic pressure

$$k_d - k_a = \kappa \cdot \left(P^H - P\right) + \mathcal{O}(P^2), \tag{1.2}$$

where κ is the expansion coefficient. Higher order terms may be needed for a precise description further away from the homeostatic state, as one can expect the linear relation to be valid only near this point. A second consequence of growth is, that cells are more tightly packed with increasing pressure. Here, a similar relation for the cell number density ρ can be expected, given by

$$k_d - k_a = \varkappa \cdot \left(\rho^H - \rho\right) + \mathcal{O}(\rho^2), \tag{1.3}$$

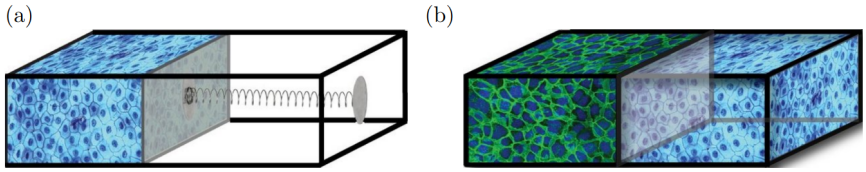

Figure 1.3: Schematic representation of the homeostatic pressure *Gedankenexperiment*. (a) Pressure stalled growth is shown by an extendable chamber setup. Cells are grown in a volume with a moving wall, which is coupled to a spring. Due to expansion of the cells, the spring is compressed until a steady state is reached. (b) Same experiment as in a, but with the spring replaced by a second tissue. The tissue with higher homeostatic pressure will compress the other one. Note, that due to the infinite compressibility of tissues on long times due to apoptosis, one tissue will eventually fill the total compartment. Color version of sketch from [7] reprinted by permission of Informa UK Limited, trading as Taylor & Francis Group, `https://www.tandfonline.com`.

where ρ^H is the cell density in homeostasis and $\varkappa$ the density response coefficient. The two expansion coefficients, κ and $\varkappa$, are connected and we can combine Eq. 1.2 & 1.3 to give the linear expansion of the pressure around its homeostatic value as a function of density, given by

$$P = P^H - \frac{\varkappa}{\kappa}\left(\rho^H - \rho\right). \tag{1.4}$$

In a second setup of the *Gedankenexperiment*, the spring is replaced by a second tissue (see Fig. 1.3). For the sake of simplicity the movable wall between the two cell populations is kept. Then, interface effects or other complex interactions between both cell populations do not play a role. Each tissue expands or tightens, until it reaches its homeostatic pressure. If one cell line has a higher homeostatic pressure, it compresses the other tissue. The tissue has practically infinite compressibility on long time scales due to apoptosis [99], which results in one cell population to go extinct.

The concept of homeostatic pressure provides a minimal explanation how mechanical interactions regulate growth and division. To further illustrate the importance of mechanics on growth, two examples of inhomogeneous growth will be discussed in the following. In the first case, the growth of multi-cellular spheroids, originally studied by Montel et al. [82, 83] and Delarue et al. [31], is discussed. Here, cells are grown within a semipermeable membrane, which allows diffusion of nutrients, but not of dextrane molecules with large molecular weight, so that external pressure can be applied on the spheroid. Immunostaining on histological slices shows, that apoptotic events take place primarily in the center of the spheroid, and division is found more frequently at the border. Thus, the core of the spheroid is dying, while the outside divides and stabilizes the core via an inflow of cells. One may argue, that nutrients cannot diffuse far enough in the center, leaving cells malnourished. However, a simple mechanical argument, as shown in detail below, suffices to explain this effect. Cell divisions introduce a strain dipole to the tissue, which exerts stresses on their environment. At the surface of a tissue, the strain field is partially cut away. Thus, it requires

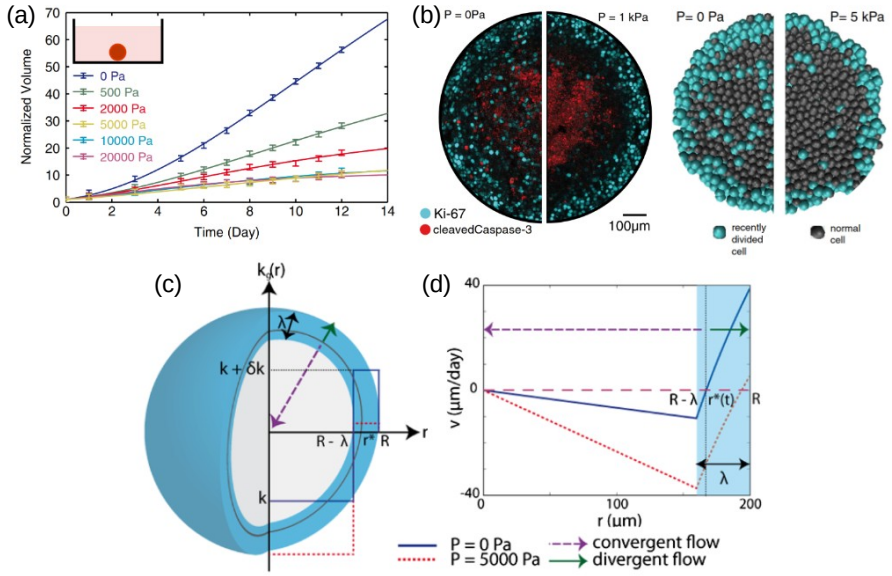

Figure 1.4: Anisotropic growth at surfaces. Experimental and theoretical results show, that tumor spheroids grow predominantly at surfaces. An effect enhanced under higher environmental pressures. (a) Spheroid growth rate over time in environments of increasing environmental pressure realized by dextrane concentration. (b) Experimental (left) and simulation (right) slice of a spheroid, where recently divided cells are colored in cyan blue at low and high environmental pressure. (bottom) (c) Schematic of anisotropic growth rate given in Eq. 1.5 and (d) resulting flow field of Eq. 1.7. Figures taken from [31, 82] by permission of the publishers.

less energy to elastically deform the cell environment in order to divide, resulting in a higher division rate at the surface. Note, that the effect of surface enhanced growth is pronounced with increasing pressure and also the growth rate of the spheroid reduces with increased pressure (see Fig. 1.4).

Assuming that the growth rate in the bulk is constant, given by k, and excess divisions δk are only possible in a surface layer of thickness λ. Then, for a spheroid of size $R(t)$, the spatially dependent growth rate $k_g(r,t)$ is given by

$$k_g(r,t) = \begin{cases} k & \text{for } r < R(t) - \lambda \\ k + \delta k & \text{for } R(t) - \lambda < r < R(t) \\ 0 & \text{for } r > R(t). \end{cases} \tag{1.5}$$

For small spheroids $R < \lambda$ the exponential growth dynamics is recovered. For spheroids larger then λ, under the assumption of a constant cell density, the volume change is given by

$$\partial_t V = k_B V + R_S \Delta k_S (36\pi)^{1/3} V^{2/3}. \tag{1.6}$$

If the bulk is apoptotic ($k < 0$), spheroid growth will stall at a finite size $R_f =$

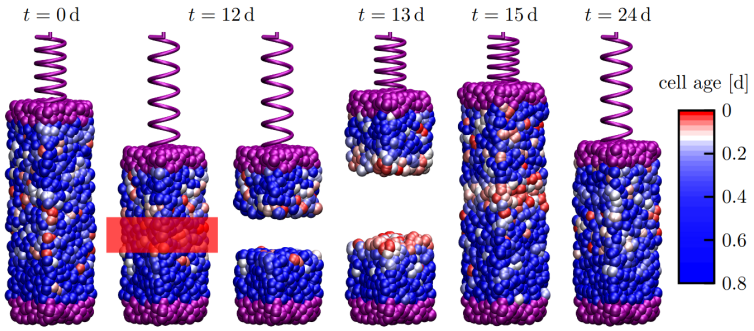

Figure 1.5: Tensile tissue growth. Simulation approach to reveal mechanical driven surface contribution to anisotropic growth and unravel tensile nature of tissue. Figure taken from [89] by permission of the publisher.

$-3\lambda\delta k/k$. The cell flow in the spheroid can be obtained from mass conservation ($\nabla v = k(r)$) and is given by

$$v(r) = \begin{cases} \frac{1}{3}kr & \text{for } r < R(t) - \lambda \\ \frac{1}{3}(k + \delta k) & \text{for } R(t) - \lambda < r < R(t). \end{cases} \tag{1.7}$$

This explains, how a inward flow ($v < 0$) stabilizes the spheroid core, while an outward flow ($v > 0$) increases the size until the steady state size R_f is reached (see Fig. 1.4).

To highlight the importance of surface enhanced growth to stabilize apoptotic bulk tissue, the idea and results originally presented by [89] are discussed as a second experiment (see Fig. 1.5). Consider a tissue, that grows in a confined volume with adhesive walls, i.e. it does not only move, if cells push against the wall, but also when they pull on the wall. In one direction, one wall is fixed, while the opposing wall is (again) a movable wall connected to a spring. Along the remaining two directions, periodic boundary conditions are implemented. While the setup is identical to the *Gedankenexperiment* discussed above, here, the focus lies on the special case of a tissue with negative homeostatic pressure. This is similar to the apoptotic bulk discussed before. For a filled volume, due to apoptosis, cells pull on the movable wall, extending the spring, until the restoring force of the spring is strong enough to increase the division rate of cells to balance apoptosis. When performing a cut through the tissue, the spring recoils and two free surfaces are created. At the surface, cells will grow with a higher rate, until the gap is closed and the spring gets extended again.

Such a tensile states has been found in epithelial tissues [114] and is assumed to act as driver of morphogenesis and homeostasis [21]. Besides the basic concepts of the homeostatic pressure theory introduced in this section, it has been successfully applied to many more questions revolving around the competition of tissues with particular focus on interfacial dynamics or in the presence of motility [18, 41, 90]. In multi-component systems, pressure alone does not predict the outcome of competition correctly and higher order effects, like co-evolution or passive cell mass, can be influential [19, 91]. Ongoing research shows, that mechanical effects can add even

more complexity. When considering additional friction with a substrate of a two-dimensional cell sheet, negative pressure does not necessarily result in a finite tissue size [125]. Friction forces balance the retrograde cell flow from the surface to the center. Thus, only highly tensile tissues stop growing at a finite size.

In conclusion, there are several aspects of growing tissues, which can be explained with help of a mechanically based framework. Cell fate control via mechanical feedback lies at the core of the homeostatic pressure or density theory. Yet, most tissues consist of heterogeneous populations, i.e. different cell types, which are created by division and differentiation. In the next section the concept how stem cells are assumed to give rise to specialized daughter cells, while maintaining their population and self-organize, is introduced.

1.3 Stem Cell Biology and Self-organisation

Life starts with a single fertilized egg, the totipotent stem cell, which gives rise to all 30-40 trillion cells of an adult human. During embryonic development, not only cell mass and number are increased, but also variability. Initially, the totipotent stem cell replicates, and then continues to give rise to specialized cells arranged according to the complex body plan of the organism. In the course of this process, stem cells with reduced potency, i.e. the variety of offspring they can produce narrows down, develop and ensure the renewal of specific tissue types. However, the process of renewal must continue until death, which is why stem cells must remain in the body for that long. In general, stem cells present a population, which gives rise to specialized cells through differentiation, while preserving its own population through division [75].

In this section, we first introduce the concept of tissue self-renewal by stem cells based on the established textbook picture and its revised adaptations. Then, we discuss different approaches to study the self-organisation of stem cells within the tissue.

1.3.1 Tissue renewal by stem cells

First evidence for adult stem cells has been found in the blood marrow in the 1950s. Hematopoietic stem cells have been proposed as "radio-protective" cells in the bone marrow, able to protect against loss of white blood cells after radiation [78]. These rare cells ($\approx 0.05\%$ of cells in the bone marrow) are capable to give rise to all types of blood cells, like red and white blood cells, and also self renew their population [84]. Division gives rise to two types of daughter cells, so called asymmetric division, where one daughter remains a stem cell and the other differentiates. To prevent genomic errors, i.e. mutations arising during DNA replication during division, stem cells are assumed to divide only rarely. But how can a small population, which rarely divides give rise to a much larger number of cells?

Stem cell divisions are assumed to trigger a cascade of division and differentiation steps. These differentiated daughter cells do not have the capability to self-renew their population for unlimited time or give rise to all other (blood) cells. Instead,

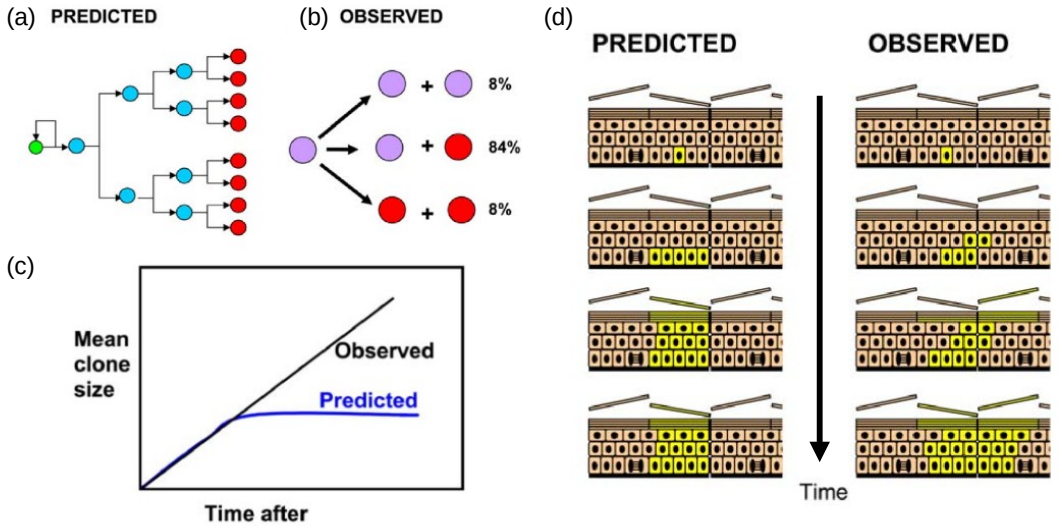

Figure 1.6: Epithelial renewal by stem cells (a) The textbook picture of epithelial renewal by stem cells and (b) revised scheme with fixed fraction of symmetric and asymmetric divisions. (c) Mean clone size over time reaches plateau for deterministic scheme, where size is set by number of rounds of symmetric divisions, but continues to expand in tissues, which is explained by revised scheme. (d) Illustrative sketch of clone size evolution in epidermis for the two schemes. The initial stem cell is marked in yellow (top) and over time generates daughter cells. Original scheme expects clones in well defined units, whereas observed clones are larger in size and spatially extended. Figures taken from [67] by permission of the publisher.

these dividing daughter cells act as an amplifier, producing the required mass of cells. A deterministic, or hard-wired, scheme of discrete division and differentiation steps builds up the necessary number and ratio of cells. Hematopoietic stem cells were one of the first stem cell systems investigated and early experiments for epithelial tissues in the 1970s did motivate that other tissues follow the same template [76, 94]. Thus, the hard-wired stem cell division-differentiation cascade became the *textbook* picture of self-renewal by stem cells [2, 25]: Stem cells divide asymmetrically and give rise to symmetrically dividing daughter cells, so called transient amplifying (TA) cells, which undergo a finite number of divisions to give rise to specialized, fully differentiated cells (see Fig. 1.6 a).

For epidermal tissues, experiments suggested that these stem cells are organized in well defined units, the *epidermal proliferation units* (EPU) [93, 94], in which stem cells slowly divide to maintain the short lived transit cell population [95]. Within these units, actively cycling and differentiating (transient) cells lie at the outside of stem cell clusters [65, 66], while slow-cycling stem cells reside in the center. Also in other tissues, like the intestinal epithelium, signs for similar mechanisms are found [117]. In this thesis, we will begin with investigating the classical picture of tissues renewed by

stem cells with infinite replication potential, which give rise to a transient cell type with limited division potential, and terminates in post-mitotic cells in chapter 2.

However, in particular in epithelia tissues, where cell transport is less efficient than in liquid blood, this has been challenged over time [67]. Advances in imaging and cell lineage tracing allowed more sophisticated clone labeling experiments, which show, that the size and shape of EPUs varies much more than predicted by a theory based on the textbook picture [23, 42, 72] (see Fig. 1.6). Another relevant observation follows from the division outcome: Cells do not strictly adhere to a fixed outcome. In the basal layer, all three possible combinations, i.e. generating two proliferating cells, two differentiated cells, and an asymmetric combination of proliferating and differentiating cell, are observed. The ratio of symmetric duplication or differentiation or asymmetric division in homeostasis must be balanced. Yet, it should not be fixed. Otherwise, the stem cell pool would not be capable to respond to increased loss of stem cells, following for example wounds. How exactly the ratios of different division outcomes are set and how a specific tissue composition is controlled remains unclear. The consequences arising from the stochastic rate based model are further investigated in chapter 3 of the thesis.

1.3.1.1 Defining stem cells by function and a unifying theory of stemness

Experimental techniques often aim to identify stem cells via their characteristic gene expression profile. This, however, complicates to find a general definition of the stem cell type. In an orthogonal approach, one can define stemness by focusing more on cellular function [25, 92]. This extends our previous discussion, in which we already found two of the six hallmarks of stemness, as proposed in literature [13] (see Fig. 1.7). First, the self-renewal potential, i.e. the capability to divide and replenish its own population, and second the ability to give rise to one or more differentiated cell types (multipotency). Other hallmarks are plasticity, the ability to alter function or type in response to environmental cues, including dedifferentition, and transplantability, the ability to be placed in a different tissue context. The latter may require the former to adjust cell fate following transplantation. Further, maintenance of genome integrity, i.e. protecting against mutagenic damages, is a requirement for longevity. Dependence on niche factors is seen as a signal induced stemness by location. Stem cells which leave the niche differentiate, while cells which revert to the niche dedifferentiate (plasticity). Although counter examples rule out stem cell quiescence, i.e. an extended period of no divisions of the stem cells or at least slow cycling rounds of divisions, as a hallmark of stemness, we incorporate slow cycling stem cells in our models, as it is observed in a number of tissues [17, 27, 113].

While many hallmarks of stemness depend also on complex signaling pathways or subcellular genomic details, it is useful to define a minimal model of stemness. Following the idea of universal principles of stem cells presented in Ref. [46], we present their hypothesis based on the condition of a homeostatic population. This theory builds on the self-renewal of stem cells and its multipotency. It does not explicitely rule out other mechanisms, which can be naturally integrated in the scheme, however,

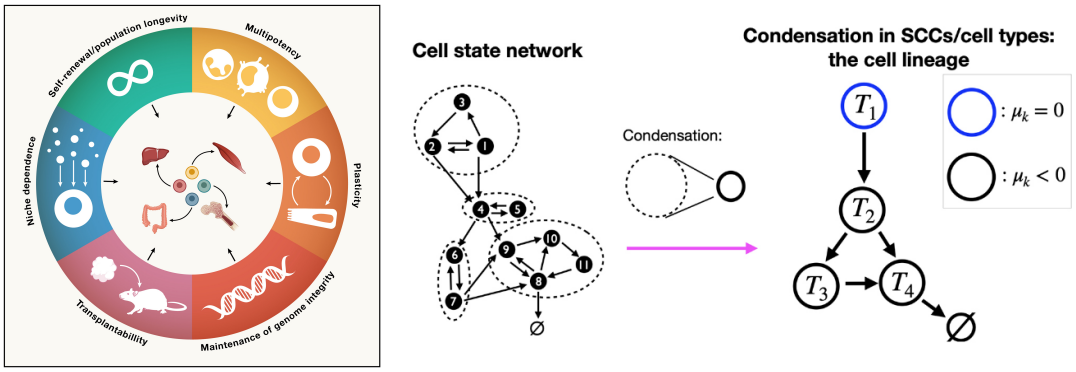

Figure 1.7: Definition of stemness. (left) Hallmarks of stem cells defined by function not by genotype, taken from [13] with permission under open access license CC-BY-4.0. (right) A universal definition of stemness based on lineage stability, where the full cell state network (left) consists of a large number of different cell types and possible transitions, which are condensed in a simplified network structure (right) with the stem cell (T_1) at the apex of the hierarchy. All cells (T_{2-4}) except the stem cell must have negative self-replication rate μ_k for stable homeostasis. Figure taken [46] by permission of the publisher.

without being a required feature by the population. Any cell of a system can be defined by its (molecular) state, which may be able to replicate. Further, this state is subject to change by differentiation or death. The combinations of possible states and change pathway make up a *cell state network* of arbitrary complexity, only limited by the condition that the network is closed (see Fig. 1.7). Transitions between states can be restricted by current cellular state, positioning, or external factors. Thus, implicitly all possible hallmarks of stemness can be included in the network, but are not a requirement for the model. While this description allows arbitrary complexity of the cell state network, condensation into classes simplifies the network description. Cells belong to the same class, if they can reach the same molecular state. As soon as an irreversible differentiation happens, the cell class changes. Now, in the simplified condensed network for every class a self-replication rate μ_k can be defined as well as transition rates between classes. Under the assumption of a stable cell population, the stem cell class (T_1 in Fig 1.7) must fulfill $\mu_1 = 0$ and all transient classes $\mu_{k>1} < 0$. Then, the system is able to balance cellular loss, but prevents overgrowth.

An important consequence of this network description is, that the stem cell type must reside at the apex of the hierarchy. This means, no influx from another state is allowed and all other states can be reached starting from the stem cell state. Eventually, such generic theory allows to include various characteristics of stemness and compile them into a hierarchical scheme. In some cases, even competing theories can be condensed in the same network. This allows us to focus on generic differentiation schemes and still obtain valuable insights transferable to more complex tissue contexts. Yet, such a cellular network focuses on coarse grained description and can not explain how the population organises within the tissue.

1.3.2 Stem cell dynamics and structure formation in epithelial tissues

In liquid systems, like blood, cells, which are produced locally by stem cells in the blood marrow, are efficiently transported through the blood vessels [29]. Renewal of epithelial tissues requires a much more homogeneous distribution of stem cells. For example in the basal layer of the epidermis, stem cells reside next to transient amplifying cells and are found on the tips of the buckles of the epidermal basal layer [65, 66]. A patterning that can result from differential cellular adhesion [74]. And in the intestine, they reside deep insight crypts [24], protected against intense wear and tear by their progeny. Besides confined niche environments, open niches, where stem cells are rather freely distributed, have also been observed [126]. Here, we want to focus on the question how stem cell distribution in epithelial tissues can be explained with help of generic models.

Recent studies have tackled different aspects of the stem cell nature to describe their distribution in epithelial tissues. Note, that most generic models are not limited to two-dimensional cell sheets, but can be directly extended to more complicated geometries. While real biological systems show high heterogeneity of cells, which results in complicated cell proliferation and differentiation mechanisms with decisions made in noisy environments [115] and sensitive to mechanical properties of the environment [36, 50], on long time scales, these converge to universal laws [71, 102]. Then, the underlying active, self-renewing nature of many particle systems, like stem cell populations, can be studied with minimal theories. We want to review two recently published models, first a model of reversible cell fate, and second an effectively coupled cell fate model controlled by a diffusing chemical, to illustrate this.

The first model, presented by Greulich et al. [45], considers cell fate decisions in a framework of cellular automata (CA, see also Sec. 1.4) simulations. Here, a simple set of update rules defines possible changes of the system. For example in the case of a stem cell type (S) and a transit cell type (T) with hierarchical uni-directional differentiation the authors define following update rules: If an S and T cell are neighbors, the S cell can "divide" to "replace" the T cell. Division can have three distinct outcomes. First, symmetric division creates two S cells, symmetric differentiation creates two T cells, and asymmetric division creates an S and a T cell, where the S and T cell can occupy the two lattice sites in one of the two possible combinations. Free lattice sides are forbidden for simplicity. This voter-like model coarsens over time [73], resulting in distinct S and T cell phases, since "divisions" can only take place at the interfaces. The final state depends on the initial configuration and cell fate probabilities. When considering reversible cell fates, or de-differentiation, such that T cells can revert back to the S cell type, no such coarsening is observed [45] and stem cells are more homogeneously distributed. Such reversible cell fate has been observed experimentally in epithelia tissues [3, 33]. Purely stochastic update rules are sufficient to generate a homogeneous stem cell distribution. However, it is not settled what controls these update rules, which have been chosen as fixed input parameter to the CA simulation. The implementation in CAs also complicates to include additional dynamics of cells and compressibility of the tissue.

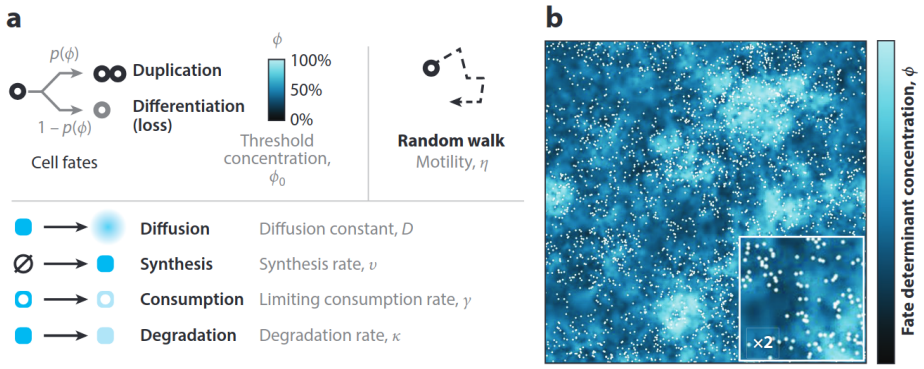

Figure 1.8: Stem cells as diffusing many-particle system. Minimal model for stem cell formation and homeostasis, where stem cells are modeled as passively diffusing, non-interacting particles. Stem cell differentiation is coupled by a chemostat ϕ, and controls outcome of stochastic division process. Fate defining chemical is consumed by the stem cells and generated by a source field. Taken from [68] by permission of the publisher.

A second approach by Joerg et al. [68] describes stem cell as a generic population of self-renewing particles. The core idea of the model is shown in Fig. 1.8. Stem cells are passively diffusing Brownian particles, which resolves the issue of lacking cell dynamics in CAs. This is a suitable model to describe the long term dynamics of stem cells, which are usually non-motile cells. The probability to duplicate, i.e. undergo a symmetric division with two stem daughter cells, is assumed to be controlled via signaling molecules, modeled as fate determinant concentration ϕ. The chemical is continuously generated, where the generation can be heterogeneous in time and space, consumed by the stem cells, and diffuses in space. This controls the local stem cell density, since in regions of high chemical concentration, stem cells duplicate more frequently, which results in higher consumption of the chemical, so that the differentiation (here: removal) probability goes up. Stem cells are effectively coupled by the signaling. This causes them to distribute homogeneous globally while locally stem cell density can vary strongly. The division mechanism together with differentiation coupling can explain heterogeneous populations, different from purely diffusing stem cells, observed for example for spermatogenic stem cells in mice [70]. This model is further capable to explain damped oscillations following perturbations, competition of species with distinct chemical uptake rates or differentiation probabilities, and various forms of large scale fluctuations, clustering effects, or neutral competition of clones.

This makes it suitable to explain experimental results and reveal long term consequences stemming from a generic form of interaction. However, the fate determinant falls short in explaining the origin of feedback. It only presents an effective long term interpretation resulting from competition to signaling cues. Also, the diffusive motion of cells is rather a consequence of microscopic effects, and in particular mechanical interactions are known to shape the cell trajectories [8]. Further, the homeostatic pressure or density theory introduced above provides a mechanistic explanation for cell fate control. Thus, naturally the question arises to which extend microscopic

mechanical interactions shape stem cell patterning and cell fate decisions in complex lineages on long time scales.

While analytical theory provides some insight on the interplay of cell fate decisions and mechanical interactions on tissue scale organisation [55, 56], computational models are able to provide deeper insight in the spatio-temporal dynamics. Thus, in the next section we introduce established computational models for tissue simulations, and select a well-suitable model for this work.

1.4 Computational modelling of cells and tissues

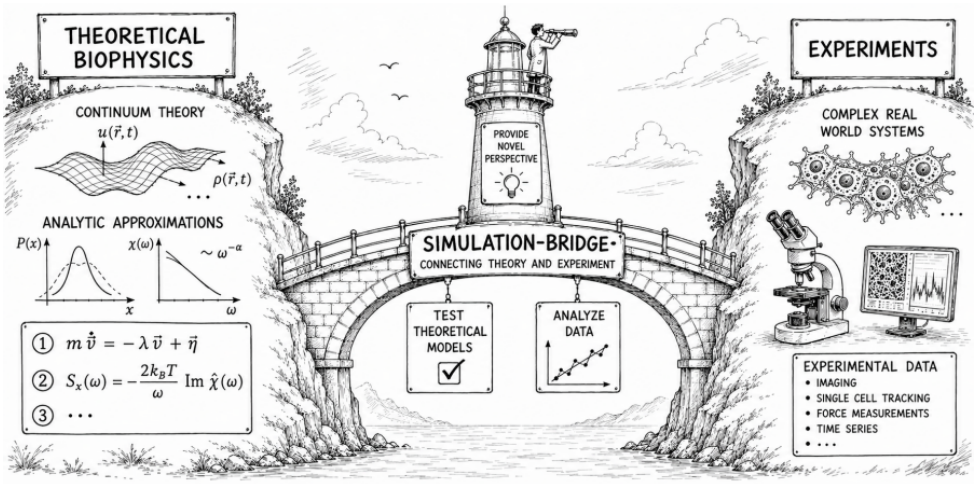

Figure 1.9: The role of computer simulations. Illustrative graphic to show how computer simulations can serve as a bridge between theory and experiments. Computational methods act as a link between theoretical approaches and complex reality, as they can test theoretical predictions or analyze data. Moreover, simulations can expand these capabilities, as they constitute self-contained experiments themselves, offering a novel perspective on the problem.

Analytic theory is mostly limited to special cases or limits of the complex biological system, even when numerical tools are applied to solve theory equations and relax approximations. While analytic theory can provide helpful insights, like population dynamics or complex pattern formations due to cell motility [55, 56], it is difficult to connect to complex experiments. But how can we advance the connection between experiments and theory?

Computer simulations provide a powerful tool to bridge between theory and experiment (see Fig.1.9): Simulation models can provide deeper insights than analytical theory alone. They can reveal emergent effects from the coupling of different microscopic details, like the discrete nature of cells, cell polarity, or detailed intercellular interactions [30]. Compared to real cellular systems, simulations have reduced complexity and implemented mechanisms are known. In particular, those mechanisms obey virtually perfect on-off switches, i.e. one can select and tune individual mecha-

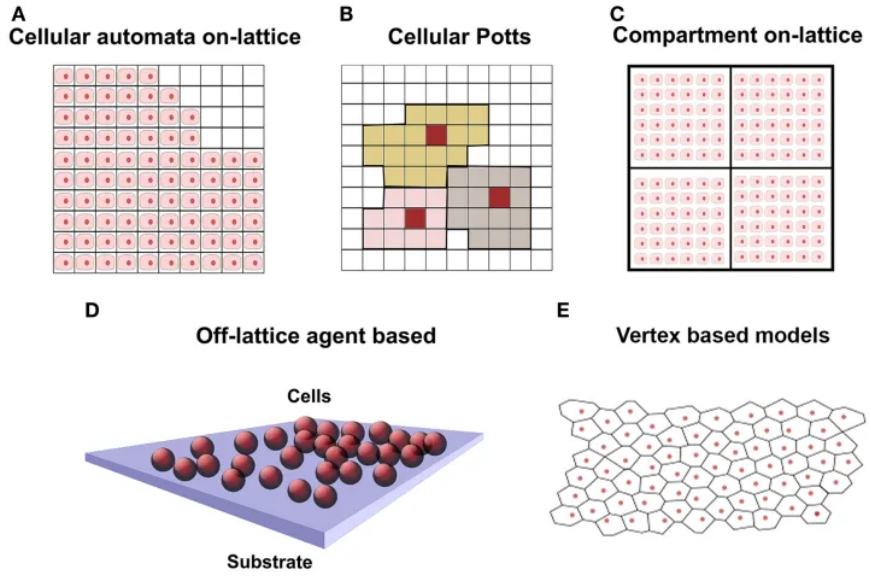

Figure 1.10: Schematic representation of discrete computational models. Illustrations of on-lattice models, like (A) Cellular Automata, (B) Cellular Potts, and (C) on-lattice compartment models, and off-lattice models, like (D) cells grown on a substrate and (E) vertex based models. Taken from [110] with permission under open access license CC-BY-4.0.

nisms in simulations to test a mechanism-based hypothesis. Furthermore, simulations allow to identify interesting parameter regimes and guide future experiments.

In the following, we focus on the generic attributes of various types of models, which are used in the field of cell and tissue modeling. Different categorization into generic model classes are feasible. For example, models can be distinguished by their underlying spatial description [110, 120] into on-lattice models (e.g. Fig. 1.10 A-C), i.e. models with predefined geometry, and off-lattice models (e.g. Fig. 1.10 D-E), where components are not bound to a fixed geometry but freely move in space. Here, we classify models with respect to their underlying mechanism. First, rule-based models are discussed, in which predefined discrete states, e.g. cell type and position, and updating rules enable to study the dynamic evolution of a system. Second, different types of off- and on-lattice models are introduced, which all have in common that the dynamics of the systems are obtained from an energy functional, reminiscent of foams. Next, we group particle-based models, which built upon agent based modeling with physical forces acting between the cells. Last, we touch on multi-scale and data-driven models, which combine different approaches or incorporate experimental results in their framework.

1.4.1 Rule based models: Cellular automata

Cellular automata (CA) are widely used to study the dynamics of discrete systems (see for example Fig. 1.10 A). Four major properties define the CA: First, the underlying

geometry, which represents a position in space, and second a finite neighborhood. Each lattice site has a defined state, for example occupied by a cell of a type chosen from a predefined number of cell types or empty, and last, transitions between states are implemented via predefined update rules.

The two spatial properties are often implemented as regular grid with nearest neighbor or next-nearest neighbor connections, but can also have complex geometries [69]. Cell states can for example be the cell types defined in a differentiation model, like stem or differentiated cell type. Updating rules include transition between states, i.e. differentiation, division by filling a connected empty site, or apoptosis, in which a site gets cleared. While the transition rules must be predefined, they do not need to be deterministic, but can be stochastic processes with given transition probabilities. Commonly, the whole grid is updated at each step of the simulations, but also stochastic or asynchronous update rules can be used.

A prominent example of CAs is Conway's game of life. Here, cells live on a regular grid with van Neumann neighborhood, i.e. only nearest neighbors along the two dimensions of the lattice are connected, thus, each cell has four neighboring cites. Three update rules define the state transition of live cells: A cell dies due to underpopulation, if less than two neighbors are live, or overpopulation, if all four neighbors are live. Only for two or three live neighbors it lives on to the next generation. Dead cells get populated, if exactly three neighbors are live. The initial configuration of the system then sets the dynamics of the system, and different patterns occur. For example still lives, i.e. structures which do not change over time, oscillators, structures which return to their initial state after a certain periodicity, or moving patterns can be observed.

The discrete nature, neighborhood, and predefined update rules allow for efficient, large scale simulations. Due to the geometry constraints of the lattice, cells have no shape or size. While most cellular processes are well resembled by (stochastic) discrete jump processes, also physical interactions must be implemented in this spirit. This only allows for a rather approximate capture of physical interactions between cells, if possible at all. CAs have been successfully applied to study (interfacial) growth dynamics [15, 69, 97], understanding the role of different cell types with distinct cell fate properties in heterogeneous populations stemming from cancer stem cells [35], and effects of reversible cell fate model on stem cell distribution [45].

1.4.2 Energy-functional, foam-like models

As a second class of models, we discuss foam-like models, which derive their dynamics from an energy functional. The contributions to the functional can describe various intrinsic and extrinsic properties of the cell. For example cell shape is included by optimizing the current cell size, i.e. area or volume, with respect to a target cell size as well as optimizing the cell perimeter. Additional effects, like cell adhesion, which is discussed in more detail below, cortical tension, external forces, or active motility forces can also be included in the energy functional. The dynamics then follow by minimizing the energy functional.

One of the most prominent example, the *Cellular Potts* model (CPM) presented by Graner and Glacier [44], describes cell sorting as a consequence of differential adhesion. In this on-lattice model, each cell is made up of individual pixels on a lattice (see Fig. 1.10 B). A cell size or area is defined by the number of pixels of the respective cell. Adjacent pixels interact with each other to model adhesion. Then, an energy functional is build from an adhesive energy, which is different for cells of the same or different type and the surrounding medium, and a target volume, which penalizes too large or too small cell sizes, and is given by

$$\mathcal{H} = \sum_{(i,j)\ \text{neighbors}} J\left(\tau(\sigma_i), \tau(\sigma_j)\right)\left(1 - \delta_{\sigma_i,\sigma_j}\right) + \lambda \sum_{\sigma} \left(a(\sigma) - A(\tau(\sigma))\right)^2 . \tag{1.8}$$

Here, i, j are the pixels or lattice sites, J defines an interaction matrix, e.g. adhesion, between cell types $\tau(\sigma)$, where σ_i is the selected cell. The current cell size $a(\sigma)$ is minimized with the type specific target cell size $A(\tau(\sigma))$. A Monte-Carlo method is used to minimize energy. First, a lattice site i is chosen at random and one of its neighbors j is selected at random. If a type conversion of j to the type of i reduces the energy functional, the update is successful and accepted. Else, the transition of j is accepted with a finite probability, which introduces noise and prohibits getting stuck in local minima.

CPM-like models can be implemented with high efficiency and allow for example to study complex tumor growth with detailed information about the micro environment [10, 12, 101]. The model has been widely applied to study for example growth, competition, and evolution of tissue and tumor spheroids [104, 109]. Also, influences of cellular motility based on local cellular remodeling dynamics, for complex invasion strategies in tumors, and surface topographies have been investigated [112, 123, 124].

In recent years, implementations of cell shape models in form of vertex models (see Fig. 1.10 E) have been widely applied to study tissue morphogenesis as a consequence of cell mechanics [4, 40]. Here, cell shape is explicitely described in form of vertices, where each vertex describes the connection of three or more cells. Vertex models are well suited to describe confluent tissues, as they are built from a connected network. Forces acting on the vertices are derived from the energy functional, which usually includes a contribution from cell perimeter and area to describe shape, and cell-cell adhesion can also be included via the contact length of adjacent cells. Cell division and apoptosis need to be carefully included in the model, as they require remodelling of the vertex structure [108] An efficient way to construct the vertex structure builds upon a *Voronoi* tessellation. Here, vertices are calculated from cell center positions, which requires that forces acting on cell centers are calculated from the energy of vertices, but allows for an efficient description of tissue remodelling [6].

Vertex models have been used to study morphogenesis [38] or the formation of cysts or interfaces between different cell types [14]. Stem cell organisation in the intestine and stem cell clone competition as a consequence of sub-cellular Wnt signaling have also been investigated with this type of models [81, 119].

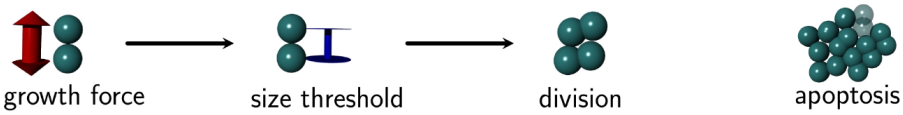

Figure 1.11: Schematic representation of two-particle growth (2PG) model. Cell growth is modeled via an active repulsive force between the two particles of a cell, until their distance exceeds a division threshold, which initiates division. During division for each old particle of the cell a new particle is placed in close vicinity at random orientation. Cell loss is modelled in a stochastic process with fixed apoptosis rate. Taken with permission granted by J. Elgeti.

1.4.3 Particle based models

In particle based models, each cell of the tissue is represented individually. Physical forces acting on the cell determine their shape and dynamics. For example, when each cell is a point particle, a spherical shape results from an isotropic, short range repulsive interaction between cells. More complex cell shapes result from anisotropic potentials or a representation of the cell constructed from multiple particles. In the same spirit, cell adhesion is then modelled as attractive force. Such a combination of attractive and repulsive forces is usually implemented in Lennard-Jones like potentials and the shape of the potential determines the "softness" and "stickiness" of cells. The force based formalism is very flexible, and more complex mechanisms, like cell motion, can be directly included in form of forces acting on the cell particles.

Different implementations have been developed to model growth, for example in form of growing rods [64, 88] or discs [62], where the respective agent size grows deterministically with a fixed rate. Other models use a dumbbell like representation, where cell shape prior to division undergoes a transformation from a spheroid to an elongated shape [8, 34, 59, 89]. Here, cellular growth is controlled by an active growth force, which makes cells susceptible to feedback from their environment.

Particle based models of growth have been applied to study various mesoscopic mechanical effects, like fluidization of tissues due to division and apoptosis [8], the role of motility on colony spreading, wound healing and alignment of division axis [9, 80], interface dynamics [18, 41], complex co-existing multi-cellular systems [19], and the role of mechanoresponse on the proliferation probability [59]. With increasing number of particles per cell, cell shape and polarity can be studied as well [30].

The aim of this thesis is to investigate the role of mechanical interactions on long term stem cell population dynamics and self-organisation. This requires large time and length scales, but can abstain from details on subcellular scales and short times. Particle-based simulations are well suited to facilitate these requirements. Here, we adapt the *two-particle growth* (2PG) model [8] (see Fig. 1.11). Details of the model are presented in each individual result chapter. Briefly stated, each cell is represented by two particles, which repel each other with an active growth force. When the distance between the two particles of a cell exceeds a fixed threshold, the cell divides. At the time of division, next to each particle of the original cell, a new particle is placed. The

position of the new particle is chosen at random. Apoptosis is modelled as stochastic removal of cells, while cell differentiation is modeled in different fashion for the respective systems under investigation and will be introduced in the corresponding chapters. Cell interactions are modelled by an attractive adhesion force and a repulsive force for volume exclusion. Random and frictional forces act within the cell and between pairs of cells. Friction is high, such that inertial effects do not play a role. Beside cell-cell friction we also include cell-substrate friction. Long time and length scales are enabled with a self-consistent dissipative particle dynamics (DPD) technique [37, 47, 60, 77, 87], which allows for large time steps to increase computational speed. Furthermore, this technique conserves momentum and preserves hydrodynamics. In addition, efficient computations rely on additional sophisticated techniques to track cellular neighborhoods, like Verlet lists, and `OpenMP` parallelization.

1.4.4 Multiscale and hybrid models and data driven modelling

In some cases, a single class of model does not suffice to construct a suitable computational framework. Cellular dynamics range over too many orders of magnitude to be compiled in a single model class. In order to build more realistic models, often referred to as digital twins or shadows, it may be necessary to combine several different techniques. The core idea of these models is to remove excessive computational costs by choosing the best suited minimal model for each component, and linking them in additional steps. Combinations of one of the previously discussed discrete models with partial differential equations (PDEs) allows to capture larger variation in scales and consider relevant effects on different orders of magnitude. For example nutrients can be modelled with continuum equations and combined with agent based simulations of growing cells [61]. Also, combination of different types of discrete models is conceivable. It is crucial, however, to correctly couple each individual technique and integrate them in a single framework. Multi-scale models have used for example a CPM for cells and elastic lattice models for the extracellular matrix [58], or in form of a vertex model for cell interactions and differential equations to model ion-transport [85]. The latter will be introduced in more detail in chapter 4, where we apply this model to test our fluctuation-response measurement.

Also, recently data driven models have been seen rising attention [16, 20, 86]. They utilize large amounts of experimental data to either reveal or predict physiological mechanisms and function or infer mechanistic models. While traditionally they have been applied to omics data sets, recent progress on cell trajectory data is experimenting with new paths. In order to generate a true digital twin or shadow of an experiment or application, combining physics-based models and data is crucial [5, 28].

1.5 Outlook on the thesis

In this thesis, we investigate in detail how two specific differentiation models coupled with mechanical interactions result in distinct stem cell population dynamics and

patterning. Further, we examine how the dynamic response can be measured from steady state fluctuation spectra. The thesis is structured as follows.

In chapter 2, we combine the 2PG simulation model and the textbook picture of epithelial renewal by stem cells, i.e. the deterministic cascade of set number of transient amplifying (TA) cell divisions following an asymmetric stem cell division. We discuss how the outflux of cells generated by the stem cell and the mechanical interactions between cells in the tissue result in stem cell separation. In particular, the role of TA cell growth as the driving force of separation is studied. We map our system on a thermal equilibrium analogy of Brownian particles interacting via an exponentially decaying potential. The parameters of the potential are derived from properties of cell colonies generated by a single stem cell and a pair of stem cells. In confluent tissues we analyze static structure formation via the pair correlation function and dynamic relaxation of these structures through the dynamic structure factor, comparing tissue simulations with our thermal equilibrium analogy. Further, we unravel the role of proliferating progeny for stem cell dynamics and how they cause surprising persistent bursts, quantified as superdiffusive motion.

In chapter 3, we remove the limitation of a fixed stem cell number due to solely asymmetric stem cell divisions. This enables dynamically adjusted stem cell numbers and tissue composition by allowing for symmetric division in combination with fixed rate differentiation. With help of a mean field theory of cell number balance, we discuss a criterion for stability of the stem cell population. Combined with numerical simulations, we can identify relevant tissue configurations. These meet the requirements of a rare stem cell population with reduced proliferation dynamics, an intermediate, quickly but limited proliferating cell type and major mass given by fully differentiated cells [100]. We study how stochasticity and symmetric divisions result in formation of cluster like stem cell niches and their dynamics. Further, we investigate the complexity of structure formation with help of clone tracing methods.

Last, we focus on measuring the mechanical response of cells in tissues, in chapter 4, and study how steady-state fluctuations can be utilized to describe the dynamic response of cells. To this end, equations, which describe a self-renewing cell population, are set in relation to a system of a Brownian particle trapped in a harmonic potential. From this mapping we derive a number of complementing statistical methods, which allow to measure the dynamic response coefficient via the variance of fluctuations. By depending only on steady state trajectories, our novel approach overcomes limitations of previous simulation methods and common experimental techniques, like stretch assays, which can be interfering or invasive. We show that our presented method is even capable of revealing underlying microscopic details of distinct growth models, and identify a non-Markovian memory effect in the 2PG model and even more complex effects in a mechano-electro-osmotic growth model. In contrast to the other two chapters, this new method is worked out for tissues consisting of a single cell type as a foundational step toward multi-cellular lineage systems.

In the concluding chapter, we present a summary and discussion of our results. Future research perspectives, which follow from the results of this thesis, are outlined.

References

[1] D. N. Alasaadi and R. Mayor. Mechanically guided cell fate determination in early development. *Cellular and Molecular Life Sciences*, 81(1), May 2024. ISSN 1420-9071. doi: 10.1007/s00018-024-05272-6. URL http://dx.doi.org/10.1007/s00018-024-05272-6.

[2] B. Alberts, A. Johnson, J. Lewis, M. Raff, K. Roberts, and P. Walter. Epidermis and Its Renewal by Stem Cells. *Molecular Biology of the Cell. 4th edition*, 2002. URL https://www.ncbi.nlm.nih.gov/books/NBK26865/. Publisher: Garland Science.

[3] M. P. Alcolea, P. Greulich, A. Wabik, J. Frede, B. D. Simons, and P. H. Jones. Differentiation imbalance in single oesophageal progenitor cells causes clonal immortalization and field change. *Nature Cell Biology*, 16(6):612–619, May 2014. ISSN 1476-4679. doi: 10.1038/ncb2963. URL http://dx.doi.org/10.1038/ncb2963.

[4] S. Alt, P. Ganguly, and G. Salbreux. Vertex models: from cell mechanics to tissue morphogenesis. *Philosophical Transactions of the Royal Society B: Biological Sciences*, 372(1720):20150520, Mar. 2017. ISSN 1471-2970. doi: 10.1098/rstb.2015.0520. URL http://dx.doi.org/10.1098/rstb.2015.0520.

[5] M. T. Barros, M. Paci, A. Tervonen, E. Passini, J. T. Koivumäki, J. A. K. Hyttinen, and K. Lenk. From multiscale biophysics to digital twins of tissues and organs: Future opportunities for in-silico pharmacology. *IEEE Transactions on Molecular, Biological, and Multi-Scale Communications*, 10(4):576–594, Dec. 2024. ISSN 2332-7804. doi: 10.1109/tmbmc.2024.3442083. URL http://dx.doi.org/10.1109/TMBMC.2024.3442083.

[6] D. L. Barton, S. Henkes, C. J. Weijer, and R. Sknepnek. Active vertex model for cell-resolution description of epithelial tissue mechanics. *PLOS Computational Biology*, 13 (6):e1005569, June 2017. ISSN 1553-7358. doi: 10.1371/journal.pcbi.1005569. URL http://dx.doi.org/10.1371/journal.pcbi.1005569.

[7] M. Basan, T. Risler, J. Joanny, X. Sastre-Garau, and J. Prost. Homeostatic competition drives tumor growth and metastasis nucleation. *HFSP Journal*, 3(4):265–272, Aug. 2009. ISSN 1955-2068. doi: 10.2976/1.3086732. URL http://dx.doi.org/10.2976/1.3086732.

[8] M. Basan, J. Prost, J.-F. Joanny, and J. Elgeti. Dissipative particle dynamics simulations for biological tissues: rheology and competition. *Physical Biology*, 8(2): 026014, Apr. 2011. ISSN 1478-3975. doi: 10.1088/1478-3975/8/2/026014. URL http://dx.doi.org/10.1088/1478-3975/8/2/026014.

[9] M. Basan, J. Elgeti, E. Hannezo, W.-J. Rappel, and H. Levine. Alignment of cellular motility forces with tissue flow as a mechanism for efficient wound healing. *Proceedings of the National Academy of Sciences*, 110(7):2452–2459, Jan. 2013. ISSN 1091-6490. doi: 10.1073/pnas.1219937110. URL http://dx.doi.org/10.1073/pnas.1219937110.

[10] E. Behle, J. M. Herold, and A. H. Schug. Simulating tumor-induced angiogenesis in macroscopic systems. *Biophysical Journal*, 123(3):279a, Feb. 2024. ISSN 0006-3495. doi: 10.1016/j.bpj.2023.11.1738. URL http://dx.doi.org/10.1016/j.bpj.2023.11.1738.

[11] M. Ben Amar and F. Jia. Anisotropic growth shapes intestinal tissues during embryogenesis. *Proceedings of the National Academy of Sciences*, 110(26):10525–10530, June 2013. ISSN 1091-6490. doi: 10.1073/pnas.1217391110. URL http://dx.doi.org/10.1073/pnas.1217391110.

[12] M. Berghoff, J. Rosenbauer, F. Hoffmann, and A. Schug. Cells in silico – introducing a high-performance framework for large-scale tissue modeling. *BMC Bioinformatics*, 21(1), Oct. 2020. ISSN 1471-2105. doi: 10.1186/s12859-020-03728-7. URL http://dx.doi.org/10.1186/s12859-020-03728-7.

[13] J. Beumer and H. Clevers. Hallmarks of stemness in mammalian tissues. *Cell Stem Cell*, 31(1):7–24, Jan. 2024. ISSN 1934-5909. doi: 10.1016/j.stem.2023.12.006. URL http://dx.doi.org/10.1016/j.stem.2023.12.006.

[14] C. Bielmeier, S. Alt, V. Weichselberger, M. La Fortezza, H. Harz, F. Jülicher, G. Salbreux, and A.-K. Classen. Interface contractility between differently fated cells drives cell elimination and cyst formation. *Current Biology*, 26(5):563–574, Mar. 2016. ISSN 0960-9822. doi: 10.1016/j.cub.2015.12.063. URL http://dx.doi.org/10.1016/j.cub.2015.12.063.

[15] M. Block, E. Schöll, and D. Drasdo. Classifying the expansion kinetics and critical surface dynamics of growing cell populations. *Physical Review Letters*, 99(24), Dec. 2007. ISSN 1079-7114. doi: 10.1103/physrevlett.99.248101. URL http://dx.doi.org/10.1103/PhysRevLett.99.248101.

[16] D. B. Brückner and C. P. Broedersz. Learning dynamical models of single and collective cell migration: a review. *Reports on Progress in Physics*, 87(5):056601, Apr. 2024. ISSN 1361-6633. doi: 10.1088/1361-6633/ad36d2. URL http://dx.doi.org/10.1088/1361-6633/ad36d2.

[17] S. J. A. Buczacki, H. I. Zecchini, A. M. Nicholson, R. Russell, L. Vermeulen, R. Kemp, and D. J. Winton. Intestinal label-retaining cells are secretory precursors expressing lgr5. *Nature*, 495(7439):65–69, Feb. 2013. ISSN 1476-4687. doi: 10.1038/nature11965. URL http://dx.doi.org/10.1038/nature11965.

[18] T. Büscher, A. L. Diez, G. Gompper, and J. Elgeti. Instability and fingering of interfaces in growing tissue. *New Journal of Physics*, 22(8):083005, Aug. 2020. ISSN 1367-2630. doi: 10.1088/1367-2630/ab9e88. URL http://dx.doi.org/10.1088/1367-2630/ab9e88.

[19] T. Büscher, N. Ganai, G. Gompper, and J. Elgeti. Tissue evolution: mechanical interplay of adhesion, pressure, and heterogeneity. *New Journal of Physics*, 22(3):033048, Mar. 2020. ISSN 1367-2630. doi: 10.1088/1367-2630/ab74a5. URL http://dx.doi.org/10.1088/1367-2630/ab74a5.

[20] P. Cahan, D. Cacchiarelli, S.-J. Dunn, M. Hemberg, S. M. C. de Sousa Lopes, S. A. Morris, O. J. Rackham, A. del Sol, and C. A. Wells. Computational stem cell biology: Open questions and guiding principles. *Cell Stem Cell*, 28(1):20–32, Jan. 2021. ISSN 1934-5909. doi: 10.1016/j.stem.2020.12.012. URL http://dx.doi.org/10.1016/j.stem.2020.12.012.

[21] G. Charras and A. S. Yap. Tensile forces and mechanotransduction at cell–cell junctions. *Current Biology*, 28(8):R445–R457, Apr. 2018. ISSN 0960-9822. doi: 10.1016/j.cub.2018.02.003. URL http://dx.doi.org/10.1016/j.cub.2018.02.003.

[22] G. Cheng, J. Tse, R. K. Jain, and L. L. Munn. Micro-environmental mechanical stress controls tumor spheroid size and morphology by suppressing proliferation and inducing apoptosis in cancer cells. *PLoS ONE*, 4(2):e4632, Feb. 2009. ISSN 1932-6203. doi: 10.1371/journal.pone.0004632. URL http://dx.doi.org/10.1371/journal.pone.0004632.

[23] E. Clayton, D. P. Doupé, A. M. Klein, D. J. Winton, B. D. Simons, and P. H. Jones. A single type of progenitor cell maintains normal epidermis. *Nature*, 446(7132):185–189, Feb. 2007. ISSN 1476-4687. doi: 10.1038/nature05574. URL `http://dx.doi.org/10.1038/nature05574`.

[24] H. Clevers. The intestinal crypt, a prototype stem cell compartment. *Cell*, 154(2): 274–284, July 2013. ISSN 0092-8674. doi: 10.1016/j.cell.2013.07.004. URL `http://dx.doi.org/10.1016/j.cell.2013.07.004`.

[25] H. Clevers and F. M. Watt. Defining adult stem cells by function, not by phenotype. *Annual Review of Biochemistry*, 87(1):1015–1027, June 2018. ISSN 1545-4509. doi: 10.1146/annurev-biochem-062917-012341. URL `http://dx.doi.org/10.1146/annurev-biochem-062917-012341`.

[26] L. d. Costa Campos, R. Hornung, G. Gompper, J. Elgeti, and S. Caspers. The role of thickness inhomogeneities in hierarchical cortical folding. *NeuroImage*, 231:117779, May 2021. ISSN 1053-8119. doi: 10.1016/j.neuroimage.2021.117779. URL `http://dx.doi.org/10.1016/j.neuroimage.2021.117779`.

[27] G. Cotsarelis, T.-T. Sun, and R. M. Lavker. Label-retaining cells reside in the bulge area of pilosebaceous unit: Implications for follicular stem cells, hair cycle, and skin carcinogenesis. *Cell*, 61(7):1329–1337, June 1990. ISSN 0092-8674. doi: 10.1016/0092-8674(90)90696-c. URL `http://dx.doi.org/10.1016/0092-8674(90)90696-C`.

[28] P. Coveney, R. Highfield, E. Stahlberg, and M. Vázquez. Digital twins and big ai: the future of truly individualised healthcare. *npj Digital Medicine*, 8(1), Aug. 2025. ISSN 2398-6352. doi: 10.1038/s41746-025-01874-x. URL `http://dx.doi.org/10.1038/s41746-025-01874-x`.

[29] G. M. Crane, E. Jeffery, and S. J. Morrison. Adult haematopoietic stem cell niches. *Nature Reviews Immunology*, 17(9):573–590, June 2017. ISSN 1474-1741. doi: 10.1038/nri.2017.53. URL `http://dx.doi.org/10.1038/nri.2017.53`.

[30] M. Dedenon, C. Blanch-Mercader, K. Kruse, and J. Elgeti. The importance of being discrete: fluctuations, defects, and density-orientation coupling in agent-based active nematics. *New Journal of Physics*, 28(2):024401, Feb. 2026. ISSN 1367-2630. doi: 10.1088/1367-2630/ae3d5c. URL `http://dx.doi.org/10.1088/1367-2630/ae3d5c`.

[31] M. Delarue, F. Montel, O. Caen, J. Elgeti, J.-M. Siaugue, D. Vignjevic, J. Prost, J.-F. Joanny, and G. Cappello. Mechanical control of cell flow in multicellular spheroids. *Physical Review Letters*, 110(13), Mar. 2013. ISSN 1079-7114. doi: 10.1103/physrevlett.110.138103. URL `http://dx.doi.org/10.1103/PhysRevLett.110.138103`.

[32] I. Di Meglio, A. Trushko, P. Guillamat, C. Blanch-Mercader, S. Abuhattum, and A. Roux. Pressure and curvature control of the cell cycle in epithelia growing under spherical confinement. *Cell Reports*, 40(8):111227, Aug. 2022. ISSN 2211-1247. doi: 10.1016/j.celrep.2022.111227. URL `http://dx.doi.org/10.1016/j.celrep.2022.111227`.

[33] G. Donati and F. M. Watt. Stem cell heterogeneity and plasticity in epithelia. *Cell Stem Cell*, 16(5):465–476, May 2015. ISSN 1934-5909. doi: 10.1016/j.stem.2015.04.014. URL `http://dx.doi.org/10.1016/j.stem.2015.04.014`.

[34] D. Drasdo and S. Höhme. A single-cell-based model of tumor growthin vitro: monolayers and spheroids. *Physical Biology*, 2(3):133–147, July 2005. ISSN 1478-3975. doi: 10.1088/1478-3975/2/3/001. URL `http://dx.doi.org/10.1088/1478-3975/2/3/001`.

[35] H. Enderling and P. Hahnfeldt. Cancer stem cells in solid tumors: Is 'evading apoptosis' a hallmark of cancer? *Progress in Biophysics and Molecular Biology*, 106(2):391–399, Aug. 2011. ISSN 0079-6107. doi: 10.1016/j.pbiomolbio.2011.03.007. URL http://dx.doi.org/10.1016/j.pbiomolbio.2011.03.007.

[36] A. J. Engler, S. Sen, H. L. Sweeney, and D. E. Discher. Matrix elasticity directs stem cell lineage specification. *Cell*, 126(4):677–689, Aug. 2006. ISSN 0092-8674. doi: 10.1016/j.cell.2006.06.044. URL http://dx.doi.org/10.1016/j.cell.2006.06.044.

[37] P. Español and P. Warren. Statistical Mechanics of Dissipative Particle Dynamics. *Europhysics Letters (EPL)*, 30(4):191–196, May 1995. ISSN 0295-5075, 1286-4854. doi: 10.1209/0295-5075/30/4/001. URL https://iopscience.iop.org/article/10.1209/0295-5075/30/4/001.

[38] R. Farhadifar, J.-C. Röper, B. Aigouy, S. Eaton, and F. Jülicher. The influence of cell mechanics, cell-cell interactions, and proliferation on epithelial packing. *Current Biology*, 17(24):2095–2104, Dec. 2007. ISSN 0960-9822. doi: 10.1016/j.cub.2007.11.049. URL http://dx.doi.org/10.1016/j.cub.2007.11.049.

[39] C. Ferrai and C. Schulte. Mechanotransduction in stem cells. *European Journal of Cell Biology*, 103(2):151417, June 2024. ISSN 0171-9335. doi: 10.1016/j.ejcb.2024.151417. URL http://dx.doi.org/10.1016/j.ejcb.2024.151417.

[40] A. G. Fletcher, M. Osterfield, R. E. Baker, and S. Y. Shvartsman. Vertex models of epithelial morphogenesis. *Biophysical Journal*, 106(11):2291–2304, June 2014. ISSN 0006-3495. doi: 10.1016/j.bpj.2013.11.4498. URL http://dx.doi.org/10.1016/j.bpj.2013.11.4498.

[41] N. Ganai, T. Büscher, G. Gompper, and J. Elgeti. Mechanics of tissue competition: interfaces stabilize coexistence. *New Journal of Physics*, 21(6):063017, June 2019. ISSN 1367-2630. doi: 10.1088/1367-2630/ab2475. URL http://dx.doi.org/10.1088/1367-2630/ab2475.

[42] S. Ghazizadeh and L. B. Taichman. Organization of stem cells and their progeny in human epidermis. *Journal of Investigative Dermatology*, 124(2):367–372, Feb. 2005. ISSN 0022-202X. doi: 10.1111/j.0022-202x.2004.23599.x. URL http://dx.doi.org/10.1111/j.0022-202x.2004.23599.x.

[43] S. M. Girvin and K. Yang. *Modern condensed matter physics*. Cambridge University Press, Cambridge, England, Feb. 2019.

[44] F. Graner and J. A. Glazier. Simulation of biological cell sorting using a two-dimensional extended potts model. *Physical Review Letters*, 69(13):2013–2016, Sept. 1992. ISSN 0031-9007. doi: 10.1103/physrevlett.69.2013. URL http://dx.doi.org/10.1103/PhysRevLett.69.2013.

[45] P. Greulich and B. D. Simons. Dynamic heterogeneity as a strategy of stem cell self-renewal. *Proceedings of the National Academy of Sciences*, 113(27):7509–7514, June 2016. ISSN 1091-6490. doi: 10.1073/pnas.1602779113. URL http://dx.doi.org/10.1073/pnas.1602779113.

[46] P. Greulich, B. D. MacArthur, C. Parigini, and R. J. Sánchez-García. Universal principles of lineage architecture and stem cell identity in renewing tissues. *Development*, 148(11), June 2021. ISSN 1477-9129. doi: 10.1242/dev.194399. URL http://dx.doi.org/10.1242/dev.194399.

[47] R. D. Groot and P. B. Warren. Dissipative particle dynamics: Bridging the gap between atomistic and mesoscopic simulation. *The Journal of Chemical Physics*, 107 (11):4423–4435, Sept. 1997. ISSN 1089-7690. doi: 10.1063/1.474784. URL http://dx.doi.org/10.1063/1.474784.

[48] P. Gross, K. V. Kumar, and S. W. Grill. How active mechanics and regulatory biochemistry combine to form patterns in development. *Annual Review of Biophysics*, 46 (1):337–356, May 2017. ISSN 1936-1238. doi: 10.1146/annurev-biophys-070816-033602. URL http://dx.doi.org/10.1146/annurev-biophys-070816-033602.

[49] C. Guha Ray and P. A. Haas. Unbuckling mechanics of epithelial monolayers under compression. *Physical Review Letters*, 134(11), Mar. 2025. ISSN 1079-7114. doi: 10.1103/physrevlett.134.118402. URL http://dx.doi.org/10.1103/PhysRevLett.134.118402.

[50] F. Guilak, D. M. Cohen, B. T. Estes, J. M. Gimble, W. Liedtke, and C. S. Chen. Control of stem cell fate by physical interactions with the extracellular matrix. *Cell Stem Cell*, 5(1):17–26, July 2009. ISSN 1934-5909. doi: 10.1016/j.stem.2009.06.016. URL http://dx.doi.org/10.1016/j.stem.2009.06.016.

[51] P. A. Haas. Geometry of t1 transitions in epithelia. *Physical Review E*, 112(4), Oct. 2025. ISSN 2470-0053. doi: 10.1103/kdnb-bxdx. URL http://dx.doi.org/10.1103/kdnb-bxdx.

[52] O. Hallatschek, S. S. Datta, K. Drescher, J. Dunkel, J. Elgeti, B. Waclaw, and N. S. Wingreen. Proliferating active matter. *Nature Reviews Physics*, 5(7):407–419, May 2023. ISSN 2522-5820. doi: 10.1038/s42254-023-00593-0. URL http://dx.doi.org/10.1038/s42254-023-00593-0.

[53] E. Hannezo, J. Prost, and J.-F. Joanny. Instabilities of monolayered epithelia: Shape and structure of villi and crypts. *Physical Review Letters*, 107(7), Aug. 2011. ISSN 1079-7114. doi: 10.1103/physrevlett.107.078104. URL http://dx.doi.org/10.1103/PhysRevLett.107.078104.

[54] E. Hannezo, J. Prost, and J.-F. Joanny. Theory of epithelial sheet morphology in three dimensions. *Proceedings of the National Academy of Sciences*, 111(1):27–32, Dec. 2013. ISSN 1091-6490. doi: 10.1073/pnas.1312076111. URL http://dx.doi.org/10.1073/pnas.1312076111.

[55] E. Hannezo, J. Prost, and J.-F. Joanny. Growth, homeostatic regulation and stem cell dynamics in tissues. *Journal of The Royal Society Interface*, 11(93):20130895, Apr. 2014. ISSN 1742-5662. doi: 10.1098/rsif.2013.0895. URL http://dx.doi.org/10.1098/rsif.2013.0895.

[56] E. Hannezo, A. Coucke, and J.-F. Joanny. Interplay of migratory and division forces as a generic mechanism for stem cell patterns. *Physical Review E*, 93(2), Feb. 2016. ISSN 2470-0053. doi: 10.1103/physreve.93.022405. URL http://dx.doi.org/10.1103/PhysRevE.93.022405.

[57] G. Helmlinger, P. A. Netti, H. C. Lichtenbeld, R. J. Melder, and R. K. Jain. Solid stress inhibits the growth of multicellular tumor spheroids. *Nature Biotechnology*, 15 (8):778–783, Aug. 1997. ISSN 1546-1696. doi: 10.1038/nbt0897-778. URL http://dx.doi.org/10.1038/nbt0897-778.

[58] J. Herold, P. Brinkmeier, M. Götz, A. Schug, and A. Streit. Large-scale modeling of the extracellular matrix on hybrid supercomputers using highly parallel stencil computations. In *ISC High Performance 2025 Research Paper Proceedings (40th International Conference)*, page 1–14. IEEE, June 2025. doi: 10.23919/isc.2025.11017726. URL http://dx.doi.org/10.23919/ISC.2025.11017726.

[59] K. Höllring, L. Nuić, L. Rogić, S. Kaliman, S. Gehrer, C. Wollnik, F. Rehfeldt, M. Hubert, and A.-S. Smith. Capturing the mechanosensitivity of cell proliferation in models of epithelium. *Proceedings of the National Academy of Sciences*, 121(45), Oct. 2024. ISSN 1091-6490. doi: 10.1073/pnas.2308126121. URL http://dx.doi.org/10.1073/pnas.2308126121.

[60] P. J. Hoogerbrugge and J. M. V. A. Koelman. Simulating Microscopic Hydrodynamic Phenomena with Dissipative Particle Dynamics. *Europhysics Letters (EPL)*, 19(3):155–160, June 1992. ISSN 0295-5075, 1286-4854. doi: 10.1209/0295-5075/19/3/001. URL https://iopscience.iop.org/article/10.1209/0295-5075/19/3/001.

[61] R. Hornung, A. Grünberger, C. Westerwalbesloh, D. Kohlheyer, G. Gompper, and J. Elgeti. Quantitative modelling of nutrient-limited growth of bacterial colonies in microfluidic cultivation. *Journal of The Royal Society Interface*, 15(139):20170713, Feb. 2018. ISSN 1742-5662. doi: 10.1098/rsif.2017.0713. URL http://dx.doi.org/10.1098/rsif.2017.0713.

[62] L. Hupe, Y. G. Pollack, J. Isensee, A. Amiri, R. Golestanian, and P. Bittihn. A minimal model of smoothly dividing disk-shaped cells, 2024. URL https://arxiv.org/abs/2409.01959.

[63] K. D. Irvine and B. I. Shraiman. Mechanical control of growth: ideas, facts and challenges. *Development*, 144(23):4238–4248, Dec. 2017. ISSN 0950-1991. doi: 10.1242/dev.151902. URL http://dx.doi.org/10.1242/dev.151902.

[64] J. Isensee, L. Hupe, R. Golestanian, and P. Bittihn. Stress anisotropy in confined populations of growing rods. *Journal of The Royal Society Interface*, 19(196), Nov. 2022. ISSN 1742-5662. doi: 10.1098/rsif.2022.0512. URL http://dx.doi.org/10.1098/rsif.2022.0512.

[65] U. B. Jensen, S. Lowell, and F. M. Watt. The spatial relationship between stem cells and their progeny in the basal layer of human epidermis: a new view based on whole-mount labelling and lineage analysis. *Development*, 126(11):2409–2418, June 1999. ISSN 1477-9129. doi: 10.1242/dev.126.11.2409. URL http://dx.doi.org/10.1242/dev.126.11.2409.

[66] P. H. Jones, S. Harper, and F. M. Watt. Stem cell patterning and fate in human epidermis. *Cell*, 80(1):83–93, Jan. 1995. ISSN 0092-8674. doi: 10.1016/0092-8674(95)90453-0. URL http://dx.doi.org/10.1016/0092-8674(95)90453-0.

[67] P. H. Jones, B. D. Simons, and F. M. Watt. Sic transit gloria: Farewell to the epidermal transit amplifying cell? *Cell Stem Cell*, 1(4):371–381, Oct. 2007. ISSN 1934-5909. doi: 10.1016/j.stem.2007.09.014. URL http://dx.doi.org/10.1016/j.stem.2007.09.014.

[68] D. J. Jörg, Y. Kitadate, S. Yoshida, and B. D. Simons. Stem cell populations as self-renewing many-particle systems. *Annual Review of Condensed Matter Physics*, 12(1):135–153, Mar. 2021. ISSN 1947-5462. doi: 10.1146/annurev-conmatphys-041720-125707. URL http://dx.doi.org/10.1146/annurev-conmatphys-041720-125707.

[69] A. Kansal, S. Torquato, G. Harsh IV, E. Chiocca, and T. Deisboeck. Cellular automaton of idealized brain tumor growth dynamics. *Biosystems*, 55(1–3):119–127, Feb. 2000. ISSN 0303-2647. doi: 10.1016/s0303-2647(99)00089-1. URL http://dx.doi.org/10.1016/S0303-2647(99)00089-1.

[70] Y. Kitadate and S. Yoshida. Regulation of spermatogenic stem cell homeostasis by mitogen competition in an open niche microenvironment. *Genes & Genetic Systems*, 97(1):15–25, Feb. 2022. ISSN 1880-5779. doi: 10.1266/ggs.21-00062. URL http://dx.doi.org/10.1266/ggs.21-00062.

[71] A. M. Klein and B. D. Simons. Universal patterns of stem cell fate in cycling adult tissues. *Development*, 138(15):3103–3111, Aug. 2011. ISSN 0950-1991. doi: 10.1242/dev.060103. URL http://dx.doi.org/10.1242/dev.060103.

[72] A. M. Klein, D. P. Doupé, P. H. Jones, and B. D. Simons. Kinetics of cell division in epidermal maintenance. *Physical Review E*, 76(2), Aug. 2007. ISSN 1550-2376. doi: 10.1103/physreve.76.021910. URL http://dx.doi.org/10.1103/PhysRevE.76.021910.

[73] A. M. Klein, D. P. Doupé, P. H. Jones, and B. D. Simons. Mechanism of murine epidermal maintenance: Cell division and the voter model. *Physical Review E*, 77(3), Mar. 2008. ISSN 1550-2376. doi: 10.1103/physreve.77.031907. URL http://dx.doi.org/10.1103/PhysRevE.77.031907.

[74] Y. Kobayashi, Y. Yasugahira, H. Kitahata, M. Watanabe, K. Natsuga, and M. Nagayama. Interplay between epidermal stem cell dynamics and dermal deformation. *npj Computational Materials*, 4(1):45, Dec. 2018. ISSN 2057-3960. doi: 10.1038/s41524-018-0101-z. URL http://www.nature.com/articles/s41524-018-0101-z.

[75] L. LAJTHA. Stem cell concepts. *Differentiation*, 14(1–3):23–33, Sept. 1979. ISSN 0301-4681. doi: 10.1111/j.1432-0436.1979.tb01007.x. URL http://dx.doi.org/10.1111/j.1432-0436.1979.tb01007.x.

[76] R. M. Lavker and T.-T. Sun. Epidermal stem cells. *Journal of Investigative Dermatology*, 81(1):S121–S127, July 1983. ISSN 0022-202X. doi: 10.1111/1523-1747.ep12540880. URL http://dx.doi.org/10.1111/1523-1747.ep12540880.

[77] M. B. Liu, G. R. Liu, L. W. Zhou, and J. Z. Chang. Dissipative particle dynamics (dpd): An overview and recent developments. *Archives of Computational Methods in Engineering*, 22(4):529–556, July 2014. ISSN 1886-1784. doi: 10.1007/s11831-014-9124-x. URL http://dx.doi.org/10.1007/s11831-014-9124-x.

[78] E. Lorenz, D. Uphoff, T. Reid, and E. Shelton. Modification of irradiation injury in mice and guinea pigs by bone marrow injections. *Journal of the National Cancer Institute*, 12(1):197–201, 1951.

[79] M. C. Marchetti, J. F. Joanny, S. Ramaswamy, T. B. Liverpool, J. Prost, M. Rao, and R. A. Simha. Hydrodynamics of soft active matter. *Reviews of Modern Physics*, 85 (3):1143–1189, July 2013. ISSN 1539-0756. doi: 10.1103/revmodphys.85.1143. URL http://dx.doi.org/10.1103/RevModPhys.85.1143.

[80] A.-K. Marel, N. Podewitz, M. Zorn, J. O. Rädler, and J. Elgeti. Alignment of cell division axes in directed epithelial cell migration. *New Journal of Physics*, 16(11): 115005, Nov. 2014. ISSN 1367-2630. doi: 10.1088/1367-2630/16/11/115005. URL http://dx.doi.org/10.1088/1367-2630/16/11/115005.

[81] F. A. Meineke, C. S. Potten, and M. Loeffler. Cell migration and organization in the intestinal crypt using a lattice-free model. *Cell Proliferation*, 34(4):253–266, Aug. 2001. ISSN 1365-2184. doi: 10.1046/j.0960-7722.2001.00216.x. URL http://dx.doi.org/10.1046/j.0960-7722.2001.00216.x.

[82] F. Montel, M. Delarue, J. Elgeti, L. Malaquin, M. Basan, T. Risler, B. Cabane, D. Vignjevic, J. Prost, G. Cappello, and J.-F. Joanny. Stress clamp experiments on multicellular tumor spheroids. *Physical Review Letters*, 107(18), Oct. 2011. ISSN 1079-7114. doi: 10.1103/physrevlett.107.188102. URL http://dx.doi.org/10.1103/PhysRevLett.107.188102.

[83] F. Montel, M. Delarue, J. Elgeti, D. Vignjevic, G. Cappello, and J. Prost. Isotropic stress reduces cell proliferation in tumor spheroids. *New Journal of Physics*, 14(5): 055008, May 2012. ISSN 1367-2630. doi: 10.1088/1367-2630/14/5/055008. URL http://dx.doi.org/10.1088/1367-2630/14/5/055008.

[84] S. J. Morrison, N. Uchida, and I. L. Weissman. The biology of hematopoietic stem cells. *Annual review of cell and developmental biology*, 11(1):35–71, 1995.

[85] A. Mukherjee, Y. Huang, J. Elgeti, S. Oh, J. G. Abreu, L. Ammar, A. R. Neliat, J. Schüttler, D.-D. Su, C. Dupre, N. C. Benites, X. Liu, L. Peshkin, M. Barboiu, H. Stocker, M. W. Kirschner, and M. Basan. Membrane potential mediates the cellular response to mechanical pressure. *Cell*, 189(1):143–160.e22, Jan. 2026. ISSN 0092-8674. doi: 10.1016/j.cell.2025.11.004. URL http://dx.doi.org/10.1016/j.cell.2025.11.004.

[86] P. J. Myers, S. H. Lee, and M. J. Lazzara. Mechanistic and data-driven models of cell signaling: Tools for fundamental discovery and rational design of therapy. *Current Opinion in Systems Biology*, 28:100349, Dec. 2021. ISSN 2452-3100. doi: 10.1016/j.coisb.2021.05.010. URL http://dx.doi.org/10.1016/j.coisb.2021.05.010.

[87] P. Nikunen, M. Karttunen, and I. Vattulainen. How would you integrate the equations of motion in dissipative particle dynamics simulations? *Computer Physics Communications*, 153(3):407–423, July 2003. ISSN 0010-4655. doi: 10.1016/s0010-4655(03)00202-9. URL http://dx.doi.org/10.1016/S0010-4655(03)00202-9.

[88] S. Orozco-Fuentes and D. Boyer. Order, intermittency, and pressure fluctuations in a system of proliferating rods. *Physical Review E*, 88(1), July 2013. ISSN 1550-2376. doi: 10.1103/physreve.88.012715. URL http://dx.doi.org/10.1103/PhysRevE.88.012715.

[89] N. Podewitz, M. Delarue, and J. Elgeti. Tissue homeostasis: A tensile state. *EPL (Europhysics Letters)*, 109(5):58005, Mar. 2015. ISSN 1286-4854. doi: 10.1209/0295-5075/109/58005. URL http://dx.doi.org/10.1209/0295-5075/109/58005.

[90] N. Podewitz, F. Jülicher, G. Gompper, and J. Elgeti. Interface dynamics of competing tissues. *New Journal of Physics*, 18(8):083020, Aug. 2016. ISSN 1367-2630. doi: 10.1088/1367-2630/18/8/083020. URL http://dx.doi.org/10.1088/1367-2630/18/8/083020.

[91] Y. G. Pollack, P. Bittihn, and R. Golestanian. A competitive advantage through fast dead matter elimination in confined cellular aggregates. *New Journal of Physics*, 24 (7):073003, July 2022. ISSN 1367-2630. doi: 10.1088/1367-2630/ac788e. URL http://dx.doi.org/10.1088/1367-2630/ac788e.

[92] Y. Post and H. Clevers. Defining adult stem cell function at its simplest: The ability to replace lost cells through mitosis. *Cell Stem Cell*, 25(2):174–183, Aug. 2019. ISSN 1934-5909. doi: 10.1016/j.stem.2019.07.002. URL http://dx.doi.org/10.1016/j.stem.2019.07.002.

[93] C. Potten. *Cell Replacement in Epidermis (Keratopoiesis) via Discrete Units of Proliferation*, page 271–318. Elsevier, 1981. ISBN 9780123644695. doi: 10.1016/s0074-7696(08)62326-8. URL http://dx.doi.org/10.1016/s0074-7696(08)62326-8.

[94] C. S. Potten. The epidermal proliferative unit: The possible role of the central basal cell. *Cell Proliferation*, 7(1):77–88, 1974. doi: https://doi.org/10.1111/j.1365-2184.1974.tb00401.x. URL https://onlinelibrary.wiley.com/doi/abs/10.1111/j.1365-2184.1974.tb00401.x.

[95] C. S. Potten. Epidermal cell production rates. *Journal of Investigative Dermatology*, 65(6):488–500, Dec. 1975. ISSN 0022-202X. doi: 10.1111/1523-1747.ep12610194. URL http://dx.doi.org/10.1111/1523-1747.ep12610194.

[96] J. Prost, J.-F. Joanny, and J. M. R. Parrondo. Generalized fluctuation-dissipation theorem for steady-state systems. *Physical Review Letters*, 103(9), Aug. 2009. ISSN 1079-7114. doi: 10.1103/physrevlett.103.090601. URL http://dx.doi.org/10.1103/PhysRevLett.103.090601.

[97] M. Radszuweit, M. Block, J. G. Hengstler, E. Schöll, and D. Drasdo. Comparing the growth kinetics of cell populations in two and three dimensions. *Physical Review E*, 79(5), May 2009. ISSN 1550-2376. doi: 10.1103/physreve.79.051907. URL http://dx.doi.org/10.1103/PhysRevE.79.051907.

[98] S. Ramaswamy. The mechanics and statistics of active matter. *Annual Review of Condensed Matter Physics*, 1(1):323–345, Aug. 2010. ISSN 1947-5462. doi: 10.1146/annurev-conmatphys-070909-104101. URL http://dx.doi.org/10.1146/annurev-conmatphys-070909-104101.

[99] J. Ranft, M. Basan, J. Elgeti, J.-F. Joanny, J. Prost, and F. Jülicher. Fluidization of tissues by cell division and apoptosis. *Proceedings of the National Academy of Sciences*, 107(49):20863–20868, Nov. 2010. ISSN 1091-6490. doi: 10.1073/pnas.1011086107. URL http://dx.doi.org/10.1073/pnas.1011086107.

[100] E. Rangel-Huerta and E. Maldonado. Transit-amplifying cells in the fast lane from stem cells towards differentiation. *Stem Cells International*, 2017(1):7602951, 2017. doi: https://doi.org/10.1155/2017/7602951. URL https://onlinelibrary.wiley.com/doi/abs/10.1155/2017/7602951.

[101] J. Rosenbauer, M. Berghoff, and A. H. Schug. Multiscale tissue modeling reveals impact of cancer treatment to tumor heterogeneity. *Biophysical Journal*, 118(3):348a, Feb. 2020. ISSN 0006-3495. doi: 10.1016/j.bpj.2019.11.2006. URL http://dx.doi.org/10.1016/j.bpj.2019.11.2006.

[102] S. Rulands, F. Lescroart, S. Chabab, C. J. Hindley, N. Prior, M. K. Sznurkowska, M. Huch, A. Philpott, C. Blanpain, and B. D. Simons. Universality of clone dynamics during tissue development. *Nature Physics*, 14(5):469–474, Feb. 2018. ISSN 1745-2481. doi: 10.1038/s41567-018-0055-6. URL http://dx.doi.org/10.1038/s41567-018-0055-6.

[103] T. Savin, N. A. Kurpios, A. E. Shyer, P. Florescu, H. Liang, L. Mahadevan, and C. J. Tabin. On the growth and form of the gut. *Nature*, 476(7358):57–62, Aug. 2011. ISSN 1476-4687. doi: 10.1038/nature10277. URL http://dx.doi.org/10.1038/nature10277.

[104] A. Shirinifard, J. S. Gens, B. L. Zaitlen, N. J. Popławski, M. Swat, and J. A. Glazier. 3d multi-cell simulation of tumor growth and angiogenesis. *PLoS ONE*, 4(10):e7190, Oct. 2009. ISSN 1932-6203. doi: 10.1371/journal.pone.0007190. URL http://dx.doi.org/10.1371/journal.pone.0007190.

[105] B. I. Shraiman. Mechanical feedback as a possible regulator of tissue growth. *Proceedings of the National Academy of Sciences*, 102(9):3318–3323, Feb. 2005. ISSN 1091-6490. doi: 10.1073/pnas.0404782102. URL http://dx.doi.org/10.1073/pnas.0404782102.

[106] A. E. Shyer, T. Tallinen, N. L. Nerurkar, Z. Wei, E. S. Gil, D. L. Kaplan, C. J. Tabin, and L. Mahadevan. Villification: How the gut gets its villi. *Science*, 342(6155):212–218, Oct. 2013. ISSN 1095-9203. doi: 10.1126/science.1238842. URL http://dx.doi.org/10.1126/science.1238842.

[107] A.-S. Smith. Alive and twitching. *Nature Physics*, 12(5):378–379, May 2016. ISSN 1745-2481. doi: 10.1038/nphys3703. URL http://dx.doi.org/10.1038/nphys3703.

[108] D. B. Staple, R. Farhadifar, J. C. Röper, B. Aigouy, S. Eaton, and F. Jülicher. Mechanics and remodelling of cell packings in epithelia. *The European Physical Journal E*, 33(2):117–127, Oct. 2010. ISSN 1292-895X. doi: 10.1140/epje/i2010-10677-0. URL http://dx.doi.org/10.1140/epje/i2010-10677-0.

[109] A. Szabó and R. M. H. Merks. Cellular potts modeling of tumor growth, tumor invasion, and tumor evolution. *Frontiers in Oncology*, 3, 2013. ISSN 2234-943X. doi: 10.3389/fonc.2013.00087. URL http://dx.doi.org/10.3389/fonc.2013.00087.

[110] D. Tartarini and E. Mele. Adult stem cell therapies for wound healing: Biomaterials and computational models. *Frontiers in Bioengineering and Biotechnology*, 3, Jan. 2016. ISSN 2296-4185. doi: 10.3389/fbioe.2015.00206. URL http://dx.doi.org/10.3389/fbioe.2015.00206.

[111] M. te Vrugt and R. Wittkowski. Metareview: a survey of active matter reviews. *The European Physical Journal E*, 48(2–3), Mar. 2025. ISSN 1292-895X. doi: 10.1140/epje/s10189-024-00466-z. URL http://dx.doi.org/10.1140/epje/s10189-024-00466-z.

[112] T. Thenard, A. Catapano, M. Mesnard, and R. Allena. A cellular potts energy-based approach to analyse the influence of the surface topography on single cell motility. *Journal of Theoretical Biology*, 509:110487, Jan. 2021. ISSN 0022-5193. doi: 10.1016/j.jtbi.2020.110487. URL http://dx.doi.org/10.1016/j.jtbi.2020.110487.

[113] H. Tian, B. Biehs, S. Warming, K. G. Leong, L. Rangell, O. D. Klein, and F. J. de Sauvage. A reserve stem cell population in small intestine renders lgr5-positive cells dispensable. *Nature*, 478(7368):255–259, Sept. 2011. ISSN 1476-4687. doi: 10.1038/nature10408. URL http://dx.doi.org/10.1038/nature10408.

[114] X. Trepat, M. R. Wasserman, T. E. Angelini, E. Millet, D. A. Weitz, J. P. Butler, and J. J. Fredberg. Physical forces during collective cell migration. *Nature Physics*, 5(6):426–430, May 2009. ISSN 1745-2481. doi: 10.1038/nphys1269. URL http://dx.doi.org/10.1038/nphys1269.

[115] L. S. Tsimring. Noise in biology. *Reports on Progress in Physics*, 77(2):026601, Jan. 2014. ISSN 1361-6633. doi: 10.1088/0034-4885/77/2/026601. URL http://dx.doi.org/10.1088/0034-4885/77/2/026601.

[116] H. Turlier, D. A. Fedosov, B. Audoly, T. Auth, N. S. Gov, C. Sykes, J.-F. Joanny, G. Gompper, and T. Betz. Equilibrium physics breakdown reveals the active nature of red blood cell flickering. *Nature Physics*, 12(5):513–519, Jan. 2016. ISSN 1745-2481. doi: 10.1038/nphys3621. URL http://dx.doi.org/10.1038/nphys3621.

[117] S. Umar. Intestinal stem cells. *Current Gastroenterology Reports*, 12(5):340–348, Aug. 2010. ISSN 1534-312X. doi: 10.1007/s11894-010-0130-3. URL http://dx.doi.org/10.1007/s11894-010-0130-3.

[118] J. van der Gucht. Grand challenges in soft matter physics. *Frontiers in Physics*, 6, Aug. 2018. ISSN 2296-424X. doi: 10.3389/fphy.2018.00087. URL http://dx.doi.org/10.3389/fphy.2018.00087.

[119] I. M. M. Van Leeuwen, G. R. Mirams, A. Walter, A. Fletcher, P. Murray, J. Osborne, S. Varma, S. J. Young, J. Cooper, B. Doyle, J. Pitt-Francis, L. Momtahan, P. Pathmanathan, J. P. Whiteley, S. J. Chapman, D. J. Gavaghan, O. E. Jensen, J. R. King, P. K. Maini, S. L. Waters, and H. M. Byrne. An integrative computational model for intestinal tissue renewal. *Cell Proliferation*, 42(5):617–636, Aug. 2009. ISSN 1365-2184. doi: 10.1111/j.1365-2184.2009.00627.x. URL http://dx.doi.org/10.1111/j.1365-2184.2009.00627.x.

[120] P. Van Liedekerke, M. Palm, N. Jagiella, and D. Drasdo. Simulating tissue mechanics with agent-based models: concepts, perspectives and some novel results. *Computational Particle Mechanics*, 2(4):401–444, Dec. 2015. ISSN 2196-4386. doi: 10.1007/s40571-015-0082-3. URL http://dx.doi.org/10.1007/s40571-015-0082-3.

[121] G. M. Whitesides and B. Grzybowski. Self-assembly at all scales. *Science*, 295(5564):2418–2421, Mar. 2002. ISSN 1095-9203. doi: 10.1126/science.1070821. URL http://dx.doi.org/10.1126/science.1070821.

[122] S. A. Wickström and C. M. Niessen. Cell adhesion and mechanics as drivers of tissue organization and differentiation: local cues for large scale organization. *Current Opinion in Cell Biology*, 54:89–97, Oct. 2018. ISSN 0955-0674. doi: 10.1016/j.ceb.2018.05.003. URL http://dx.doi.org/10.1016/j.ceb.2018.05.003.

[123] I. M. Wortel, I. Niculescu, P. M. Kolijn, N. S. Gov, R. J. de Boer, and J. Textor. Local actin dynamics couple speed and persistence in a cellular potts model of cell migration. *Biophysical Journal*, 120(13):2609–2622, July 2021. ISSN 0006-3495. doi: 10.1016/j.bpj.2021.04.036. URL http://dx.doi.org/10.1016/j.bpj.2021.04.036.

[124] I. M. N. Wortel and J. Textor. Interpreting t-cell search "strategies" in the light of evolution under constraints. *PLOS Computational Biology*, 19(2):e1010918, Feb. 2023. ISSN 1553-7358. doi: 10.1371/journal.pcbi.1010918. URL http://dx.doi.org/10.1371/journal.pcbi.1010918.

[125] C. Yao and J. Elgeti. Free growth under tension. *SciPost Physics*, 19(4), Oct. 2025. ISSN 2542-4653. doi: 10.21468/scipostphys.19.4.097. URL http://dx.doi.org/10.21468/SciPostPhys.19.4.097.

[126] S. Yoshida. Open niche regulation of mouse spermatogenic stem cells. *Development, Growth & Differentiation*, 60(9):542–552, Dec. 2018. ISSN 0012-1592, 1440-169X. doi: 10.1111/dgd.12574. URL https://onlinelibrary.wiley.com/doi/10.1111/dgd.12574.

2 Mechanically driven stem cell separation via proliferating daughter cells

Abstract

The homeostasis of epithelial tissue relies on a balance between the self-renewal of stem cell populations, cellular differentiation, and loss. Although this balance needs to be tightly regulated to avoid pathologies, such as tumor growth, the regulatory mechanisms, both cell-intrinsic and collective, which ensure tissue steady-state are still poorly understood. Here, we develop a computational model that incorporates basic assumptions of stem cell renewal into distinct populations and mechanical interactions between cells. We find that the model generates unexpected dynamic features: stem cells repel each other in the bulk tissue and are thus found rather isolated, as in a number of in vivo contexts. By mapping the system onto a gas of passive Brownian particles with effective repulsive interactions, that arise from the generated flows of differentiated cells, we show that we can quantitatively describe such stem cell distribution in tissues. The interaction potential between a pair of stem cells decays exponentially with a characteristic length that spans several cell sizes, corresponding to the volume of cells generated per stem cell division. Our findings may help understanding the dynamics of normal and cancerous epithelial tissues.

2.1 Introduction

Tissue renewal through cell division to balance the constant loss of cells is a hallmark of life in multicellular organisms. It is widely accepted that for most tissue types, stem cells (SC) play a key role in this complex process [23, 41]. Stem cells have the potential to proliferate and self renew over long timescales, continuously generating various types of differentiated cells required for physiological tissue function. Such tissue maintenance via small populations of stem cells requires fine-tuned fate choices to ensure not only a constant and well-defined ratio of cellular types, but also stable tissue size and overall cellular numbers.

Equally important, however, is a homogeneous positioning of stem cells across the tissue, such that lost cells can quickly be replenished. If all stem cells were to segregate from progeny, tissue function and maintenance could be compromised. Indeed, in a lattice model without mechanical interactions, proliferating and non-proliferating cells have been shown to require reversible differentiation in a manner dependent on relative local cell numbers to avoid non-homeostatic behavior, such as phase separation of cell types [21]. Other types of fate control that have been recently explored

theoretically and experimentally are an effective fate determinant field of a diffusible chemical. It is homogeneously supplied but consumed by stem cells, thus, providing a biochemical negative-feedback mechanism for stem cell density, which can also reproduce homogeneous distribution of stem cells within the tissue [34].

In recent years, mechanical forces have been shown to be crucial regulators for tissue growth and homeostasis. A key concept is the *homeostatic pressure*, which is the pressure at which cellular division and apoptosis are balanced, under the generic assumption that these processes depend on mechanical forces. Based on this concept, competition between different tissues [5], tissue fluidization [52], negative bulk homeostatic pressure [49], interface dynamics during competition [10, 18, 50], and the evolution of tissue [11] could be explained. However, these studies always considered situations without the possibility of conversion between cellular types and change in self-renewal potential, which is by definition key to understand stem cell dynamics in tissues. This raises the question of whether purely mechanical interactions, which must occur in any confluent tissue with cell renewal and loss, could be a factor in the regulation of stem cell dynamics and positioning.

Here, we study the interaction and distribution of stem cells in self-renewing tissues in the presence of mechanical interactions only. As a minimal hierarchical scheme of tissues with stem and differentiated cells (Fig. 2.1a), we take a classical model [1], where stem cells (SC) asymmetrically divide into a stem and a transient amplifying (TA) cell. The TA cells can undergo a number N_{TA} of symmetric divisions before terminally differentiating into non-proliferative cells (TD). Although this is an oversimplified picture [33], we show that it already gives rise to complex dynamics and provides a computational framework which can be readily generalized to more realistic stochastic models of cell differentiation. For instance effects of the stem cell environment, the so called niche, on fate decisions [27, 38] or self-controlled fate decisions such as in "open niche" [62], where all cells have the same differentiation potential. Implementing the renewal scheme into the two particle growth model [6] (sec. 2.2 and App. 2.B), we find that the resulting tissue is characterized by well separated SCs surrounded by a small cloud of TA cells in a sea of TD cells in two (see Fig. 2.1b), and three dimensions (see sec. 2.6). The cause of the homogeneous distribution of stem cells in the tissue on larger distances lies in the of outflux of cells from the stem cells, and short-range mechanical interactions. Surprisingly, we find that this repulsion and distribution of SC in the tissue can be effectively described by a simple thermodynamic picture with SCs behaving like soft repulsive colloids in a thermal bath. The length scale of the soft repulsive potential is set by the volume of cells generated per stem cell division.

In section 2.3, we first discuss the dynamics of single stem cells to determine the length scale of the interaction, and to study how the cloud of their progeny around them impacts their movements. Subsequently, in section 2.4, we study the dynamics of SC pairs. From their distance distribution function, we infer the amplitude of the effective repulsive potential that is mediated by the outward flow of differentiated cells that they each produce. In section 2.5, we show that the distribution of stem cells in a bulk tissue can be described by this effective pair interaction. In three dimensions,

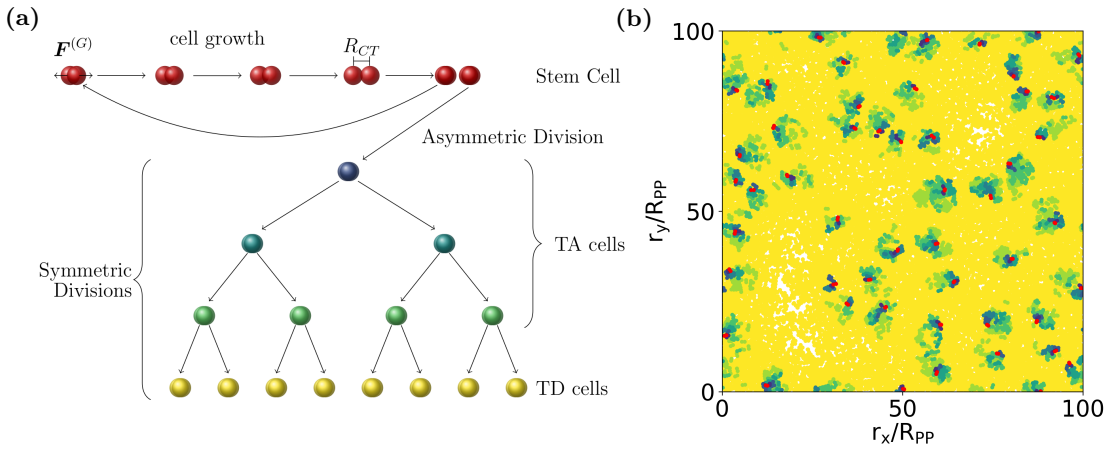

Figure 2.1: Stem cell (SC) division and differentiation scheme leads to well-separated SC arrangement. (a) Schematic illustration of growth, division, and differentiation implemented in the two-particle growth model. SCs grow by an active growth force $F^{(G)}$ and divide when the two particles of a cell are separated by a threshold distance R_{ct}. A SC divides always asymmetrically in one SC daughter and one TA daughter cell. TA cells still grow, but their maximal number of divisions are limited. They always divide symmetrically, and in the final step both daughters are TD cells. TA and TD cells are removed with the same, finite apoptosis rate k_a. (b) In bulk simulations, SCs are distributed all over the tissue, and rarely at close distance. Each SC is surrounded by a halo of TA and TD cells. The main mass is made up by non-growing TD cells. The same color scheme as in Fig. 2.1a is applied with finer gradation for TA cells, which can divide up to five times. The simulation was performed in a squared two-dimensional box with box length 100 R_{PP}. After equilibration, the average cell density is $\rho \sim 1.58/R_{PP}$, and the snapshot was taken after 25 generations.

we find that the repulsive interaction of stem cells is also preserved (see sec. 2.6). Last, we demonstrate independence of the homeostatic pressure controlled division mechanism, by replacing it with a stochastic one, in section2.7. This shows that our results are primarily driven by mechanical interactions and proliferation generated outflow of cells.

2.2 Simulation model

Each cell in the simulation model consists of two particles, which interact via a repulsive force to model growth. When the particle distance reaches a size threshold, a cell divides and two new particles are placed at random at very short distance next to the old ones. Particles of different cells interact via an attractive and a repulsive force, to model adhesion and volume exclusion, respectively. The length R_{PP}, up to which inter-cellular interactions are present, defines the length scale of our model and depicts the cell size. TA and TD cell removal is modeled in a stochastic process with fixed rate k_a, which defines the timescale of the model. Note that the division rate k_d is not fixed and will follow from the other model parameters. Random and dissipative forces are included by dissipative particle thermostat. Together with a

self-consistent velocity Verlet integrator for the Langevin equations, this enables efficient calculations, correctly accounting for the overdamped dynamics required for tissue simulations, as discussed in detail in App. 2.D.3. Cells follow a classical differentiation model [1], see Fig. 2.1a, and have all identical interaction parameters. Solely stem cells do not die ($k_a = 0$), and TD cells do not actively grow ($G = 0$) to prevent divisions. All simulations in this work are initialized with SCs only. More details on the model can be found in App. 2.B and previous works [6, 10, 11, 49, 50].

2.3 Isolated stem cell

To understand the separation of stem cells in bulk tissue, we begin our analysis by studying the dynamics of a single SC and its offspring. We start with an isolated stem cell and shortly thereafter find it surrounded by a cloud of progeny that maintains a certain size throughout the simulation time. (see Fig. 2.2a).

Assuming equal division rates k_d for SC and TA cells and neglecting TA cell loss on average $2^{N_{TA}}$ growing cells are present at a time, with N_{TA} the maximum allowed number of TA cell division cycles. Further, $2^{N_{TA}}$ TD cells are produced in each cycle. Thus, each stem cell division can produce at most $2^{N_{TA}+1}$ progeny. However, due to the stochastic loss rate k_a of TA and TD cells in our model (which can occur either due to apoptosis in monolayers, or out-of-plane delamination in multilayered tissues such as the epidermis) we arrive at a lower effective number $\langle N_p \rangle < 2^{N_{TA}+1}$(see Fig. 2.2c). On average, the stem cell is thus surrounded by a circular arrangement of its offspring, with a characteristic length $L_p = \sqrt{\langle N_p \rangle / \rho\pi}$, where ρ denotes the cell density (see Fig. 2.2d). Note that k_d is not fixed in our simulation model, but controlled by pressure [5, 45, 49]. An increase of TA cell generations can thus decreases the proliferation rate and effective cell number further (see App.2.C Fig. 2.C.1).

However, the average hides an important aspect of the dynamics. While in some instances the SC is indeed in the center of the cell mass, it is also often found at the boundary due to the stochastic nature of the orientation of asymmetric divisions. When the SC is located at the boundary, the divisions of the TA cells result in an effective propulsion of the SC and persistent directed motion (App. 2.D Fig. 2.D.1).

Correspondingly, the mean squared displacement (MSD) of the stem cell shows a regime of active motion up to about the lifetime of one generation, and a regime of activity enhanced long-term diffusion thereafter (see Fig. 2.4a and App. 2.D Fig. 2.D.2). In analogy to active Brownian particles (ABPs) or Run'n'Tumble particles, the MSD of stem cells can be described in terms of a translation diffusion coefficient D_t, a characteristic rotational time τ_R, which confirms decorrelation of the SC motion after about one cell generation, and a propulsion velocity v_0 (see App. 2.D.1). The fitted values for τ_R are about one half to one apoptosis times and correspond to the decorrelation of directed motion. For the propulsion velocity we find a maximum for $N_{TA} = 6$, indicating an optimal population size for sped-up motion.

We quantify the active outbursts of SC motion by the displacement distribution of the stem cell, i. e. the probability that the SC undergoes a given displacement within

a fraction of a generation (*here* $0.2/k_a$ see App. 2.D Fig. 2.D.4a). Heavy tails in the distribution display the persistent motion during outburst. When a stem cell is displaced from the center of mass of the cell population the heaviness of the tail increases strongly (see App. 2.D Fig. 2.D.4b).

2.4 Stem cell interaction

In order to derive an effective pair interaction, we initialize the simulation with two stem cells in a large periodic box. Each stem cell generates its own progeny populations, which form an aggregate via which stem cells effectively repel each other (see Fig. 2.2b). Loss of cells in the region between stem cells can lead to two separate cell populations, both behaving as described in the previous section. In simulations with periodic boundary conditions, they eventually collide again and SC rejection can be observed yet again. We quantify the stem cell repulsion by measuring the pair correlation function

$$g(r) = \left\langle \sum_{m,n\neq m}^{N_{SC}} \Theta_H\left(r - r_{mn}(t_i)\right) \Theta_H\left(r_{mn}(t_i) - (r+\delta r)\right) / \Omega(r) \right\rangle$$

in an annulus ranging from r to $r+\delta r$, where $\Theta_H(x)$ is the Heaviside function and $r_{mn}(t_i) = |\boldsymbol{r}_m(t_i) - \boldsymbol{r}_n(t_i)|$ the stem cell pair distance, measured applying minimum image convention. The average combines data from different times and independent runs to improve statistics and the sum runs over pairs of SC. In order to normalize $g(r)$, and to take into account the radial bin size, we divide by a geometrical scaling constant $\Omega(r) = L_{XY}^2/[4(N_{SC}-1)((r+\delta r)^2 - r^2)]$. The probability to find two SCs at short distances is strongly reduced, and reaches a plateau at larger distances, where the cell clouds are out of contact again (see Fig. 2.2e).

Next we utilize an analogy to thermal equilibrium to derive an effective repulsive pair potential $V(r) = V_0 \exp\{-r/L_{rep}\}$ of very soft colloids. The repulsion length L_{rep} is set to the characteristic length L_p of progeny around the SC. In equilibrium, the pair correlation function follows from Boltzmann statistics

$$G(r) = G_0 \exp\{-\beta V_0 \exp\{-r/L_p\}\}, \tag{2.1}$$

with $\beta = 1/k_B T_{eff}$ and effective temperature T_{eff}. The prefactor G_0 is obtained from the normalization condition $\int G(x)dx = 1$. We determine the effective potential strength βV_0 by fitting $G(r)$ to $g(r)$ and find good agreement of this simple model with our data. Results are shown in Figure 2.2e+2.2f. The decrease of βV_0 with N_{TA} corresponds to a softening of the potential, which could be due to an increasingly asymmetric distribution of TA cells.

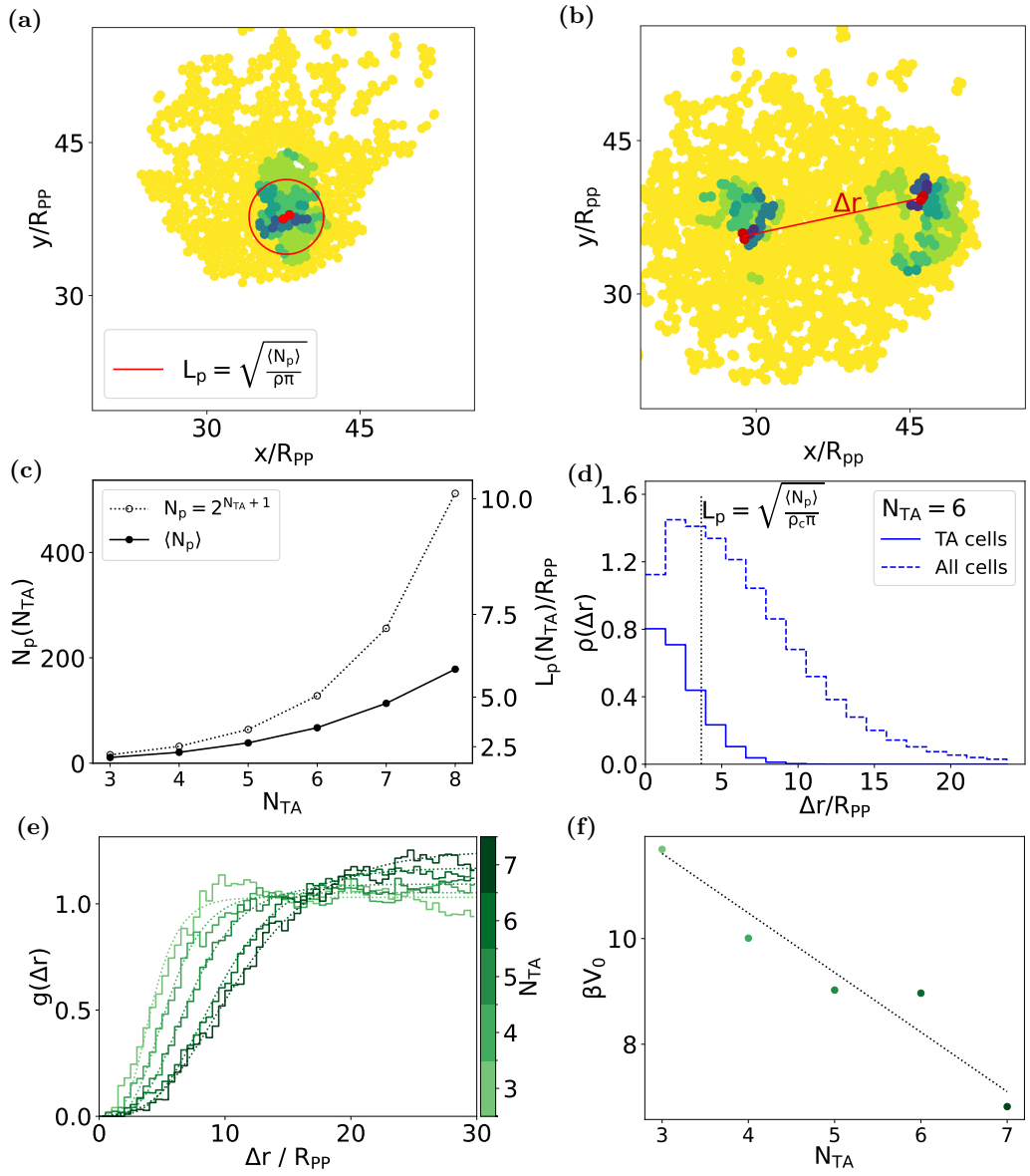

Figure 2.2: Interaction parameter determination. (a) Snapshot of isolated SC and (b) two interacting SCs. (c) Cell number generated in each SC division cycle, i. e. sum of TA cell and latest TD cells, for the upper limit $N_p = 2^{N_{TA}+1}$ (open circles, dotted line) and measured from simulation by averaging over time $\langle N_p \rangle$ (filled circles, solid line) as function of N_{TA}. The latter is used to determine the characteristic progeny distance L_p, which is used on the right y-axis label. (d) Cell density of TA (solid line) and all daughter cells (dashed line) around SC, where L_p derived from average measured progeny number N_p is marked by dotted line, for $N_{TA} = 6$. (e) pair correlation $g(\Delta r)$ as function of SC distance Δr for a pair of SCs. N_{TA} is coded in color. Fit shows interaction via repulsive potential and obtained interaction strength βV_0 is shown in (f) as a function of N_{TA}. Multiple independent long simulation runs of these systems for each N_{TA} are used to determine the interaction parameters. Simulations are initialized from a single SC (a, c, d) and two SCs in contact (b, e, f) and averages are taken in steady state, i. e. after reasonably long time after initialization.

2.5 Confluent tissue maintained by stem cells

We perform tissue simulations for different N_{TA}, and vary the number of stem cells N_{SC} in the simulation such that the average total cell density is approximately the same for different simulations. We compare these tissue simulation with Brownian dynamics (BD) simulations of thermal colloid particles interacting via the proposed effective repulsion. The interaction parameters, obtained in section 2.4, are used without further adaptions. Snapshots for the mechanical model and the thermal colloid model are shown in Figure 2.3a and 2.3b, respectively.

Clearly, SCs are well separated, and homogeneously distributed over the system. To quantify this separation, we measure again the pair correlation function for both systems (see Fig. 2.3c). The pair correlation function reveals a strong depletion of stem cells from the vicinity of another on length scales set by the amount of progenitors they generate. Interestingly, we find that the colloid system (dotted lines) reproduces well the results from the tissue simulations (solid lines) even in confluent tissues. Note that this requires a rather soft colloidal interaction on length scales much larger than the (stem) cell size.

We further quantify the stem cell separation with a cluster analysis. We consider that SCs which are found at a distance smaller than d belong to the same cluster, and calculate the cluster size distribution function $\mathcal{N}(n) = p(n) \cdot n$, where $p(n)$ is the probability of a cluster of n SCs, and average cluster size $\langle n \rangle$. If we take the distance threshold d equal to the cells interaction range R_{pp}, as commonly done for cluster analysis, we identify close to no clusters at all ($\mathcal{N}(n = 2) = 0.024$ and $\mathcal{N}(n = 3) = 0.00014$, for $N_{TA} = 5$). By choosing a larger cutoff $d = 2L_p$ on the basis of their progeny, we find some small clusters, but still not any large clusters (see Fig. 2.3d and App. 2.E Fig. 2.E.2), a feature indicative of SC separation, which is also reproduced in the colloidal systems.

To obtain more insight in the structural dynamics of both systems, we additionally calculate the MSD of SC, and the intermediate scattering function

$$S(q,t) = \left\langle \sum_{m=1}^{N_{SC}} \sum_{n=1}^{N_{SC}} e^{i\boldsymbol{q}\boldsymbol{r}_m(t)} e^{-i\boldsymbol{q}\boldsymbol{r}_n(0)} \right\rangle,$$

where $\langle \cdot \rangle$ denotes a time average and we calculate the over $S(q,t)$ with wave vector $q = |\boldsymbol{q}|$ (see Fig. 2.4b).

The MSD of SCs in tissues shows the same superdiffusive behaviour as found for an isolated SC in free space (see Fig. 2.4a). However, the displacement is reduced in confluent tissue due to the increased cell density. We find, that this affects mainly the translational diffusion coefficient and propulsion velocity, while the reorientation remains in the same order of magnitude as for isolated SC (see App.2.D Fig. 2.D.3). The thermal colloid system on the other hand shows normal diffusion, as should be. Because the Boltzmann description does not provide any timescales, we use the short-term diffusive limit of colloids and SCs in tissues to fix the timescale. The short-term diffusion coefficient can also be calculated from the relaxation of the intermediate

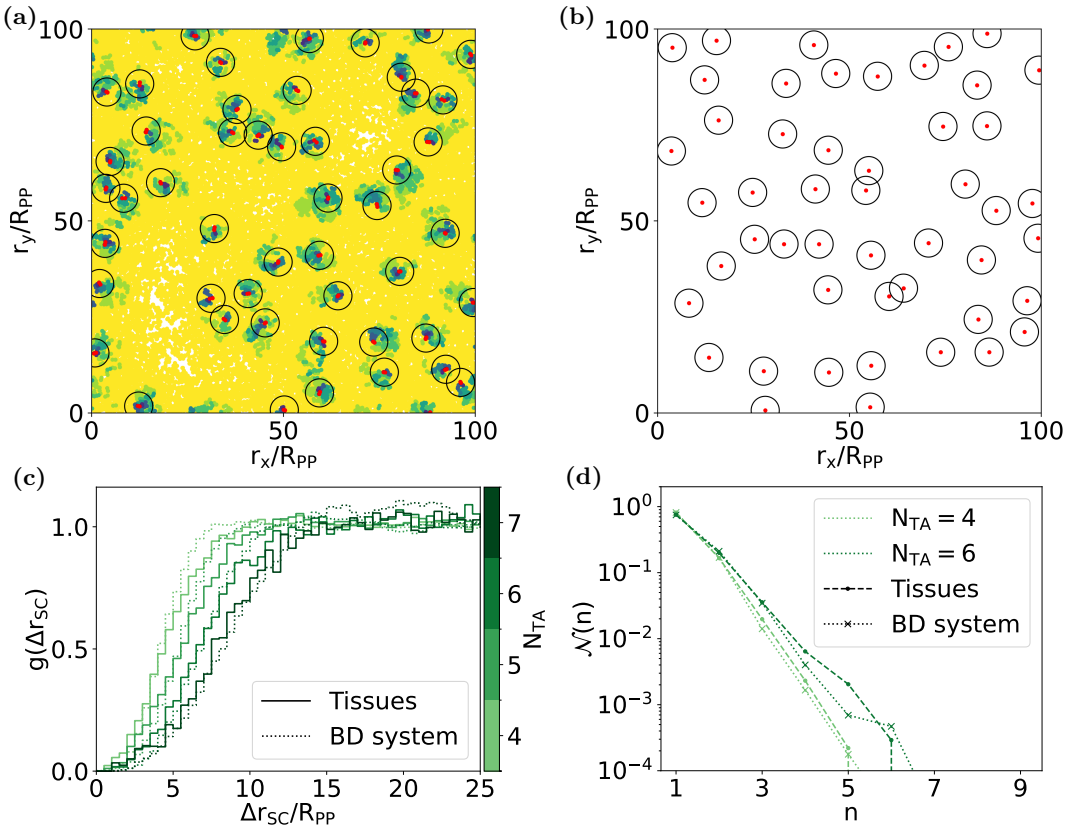

Figure 2.3: SC separation in bulk tissue is explained by equilibrium model with simple repulsive interaction. (a) Snapshot of the tissue simulation for $N_{TA} = 7$ and (b) respective thermal colloid simulation. The characteristic progeny length scale is displayed by circles. (c) The SC and particle pair correlation functions, measured from simulations of the two-particle growth model (solid lines) and thermal colloids, interacting with the assumed repulsive interaction (dotted lines), are shown for color coded N_{TA}. (d) Cluster size distribution function for SCs in tissues (dots, dashed line) and thermal colloids (cross, dotted line) for color coded N_{TA}. Distance threshold for clustering is set to $d = 2L_p$, much larger than the cell size, in order to see any clustering at all. The number of SCs was chosen such that the cell density in all simulations is $\sim 1.58\,\text{cells}/R_{PP}$, and the number of thermal colloids equals the number of SCs. Interaction parameters of colloids were extracted from single and two SC simulations. Note the astonishing agreement between both systems. Simulations are initialized with fixed number of SCs or thermal colloids at regularly spaced distances and averages are taken in steady state, i. e. after reasonably long time after initialization.

scattering function as $D_{eff} = -\log\{S(q,t)/S(q,0)\}/(q^2 t)$ in the short time limit. After aligning the time scale of the thermal colloid system, we find that this effective diffusion is approximately the same for both systems (see App. 2.E Fig. 2.E.3). For large q, D_{eff} is constant, while for small q, finite-size effects of the simulation area come into play.

For zero time lag ($S(q, \Delta t = 0)$), we find a plateau, corresponding to the autocor-

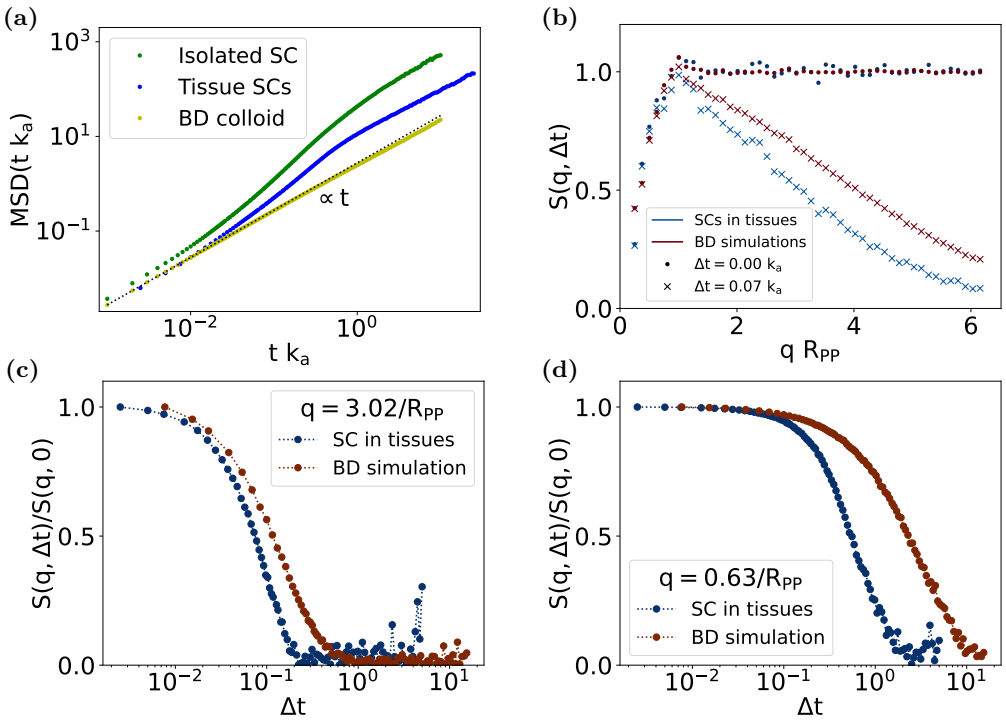

Figure 2.4: Dynamics of SC and BD simulations. (a) Mean squared displacement (MSD) for isolated SC (green) and SCs in tissue (blue), both with $N_{TA} = 4$, and respective thermal colloid system (yellow). In the tissue model, we find superdiffusive SCs. Their displacement gets reduced with increased cell density in confluent tissues. Time scale of thermal colloid system was aligned with the short term diffusion of SC in tissues. (b) Dynamic structure factor (DSF) as function of wavevector for $t = 0$ and $t = 0.07k_a$. Relaxation of the DSF as function of time for (c) small structures ($q = 3.08/R_{PP}$ or $\lambda_q = 2.03R_{PP}$, i. e. twice the cell diameter) and (d) large structures ($q = 0.69/R_{PP}$ or $\lambda_q = 9.11R_{PP}$, i. e. comparable to "weakly" interacting stem cells). Small structures relax at comparable timescale, whereas large structures relax faster in the tissue model due to the superdiffusive behavior of stem cells. Simulations are initialized with fixed number of SCs or thermal colloids at regularly spaced distances and averages are taken in steady state, i. e. after reasonably long time after initialization.

relation term ($n = m$). With a finite time lag, the scattering function starts to decay with q (see Fig. 2.4b for $\Delta t = 0.02k_a$). For tissues and colloids, we show the relaxation of small and large structures in Fig. 2.4c and Fig. 2.4d, respectively. Because we match the timescale of both systems for the short-term diffusion, we find that small structures relax at similar times. Still, SCs in tissue show faster relaxation compared to the BD system. For larger structures (small q), the SCs in tissue relax significantly faster compared to the thermal colloids due to their superdiffusive motion. The enhanced relaxation with increased structure size holds for all q as can be seen from the half life relaxation time (see App. 2.E Fig. 2.E.3).

2.6 Stem cell repulsion in three dimensions

Many biological tissues are not restricted to two dimensions, but extend to the third dimension, which is especially the case in cancer, where cells grow out of plane and form spheroidal tumors. We show that the effect of repulsion by progeny is not limited to two dimensions and can also be found in tissue simulations in three dimensions (see Fig. 2.5). Qualitatively, the pair correlation function shows the same repulsion of SC at a distance corresponding to the volume of their progenitors. Note that here the geometric normalization of the pair correlation function is the volume of a sphere instead of the area of a circle around the stem cell.

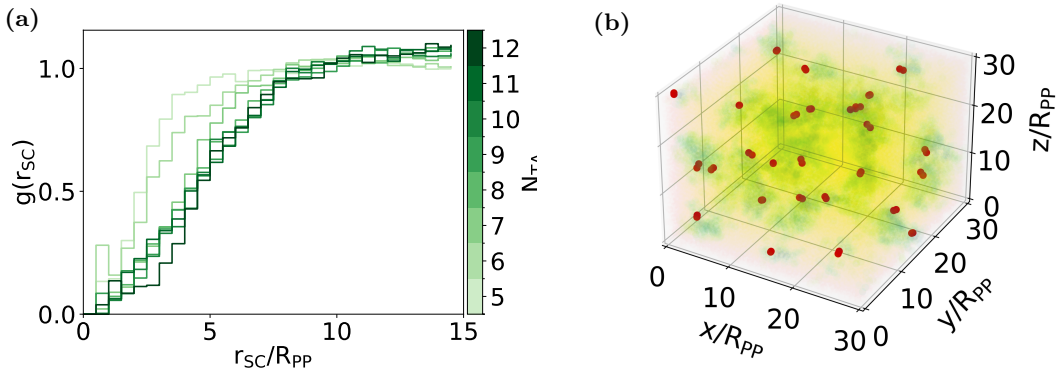

Figure 2.5: Stem Cell repulsion qualitatively remains in three dimensions. (a) Pair correlation function for stem cells in three dimensions shows reduced probability to find SCs at short distances, and plateau at longer distances. (b) Snapshot for a three dimensional tissue with $N_{TA} = 10$ after 50 generations. All simulations are performed with 27 SCs in a cubic box with box length 30 R_{PP}.

2.7 Independence of homeostatic pressure controlled divisions

Stem cells interacting effectively via their (growing) progeny is a robust effect in tissues with mechanical cell-cell interactions. We show this by replacing the division after reaching a size threshold, which introduces a feedback on the homeostatic pressure, by stochastic divisions with fixed rate k_d. This rate is set to the measured division rate in the size threshold division model for an exemplary tissue with $N_{TA} = 6$. Details on the implementation can be found in Appendix 2.F.

The distribution of TA cells around the SC remains almost unchanged (see Fig. 2.6a), thus, also the SC pair correlation function of both models remains the same (see Fig.2.6b). The SC dynamics, measured by the MSD, remains unchanged as well (see App. 2.F Fig. 2.F.2). Thus, the mechanical cell-cell interactions in the model and outflux of cells from the SC are generating an effective SC repulsion, but not the feedback of growth and division on pressure in the tissue.

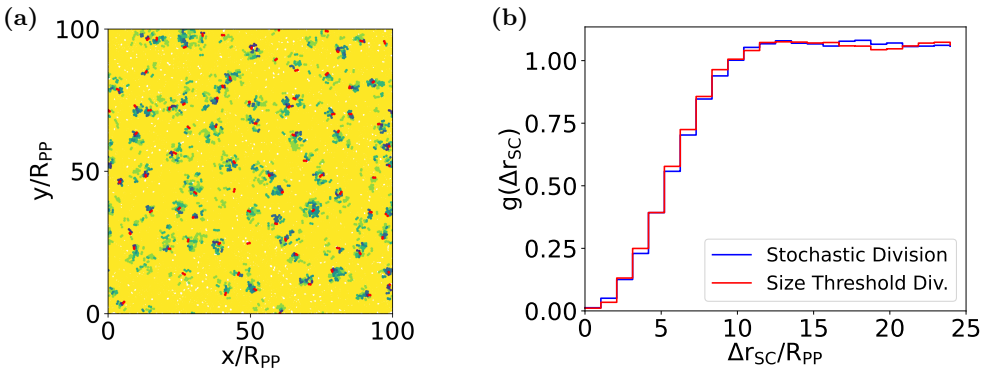

Figure 2.6: Relevance of homeostatic pressure growth control. (a) Snapshot for deterministic TA cell differentiation ($N_{TA} = 6$) in the model with stochastic division mechanism. (b) Pair correlation function for simulation model with division after reaching a size threshold (red) and stochastic divisions (blue).

2.8 Discussion and conclusion

In this work, we have studied the dynamics of stem cells in self-renewing tissues driven by mechanical interactions. Due to the constant outward flow of progeny generated by stem cells, we find that SCs effectively repel each other and spontaneously organize into dispersed structures with a corona of their progeny. This provides an updated and more biophysical view of the classical concept of proliferating units in tissues, in which size and shape of self-renewing domains are flexible, but still organized by stem cells which are robustly present within each unit [56].

Interestingly, we find that the interaction between stem cells can be largely described in a simplified fashion with help of an effective equilibrium approach. The assumption purely repulsive interaction and determination of the interaction length from the spatial requirements for the progeny produced by each stem cell division allows us to characterize SCs like very soft colloids, which interact via this effective repulsive interaction – much larger than the cell size. Further, we have shown that this simplified model reproduces the structural results of the two-particle growth model in confluent tissues. The pair correlation function of the thermal colloids is remarkably similar to that of actively growing cells. The dynamics however are different. We show evidence of an active and persistent self-propulsion force acting on SCs due to the surrounding growing cells. We systematically characterize these, in particular in terms of the statistics and active nature of their persistent random walks. As a result of this proliferation-driven movements, the confluent tissue shows faster relaxation characteristics on long time and length scales. The only detectable difference between the actively growing tissue and the thermal colloid system was found in the dynamic structure factor. It shows a speedup of large structure relaxations in the tissue model due to its active nature, and thus confirms that the active system can be mapped surprisingly well to an thermal equilibrium system.

The derivation of an effective interaction using nearest neighbor distribution func-

tions and mapping it on particle systems may lack sensitivity to certain characteristics of the interaction, especially with increasing density [9, 60]. However, they are still able to capture the main influences of the interaction. Further, replacing the passive Brownian particle system by an active one, is very likely to fail as the continuously decrease of activity enhanced motion cannot be derived from first principles of infinitely diluted systems [14].

Small populations of SCs dispersed within the tissue were also shown to be particularly susceptible to tumor formation in mouse epidermis [57] as well as to have large contribution upon wound healing [3], which could also be investigated via our simulation framework. Furthermore, spermatogenic stem cells are also found to be well separated in the planar basal layer in mouse testis, and show a striking similarity to the stem cell arrangement found in our simulations [25]. Other models of the formation of epithelial protrusions and location of stem cells on the tips of these have been studied previously using a particle-based model [35]. By adding substrate deformability and cell type dependent adhesion forces, the model displayed a stable stratified epithelium with stem cells located at protrusions. It will be interesting to combine these models.

The homogeneous distribution of stem cells arising from our purely mechanical feedback model may complement previous studies [21, 34], in which this was achieved with help of a reversible differentiation scheme or biochemical feedback mechanisms based on diffusible signals. However, in reality, a combination of several of these mechanisms will likely be relevant, also depending on the tissue type. In particular, stochastic cell fate models may be of great interest in the future and could facilitate the description of the plasticity of cells during tissue repair [51, 59]. Also, there exists evidence that more than one SC type maintains some tissues [20, 43] or that cell fates are reversible processes [21, 37], which could be readily integrated in our simulation framework. In the presence of local niches, it has also been shown that the ratio of proliferation to random cell movements determines the effective number of stem cells via a mechanism of stochastic competition for space, although this has not been modeled via explicit mechanical simulations [4, 13]. Until now, the vanishing apoptosis rate of SCs and restriction to only asymmetric SC divisions in our model are limiting factors. Allowing for SC apoptosis, or other processes which reduce the SC number, requires symmetric duplication to balance the SC loss to retain their unique identity in the lineage architecture [22]. Furthermore, it would be interesting to see if a purely mechanical model is able to capture the alternation from a quiescent long-lived SC to produce rapidly dividing short-lived progeny during wound repair [31, 32, 47].

In this work, we find surprising motility of cells emerging from the interaction of cells with each other. While epithelial cells are generally not motile, motility occurs after epithelial-mesenchymal transformation (EMT) [26], or in some cell lines, in particular MDCK. Active cell migration has been the subject of related work [7, 19, 42] and recent findings show that active cell migration does play a role in tissue renewal [36], thus, displaying a promising extension of our work in future studies.

Many aspects of growing tissues have not been addressed in this work. In particular we did not address the role of boundaries and interfaces. Especially in competition

setups [10, 11, 18, 50, 61] the interface plays a dominant role over the resulting structure. Similarly, three dimensional cell culture is often performed in tissue spheroids, where growth at the surface stabilizes the internal tissue [15, 45, 46, 49] and the dynamics can drive phase separation [53, 54]. A second aspect not addressed here is the rheology or flow response of the tissue. "Analogies between growing dense active matter and soft driven glasses" [58] have been discussed a lot in the literature. In particular, if tissues are generically liquid-like due to cell turnover [44, 52], and if cell density [2], cell shape [8], or cell-cell adhesion [19] drive a glass like transition on timescales short compared to cell turnover. For a review of further unique properties of self replicating systems like injection of degrees of freedom or giant fluctuations see [24].

Finally, our results might contribute to a better understanding of the growth and dynamics of cancer. In the cancer stem cell (CSC) hypothesis, it is assumed that malignant tissue follows the same underlying stem cell dynamics. Therapies, which target fast growing tissue, fail, since the stem cells evade. A better understanding of the dynamics of CSCs could improve their detection and the design of therapies. Our results would suggest, that CSCs are isolated and well spread throughout the tumor. To further tackle these questions, it will be necessary to combine our model, with models of cellular competition [5, 11, 18, 49, 50], and taking the cell cycle explicitly into account might be essential [39, 40]

Acknowledgements

Funding information JE and JK gratefully acknowledge financial support from the Initiative and Networking Fund (IVF) via the grant number ERC-RA-004. Simulations were performed with computing resources granted by RWTH Aachen University under project 'rwth0475'.

Data accessibility Source code, simulation data, and analysis scripts is made publicly available on zenodo.org (`https://doi.org/10.5281/zenodo.8410956`).

Supplementary Information - Chapter 2

2.A Supplementary animations of tissue simulations

Supplementary animations of tissue simulations can be found next to the source code, simulation data, and analysis scripts on *zenodo.org* (`10.5281/zenodo.8410957`). Uploaded animations are:

- *S1 Video* **Confluent tissue.** Animation of confluent tissue shown in Fig. 2.1b.
- *S2 Video* **Isolated stem cell.** Animation of isolated SC performing random walk with long persistent segments (see Fig. 2.2a and sec. 2.D).
- *S3 Video* **Stem cell interaction.** Animation of two SCs interacting with each other via their progeny (see Fig. 2.2b).
- *S4 Video* **Interaction in Tissue and BD simulations.** Animation of confluent tissue and thermal colloids (see Fig. 2.3a and Fig. 2.3b).

2.B Simulation model

The described SC model is implemented in the two-particle growth (2PG) model of Refs. [6, 49] and has been adapted in Refs. [10, 11, 18].

Each cell is described by two particles, which repel each other via an active growth force

$$F_{ij}^{(G)} = \frac{G}{(r_{ij} - r_0)^2} \hat{\boldsymbol{r}}_{ij} \tag{2.2}$$

with unit vector $\hat{\boldsymbol{r}}_{ij}$, distance r_{ij} between the two particles, a constant r_0, and growth strength G. For non-growing cells, like TD cells, the growth strength is set to zero, $G_{TD} = 0$, and for the sake of simplicity SC and TA cells have the same growth force, $G_{SC} = G_{TA}$.

To prevent overlap of cells, particles of different cells interact via a soft repulsive volume-exclusion force

$$\boldsymbol{F}_{ik}^{(V)} = f_0 \left(\frac{R_{PP}^5}{r_{ik}^5} - 1 \right) \hat{\boldsymbol{r}}_{ij}, \text{ for } r_{ik} < R_{PP} \tag{2.3}$$

with exclusion strength f_0 and interaction length R_{PP}, which sets the length scale of our simulations. Further, cells in contact interact via an attractive adhesion force of the form

$$\boldsymbol{F}_{ik}^{(V)} = -f_1 \hat{\boldsymbol{r}}_{ik}, \text{ for } r_{ik} < R_{PP} \tag{2.4}$$

with adhesion strength f_1.

We employ a dissipative particle dynamics-type thermostat [28], with an effective temperature T, to account for energy dissipation

$$F_{ij}^{(D)} = \gamma \cdot \left(1 - \frac{dr}{rt}\right)^2 \cdot (\boldsymbol{v}_{ij} \cdot \hat{\boldsymbol{r}}_{ij})\, \hat{\boldsymbol{r}}_{ij} \tag{2.5}$$

and random fluctuations

$$F_{ij}^{(R)} = \sigma\xi \cdot \hat{\boldsymbol{r}}_{ij} \tag{2.6}$$

where γ and σ are related to fulfill the fluctuation-dissipation theorem [17]. Also, background dissipation is taken into account as

$$\boldsymbol{F}_i^B = -\gamma_b \boldsymbol{v}_i. \tag{2.7}$$

A self-consistent velocity-Verlet algorithm [48] is implemented to integrate the equations of motion, and all simulations were performed with periodic boundary conditions.

Cell division is performed, when the two particles of one cell are separated by a critical threshold R_{ct}. A new particle is randomly placed near each original particle in a distance R_d, and the two new particle pairs form the two daughter cells. Differentiation is implemented at the time of division as described above, and the number of divisions of TA cells is tracked by an internal variable. No mechanism is implemented to prevent (non-growing) TD cells from separating. However, we observe only a marginal number of TD cell divisions in simulations of isolated SCs and SC pairs in free space, and none for confluent tissues. The TD cell size in confluent tissues is always far below the division threshold (see Fig.2.F.1), but slightly increases with distance, which is found more pronounced for TD cells generated by SCs in free space (data not shown).

TA and TD cells are stochastically removed from the simulation with a finite apoptosis rate k_a. For simplicity, the same rate is chosen for different cell types. Time is measured in terms of the inverse apoptosis rate, and referred to as "generation".

The standard parameter set for our simulations are given in Tab. 2.B.1. However, not all of these simulation parameters, have a direct conversion to physical units. As discussed in [6] one has to chose well defined measurable quantities, such as apoptosis rate and range of the pair potential as rescaling units for inverse time and particle diameter, to allow for conversion to physical units and comparison with experiments.

As the number of stem cells in our simulation is fixed by only allowing for asymmetric divisions and no apoptosis, we initialize all simulations with the required number of stem cells, placed at regular distances within the unit box with periodic boundary conditions.

Table 2.B.1: Simulation parameters of the standard tissue.

Parameter	Symbol	Value
Time step	Δt	0.001
Pair potential interaction range	R_{PP}	1
Cell expansion constant	r_0	1
Division distance threshold	R_{ct}	0.8
New cell particle initial distance	R_d	10^{-5}
Growth-force strength	G	50
Mass	m	1
Intra-cell dissipation coefficient	γ_c	100
Inter-cell dissipation coefficient	γ_t	50
Background dissipation coefficient	γ_c	0.1
Apoptosis rate	k_a	0.01
Noise intensity	k_BT	0.1
Repulsive cell-cell potential coefficient	f_0	2.39566
Attractive cell-cell potential coefficient	f_1	3.0

2.C Division rate of isolated SC

Assuming equal division rates k_d for all types of proliferating cells, we can derive an average cell number from number balance for each cell type

$$\begin{aligned} n_{SC} &= \langle n_{SC} \rangle = const. \\ \langle n_i \rangle &= 2^{i-1} \left(\frac{k_d}{k_d + k_a} \right)^i n_{SC} \\ \langle n_{TD} \rangle &= \left(\frac{2k_d}{k_d + k_a} \right)^{N_{TA}} \frac{k_d}{k_a} n_{SC}, \end{aligned} \tag{2.8}$$

where i denotes the TA cell cycle. k_d is obtained from fitting these equations to the cell numbers obtained from simulations of isolated SCs. With increasing N_{TA}, the division rate decreases (see Fig. 2.C.1).

2.D Stem cell motion

Here, we give some additional insight in the SC motion of isolated SCs and SCs in tissues, which are also discussed in the main text.

An exemplary single stem cell snapshot for $N_{TA} = 4$ is shown, where the SC trajectory over ten generations illustrates the motion of the SC, and accompanied The full trajectory of the SC and center of mass of the respective single stem cell simulation along both directions of the simulation plane (see Fig. 2.D.1).

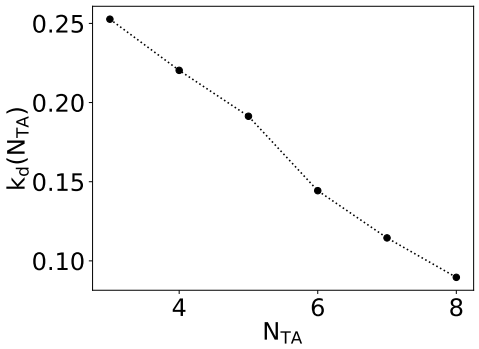

Figure 2.C.1: Division rate k_d as function of N_{TA} for proliferating cells in isolated SC simulations.

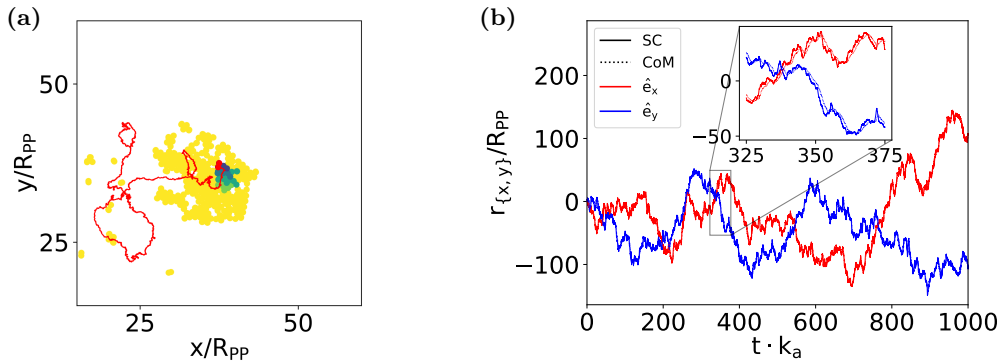

Figure 2.D.1: (a) Snapshot of cell population generated by a single SC with trajectory of SC over the ten cell generations (red line). (b) Trajectory of isolated SC (solid line) and center of mass (CoM) of cell population (dotted line) along $\hat{e}_x$ (red) and $\hat{e}_y$ (blue). Inset shows time close-up to highlight how the center of mass follows the stem cell motion. Both, SC and CoM trajectory perform a random walk with surprisingly long persistent segments, a reminiscent of Run'n'Tumble-like motion. Simulation with $N_{TA} = 4$ is shown.

2.D.1 Mean squared displacement of isolated stem cells and stem cells in tissues

For active Brownian particles (ABPs) in two-dimensions the mean squared displacement MSD is given as [16, 29]

$$MSD = 4\ D_t \Delta t + \frac{v_0^2 \tau_R^2}{2} \left[\frac{2\Delta t}{\tau_R} + e^{-2\Delta t/\tau_R} - 1 \right], \tag{2.9}$$

with translational diffusion coefficient D_t, characteristic time scale for rotational diffusion τ_R, and propulsion velocity v_0. In the short-time limit $dt \ll \tau_R$ the effective diffusion is given by $MSD_{dt \ll \tau_R} \approx 4 D_t dt$. For long-time diffusion the effective diffusion is enhanced and the MSD found to be $MSD \approx (4D_t + v_0^2 \tau_R)\ dt$, again linear in time. Between these two regimes, ballistic motion is observed, and non-linear terms

enters the MSD, $MSD \approx 4D_t dt + v_0^2 dt^2$.

In the tissue simulations, the stem cells are not ABPs, but move actively due to propulsion by progeny. However, we can quantify the dynamics of the stem cell motion in terms of D_t, τ_R, and v_0 to gain a deeper understanding. Also different models of self-propelling particles, like ABPs and Run'n'Tumble particles have been shown to be equivalent on larger scales [12, 55], so that we can describe them using the same theory, without making strong assumptions on the underlying propulsion mechanisms.

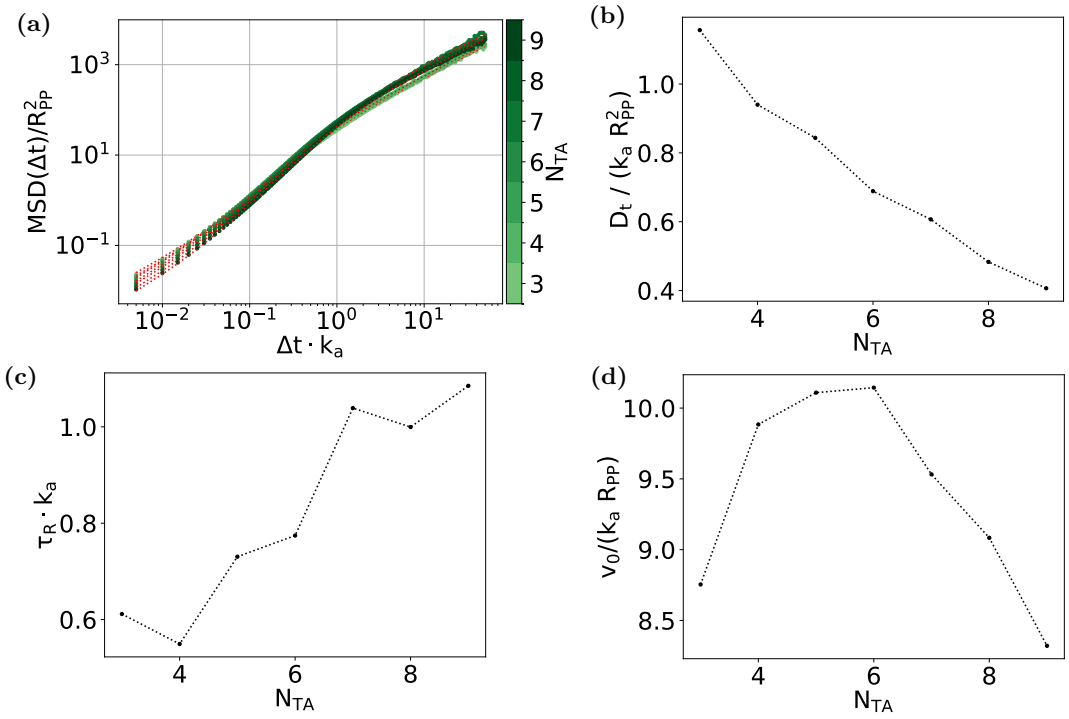

Figure 2.D.2: (a) Mean squared displacement for isolated SCs with different N_{TA} (color coded) and fit of ABP model (red dotted lines). (b) Translational diffusion coefficient D_t, (c) characteristic rotational diffusion time τ_R, and (d) propulsion velocity v_0 obtained from fit function in (a).

From the MSDs for simulations of SCs with varying number of TA cell cycles N_{TA} (see Fig. 2.D.2), one can see that the displacement does vary little with a change of N_{TA}. In particular the short-time diffusion decreases with N_{TA}, which could be due to blocking of cell motion at higher density. This resembles the decrease of the translational diffusion coefficient D_t with N_{TA}. The long-time diffusion first increases with N_{TA}, but then starts to decrease again. Possibly, in increasing number of TA cells around the stem cell initially increases the propulsion force on the stem cell, but saturates at higher number of progeny, which form a more dense halo around the stem cell for more TA cell cycles. The non-monotonic fit parameter for the self propulsion velocity, with maximum at $N_{TA} = 6$, and increasing characteristic rotational diffusion time τ_R show, that the decrease in propulsion velocity does cause the effective decrease

of the long-time diffusion with $N_{TA} > 6$. The characteristic rotational diffusion time τ_R is found to be in the range from half to more than one apoptosis time, which corresponds to a loss of orientation after times larger than one cell generation.

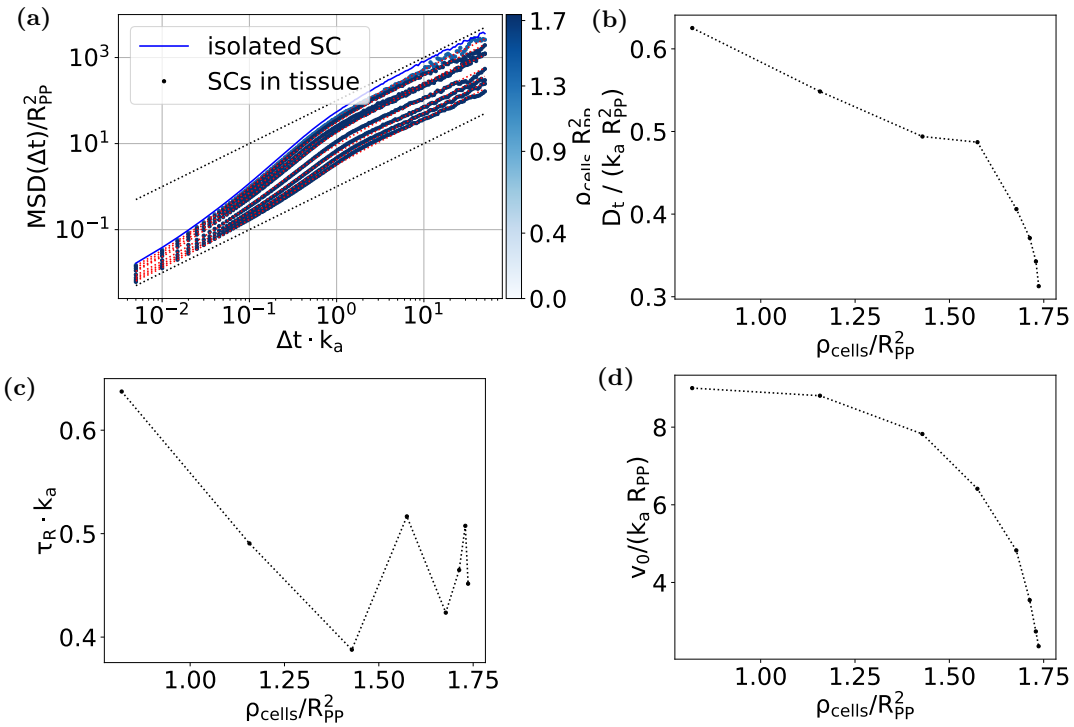

Figure 2.D.3: (a) Mean squared displacement for SCs in tissue with different cell density (color coded) controlled by the stem cell number, with $N_{TA} = 6$. (b) Translational diffusion coefficient D_t, (c) characteristic rotational diffusion time τ_R, and (d) propulsion velocity v_0 obtained from fit function in (a).

In tissues, we still can apply the MSD theory to fit to the SC displacement (see Fig. 2.D.3). With increasing cell density, controlled by an increase in SC numbers, we find that the translational diffusion coefficient D_t and propulsion velocity v_0 decrease, and the SC motion freezes out. The rotational diffusion time is not as strongly effected by the cell density, and approximately half the value compared to the case of an isolated SC, since it is mainly affected by the apoptosis rate.

2.D.2 Displacement distribution

To quantify the persistent motion further, we calculate the displacement distribution function and find heavy tails. The heaviness of the tails increases, when the SC is located further away from the center of mass in the boundary region of the cell population (see Fig. 2.D.4).

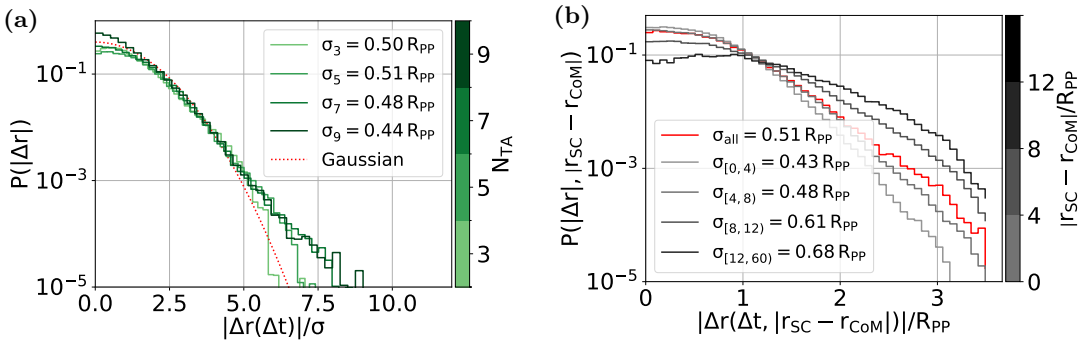

Figure 2.D.4: (a) Displacement distribution for an isolated stem cell with different N_{TA} (green color gradient) over normalized displacement. Red dotted line displays normal displacement (Gaussian). Heavy tails emerge from long consistent segments of random walk. (b) Displacement distribution as in (a) for isolated SC with $N_{TA} = 5$, where color gradient (grey) encodes SC-to-CoM distance. With increasing distance heaviness of tails increases. All displacements are calculated for a time step of $\Delta t\ k_a = 0.2$ generations, combining data of multiple long simulation runs.

2.D.3 Overdamped dynamics

The applied self-consistent velocity Verlet integration of the Langevin equations allows for large integration time steps and therefore provides significant faster computations [30]. Effectively, using a finite mass and velocity Verlet integration corresponds to using a higher order integrator with a physically interpretable control parameter, the mass of cells. However, care has to be taken to reproduce overdamped dynamics, which is achieved by setting mass and friction coefficients such that the viscous relaxation time is much shorter than all other relevant timescales, i. e. that viscous drag dominates over inertia even at short timescales. Because inertial effects scale with the mass of the particles, correct reproduction of overdamped dynamics can be verified by showing independence of the results on mass. As an example, we measured the self propulsion of a single stem cell over two orders of magnitude in mass (see Fig. 2.D.5). The results are virtually indistinguishable, confirming correct reproduction of overdamped dynamics .

2.E Additional results for simulations of stem cells in tissues

2.E.1 Cell densities in confluent tissues

In confluent tissue simulations, we chose the SC number and N_{TA} such that an uninterrupted tissue evolves. Still, the TD cell density around SCs remains very similar to the case of isolated SCs. The TD cells are located closer to the SCs and form a more dense conglomerate. Exemplary cell densities for $N_{TA} = 6$ are shown in Fig. 2.E.1a.

The total cell density of tissues with different N_{TA} is controlled by the number of SCs in the simulation, and chosen such that they are all very similar (see Fig. 2.E.1b).

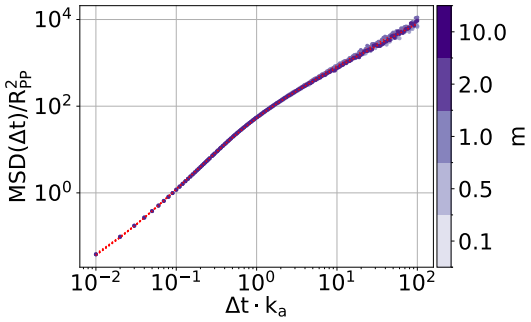

Figure 2.D.5: Mean squared displacement for isolated SCs for simulations with different cell masses m (purple color gradient). All simulations are performed with $N_{TA} = 6$.

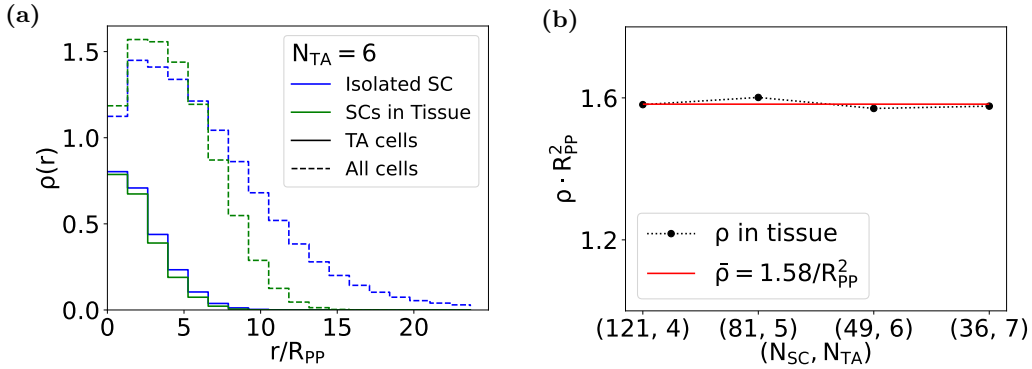

Figure 2.E.1: (a) Cell density of TA (solid line) and all (dashed line) cells around the SC for simulations of an isolated SC (blue) and SCs in tissue (green). In tissue, distance is measured to the closest SC. (b) Average cell density of tissue simulations as function of N_{SC}, the fixed number of SC, N_{TA} obtained from average cell number over box area.

2.E.2 Cluster analysis

To quantify the clustering of SCs in tissues, we calculate the cluster size distribution function is given by

$$\mathcal{N}(n) = \frac{1}{N_{SC}} n\ p(n) \tag{2.10}$$

and represents the fraction of SCs belonging to a cluster of size n, where $p(n)$ is the number of clusters of size n. The distribution is normalized such that $\sum_{i=1}^{N_SC} = 1$. The average cluster size is given as

$$\langle n \rangle = \frac{\sum_n np(n)}{\sum_n p(n)} \tag{2.11}$$

Cells in a distance less than the characteristic TA cell distance estimated from cell numbers belong to the same cluster. Results are shown in Fig. 2.E.2.

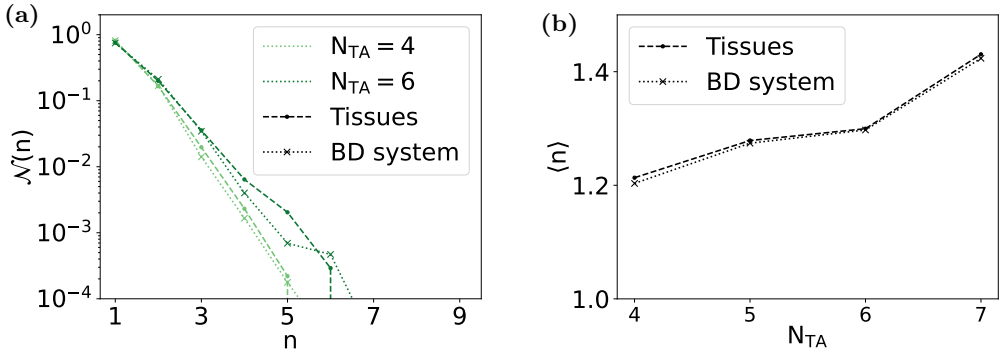

Figure 2.E.2: (a) Same as Fig. 2.3d (b) Average cluster size as function of N_{TA} remains clearly below two SC.

2.E.3 Effective diffusion coefficient and relaxation

The timescale for the thermal colloid simulation in the main text was adjusted by matching the short term diffusion obtained from the MSD of SCs in the tissue simulations. Here, we calculate the effective diffusion coefficient D_{eff} from the intermediate structure factor. For the relaxation of structures it holds

$$\frac{S(q,\Delta t)}{S(q,0)} = e^{-D_{eff}(q)\ \Delta t\ q^2 \Delta t}, \tag{2.12}$$

which yields

$$D_{eff}(q) = \log\left\{\frac{S(q,\Delta t)}{S(q,0)}\right\}/(q^2\Delta t). \tag{2.13}$$

Now, we can measure the effective diffusion for short time lags (here: $0.02k_a$) and see that both models show the same short term diffusivity, as should be (see Fig. 2.E.3a).

The relaxation of structures is obtained from the half-life relaxation time of $S(q,t)/S(q,0)$. We find that this time decreases with q, which means that smaller structures relax faster. Further, in the tissue model structures relax faster than in the thermal colloid system and the relaxation speeds up with structure size (see Fig. 2.E.3b).

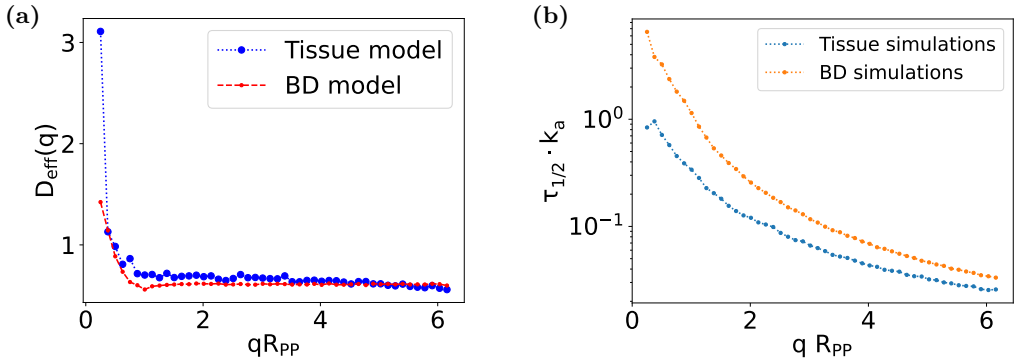

Figure 2.E.3: (a) Effective diffusion coefficient D_{eff} measured from structure factor relaxation for $\Delta t = 0.2k_a$. (b) Relaxation half life time as function of q.

2.F Stochastic division rate model

The observed separation of stem cell in tissues is a generic effect arising from short range mechanical interactions between pairs of cells. To highlight this, we replace the size-threshold division (STD) mechanism by a stochastic division with fixed rate $\tilde{k}_d$ (SDR). This turns off the homeostatic pressure control on divisions. We determine the simulation parameter $\tilde{k}_d$ for the SDR model from measurements of k_d in the STD model. Only the case of tissues with $N_{TA} = 5$ is examined.

To implement, that cells do not divide at too small size and cause computational flaws, we replace the growth force by a damped harmonic oscillator

$$\boldsymbol{F}_{i,j}^{Gharm.} = -k\boldsymbol{x} - \gamma_k \dot{\boldsymbol{x}}, \tag{2.14}$$

where $k = 100$ is the spring constant, and $\gamma_k = 20$ the damping coefficient, chosen in a way to realize critical damping with relaxation time faster than the average division time. The deflection $\boldsymbol{x} = (|\boldsymbol{r}_i - \boldsymbol{r}_j| - R_{rest})\,\hat{\boldsymbol{e}}_{ij}$ is given by the difference between cell size and rest length R_{rest}. We set the rest length of proliferating cells, i.e. SC and TA cells, to $R_{rest}^{SC,TA} = R_{ct} = 0.8R_{PP}$ and for TD cells to $R_{rest}^{TD} = 0.1R_{PP}$.

Despite the fact that we tune the oscillator such that cells grow quickly to a adequate size, some cells divide at very small size and cause computational chaos. To prevent this, we introduce a minimum division size, much smaller than the division size threshold used previously. With $R_{min} = 0.15R_{PP}$ we can ensure stable behavior of the computational model after division.

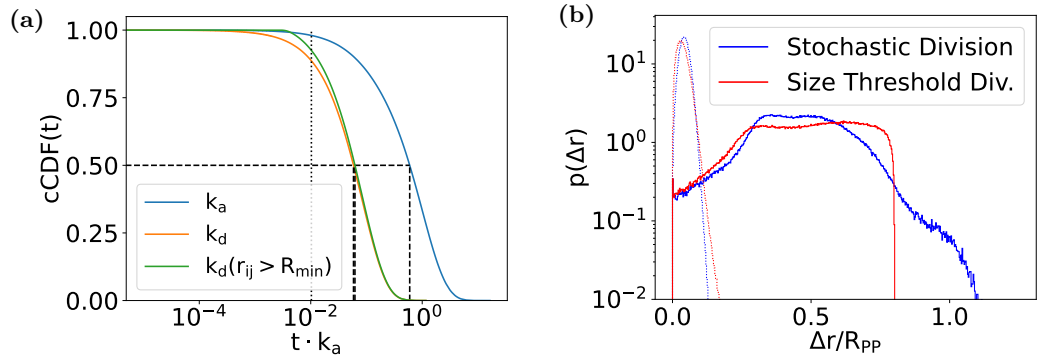

Figure 2.F.1: (a) Complementary cumulative distribution function (cCDF) for apoptosis (blue), division events including prevented divisions due to small size (orange), and performed divisions (green). Black dotted line highlights longest time for a prevented division event. Black dashed lines display median of each cCDF. (b) Cell size distribution for proliferating (SC and TA cells, solid line) and TD cells (dotted lines) in the stochastic division model (blue) and for size threshold divisions (red).

Figure 2.F.1a displays the complementary cumulative distribution function (cCDF) of apoptosis, division, and non-permitted division events, i.e. division events at too small cell size. Only a small fraction of events at very short times is permitted and thus, we sufficiently removed the size-threshold division mechanism. Further, the cell size distribution (see Fig. 2.F.1b) shows, that TD cells in both models match

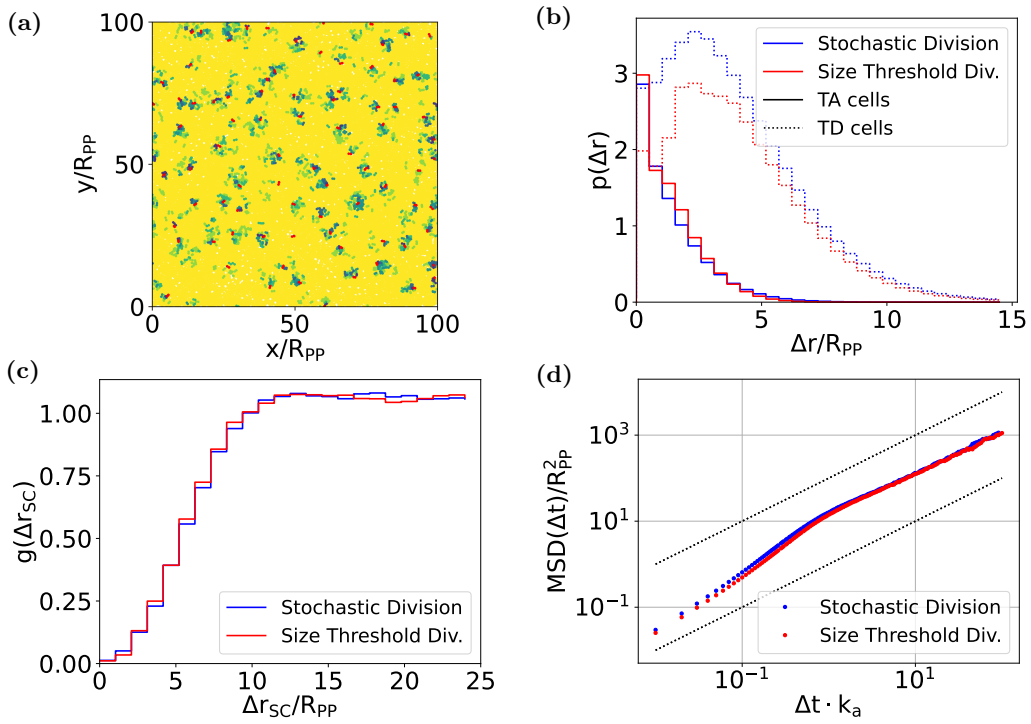

Figure 2.F.2: (a) Snapshot for stochastic division model, (b) TA and TD cell distribution around nearest neighbor SC in tissue, (c) pair correlation function, and (d) Mean squared displacement for the respective models. For comparison, stochastic division model is shown by blue lines together with results for model with size threshold division for $N_{TA} = 5$.

each other well, and for growing cells, we find that the hard division size threshold changes to a blurred tail. The stochastic division model has equal number of TA cells, both in total and for each generation, and did produce only slightly more TD cells. However, cell numbers fluctuate more, which can be to the detriment of stable tissue homeostasis.

When comparing both models, we find that SCs are still surrounded by their TA cell cloud. In the stochastic division model the TA cell arrangement around the stem cells looks more fringed compared to the deterministic model but no large differences can be found in the measured TA cell distribution (see Fig. 2.F.2a, 2.F.2b). Still, for both models, the pair correlation function agree very well (see Fig. 2.F.2c) and the activity of SC in the tissue remains almost unchanged (see Fig. 2.F.2d).

We conclude that the results discussed in the main text are not a consequence of homeostatic pressure growth control, but result from the constant cell outflux generated by the SC. Yet, the pressure feedback on divisions is beneficial to balance cell numbers in the tissue to ensure homeostasis.

References

[1] B. Alberts, A. Johnson, J. Lewis, M. Raff, K. Roberts, and P. Walter. Epidermis and Its Renewal by Stem Cells. *Molecular Biology of the Cell. 4th edition*, 2002. URL https://www.ncbi.nlm.nih.gov/books/NBK26865/. Publisher: Garland Science.

[2] T. E. Angelini, E. Hannezo, X. Trepat, M. Marquez, J. J. Fredberg, and D. A. Weitz. Glass-like dynamics of collective cell migration. *Proceedings of the National Academy of Sciences*, 108(12):4714–4719, Feb. 2011. ISSN 1091-6490. doi: 10.1073/pnas.1010059108. URL http://dx.doi.org/10.1073/pnas.1010059108.

[3] M. Aragona, S. Dekoninck, S. Rulands, S. Lenglez, G. Mascré, B. D. Simons, and C. Blanpain. Defining stem cell dynamics and migration during wound healing in mouse skin epidermis. *Nature Communications*, 8(1):14684, Apr. 2017. ISSN 2041-1723. doi: 10.1038/ncomms14684. URL http://www.nature.com/articles/ncomms14684.

[4] M. Azkanaz, B. Corominas-Murtra, S. I. J. Ellenbroek, L. Bruens, A. T. Webb, D. Laskaris, K. C. Oost, S. J. A. Lafirenze, K. Annusver, H. A. Messal, S. Iqbal, D. J. Flanagan, D. J. Huels, F. Rojas-Rodríguez, M. Vizoso, M. Kasper, O. J. Sansom, H. J. Snippert, P. Liberali, B. D. Simons, P. Katajisto, E. Hannezo, and J. van Rheenen. Retrograde movements determine effective stem cell numbers in the intestine. *Nature*, 607(7919):548–554, July 2022. ISSN 0028-0836, 1476-4687. doi: 10.1038/s41586-022-04962-0. URL https://www.nature.com/articles/s41586-022-04962-0.

[5] M. Basan, T. Risler, J. Joanny, X. Sastre-Garau, and J. Prost. Homeostatic competition drives tumor growth and metastasis nucleation. *HFSP Journal*, 3(4):265–272, Aug. 2009. ISSN 1955-2068. doi: 10.2976/1.3086732. URL https://www.tandfonline.com/doi/full/10.2976/1.3086732.

[6] M. Basan, J. Prost, J.-F. Joanny, and J. Elgeti. Dissipative particle dynamics simulations for biological tissues: rheology and competition. *Physical Biology*, 8(2):026014, Apr. 2011. ISSN 1478-3975. doi: 10.1088/1478-3975/8/2/026014. URL https://iopscience.iop.org/article/10.1088/1478-3975/8/2/026014.

[7] M. Basan, J. Elgeti, E. Hannezo, W.-J. Rappel, and H. Levine. Alignment of cellular motility forces with tissue flow as a mechanism for efficient wound healing. *Proceedings of the National Academy of Sciences*, 110(7):2452–2459, Jan. 2013. ISSN 1091-6490. doi: 10.1073/pnas.1219937110. URL http://dx.doi.org/10.1073/pnas.1219937110.

[8] D. Bi, X. Yang, M. C. Marchetti, and M. L. Manning. Motility-driven glass and jamming transitions in biological tissues. *Physical Review X*, 6(2), Apr. 2016. ISSN 2160-3308. doi: 10.1103/physrevx.6.021011. URL http://dx.doi.org/10.1103/PhysRevX.6.021011.

[9] P. G. Bolhuis and A. A. Louis. How To Derive and Parameterize Effective Potentials in Colloid-Polymer Mixtures. *Macromolecules*, 35(5):1860–1869, Feb. 2002. ISSN 0024-9297, 1520-5835. doi: 10.1021/ma010888r. URL https://pubs.acs.org/doi/10.1021/ma010888r.

[10] T. Büscher, A. L. Diez, G. Gompper, and J. Elgeti. Instability and fingering of interfaces in growing tissue. *New Journal of Physics*, 22(8):083005, Aug. 2020. ISSN 1367-2630. doi: 10.1088/1367-2630/ab9e88. URL https://iopscience.iop.org/article/10.1088/1367-2630/ab9e88.

[11] T. Büscher, N. Ganai, G. Gompper, and J. Elgeti. Tissue evolution: mechanical interplay of adhesion, pressure, and heterogeneity. *New Journal of Physics*, 22(3):033048, Mar. 2020. ISSN 1367-2630. doi: 10.1088/1367-2630/ab74a5. URL https://iopscience.iop.org/article/10.1088/1367-2630/ab74a5.

[12] M. E. Cates and J. Tailleur. When are active Brownian particles and run-and-tumble particles equivalent? Consequences for motility-induced phase separation. *EPL (Europhysics Letters)*, 101(2):20010, Jan. 2013. ISSN 0295-5075, 1286-4854. doi: 10.1209/0295-5075/101/20010. URL https://iopscience.iop.org/article/10.1209/0295-5075/101/20010.

[13] B. Corominas-Murtra, C. L. G. J. Scheele, K. Kishi, S. I. J. Ellenbroek, B. D. Simons, J. van Rheenen, and E. Hannezo. Stem cell lineage survival as a noisy competition for niche access. *Proceedings of the National Academy of Sciences*, 117(29):16969–16975, July 2020. ISSN 0027-8424, 1091-6490. doi: 10.1073/pnas.1921205117. URL http://www.pnas.org/lookup/doi/10.1073/pnas.1921205117.

[14] J. Decayeux, J. Fries, V. Dahirel, M. Jardat, and P. Illien. Isotropic active colloids: explicit vs. implicit descriptions of propulsion mechanisms, 2023. ISSN 1744-6848. URL http://dx.doi.org/10.1039/D3SM00763D.

[15] M. Delarue, J.-F. Joanny, F. Jülicher, and J. Prost. Stress distributions and cell flows in a growing cell aggregate. *Interface Focus*, 4(6):20140033, Dec. 2014. ISSN 2042-8901. doi: 10.1098/rsfs.2014.0033. URL http://dx.doi.org/10.1098/rsfs.2014.0033.

[16] J. Elgeti, R. G. Winkler, and G. Gompper. Physics of microswimmers—single particle motion and collective behavior: a review. *Reports on Progress in Physics*, 78(5):056601, May 2015. ISSN 0034-4885, 1361-6633. doi: 10.1088/0034-4885/78/5/056601. URL https://iopscience.iop.org/article/10.1088/0034-4885/78/5/056601.

[17] P. Español and P. Warren. Statistical Mechanics of Dissipative Particle Dynamics. *Europhysics Letters (EPL)*, 30(4):191–196, May 1995. ISSN 0295-5075, 1286-4854. doi: 10.1209/0295-5075/30/4/001. URL https://iopscience.iop.org/article/10.1209/0295-5075/30/4/001.

[18] N. Ganai, T. Büscher, G. Gompper, and J. Elgeti. Mechanics of tissue competition: interfaces stabilize coexistence. *New Journal of Physics*, 21(6):063017, June 2019. ISSN 1367-2630. doi: 10.1088/1367-2630/ab2475. URL https://iopscience.iop.org/article/10.1088/1367-2630/ab2475.

[19] S. Garcia, E. Hannezo, J. Elgeti, J.-F. Joanny, P. Silberzan, and N. S. Gov. Physics of active jamming during collective cellular motion in a monolayer. *Proceedings of the National Academy of Sciences*, 112(50):15314–15319, Dec. 2015. ISSN 1091-6490. doi: 10.1073/pnas.1510973112. URL http://dx.doi.org/10.1073/pnas.1510973112.

[20] C. Gomez, W. Chua, A. Miremadi, S. Quist, D. Headon, and F. Watt. The Interfollicular Epidermis of Adult Mouse Tail Comprises Two Distinct Cell Lineages that Are Differentially Regulated by Wnt, Edaradd, and Lrig1. *Stem Cell Reports*, 1(1):19–27, June 2013. ISSN 22136711. doi: 10.1016/j.stemcr.2013.04.001. URL https://linkinghub.elsevier.com/retrieve/pii/S2213671113000076.

[21] P. Greulich and B. D. Simons. Dynamic heterogeneity as a strategy of stem cell self-renewal. *Proceedings of the National Academy of Sciences*, 113(27):7509–7514, July 2016. ISSN 0027-8424, 1091-6490. doi: 10.1073/pnas.1602779113. URL https://pnas.org/doi/full/10.1073/pnas.1602779113.

[22] P. Greulich, B. D. MacArthur, C. Parigini, and R. J. Sánchez-García. Universal principles of lineage architecture and stem cell identity in renewing tissues. *Development*, 148(11), June 2021. ISSN 1477-9129. doi: 10.1242/dev.194399. URL http://dx.doi.org/10.1242/dev.194399.

[23] P. A. Hall and F. M. Watt. Stem cells: the generation and maintenance of cellular diversity. *Development*, 106(4):619–633, Aug. 1989. ISSN 0950-1991, 1477-9129. doi: 10.1242/dev.106.4.619. URL https://journals.biologists.com/dev/article/106/4/619/36304/Stem-cells-the-generation-and-maintenance-of.

[24] O. Hallatschek, S. S. Datta, K. Drescher, J. Dunkel, J. Elgeti, B. Waclaw, and N. S. Wingreen. Proliferating active matter. *Nature Reviews Physics*, 5(7):407–419, May 2023. ISSN 2522-5820. doi: 10.1038/s42254-023-00593-0. URL http://dx.doi.org/10.1038/s42254-023-00593-0.

[25] K. Hara, T. Nakagawa, H. Enomoto, M. Suzuki, M. Yamamoto, B. D. Simons, and S. Yoshida. Mouse Spermatogenic Stem Cells Continually Interconvert between Equipotent Singly Isolated and Syncytial States. *Cell Stem Cell*, 14(5):658–672, May 2014. ISSN 19345909. doi: 10.1016/j.stem.2014.01.019. URL https://linkinghub.elsevier.com/retrieve/pii/S1934590914000496.

[26] E. Hay. An overview of epithelio-mesenchymal transformation. *Cells Tissues Organs*, 154(1):8–20, 1995. ISSN 1422-6421. doi: 10.1159/000147748. URL http://dx.doi.org/10.1159/000147748.

[27] M.-K. Hayward, J. M. Muncie, and V. M. Weaver. Tissue mechanics in stem cell fate, development, and cancer. *Developmental Cell*, 56(13):1833–1847, July 2021. ISSN 15345807. doi: 10.1016/j.devcel.2021.05.011. URL https://linkinghub.elsevier.com/retrieve/pii/S1534580721004408.

[28] P. J. Hoogerbrugge and J. M. V. A. Koelman. Simulating Microscopic Hydrodynamic Phenomena with Dissipative Particle Dynamics. *Europhysics Letters (EPL)*, 19(3):155–160, June 1992. ISSN 0295-5075, 1286-4854. doi: 10.1209/0295-5075/19/3/001. URL https://iopscience.iop.org/article/10.1209/0295-5075/19/3/001.

[29] J. R. Howse, R. A. L. Jones, A. J. Ryan, T. Gough, R. Vafabakhsh, and R. Golestanian. Self-Motile Colloidal Particles: From Directed Propulsion to Random Walk. *Physical Review Letters*, 99(4):048102, July 2007. ISSN 0031-9007, 1079-7114. doi: 10.1103/PhysRevLett.99.048102. URL https://link.aps.org/doi/10.1103/PhysRevLett.99.048102.

[30] R. E. Isele-Holder, J. Jäger, G. Saggiorato, J. Elgeti, and G. Gompper. Dynamics of self-propelled filaments pushing a load. *Soft Matter*, 12(41):8495–8505, 2016. ISSN 1744-6848. doi: 10.1039/c6sm01094f. URL http://dx.doi.org/10.1039/C6SM01094F.

[31] M. Ito, Y. Liu, Z. Yang, J. Nguyen, F. Liang, R. J. Morris, and G. Cotsarelis. Stem cells in the hair follicle bulge contribute to wound repair but not to homeostasis of the epidermis. *Nature Medicine*, 11(12):1351–1354, Dec. 2005. ISSN 1078-8956, 1546-170X. doi: 10.1038/nm1328. URL https://www.nature.com/articles/nm1328.

[32] V. Jaks, N. Barker, M. Kasper, J. H. van Es, H. J. Snippert, H. Clevers, and R. Toftgård. Lgr5 marks cycling, yet long-lived, hair follicle stem cells. *Nature Genetics*, 40(11):1291–1299, Nov. 2008. ISSN 1061-4036, 1546-1718. doi: 10.1038/ng.239. URL https://www.nature.com/articles/ng.239.

[33] P. H. Jones, B. D. Simons, and F. M. Watt. Sic Transit Gloria: Farewell to the Epidermal Transit Amplifying Cell? *Cell Stem Cell*, 1(4):371–381, Oct. 2007. ISSN 19345909. doi: 10.1016/j.stem.2007.09.014. URL https://linkinghub.elsevier.com/retrieve/pii/S1934590907001841.

[34] D. J. Jörg, Y. Kitadate, S. Yoshida, and B. D. Simons. Competition for Stem Cell Fate Determinants as a Mechanism for Tissue Homeostasis. Technical Report arXiv:1901.03903, arXiv, Jan. 2019. URL http://arxiv.org/abs/1901.03903.

[35] Y. Kobayashi, Y. Yasugahira, H. Kitahata, M. Watanabe, K. Natsuga, and M. Nagayama. Interplay between epidermal stem cell dynamics and dermal deformation. *npj Computational Materials*, 4(1):45, Dec. 2018. ISSN 2057-3960. doi: 10.1038/s41524-018-0101-z. URL http://www.nature.com/articles/s41524-018-0101-z.

[36] A. Kopf and M. Sixt. Gut homeostasis: Active migration of intestinal epithelial cells in tissue renewal. *Current Biology*, 29(20):R1091–R1093, Oct. 2019. ISSN 0960-9822. doi: 10.1016/j.cub.2019.08.068. URL http://dx.doi.org/10.1016/j.cub.2019.08.068.

[37] A. D. Lander. The 'stem cell' concept: is it holding us back? *Journal of Biology*, 8(8): 70, 2009. doi: 10.1186/jbiol177. URL https://doi.org/10.1186/jbiol177.

[38] S. W. Lane, D. A. Williams, and F. M. Watt. Modulating the stem cell niche for tissue regeneration. *Nature Biotechnology*, 32(8):795–803, Aug. 2014. doi: 10.1038/nbt.2978. URL https://doi.org/10.1038/nbt.2978.

[39] J. Li, S. K. Schnyder, M. S. Turner, and R. Yamamoto. Role of the Cell Cycle in Collective Cell Dynamics. *Physical Review X*, 11(3):031025, July 2021. ISSN 2160-3308. doi: 10.1103/PhysRevX.11.031025. URL https://link.aps.org/doi/10.1103/PhysRevX.11.031025.

[40] J. Li, S. K. Schnyder, M. S. Turner, and R. Yamamoto. Competition between cell types under cell cycle regulation with apoptosis. *Physical Review Research*, 4(3):033156, Aug. 2022. ISSN 2643-1564. doi: 10.1103/PhysRevResearch.4.033156. URL https://link.aps.org/doi/10.1103/PhysRevResearch.4.033156.

[41] G. Mannino, C. Russo, G. Maugeri, G. Musumeci, N. Vicario, D. Tibullo, R. Giuffrida, R. Parenti, and D. Lo Furno. Adult stem cell niches for tissue homeostasis. *Journal of Cellular Physiology*, 237(1):239–257, Jan. 2022. ISSN 0021-9541, 1097-4652. doi: 10.1002/jcp.30562. URL https://onlinelibrary.wiley.com/doi/10.1002/jcp.30562.

[42] A.-K. Marel, N. Podewitz, M. Zorn, J. O. Rädler, and J. Elgeti. Alignment of cell division axes in directed epithelial cell migration. *New Journal of Physics*, 16(11):115005, Nov. 2014. ISSN 1367-2630. doi: 10.1088/1367-2630/16/11/115005. URL http://dx.doi.org/10.1088/1367-2630/16/11/115005.

[43] G. Mascré, S. Dekoninck, B. Drogat, K. K. Youssef, S. Brohée, P. A. Sotiropoulou, B. D. Simons, and C. Blanpain. Distinct contribution of stem and progenitor cells to epidermal maintenance. *Nature*, 489(7415):257–262, Sept. 2012. ISSN 0028-0836, 1476-4687. doi: 10.1038/nature11393. URL https://www.nature.com/articles/nature11393.

[44] D. A. Matoz-Fernandez, K. Martens, R. Sknepnek, J. L. Barrat, and S. Henkes. Cell division and death inhibit glassy behaviour of confluent tissues. *Soft Matter*, 13(17): 3205–3212, 2017. ISSN 1744-6848. doi: 10.1039/c6sm02580c. URL http://dx.doi.org/10.1039/C6SM02580C.

[45] F. Montel, M. Delarue, J. Elgeti, L. Malaquin, M. Basan, T. Risler, B. Cabane, D. Vignjevic, J. Prost, G. Cappello, and J.-F. Joanny. Stress clamp experiments on multicellular tumor spheroids. *Physical Review Letters*, 107(18), Oct. 2011. ISSN 1079-7114. doi: 10.1103/physrevlett.107.188102. URL http://dx.doi.org/10.1103/PhysRevLett.107.188102.

[46] F. Montel, M. Delarue, J. Elgeti, D. Vignjevic, G. Cappello, and J. Prost. Isotropic stress reduces cell proliferation in tumor spheroids. *New Journal of Physics*, 14(5):055008, May 2012. ISSN 1367-2630. doi: 10.1088/1367-2630/14/5/055008. URL http://dx.doi.org/10.1088/1367-2630/14/5/055008.

[47] M. E. Page, P. Lombard, F. Ng, B. Göttgens, and K. B. Jensen. The Epidermis Comprises Autonomous Compartments Maintained by Distinct Stem Cell Populations. *Cell Stem Cell*, 13(4):471–482, Oct. 2013. ISSN 19345909. doi: 10.1016/j.stem.2013.07.010. URL https://linkinghub.elsevier.com/retrieve/pii/S1934590913003184.

[48] I. Pagonabarraga, M. H. J. Hagen, and D. Frenkel. Self-consistent dissipative particle dynamics algorithm. *Europhysics Letters (EPL)*, 42(4):377–382, May 1998. ISSN 0295-5075, 1286-4854. doi: 10.1209/epl/i1998-00258-6. URL https://iopscience.iop.org/article/10.1209/epl/i1998-00258-6.

[49] N. Podewitz, M. Delarue, and J. Elgeti. Tissue homeostasis: A tensile state. *EPL (Europhysics Letters)*, 109(5):58005, Mar. 2015. ISSN 0295-5075, 1286-4854. doi: 10.1209/0295-5075/109/58005. URL https://iopscience.iop.org/article/10.1209/0295-5075/109/58005.

[50] N. Podewitz, F. Jülicher, G. Gompper, and J. Elgeti. Interface dynamics of competing tissues. *New Journal of Physics*, 18(8):083020, Aug. 2016. ISSN 1367-2630. doi: 10.1088/1367-2630/18/8/083020. URL https://iopscience.iop.org/article/10.1088/1367-2630/18/8/083020.

[51] M. D. Prater, V. Petit, I. Alasdair Russell, R. R. Giraddi, M. Shehata, S. Menon, R. Schulte, I. Kalajzic, N. Rath, M. F. Olson, D. Metzger, M. M. Faraldo, M.-A. Deugnier, M. A. Glukhova, and J. Stingl. Mammary stem cells have myoepithelial cell properties. *Nature Cell Biology*, 16(10):942–950, Oct. 2014. ISSN 1465-7392, 1476-4679. doi: 10.1038/ncb3025. URL https://www.nature.com/articles/ncb3025.

[52] J. Ranft, M. Basan, J. Elgeti, J.-F. Joanny, J. Prost, and F. Julicher. Fluidization of tissues by cell division and apoptosis. *Proceedings of the National Academy of Sciences*, 107 (49):20863–20868, Dec. 2010. ISSN 0027-8424, 1091-6490. doi: 10.1073/pnas.1011086107. URL http://www.pnas.org/cgi/doi/10.1073/pnas.1011086107.

[53] S. Sinha and D. Thirumalai. Self-generated persistent random forces drive phase separation in growing tumors. *The Journal of Chemical Physics*, 153(20), Nov. 2020. ISSN 1089-7690. doi: 10.1063/5.0026590. URL http://dx.doi.org/10.1063/5.0026590.

[54] S. Sinha, A. N. Malmi-Kakkada, X. Li, H. S. Samanta, and D. Thirumalai. Spatially heterogeneous dynamics of cells in a growing tumor spheroid: comparison between theory and experiments. *Soft Matter*, 16(22):5294–5304, 2020. ISSN 1744-6848. doi: 10.1039/c9sm02277e. URL http://dx.doi.org/10.1039/C9SM02277E.

[55] A. P. Solon, M. E. Cates, and J. Tailleur. Active brownian particles and run-and-tumble particles: A comparative study. *The European Physical Journal Special Topics*, 224(7): 1231–1262, July 2015. ISSN 1951-6355, 1951-6401. doi: 10.1140/epjst/e2015-02457-0. URL http://link.springer.com/10.1140/epjst/e2015-02457-0.

[56] L. R. Strachan and R. Ghadially. Tiers of Clonal Organization in the Epidermis: The Epidermal Proliferation Unit Revisited. *Stem Cell Reviews*, 4(3):149–157, Sept. 2008. ISSN 1550-8943, 1558-6804. doi: 10.1007/s12015-008-9020-6. URL http://link.springer.com/10.1007/s12015-008-9020-6.

[57] A. Sánchez-Danés, E. Hannezo, J.-C. Larsimont, M. Liagre, K. K. Youssef, B. D. Simons, and C. Blanpain. Defining the clonal dynamics leading to mouse skin tumour initiation. *Nature*, 536(7616):298–303, Aug. 2016. ISSN 0028-0836, 1476-4687. doi: 10.1038/nature19069. URL http://www.nature.com/articles/nature19069.

[58] E. Tjhung and L. Berthier. Analogies between growing dense active matter and soft driven glasses. *Phys. Rev. Res.*, 2:043334, Dec 2020. doi: 10.1103/PhysRevResearch.2.043334. URL https://link.aps.org/doi/10.1103/PhysRevResearch.2.043334.

[59] A. Van Keymeulen, A. S. Rocha, M. Ousset, B. Beck, G. Bouvencourt, J. Rock, N. Sharma, S. Dekoninck, and C. Blanpain. Distinct stem cells contribute to mammary gland development and maintenance. *Nature*, 479(7372):189–193, Nov. 2011. ISSN 0028-0836, 1476-4687. doi: 10.1038/nature10573. URL https://www.nature.com/articles/nature10573.

[60] H. Wang, F. H. Stillinger, and S. Torquato. Sensitivity of pair statistics on pair potentials in many-body systems. *The Journal of Chemical Physics*, 153(12):124106, Sept. 2020. ISSN 0021-9606, 1089-7690. doi: 10.1063/5.0021475. URL https://pubs.aip.org/jcp/article/153/12/124106/77334/Sensitivity-of-pair-statistics-on-pair-potentials.

[61] J. J. Williamson and G. Salbreux. Stability and roughness of interfaces in mechanically regulated tissues. *Physical Review Letters*, 121(23), Dec. 2018. ISSN 1079-7114. doi: 10.1103/physrevlett.121.238102. URL http://dx.doi.org/10.1103/PhysRevLett.121.238102.

[62] S. Yoshida. Open niche regulation of mouse spermatogenic stem cells. *Development, Growth & Differentiation*, 60(9):542–552, Dec. 2018. ISSN 0012-1592, 1440-169X. doi: 10.1111/dgd.12574. URL https://onlinelibrary.wiley.com/doi/10.1111/dgd.12574.

3 Mechanics and fate stochasticity shape stem cell distribution in tissues

Abstract

Balancing cellular loss in tissues requires fine balance of cell proliferation and differentiation. In differentiated tissues consisting of a single cell type, a mechanical regulation of proliferation has been proposed to underlie growth-control and homeostatic steady-states. Yet, how tissues containing different cell types with distinct proliferation rates, mechanical interactions, and spatial self-organization retain robust homeostasis of cell proportions remains poorly understood. Here, we combine particle-based mechanical models of proliferative tissues with a classical hierarchy of stem, progenitor, and differentiated cells, undergoing stochastic fate choices, and show that mechanical feedback alone is sufficient to stabilize populations. We derive analytically and computationally a phase diagram of possible stable states, in particular those maintained either via slow and rare stem cells with short-lived progenitors or no stem cells and long-lived progenitors. Our simulations uncover that mechanical control of growth is sufficient, in the absence of any codes of adhesion or extrinsic niche signals, to cause stable spatial structures, with small stem cell clusters forming and maintaining dynamical renewal units. Our results demonstrate how complex spatial structures can emerge in minimal stochastic and mechanical simulations with impact to understand the homeostasis of multi-cellular systems.

3.1 Introduction

A hallmark of higher multicellular life is to control cell fate decisions, i. e. proliferation and differentiation, to balance cell loss and maintain a functional tissue composition and structure. This means that feedback mechanisms must exist, not only to ensure that cell proliferation exceeds cell loss during development and growth, but also that the two are exactly balanced at homeostasis. However, the mechanisms ensuring this balance remain a fundamental open question of cell biology and biophysics.

In recent years, mechanical interactions between cells have gotten increasing attention [23]. Because cell growth and division exerts compressive forces within a tissue, and because different cellular events like division or apoptosis have been shown to be mechano-sensitive, i.e. dependent on the mechanical state of the tissue [1, 3, 13, 15, 22, 32, 37, 39, 40, 41, 42, 46, 54, 56], mechanical feedback has emerged as a natural candidate mechanism to ensure homeostasis. Furthermore, these types of modelling approaches have predicted a number of non-trivial features,

such as the visco-elastic properties of tissues in the presence of division and apoptosis [3, 12, 40, 46, 48], the competition between different tissues, interface dynamics, and the evolution of coexisting species [7, 8, 18, 47, 49].

However, these modelling approaches have so far largely concentrated on tissues made of a single cell type, or of different cell types that are independent from each others, i.e. no interconversion from one type to the other. This is a critical limitation, as homeostasis does not only entail the stability of cell numbers and density, but also the stable and correct proportions of different cell types. In particular, most adult tissues are maintained by adult stem cells [17, 53], which can both self-renew, and give rise to tissue specific, specialized cell types [5]. Despite the increasing insights in quantifying the dynamics of stem fate choices, for instance via lineage tracing methods or proliferation kinetic measurements, we still know comparatively little into the mechanisms of fate choices and the design principles leading to spatio-temporal coordination between cell types [6], beyond generic theoretical features common to large classes of models [20]. A first class involves either cell-level asymmetric divisions, in which case the question of fate proportion stability becomes trivial, as it is hard-coded in the division patterns of each individual cells. However, how this would act in fluctuating environments exposed to external perturbations remains unclear, as the model lacks adaptability. Population-level asymmetry, characterized by a mix of symmetric and asymmetric stem cell fate choices [9], presents an alternative way to control cell fate, while being adaptable. In that case, fate outcomes must be balanced at the population level, yet, how this is mechanistically encoded remains unclear. Experimentally, a variety of biochemical pathways, like *Wnt*, *TP53*, or *RAS*, have been shown to play a crucial role in controlling the cell cycle, i.e. growth, division, but also differentiation, and deregulation of these pathways is found in carcinoma [33, 45, 58], but how to relate these to collective fate decisions remain unclear.

Here, we aim to generalize models of tissue growth with mechanical feedback to complex tissues with stochastic fate choices. We consider a generic hierarchy of stochastically dividing stem (S) and progenitor/transit-amplifying (T) cells, which in principle have infinite self-renewing capacity, as well as non-proliferative differentiated (D) cells. We utilize compartment-based analytic theory and stochastic particle-based simulations to derive and understand a phase diagram of possible parameter combinations leading to stable tissues. Using the simulations, we further explore the structure and dynamics of stochastically differentiating tissues with mechanical feedback. Interestingly, these are fundamentally shaped by the stochasticity of fate choices, which lead to stable clustering of stem cells, in stark contrast to a situations of deterministic fate choices, which had led to sharp repulsion and separation of single stem cells within the tissue [31]. Overall, we demonstrate that niche-like stem cell clusters can arise in a self-organized manner, simply as a result of an interplay between tissue mechanics and cell fate stochasticity.

3.2 Mechanical control of fate proportions in stem-cell derived tissues

We consider a minimal model of complex tissues, where S and T cells symmetrically proliferate with rates d_S and d_T, respectively. In addition to this, both populations can stochastically differentiate into T and D cells at rates c_S and c_T, respectively. D cells are post-mitotic, i.e. non-growing, cells and lost with constant rate k_a. In the absence of feedback, such scenario is structurally unstable, and such model only has a steady state with extreme parameter fine-tuning (e.g. $d_S = c_S$), and still prone to stochastic drift, as the rates do not adapt to the number of cells. Coupling the growth rates to be modulated by local mechanical pressure, solves this issue as we will see below. A schematic of this model can be found in Fig. 3.2.1 (A). While our model only includes symmetric divisions, the effective outcome of a division can be asymmetric, i. e. one cell undergoes another division whereas the other differentiates [24].

We implement this lineage model into the two particle growth model, which considers cell mechanics and its feedback on divisions [4, 31, 46] (See Sec. 3.3). Thanks to the mechanical feedback on growth, we always find a stable steady state, independent of parameter tuning or initial conditions. Fig. 3.2.1 (B) shows that the mechanical feedback inherent to our simulations lies at the core of the stability: After randomly removing 10 % of the cells, division rates rise in response to lower cell density until the steady state is reached again.

The compositions and structure, however, varies greatly with cell type specific rates. Initially starting from a dense tissue with randomly assigned cell types, steady states with very different cell compositions, with S, T, or D cell rich regions (see Fig. 3.2.1 (C)) are found depending on the differentiation rates. This includes regions in which the S cell goes extinct but the tissue is continuously maintained by the transient cell type, as well as regions where the tissue loses integrity.

To better understand the different regions of the phase diagram and how to control the cell cycle dynamics to arrive at a biological relevant parameter range, we derive a coarse grained approximation, based on compartment models of each cell type [27], for cell fate proportions, starting with the dynamic equations describing the introduced model, given by

$$\begin{aligned} \partial_t n_S(t) &= [d_S(\mathcal{P}) - c_S]\ n_S(t) \\ \partial_t n_T(t) &= [d_T(\mathcal{P}) - c_T]\ n_T(t) + c_S\ n_S(t)\ , \\ \partial_t n_D(t) &= c_T\ n_T(t) - k_a\ n_D(t) \end{aligned} \tag{3.1}$$

where $n_i(t)$ are the cell numbers of cell types $i \in (S, T, D)$, and d_S, d_T, c_S, c_T, and k_a the division, differentiation, and loss rates, with explicit dependence on the system pressure $\mathcal{P}$ in the division rates. Note that this dependence on pressure is just the lowest order expansion of the growth rate on mechanics [3]. We focus here on the steady state, i.e. the *homeostatic* state, where the numbers of cells of each type do not change over time ($\partial_t n_i = 0$). The steady state tissue pressure is referred to as *homeostatic pressure* $\mathcal{P}^H$. Note that throughout this work the superscript H always defines the value of a variable in the homeostatic state.

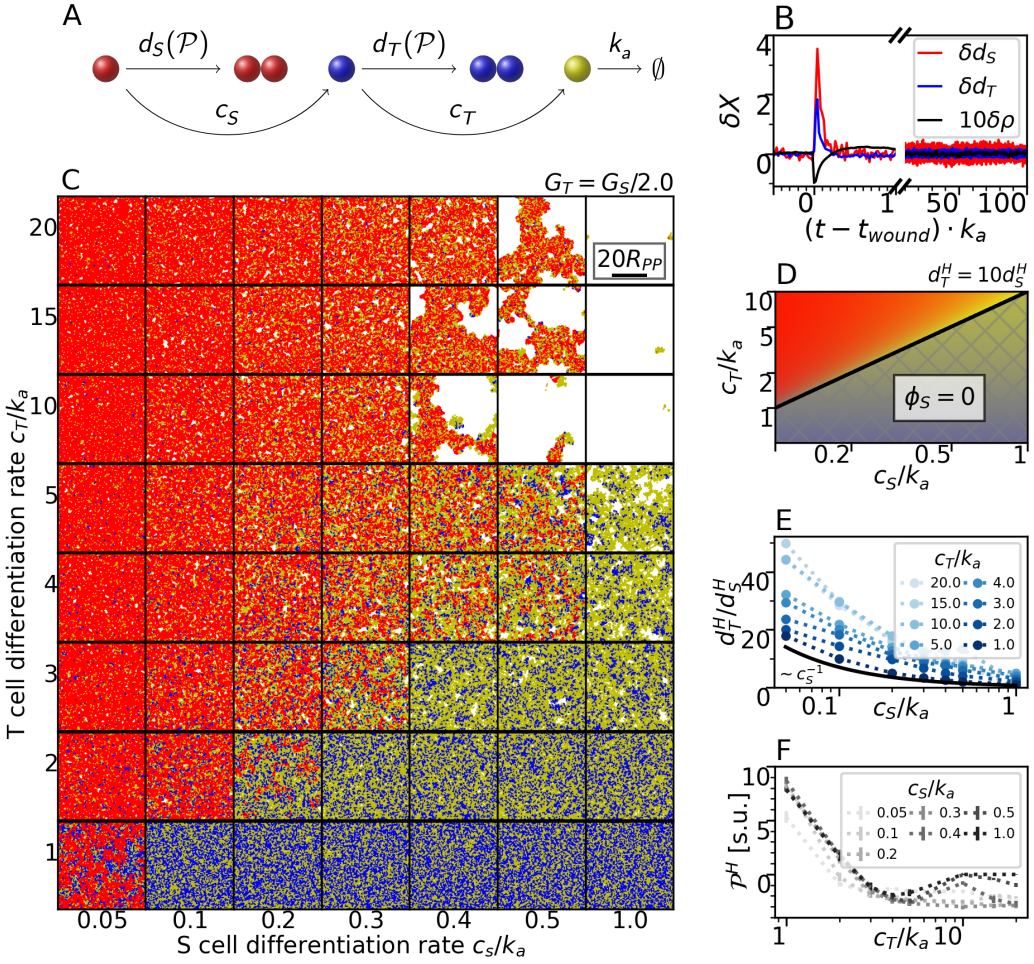

Figure 3.2.1: Homeostasis of S cell derived tissues via mechanical control.
(A) Schematic representation of the S (red) T (blue) D (yellow) cell type model. This color code to specify cell type is applied throughout the whole work. (B) Response to a "wound", i.e. at $t = t_{wound}$, 10 % of cells are removed at random from the simulation of $\mathcal{T}^S_{rare}$(def. in Fig. 3.3.1), where $\delta X = X(t)/X^H - 1$ for S and T cell division and total cell density (black, tenfold amplified for visibility) is shown. (C) Simulation snapshot phase diagram in steady state for variation of S and T cell differentiation rates $c_{(S,T)}$ for fixed $G_T/G_S = 2$. (D) Corresponding cell number fraction phase diagram following from Eqs. 3.2. Black line marks transition to S cell free region (hashed). (E) T cell division rate in homeostasis d_T^H divided by $d_S^H = c_S$ and (F) measured homeostatic pressure $\mathcal{P}^H$ in simulation units are shown for simulation phase space (B) as function of c_S and c_T.

From the dynamic equation for the S cell, we can then derive the homeostatic condition under which the S cell division rate balances its differentiation rate ($d_S^H = c_S$). Note that this condition is no longer just a requirement of stability, but a result of the mechanical feedback: Excess divisions will lead to an increase in pressure, which in turn will result in a decrease of divisions until numbers are back to their steady state value and the condition $d_S = c_S$ is satisfied again. Steady state of T cells implies that the loss through differentiation is balanced by self-renewal plus influx of differentiating S cells. Similarly, the flux of D cells generated by T cell differentiation has to be balanced by loss of D cells. This allows us to derive the steady state cell number fractions $\phi_i^H = n_i^H/N^H$, where $N^H = n_S^H + n_T^H + n_D^H$, as functions of the differentiation and homeostatic division rates, given by

$$\begin{aligned}
\phi_S^H &= \frac{1}{1 + \frac{c_S}{c_T - d_T^H}\left(1 + \frac{c_T}{k_a}\right)} \\
\phi_T^H &= \frac{c_S}{(c_T - d_T^H)}\phi_S^H = \frac{c_S}{c_T - d_T^H + c_S\left(1 + \frac{c_T}{k_a}\right)} \\
\phi_D^H &= \frac{c_T}{k_a}\,\frac{c_S}{(c_T - d_T^H)}\phi_S^H = \frac{c_S\; c_T/k_a}{c_T - d_T^H + c_S\left(1 + \frac{c_T}{k_a}\right)}\;.
\end{aligned} \tag{3.2}$$

A phase diagram for cell number fractions as function of the S and T cell differentiation rate qualitatively displays the same trends as particle simulations as illustrated by simulation snapshots (see Fig. 3.2.1 B&D).

Vice versa, we also derive the differentiation rates as functions of homeostatic variables (see SI Sec. 3.B), which allows us to tune simulation parameters to match specific tissues. First, we envision a realistic tissue composition defined by set cell number fractions $\phi_{S,T,D}^H$. Then, based on the measured or presumed division rates of S cells, which are typically slow cycling, and T cells, which divide frequently, Eq. 3.3 guide us with differentiation rates to use in the particle based simulations.

To go further, we also write linear expansions for the division rates $d_S(\mathcal{P})$, $d_T(\mathcal{P})$ as a function of pressure $\mathcal{P}$, which describe how S and T cells adapt their division with respect to pressure variations and depend in general on the mechanical properties of cells and configuration of the tissue (see SI Sec. 3.B). The homeostatic pressure is set when either $d_S^H = c_S$ and $d_T^H < c_T$ or $d_S^H < c_S$ and $d_T^H = c_T$. In the latter case S cells go extinct. In the case where S cells are present, the homeostatic pressure decreases with increasing S cell differentiation rate as also observed in our simulations (see Fig. 3.2.1 (F)). The homeostatic pressure can be negative for tensile tissues, but this has a lower bound. Below this limit, the tissue begins to rip and is losing confluency, as seen in the top right corner of Fig. 3.2.1 (C). For such non-confluent tissues, the global system pressure vanishes ($\mathcal{P} = 0$, see Fig.3.2.1 (F)). Similar analysis of the T cell division rates (see SI 3.B) reveals more in depth insight in its effect on the cell composition, and we also demonstrate (see SI Fig. 3.D.1), how division rates can be controlled by changing the mechanical properties of cells, exemplarily shown by varying the T cell growth coefficient G_T.

Stem cell rare ($\mathcal{T}^S_{rare}$)		Stem cell rich ($\mathcal{T}^S_{rich}$)	
$c_S = 0.2k_a$	$\phi^H_S = 7.0\%$	$c_S = 0.3k_a$	$\phi^H_S = 25.5\%$
$c_T = 3.0k_a$	$\phi^H_T = 22.6\%$	$c_T = 3.0k_a$	$\phi^H_T = 18.1\%$
$G_T = 2.41G_S$	$\phi^H_D = 70.3\%$	$G_T = 2.00G_S$	$\phi^H_D = 56.4\%$
$d^H_T = 14.7d_S$	$\mathcal{P}^H = -1.33$	$d^H_T = 8.6d_S$	$\mathcal{P}^H = -1.54$

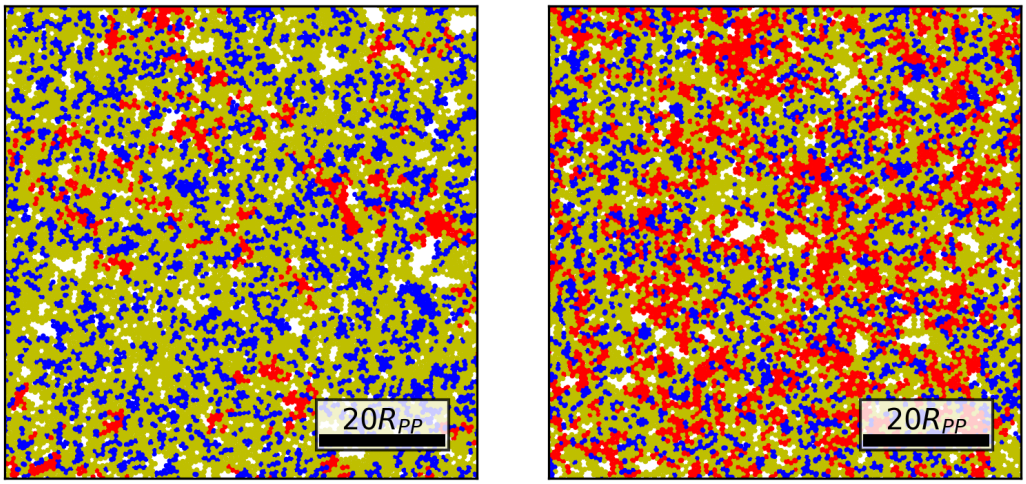

Figure 3.3.1: Details of selected tissues chosen for detailed analysis. Stem cell rare ($\mathcal{T}^S_{rare}$, left) and rich ($\mathcal{T}^S_{rich}$, right) tissues studied in detail. Simulation parameters (c_S, c_T, $G_T/G_S|_{G_S=35}$) and resulting tissue properties (d^H_T, ϕ^H_S, ϕ^H_T, ϕ^H_D, $\mathcal{P}^H$) are given in the table together with a tissue snapshot in steady state. Stem (red), transient (blue), and differentiated (yellow) cells are drawn with cell size set to distance at which attractive and repulsive forces balance, and scale for 20 interaction radii R_{PP} is given.

3.3 Agent-based simulations of stem cell derived tissues

To go beyond understanding the average fate proportions of tissues, we then turned to particle-based simulations allowing us to understand stem cell dynamics in space and time. Following our previous work [31] we extend the two-particle growth model [4] to include stochastic cell fate. Here, we present only the essential aspects of the model for this work (see SI 3.C for full details). In essence, cells are modeled as soft attractive particles with stress-dependent growth. Differentiation and cell loss are modelled as instantaneous stochastic processes with fixed rates. This allows us to set directly c_S, c_T, and k_a in simulations, where k_a depicts the time scale of our simulations, i. e. we measure time in D cell generations.

While differentiation rates are explicit simulation parameter, the division rates are not. Instead, they follow from the interactions between particles, their mechanical properties and the tissue composition [4, 7, 8, 46], via the same mechanical control mechanism discussed in the previous section. We confirmed in simulations that this

lead, as expected from the analytics, to robust stabilization of fate properties.

For instance, in Fig. 3.2.1, we show a phase diagram in the $c_T - c_S$-plane, fitting well to the predicted phase behavior from number balance (Eq. 3.2), and we present further dependencies between parameters and observables in the SI. Taken together, this shows that our simulations are a versatile tool for simulating the mechanodynamics of stem cell derived tissues.

The main advantage of simulations lies in their ability to provide insight in the spatio-temporal dynamics of tissues, while the mean field equations presented above allow us to specifically tune the cell cycle dynamics in simulations to obtain biological relevant tissue compositions and dynamics. For the remainder of this work, we define two tissues (see Fig. 3.3.1): (i) The *stem cell rare tissue* ($\mathcal{T}^S_{rare}$) consists of approximately $\phi^H_S \approx 7\%$ stem cells, $\phi^H_T \approx 23\%$ T cells and $\phi^H_D \approx 70\%$ D cells. (ii) The *stem cell rich tissue* ($\mathcal{T}^S_{rich}$) consists of approximately $\phi^H_S \approx 25\%$ stem cells, $\phi^H_T \approx 18\%$ T cells and $\phi^H_D \approx 56\%$ D cells.

In both tissues, stem cells are slow cycling: The measured T cell division rate is about one order of magnitude faster than the stem cells division rate d^H_S (see Fig. 3.2.1 (E) & 3.3.1). These numbers are in the range reported for the interfollicular epidermis [35], in which stem cells divide 4-6 times per year and long-lived progenitor cells about once per week. Robustness of our results is confirmed by additional tissue configurations (see SI 3.E), which cover a broader range of tissue compositions and cell fate rates but are not shown in the main text for the sake of clarity.

3.4 Self-organized formation of stem cell clusters in stem cell derived tissues

Interestingly, we find that that stem cells form well-defined spatial structures, with isolated niche-like stem cell clusters that remain relatively stationary in time, despite the fact that we have not implemented any specific adhesion between stem cells. Furthermore, this is in stark contrast both to previous works in the absence of mechanical interactions, where stem cell domains grow and phase separate over time [21], as well as our previous work with deterministic and asymmetrically dividing stem cells, which led to isolated stem cells due to effective and active proliferation-induced repulsion. This suggests that mechanical and stochastic effects cooperate to give rise to complex spatio-temporal patterns of finite-sized stem cell clusters, reminiscent of the concept of stem cell niches [25, 60], yet without any extrinsic spatially modulated cures from the substrate.

To systematically quantify our observed stem cell clusters, we use several metrics which could serve as guides for future quantification in experimental datasets. Firstly, we compute the stem cell pair correlation function $g(r)$, which measures the relative density of S cells in the neighborhood of other S cells (see SI 3.E.1). The niche like structure manifests itself in an increased S cell density in the vicinity of a S cell, i. e. within around ten cell sizes R_{PP}. For the low S cell fraction $\mathcal{T}^S_{rare}$, the integrated size of the peak $\int_0^{r^*_1} dr g(r) - 1 \approx 30$, where the first root of $g(r^*_1) = 1$ defines the upper

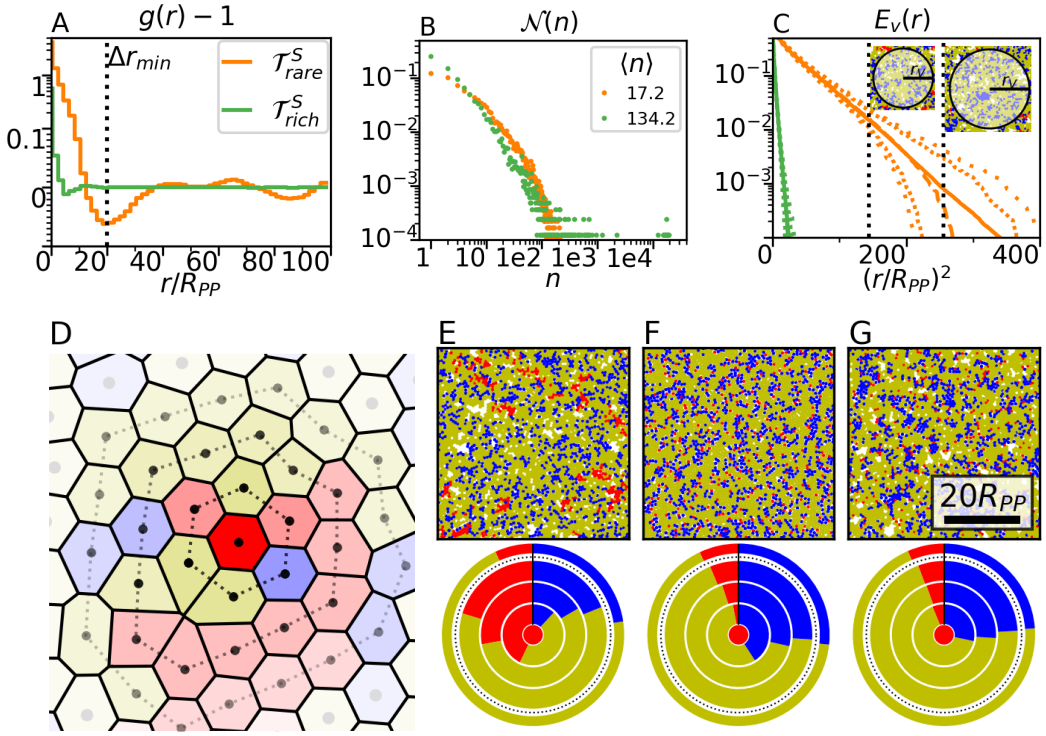

Figure 3.4.1: Spatial structure and niche formation (A) Stem cell pair correlation function $g(r)$ over pair distance $r = |\boldsymbol{r}_i - \boldsymbol{r}_j|$, with linear y-scale between $(-0.1, 0.1)$ and logarithmic y-scale else. (B) Cluster size distribution function $\mathcal{N}(n)$ for density based clustering with intra-cluster distance threshold $2R_{PP}$. Average cluster sizes $\langle n \rangle$ are given in legend. (C) Void exclusion functions $E_V(r)$ over squared distance (solid line for entire data set), following an exponential decay. Percentiles of $E_V(r)$ of *individual* snapshots are shown in loosely dotted (3^{rd} & 97^{th}), finely dotted (10^{th} & 90^{th}), and dashed (50^{th}) lines. Dashed vertical black lines denote example snapshots at void areas marked by dotted vertical lines. (D) Representative snapshot of the tissue used to construct cell neighborhoods. Cells of first, second, and third order are connected by dotted line and color opacity is gradually reduced with increasing order. (E-G) Snapshots (top row) of various differentiation models, (E) slow cycling S cells and stochastic differentiation $\mathcal{T}^S_{rare}$, (F) fast cycling and (G) slow cycling stem cells with deterministic differentiation. For each system, corresponding neighborhood statistics (bottom row) are shown in pie charts around S cells (inner circle). Each ring represents neighbor statistics of first to third order and outermost ring, separated by dashed line, shows the global cell number fractions.

bound, is a measure for the number of stem cells in a niche. The subsequent large minimum for small S cell fraction indicates an effective repulsion of S cell niches from the intermediate vicinity. The higher order peaks at even larger distances ($r \sim 50R_{PP}$) indicates a higher order structure formation of niches having well defined distances. This is further confirmed by a peak in the number fluctuations (see SI 3.E). On the contrary, in the stem cell rich tissue $\mathcal{T}^S_{rich}$, the pair correlation function decays much

quicker, shows only a small minimum and is about unity thereafter, corresponding to limited S cell condensation with no significant further structure.

Next, we turned to the cluster size distribution. Defining all S cells within a distance of twice the cell diameter ($2R_{PP}$) to belong to the same cluster, we find a mean cluster size of 17 cells for the S cell rare tissue, while for the S cell rich tissue, the mean cluster size reaches above 100, and we observe some huge, system spanning clusters.

Finally, we expand our observation by the study of the S cell-free regions. The void exclusion function $E_V(r)$ measures the probability that a random point has no S cell within a distance r. For randomly distributed particles, $E_V = \exp(-\rho\pi r^2)$. Indeed we find an exponential decay of E_V over a large range. However, the scaling is described by an effectively rescaled S cell density, due to clustering of S cells. For the S cell rare tissue, the prefactor corresponds to a much reduced S cell density of 0.8%, one order of magnitude smaller than the actual S cell density, consistent with the strong niche-like cluster formation discussed above. The percentiles of the void exclusion function across individual snapshots reveals further, that every snapshot contains at least one large void. Vice versa, the void exclusion function for the SC-rich tissue the exponential decay is less clear and roughly corresponds to densities of $6-14\%$, about half to one fourth of the actual S cell density. Here, the percentiles reveal that large voids are absent across the whole simulation.

Such local clustering of S cells and long range order is in stark contrast to asymmetrically dividing S cells with deterministic T cell duplication which results in an effective repulsion isolating individual stem cells, as we showed in our previous work [31]. Due to the symmetric divisions, an S cell pair is created next to each other, causing an increased probability to find two S cells at short distances before they separate from each other. The homeostatic control then causes long ranged self-organization of cells.

Finally, snapshots reveal another important feature: S cells are not dominantly surrounded by T cells as one might expect, and as we found in previous work with deterministic fate choices [31]. Indeed, quantifying (Fig. 3.4.1, see SI for method) the neighborhood composition reveals that T cells are even depleted from the S cell neighborhood. This is in stark comparisons to simulations that we performed with similar fate composition as $\mathcal{T}^S_{rare}$but with a deterministic differentiation scheme, where for slow and fast cycling stem cells, stem cells are largely surrounded by transient cells as expected. This underlines that inference of cell lineages and hierarchy from neighbourhood relations in static snapshots is prone to errors, that can be avoided by tracking dynamic relations.

3.5 Long-term temporal dynamics of stem cell clusters

Beyond these static spatial correlations, simulations allow us direct access to several temporal dynamics of stem cell tissues, such as lineage histories or cluster stability over time. Simulation movies (see 3.A) and stem cell spatial distribution maps (see Fig. 3.5.1) suggest that S cell clusters form stable units, which fluctuate in size, yet only diffuse spatially at a very slow pace. The remarkable stability of S cell

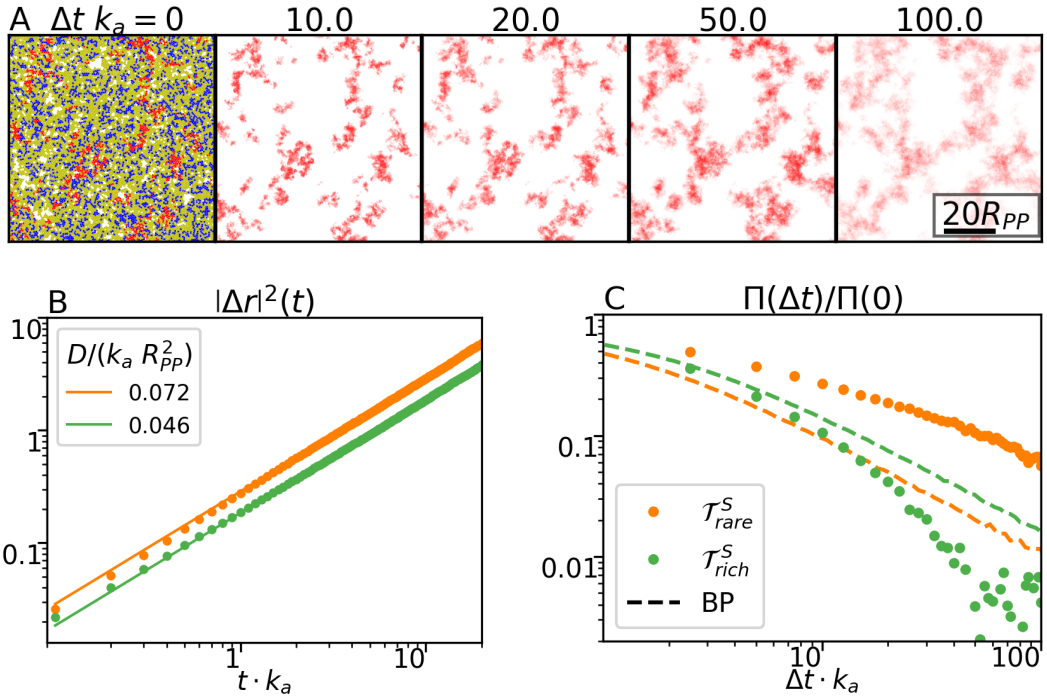

Figure 3.5.1: Temporal stability of stem-cell clusters (A) Stem cell spatial distribution map following the initial configuration (left) at time lags of 10, 20, 50 and 100 D cell generations. Stem cell trajectories with opacity such that pixels, which are constantly occupied by an S cell, are fully red. Lighter or white regions correspond to low or no stem cell frequency, respectively. (B) Mean squared displacement of stem cells over time, measured from trajectories up to time of division or differentiation. (C) Density-fluctuation correlation function over time for tissue simulations (dots) and Brownian particle (BP) simulations (dashed line) with diffusion coefficient derived from (B) and BP number equal to mean stem cell number.

clusters for $\mathcal{T}^S_{rare}$is highlighted by spatial distribution maps for S cell trajectories (see Fig. 3.5.1 A). Integrating stem cell densities, and displaying them over increasing time intervals shows, how clusters are remodeled but their overall structure remains unchanged for times much longer than the stem cell generation. This suggests that stable niche-like structures can be formed even in the presence of any external spatial signals.

We quantify this remarkable stability by the autocorrelation function for density fluctuations of S cells, given by $\Pi_S(t) = \langle \Delta\rho_S(\boldsymbol{r}, t_0 + t) \cdot \Delta\rho_S(\boldsymbol{r}, t_0)\rangle_{\boldsymbol{r},t_0}$, with $\Delta\rho_S(\boldsymbol{r}, t) = \rho_S(\boldsymbol{r}, t) - \rho_S^H$ in subvolumes of size $1R_{PP}^2$. As a guide, we compare the decay with a system of non-interacting Brownian particles, with diffusion coefficients derived from the single stem cell motion (see below). In the stem cell rare tissue, we find much slower decorrelation, evidencing more stable structures. On the other hand, in the stem cell rich tissue, density fluctuations decorrelate quicker than the passive system.

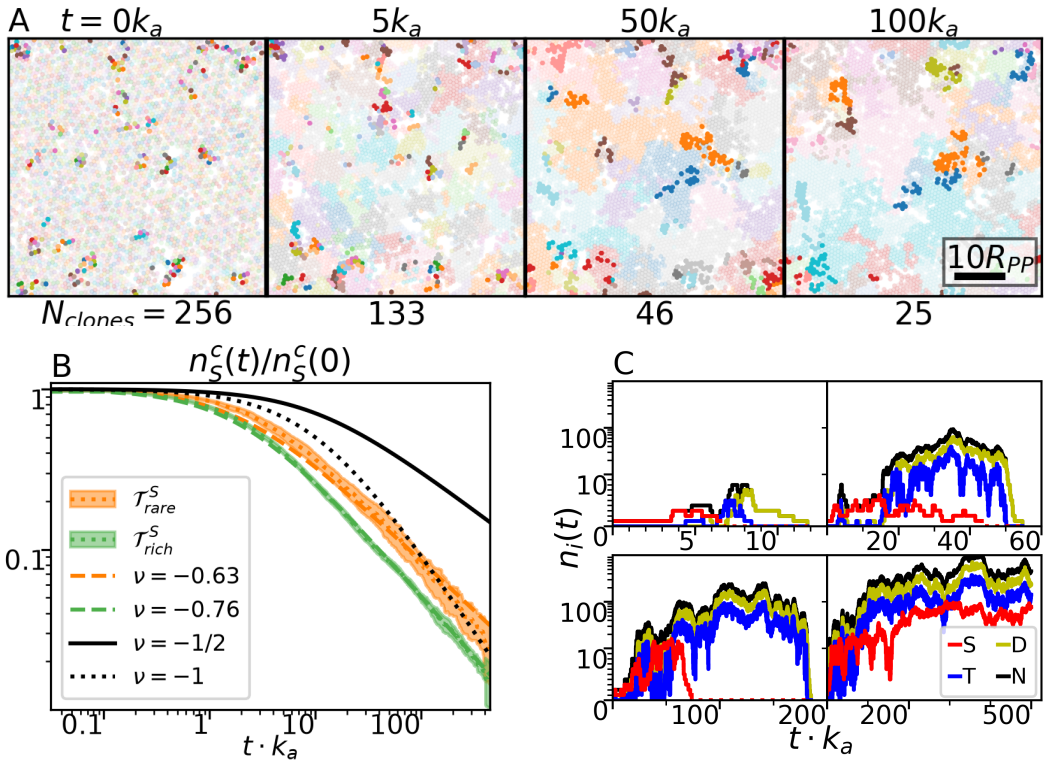

Figure 3.5.2: Lineage tracing in mechanical simulations. (A) Example of tissue clone evolution over time, where each clone is shown in different color, with reduced opacity for T and D cells to emphasize the S cell positions. Cells were marked with unique labels in the beginning and pass this over to daughter cells. (B) Fraction of surviving stem cell clones over time. Dotted line shows average over 12 independent runs and filled region standard deviation of clone fraction. $(c_S \cdot t + 1)^\nu$ is shown for different exponents, given in legend, where dashed colored lines are best fit to data of $\mathcal{T}^S_{rare}$and $\mathcal{T}^S_{rich}$. (C) Average number of clones per cluster over time for one short lived clone, two unlasting, and one surviving clone. Note the different time scales.

Additionally, we track individual S cells up to the time of division or differentiation, to quantify the mobility of individual cells. From this data, we calculate the SC mean squared displacement, which is found to be well described by passive diffusion $|\Delta r|^2 = 2dDt$, with dimension $d = 2$ (see Fig. 3.5.1). The diffusion coefficient corresponds to approximately half to one cell size per stem cell generation, consistent with previous simulations of homogeneous, mono-clonal tissues [48]. However, this is in stark contrast to our earlier work, in which we studied a hierarchical scheme with fixed number of symmetric T cell divisions and asymmetric S cell divisions only, where we found superdiffusion of the S cell induced by progeny propulsion. This points out, that the division-differentiation scheme does not only influence the structural properties, but also the dynamics of cells.

Finally, the ability to follow individual cell trajectories enables us to get detailed, time resolved information on the evolution of cell lineages. Similarly to lineage tracing experiments, we label cells in the homeostatic state at a specific time point, and trace their progeny over time. As expected from netural drift, snapshots (see Fig. 3.5.2) reveal, that with time the total number of surviving clones decreases and the size of individual clones increases, as S cell clusters become monoclonal. Interestingly, S and T cells are non-trivially distributed, as clones can extend such that T cell contributions diverge from their S cell origin. This extends our previous, static, analysis confirmed unexpected neighborhood distributions arising from stochasticity and mechanical interactions.

Measuring the clone survival fraction over time (Fig. 3.5.2 B), we find that neutral drift theory, which predicts a decay of $1/(1+c_s t)^{\nu}$, with $\nu = 1$ in two dimensions [30], does not fit the data well. Instead, we can describe the decay better with exponents $\nu = -0.63$ and -0.76 for the stem cell rare and rich tissues, respectively, which hints to the fact that mechanical interactions create spatio-temporal structures that are not captured well by mean-field analytical approximations. We illustrate this by plotting the temporal evolution of specific clones in Fig. 3.5.2 C. We find that all clones which lose their stem cell eventually go extinct. However, they can exist for an extended period due to T cells , resulting in very long correlations not captured by simple neutral drift, a prediction which could be tested in experiments by combining intravital live-imaging with reporters of cell fate.

3.6 Discussion

Combining analytical theory and minimal mechanical simulations, we map a phase diagram of possible composition for cycling tissues composed of a hierarchy of stem cells, progenitors, and differentiated cells. We uncover how a mechanical regulation of growth can generically give rise to well-defined homeostatic states with different possible cell type fractions, and derive conditions for the stability of each cellular compartment. Agent based simulations confirm these theoretical predictions, but also provide novel insights in the spatial structure and temporal dynamics of stem cell self-organization. In particular, we find, that for low stem cell densities, stable and long range order emerges, even in the absence of external signaling. This order manifests as localized stem cell clusters which are well-spaced from each other and are very stable over time. Furthermore, stochasticity of fate choices, together with our mechanical regulation of growth, result in highly non-trivial neighborhood relationships, with progenitors being statistically further from stem cell clusters than differentiated cells, despite directly originating from stem cells. We contrast these findings with previous results not considering mechanical interactions [21, 28], as well as results without stochastic fate choices [31], which both show very different large-scale spatio-temporal dynamics. In this work, we remained agnostic about the molecular mechanisms underpinning how local pressure changes proliferation. However, how biological cells sense and react to mechanics is an ongoing field of research,

where recent findings suggest that membrane potential serves as a mechanotransductive sensor for pressure and thus regulates growth [42]. Further model extensions could therefore concentrate on understanding how specific models of mechano-sensing impact on global tissue dynamics.

Importantly, extensive experimental work has been done over recent years to extract cellular dynamics and fate choices from snapshots, for instance staining of putative fate markers or lineage tracing methods [6, 30]. For instance, the existence of stem cell clusters in epidermal cultures in vitro has been proposed to be linked to stem cell adhesion [29], although our simulations suggest they could arise without any specific adhesion code. Our neighborhood probability analysis and clone tracing (Fig. 3.4.1 (D-G) & 3.5.2 (A)) also suggests that caution should be taken in simply assuming that neighboring cells are immediate progenies of stem cells, in particular in noisy systems [10]. Overall, combining our simulations with static experimental data should allow to infer, from detailed spatial correlation and tissue structure, some of the key microscopic details of the underlying division and differentiation schemes, which poses a valuable tool to test biological hypotheses. Finally, our simulations also make a number of detailed predictions on the dynamics of stem cell clusters and organization within cycling tissues. Over recent years, advances in intravital imaging have allowed unprecedented insights into the dynamics of renewal, for instance in epidermis or intestine [2, 36, 38, 50, 52, 55]. In particular when combined with live-reporters of cell fate or state, these datasets would be ideal to test our experimental findings, in particular temporal correlations between fate transition and local mechanical properties or relative cell densities, as well as the temporal stability of clusters of different cell types. Recent literature has also shown that different cell types within the same tissue are endowed with very different mechanical properties [39, 51, 57, 59], From a more theoretical perspective, potential future extension of our model could be to generalize it to 3D tissues, for instance skin where differentiation is coupled to stratification to upper layers [51], consider models with cell fate reversibility [21], which can be more flexibility to cellular responses. Finally, considering in our simulations the role of interactions between cells and their micro environment, for instance substrate geometry or stiffness, would likely lead to interesting phase diagram which could be further compared with experiments [11, 14, 19, 34].

Supplementary Information - Chapter 3

3.A Data availability

All original code has been deposited at Zenodo at `https://doi.org/10.5281/zenodo.18245707` and **will be/is** publicly available as of the date of publication. This includes: simulation source code, simulation data, and analysis scipts. We also provide demonstrative animations of selected simulations in this repository. Simulations include:

1. *S1-TissueAnimation-RandomCellLoss*: animated simulation snapshots of $\mathcal{T}^S_{rich}$ with 10% random cell loss.
2. *S2a-TissueAnimation-SCrare*: animated simulation snapshots of $\mathcal{T}^S_{rare}$
3. *S2a-TissueAnimation-SCrich*: animated simulation snapshots of $\mathcal{T}^S_{rich}$
4. *S3-TissueAnimation-CloneTracing*: animated simulation snapshots of clone tracing in $\mathcal{T}^S_{rare}$

3.B Auxiliary information for continuum theory

Setting differentiation rates: In order to tune cell number fractions, we have derived the dependence of $\phi^H_{S,T,D}$ on cell fate rates. In simulations, however, we aim to tune the cell fate rates with a certain configuration in mind. Thus, we rewrite Eq. 3.2 to derive equations for the differentiation rates.

$$\begin{aligned} c_T &= \frac{\phi^H_D}{\phi^H_T} k_a = d^H_T + c_S \frac{\phi^H_S}{\phi^H_T} \\ c_S &= d^H_S = \frac{\phi^H_D k_a - \phi^H_T d^H_T}{\phi^H_S}. \end{aligned} \tag{3.3}$$

Note that the T cell division rate is not a simulation parameter, but follows the mechanical properties of cells, and thus requires accurate adjustment of parameters like for example the growth coefficients $G_{S.T}$.

Pressure dependence of division rates: In first order, we can expand the S and T cell division rates as a function of pressure $\mathcal{P}$ as

$$\begin{aligned} d_S(\mathcal{P}) &= d^0_S - \delta_S \left(\mathcal{P} - \mathcal{P}^0\right) \\ d_T(\mathcal{P}) &= d^0_T - \delta_T \left(\mathcal{P} - \mathcal{P}^0\right), \end{aligned} \tag{3.4}$$

where $d^0_{S,T}$ is the division rate of the system at pressure $\mathcal{P}^0$, an arbitrary expansion point. In homeostasis ($c_S = d_S$), we consequently can rewrite the first equation as $\mathcal{P}^H - \mathcal{P}^0 = (d^0_S - c_S)/\delta_S$. Inserting this into $d_T(\mathcal{P}^H)$ yields $d^H_T = d^0_T + \delta_T/\delta_S\,(c_S - d^0_S)$.

Average number of T cell cycles: In Sec. 3.4 and Fig. 3.4.1 D-G we compare the stochastic differentiation model with a deterministic differentiation model. In the latter, the number of T cell cycles is set by a hard-coded variable N_T, such that T cells, which have divided N_T times, terminally differentiate automatically. In order to compare both systems, we need to chose an integer N_T, that results in comparable cell number fractions. The number of T cells produced per S cell division in the stochastic model can be derived from the T cell number balance equation $0 = c_S \cdot 1 + (d^H_T - c_S) n_T$. Consequently, $n_T = c_S/(c_S - d^H_T)$ T cells are produced per S cell division. In the deterministic model, on the other hand, we have shown that each stem cell division can produce 2^{N_T} T cells. Thus, we have to set $N_T = \log_2(c_S/(c_T - d^H_T))$, where dT^H is measured in simulations. For $\mathcal{T}^S_{rare}$, we set $N_T = 6$ in the deterministic model with slow cycling stem cells. For fast cycling stem cells, we cannot estimate the number, but have to test it via simulations, and find that $N_T = 3$ results in comparable cell number fractions.

3.C Two particle growth model (2PG) and simulation setup

The different stem cell differentiation models described in the main text are implemented in the two-particle growth (2PG) model of Refs. [4, 46] and has been adapted in Refs. [7, 8, 18, 31]. In the following, we requote the description already presented in [31] and extend it where needed.

Each cell is described by two particles, which repel each other via an active growth force

$$F^{(G)}_{ij} = \frac{G}{(r_{ij} - r_0)^2} \hat{\boldsymbol{r}}_{ij} \tag{3.5}$$

with unit vector $\hat{\boldsymbol{r}}_{ij}$, distance r_{ij} between the two particles, a constant r_0, and growth strength G. For non-growing cells, like D cells, the growth strength is set to zero, $G_D = 0$.

To prevent overlap of cells, particles of different cells interact via a soft repulsive volume-exclusion force

$$\boldsymbol{F}^{(V)}_{ik} = f_0 \left(\frac{R^5_{PP}}{r^5_{ik}} - 1 \right) \hat{\boldsymbol{r}}_{ij}, \text{ for } r_{ik} < R_{PP} \tag{3.6}$$

with exclusion strength f_0 and interaction length R_{PP}, which sets the length scale of our simulations. Further, cells in contact interact via an attractive adhesion force of the form

$$\boldsymbol{F}^{(V)}_{ik} = -f_1 \hat{\boldsymbol{r}}_{ik}, \text{ for } r_{ik} < R_{PP} \tag{3.7}$$

with adhesion strength f_1.

We employ a dissipative particle dynamics-type thermostat [26], with an effective temperature T, to account for energy dissipation

$$F_{ij}^{(D)} = \gamma \cdot \left(1 - \frac{dr}{rt}\right)^2 \cdot (\boldsymbol{v}_{ij} \cdot \hat{\boldsymbol{r}}_{ij})\, \hat{\boldsymbol{r}} \tag{3.8}$$

and random fluctuations

$$F_{ij}^{(R)} = \sigma\xi \cdot \hat{\boldsymbol{r}}_{ij} \tag{3.9}$$

where γ and σ are related to fulfill the fluctuation-dissipation theorem [16]. Also, background dissipation is taken into account as

$$\boldsymbol{F}_i^B = -\gamma_b \boldsymbol{v}_i. \tag{3.10}$$

A self-consistent velocity-Verlet algorithm [43] is implemented to integrate the equations of motion, and all simulations were performed with periodic boundary conditions in 2D.

Cell division is performed, when the two particles of one cell are separated by a critical threshold R_{ct}. A new particle is randomly placed near each original particle in a distance R_d, and the two new particle pairs form the two daughter cells. For the model described in Fig. 3.2.1, differentiation is implemented as stochastic process with fixed rates c_S and c_T. In the deterministic model discussed in Sec. 3.4, differentiation takes place at the time of division, where for T cells an internal variable tracks the number of divisions and triggers terminal differentiation, when the maximum number of divisions is reached.

D cells are stochastically removed from the simulation with a finite apoptosis rate k_a. Time is measured in terms of the inverse apoptosis rate, and referred to as "generation".

In addition to the tissue specific parameters given in the table in Fig. 3.3.1, the standard parameter set for our simulations are given in Tab. 3.C.1. However, not all of these simulation parameters, have a direct conversion to physical units. As discussed in [4] one has to chose well defined measurable quantities, such as apoptosis rate and range of the pair potential as rescaling units for inverse time and particle diameter, to allow for conversion to physical units and comparison with experiments.

As simulation for large areas have high computational cost, we performed the screening of the parameter space in smaller areas of size $50R_{PP} \times 50R_{PP}$ for 500 generations, starting with a random cell configuration with 10 % stem cells. Large tissues of size $200R_{PP} \times 200R_{PP}$ were simulated by patches of these smaller simulations. Care has been taken, that patches are not correlated, when stitched together, and that the system equilibrates before measurements are conducted (see below).

3.C.1 Brownian dynamics simulations

In the main text (Sec. 3.5), we compare results obtained with the agent based model with a passive Brownian particle (BP) model to understand the difference in static and

Table 3.C.1: Standard parameter set of agent based tissue simulations.

Parameter	Symbol	Value
Time step	Δt	0.001
Pair potential interaction range	R_{PP}	1
Cell expansion constant	r_0	1
Division distance threshold	R_{ct}	0.8
New cell particle initial distance	R_d	10^{-5}
Mass	m	1
Intra-cell dissipation coefficient	γ_c^{ST}, γ_c^D	$2G_{ST}$, $2G_T$
Inter-cell dissipation coefficient	γ_t	50
Background dissipation coefficient	γ_c	0.1
Apoptosis rate	k_a	0.01
Noise intensity	k_BT	0.1
Repulsive cell-cell potential coefficient	f_0	2.39566
Attractive cell-cell potential coefficient	f_1	10.0

dynamic properties. The BP model diffusion is simulated by solving the differential equation

$$\partial_t \boldsymbol{r}(t) = \sqrt{2D}\xi(t) \tag{3.11}$$

with diffusion coefficient D obtained from measurements of the stem cell MSD in the 2PG model and ξ describing white noise, which is mean centered $\langle \xi(t) \rangle_t = 0$ and uncorrelated $\langle \xi(t)\xi(t') \rangle = \delta(t - t')$.

3.D Parameter selection: Growth rate variation

In Sec. 3.2 of the main text, we showed how the differentiation rates of S and T cells change the cell number fractions. Further, the theory predicts that also the T cell division rate d_T does affect these ratios. Above, we have seen, that mechano-response ($\delta_{S,T}$) of different cell types shows mutual interference. To highlight that division rates adjust as a consequence of the mechanical interactions, we vary the stem cell growth coefficient, keeping G_T and γ_c^S/G_S constant. Again, we find good agreement of simulations and prediction from the cell number balance equations (see Fig. 3.D.1 (A)&(B)), and how G_S allows to fine tune the T cell division rate, due to change in pressure. Also, division rates and pressure change in the same fashion as discussed in the main text (see Fig. 3.D.1 (C)&(D)).

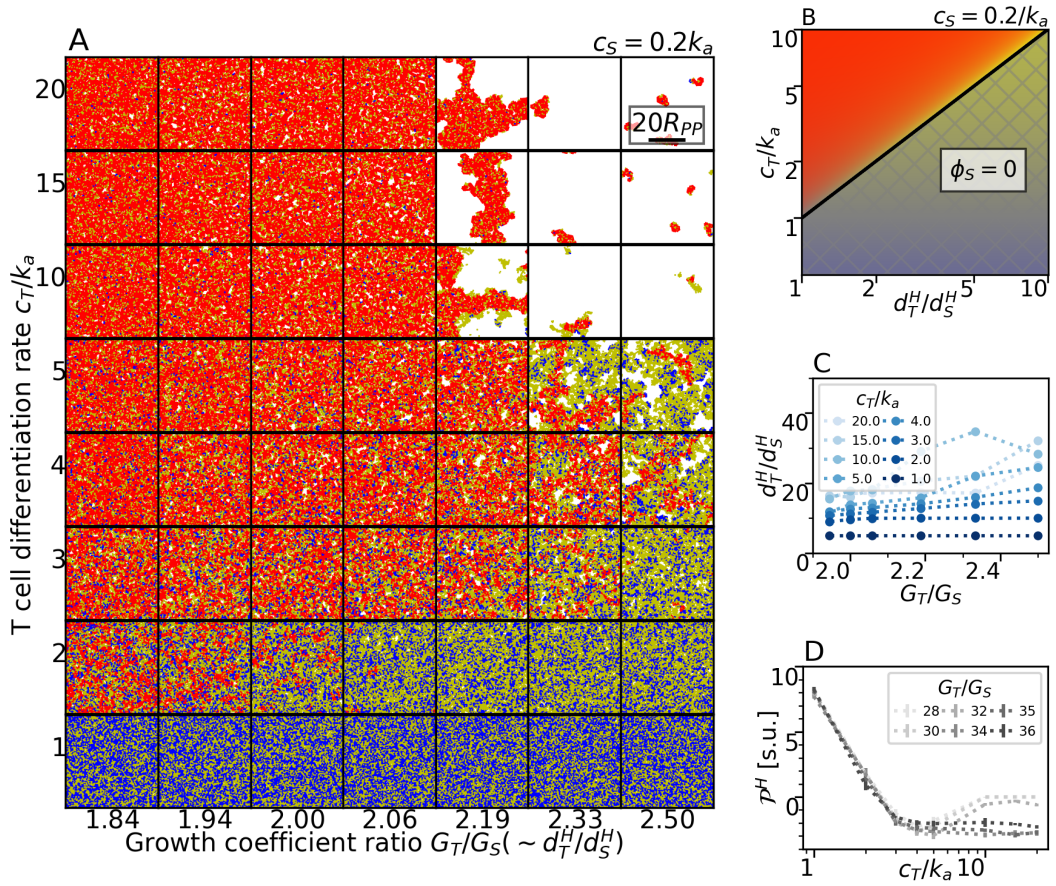

Figure 3.D.1: Parameter sweep division rate and growth coefficient. (A) Simulation snapshot phase space for $G_S - c_T$ variation, (B) corresponding phase diagram for cell number fractions from Eq. 3.2, (C) T cell division rate, and (D) homeostatic pressure for measurements in (A).

3.E Additional tissue configurations to show robustness of main text results and observables

We utilize several observables, which we define here in addition with results for three more tissues, to show the robustness of our results (see Fig. 3.E.1). Beside another stem cell rare $\mathcal{T}^{S\prime}_{rare}$and rich $\mathcal{T}^{S\prime}_{rich}$tissue, we also select a tissue of intermediate stem cell fraction. The intermediate tissue is very similar to $\mathcal{T}^{S\prime}_{rare}$, only differing only in the stem cell growth coefficient by less than 2%, which already leads to a doubling of the S cell fraction.

Stem cell rare II ($\mathcal{T}^{S\prime}_{rare}$)		Stem cell mid ($\mathcal{T}^{S}_{intermed}$)		Stem cell rich II ($\mathcal{T}^{S\prime}_{rich}$)	
$c_S = 0.2k_a$	$\phi_S^H = 5.9\%$	$c_S = 0.2k_a$	$\phi_S^H = 11.5\%$	$c_S = 0.3k_a$	$\phi_S^H = 26.4\%$
$c_T = 2.0k_a$	$\phi_T^H = 30.9\%$	$c_T = 2.0k_a$	$\phi_T^H = 29.0\%$	$c_T = 3.0k_a$	$\phi_T^H = 11.8\%$
$G_T = 2.03G_S$	$\phi_D^H = 63.2\%$	$G_T = 2.00G_S$	$\phi_D^H = 59.5\%$	$G_T = 2.00G_S$	$\phi_D^H = 60.8\%$
$d_T^H = 9.8d_S$	$\mathcal{P}^H = 1.64$	$d_T^H = 9.56d_S$	$\mathcal{P}^H = 1.43$	$d_T^H = 7.7d_S$	$\mathcal{P}^H = -2.55$
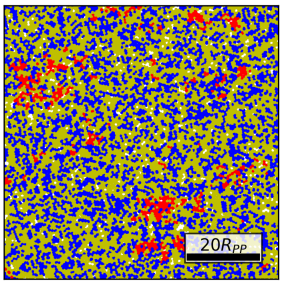		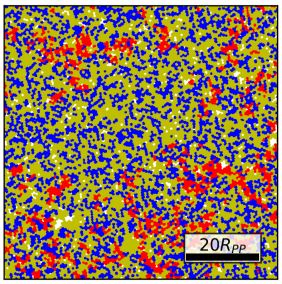		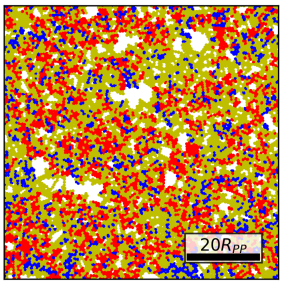	

Figure 3.E.1: Additional stem cell rare ($\mathcal{T}^{S\prime}_{rare}$, left) and rich ($\mathcal{T}^{S\prime}_{rich}$, right) tissues and an intermediate tissue ($\mathcal{T}^{S}_{intermed}$, middle) to show robustness of results. Simulation parameters (c_S, c_T, G_T/G_S) and resulting tissue properties (ϕ_S^H, ϕ_T^H, ϕ_D^H, $\mathcal{P}^H$, d_T^H/d_S^H) are given in the table together with a tissue snapshot in steady state. Stem (red), transient (blue), and differentiated (yellow) cells are drawn with cell size set to distance at which attractive and repulsive forces balance, and scale for 20 interaction radii R_{PP} is given.

3.E.1 Static properties

Pair correlation function $g(r)$ The pair correlation function measures the likelihood to find two particles at a distance r. It is defined as

$$g(r) = \left\langle \sum_{m,n\neq m}^{n_S(t)} \Theta_H\left(r - r_{mn}(t_i)\right)\Theta_H\left(r_{mn}(t_i) - (r+\delta r)\right)/\Omega(r,t) \right\rangle_t , \tag{3.12}$$

where $r_{mn}(t_i) = |\boldsymbol{r}_m(t_i) - \boldsymbol{r}_n(t_i)|$ is the pair distance, using the center of mass of cells, Θ_H Heaviside functions, used to construct a measurement annulus of width δr, and Ω a normalization factor given by

$$\Omega(r,t) = L_{XY}^2/[4(n_S(t)-1)((r+\delta r)^2 - r^2)].$$

For randomly distributed particles $g(r) = 1$, which is why we display $g(r) - 1$ in Fig. 3.3.1 (A)+3.E.2 (A). While we employ the pair correlation function for stem cell pairs, it can be generally be used to measure the pair correlation of other particle types, or cross type correlations.

In both stem cell rare tissues, and also in the tissue with intermediate stem cell fraction, we find a strong accumulation at short distances and depletion afterwards. However, the process is not as distinct for intermediate stem cell fraction, suggesting that niche formation is a feature which gets more pronounced with reduced stem cell

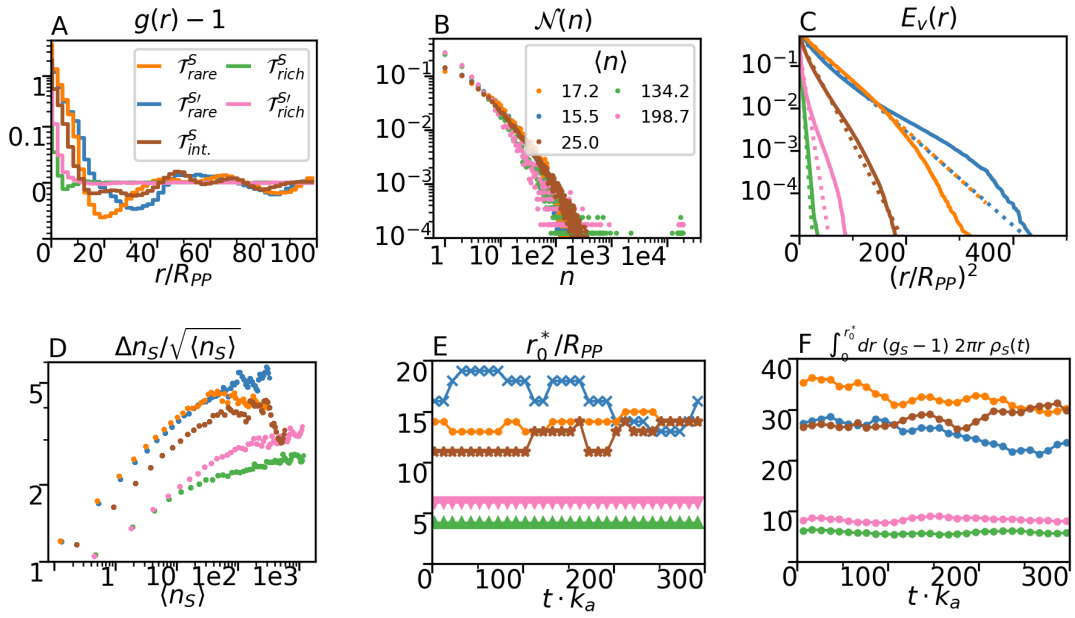

Figure 3.E.2: Niche formation and static structure. Niche formation in tissues of different stem cell densities, as described in the legend in subplot (A). (A) Pair correlation function, (B) cluster size distribution function, and (C) void exclusion function as shown in Fig. 3.4.1 in the main text. (D) shows the number fluctuations over mean cell numbers and (E) the first root of $g(r) - 1$ and (F) the integral of $(g(r) - 1)2\pi r\rho(r)$ from zero to this value.

fraction.

To quantify the short range excess of particles, we calculate the integral

$$\mathcal{I}_g = 2\pi \int_0^{r_0^*} [g(r) - 1]\, \rho(r)\; dr, \tag{3.13}$$

where r_0^* is the first root of $g(r) = 1$ and $\rho(r)$ the particle density, i.e. stem cell density.

Both, the first root r_0^* and integral $\mathcal{I}_g$ are shown as function of time, i.e. calculated for individual snapshots, in Fig. 3.E.2 (E)&(F). This acts as measure of coarsening of the system, i.e. how structure shapes over time. We do not find any variation for the stem cell rich tissues. In stem cell rare tissues, we do see small changes on very long times caused by the steady state fluctuations, which become more visible at reduced S cell densities. However, there is no clear trend towards a coarsening of structures, as independent simulations confirm. Also, the intermediate configuration does not show clear indications for coarsening on the already long times simulated for all tissues. While the presented data to confirm absence of coarsening is shown from aggregated S cell distance data of four subsequent frames, spanning 10 D cell generations, we also looked in data of each independent snapshot and could not find any difference,

except that noise increases for lower statistics.

Clustering We calculate the cluster size distribution function

$$\mathcal{N}(n) = n \cdot p(n), \tag{3.14}$$

where n is the cluster size and $p(n)$ the probability to find a cluster of size n (see Fig. 3.E.2 (B)). Clusters are searched using the `DBSCAN` algorithm with a cluster distance threshold of $2R_{PP}$ as implemented in [44].

Similar to the effective repulsion quantified via the pair correlation function, cluster sizes do increase with stem cell fraction, until percolated structures can be found for the stem cell rich tissues. For higher stem cell fractions, percolation eventually leads to the absence of isolated stem cells. However, clusters sizes are not proportional to the stem cell fraction and grow slower in size.

Void exclusion function All previously discussed quantities are measured from particle positions. In simulations, however, we find that in particular the existence of large stem cell free regions is a remarkable feature. To quantify this, we measure the distance to the closest stem cell from a randomly chosen point. For each snapshot, we chose as many random points as stem cells and from the distance array construct the complementary cumulative distribution function ($cCDF_V$, see Fig. 3.E.2 (C)). In Fig. 3.3.1, we show the percentiles for individual snapshots, and in addition calculate the $cCDF_V$ from the distances of all snapshots combined to highlight how the analysis of individual snapshots can differ at low S cell densities.

Number fluctuations Accumulation of SCs can further be analyzed by the number fluctuations: For increasing size of square subvolumes, we measure the particle number and its variance. Then, the variance divided by the square root of the mean number is plotted over the mean particle number (see Fig. 3.E.2 (D)). When particles are randomly distributed, the variance is expected to grow with the square root of the mean number, and thus should be constant at unity. In tissue simulations, we do find that stem cell number fluctuations are increased by a factor up to approximately five. Above subvolume lengths of approximately $20R_{PP}$, fluctuations begin to flatten. The broader and lower peak for higher SC-densities in turn is consistent with limited aggregation of SCs. Generally, the increase of fluctuations on short lengths and plateau at larger distances supports our finding of long range order and global homeostasis.

Neighborhood analysis We show simulation results for different microscopic models, which all result in the same homeostatic cell number fractions (see Sec.3.4 - Fig. 3.3.1). However, the local configurations are not the same. This is quantified via a neighborhood likelihood composition. First, we perform a Delaunay triangulation, i.e. a graph connecting cell centers, for all cells to construct a neighbor list for each cell. Then, we recursively generate nearest, next-nearest, and second-next-nearest neighbor lists. To

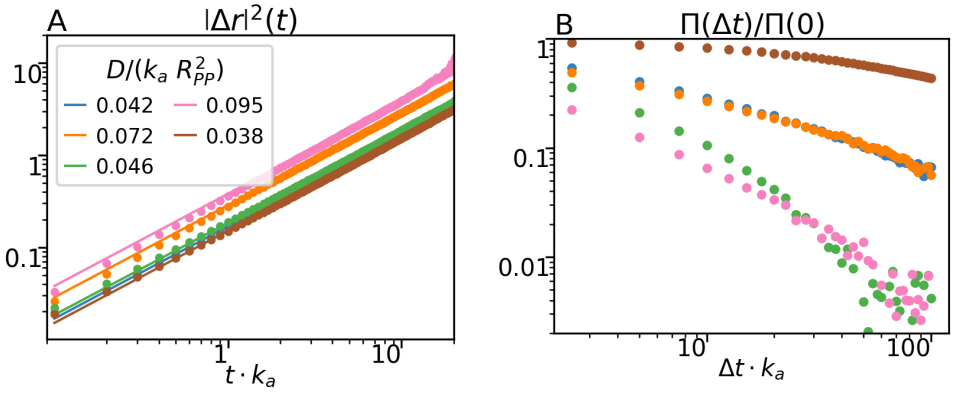

Figure 3.E.3: MSD and Density fluctuations. (A) Stem cell dynamics (MSD) and (B) stem cell density fluctuation correlation function in tissues of different stem cell densities (colors as in Fig. 3.E.2).

avoid overcounting for higher order neighbors, we utilize an exclusion list, in which we store the cells already counted at lower order. Finally, we merge these neighbor lists to calculate the average fraction of S, T, and D cells in first to third order around stem cells. Data from all stem cells of multiple simulation frames is aggregated. To visualize the results, we select an exemplary tissue section and visualize cells via a Voronoi diagram with the usual color coding and increasing shading for higher order neighbors.

3.E.2 Dynamic properties

Mean squared displacement For each tissue configuration, we find the mean squared displacement in the same order of magnitude, around half a cell diameter per S cell generation (see Fig. 3.E.3 (A)). Also, in each tissue a linear slope describes the data well, confirming that no superdiffusive behavior is found.

Density fluctuation autocorrelation and conditional probability From the stem cell trajectories, we measure local stem cell densities in small boxes of edge length $1R_{PP}$. Then, we calculate the difference $\Delta\rho_S(\boldsymbol{r},t) = \rho_S(\boldsymbol{r},t) - \rho_S^H$ between local $\rho_S(\boldsymbol{r},t)$ and global ρ_S^H stem cell density for all subvolumes of the whole simulation volume (see Fig. 3.E.3 (B)).

We find the most stable stem cell niches for the intermediate tissue. In contrast to the stem cell rare tissues, the slight increase in stem cell density paired with slow dynamics seems to stabilize niches. Stem cell rich tissues show fast decorrelation, but also have the fastest differentiation dynamics.

References

[1] B. Alric, C. Formosa-Dague, E. Dague, L. J. Holt, and M. Delarue. Macromolecular crowding limits growth under pressure. *Nature Physics*, 18(4):411–416, Feb. 2022. ISSN 1745-2481. doi: 10.1038/s41567-022-01506-1. URL http://dx.doi.org/10.1038/s41567-022-01506-1.

[2] M. Azkanaz, B. Corominas-Murtra, S. I. J. Ellenbroek, L. Bruens, A. T. Webb, D. Laskaris, K. C. Oost, S. J. A. Lafirenze, K. Annusver, H. A. Messal, S. Iqbal, D. J. Flanagan, D. J. Huels, F. Rojas-Rodríguez, M. Vizoso, M. Kasper, O. J. Sansom, H. J. Snippert, P. Liberali, B. D. Simons, P. Katajisto, E. Hannezo, and J. van Rheenen. Retrograde movements determine effective stem cell numbers in the intestine. *Nature*, 607 (7919):548–554, July 2022. ISSN 1476-4687. doi: 10.1038/s41586-022-04962-0. URL http://dx.doi.org/10.1038/s41586-022-04962-0.

[3] M. Basan, T. Risler, J. Joanny, X. Sastre-Garau, and J. Prost. Homeostatic competition drives tumor growth and metastasis nucleation. *HFSP Journal*, 3(4):265–272, Aug. 2009. ISSN 1955-2068. doi: 10.2976/1.3086732. URL http://dx.doi.org/10.2976/1.3086732.

[4] M. Basan, J. Prost, J.-F. Joanny, and J. Elgeti. Dissipative particle dynamics simulations for biological tissues: rheology and competition. *Physical Biology*, 8(2):026014, Apr. 2011. ISSN 1478-3975. doi: 10.1088/1478-3975/8/2/026014. URL http://dx.doi.org/10.1088/1478-3975/8/2/026014.

[5] J. Beumer and H. Clevers. Hallmarks of stemness in mammalian tissues. *Cell Stem Cell*, 31(1):7–24, Jan. 2024. ISSN 1934-5909. doi: 10.1016/j.stem.2023.12.006. URL http://dx.doi.org/10.1016/j.stem.2023.12.006.

[6] C. Blanpain and B. D. Simons. Unravelling stem cell dynamics by lineage tracing. *Nature Reviews Molecular Cell Biology*, 14(8):489–502, July 2013. ISSN 1471-0080. doi: 10.1038/nrm3625. URL http://dx.doi.org/10.1038/nrm3625.

[7] T. Büscher, A. L. Diez, G. Gompper, and J. Elgeti. Instability and fingering of interfaces in growing tissue. *New Journal of Physics*, 22(8):083005, Aug. 2020. ISSN 1367-2630. doi: 10.1088/1367-2630/ab9e88. URL http://dx.doi.org/10.1088/1367-2630/ab9e88.

[8] T. Büscher, N. Ganai, G. Gompper, and J. Elgeti. Tissue evolution: mechanical interplay of adhesion, pressure, and heterogeneity. *New Journal of Physics*, 22(3):033048, Mar. 2020. ISSN 1367-2630. doi: 10.1088/1367-2630/ab74a5. URL http://dx.doi.org/10.1088/1367-2630/ab74a5.

[9] E. Clayton, D. P. Doupé, A. M. Klein, D. J. Winton, B. D. Simons, and P. H. Jones. A single type of progenitor cell maintains normal epidermis. *Nature*, 446(7132):185–189, Feb. 2007. ISSN 1476-4687. doi: 10.1038/nature05574. URL http://dx.doi.org/10.1038/nature05574.

[10] B. Corominas-Murtra, C. L. G. J. Scheele, K. Kishi, S. I. J. Ellenbroek, B. D. Simons, J. van Rheenen, and E. Hannezo. Stem cell lineage survival as a noisy competition for niche access. *Proceedings of the National Academy of Sciences*, 117(29):16969–16975, July 2020. ISSN 1091-6490. doi: 10.1073/pnas.1921205117. URL http://dx.doi.org/10.1073/pnas.1921205117.

[11] A. M. Cozzolino, V. Noce, C. Battistelli, A. Marchetti, G. Grassi, C. Cicchini, M. Tripodi, and L. Amicone. Modulating the substrate stiffness to manipulate differentiation of resident liver stem cells and to improve the differentiation state of hepatocytes. *Stem Cells International*, 2016(1), Jan. 2016. ISSN 1687-9678. doi: 10.1155/2016/5481493. URL http://dx.doi.org/10.1155/2016/5481493.

[12] M. Delarue, F. Montel, O. Caen, J. Elgeti, J.-M. Siaugue, D. Vignjevic, J. Prost, J.-F. Joanny, and G. Cappello. Mechanical control of cell flow in multicellular spheroids. *Physical Review Letters*, 110(13), Mar. 2013. ISSN 1079-7114. doi: 10.1103/physrevlett.110.138103. URL http://dx.doi.org/10.1103/PhysRevLett.110.138103.

[13] M. Delarue, F. Montel, D. Vignjevic, J. Prost, J.-F. Joanny, and G. Cappello. Compressive stress inhibits proliferation in tumor spheroids through a volume limitation. *Biophysical Journal*, 107(8):1821–1828, Oct. 2014. ISSN 0006-3495. doi: 10.1016/j.bpj.2014.08.031. URL http://dx.doi.org/10.1016/j.bpj.2014.08.031.

[14] Z. Dunajova, S. Tasciyan, J. Majek, J. Merrin, E. Sahai, M. Sixt, and E. Hannezo. Substrate heterogeneity promotes cancer cell dissemination through interface roughening. *bioRxiv*, May 2025. doi: 10.1101/2025.05.20.655037. URL https://www.biorxiv.org/content/early/2025/09/25/2025.05.20.655037.

[15] G. T. Eisenhoffer, P. D. Loftus, M. Yoshigi, H. Otsuna, C.-B. Chien, P. A. Morcos, and J. Rosenblatt. Crowding induces live cell extrusion to maintain homeostatic cell numbers in epithelia. *Nature*, 484(7395):546–549, Apr. 2012. ISSN 1476-4687. doi: 10.1038/nature10999. URL http://dx.doi.org/10.1038/nature10999.

[16] P. Español and P. Warren. Statistical Mechanics of Dissipative Particle Dynamics. *Europhysics Letters (EPL)*, 30(4):191–196, May 1995. ISSN 0295-5075, 1286-4854. doi: 10.1209/0295-5075/30/4/001. URL https://iopscience.iop.org/article/10.1209/0295-5075/30/4/001.

[17] E. Fuchs and T. Chen. A matter of life and death: self-renewal in stem cells. *EMBO reports*, 14(1):39–48, Dec. 2012. ISSN 1469-3178. doi: 10.1038/embor.2012.197. URL http://dx.doi.org/10.1038/embor.2012.197.

[18] N. Ganai, T. Büscher, G. Gompper, and J. Elgeti. Mechanics of tissue competition: interfaces stabilize coexistence. *New Journal of Physics*, 21(6):063017, June 2019. ISSN 1367-2630. doi: 10.1088/1367-2630/ab2475. URL http://dx.doi.org/10.1088/1367-2630/ab2475.

[19] M. Grelier, C. U. Martin, M. Milas, L. Bruskin-Pevzner, Y. Segal, M. Ramani, L. Nuić, G. Le Saux, A.-S. Smith, and M. Schvartzman. Heterogeneity in environmental stiffness alone can guide cells and shape tissues. *bioRxiv*, Oct. 2025. doi: 10.1101/2025.10.10.681597. URL https://www.biorxiv.org/content/early/2025/10/10/2025.10.10.681597.

[20] P. Greulich. Quantitative modelling in stem cell biology and beyond: How to make best use of it. *Current Stem Cell Reports*, 9(4):67–76, Dec. 2023. ISSN 2198-7866. doi: 10.1007/s40778-023-00230-7. URL http://dx.doi.org/10.1007/s40778-023-00230-7.

[21] P. Greulich and B. D. Simons. Dynamic heterogeneity as a strategy of stem cell self-renewal. *Proceedings of the National Academy of Sciences*, 113(27):7509–7514, June 2016. ISSN 1091-6490. doi: 10.1073/pnas.1602779113. URL http://dx.doi.org/10.1073/pnas.1602779113.

[22] S. A. Gudipaty, J. Lindblom, P. D. Loftus, M. J. Redd, K. Edes, C. F. Davey, V. Krishnegowda, and J. Rosenblatt. Mechanical stretch triggers rapid epithelial cell division through piezo1. *Nature*, 543(7643):118–121, Feb. 2017. ISSN 1476-4687. doi: 10.1038/nature21407. URL http://dx.doi.org/10.1038/nature21407.

[23] O. Hallatschek, S. S. Datta, K. Drescher, J. Dunkel, J. Elgeti, B. Waclaw, and N. S. Wingreen. Proliferating active matter. *Nature Reviews Physics*, 5(7):407–419, May 2023. ISSN 2522-5820. doi: 10.1038/s42254-023-00593-0. URL http://dx.doi.org/10.1038/s42254-023-00593-0.

[24] E. Hannezo, J. Prost, and J.-F. Joanny. Growth, homeostatic regulation and stem cell dynamics in tissues. *Journal of The Royal Society Interface*, 11(93):20130895, Apr. 2014. ISSN 1742-5662. doi: 10.1098/rsif.2013.0895. URL http://dx.doi.org/10.1098/rsif.2013.0895.

[25] M. R. Hicks and A. D. Pyle. The emergence of the stem cell niche. *Trends in Cell Biology*, 33(2):112–123, Feb. 2023. ISSN 0962-8924. doi: 10.1016/j.tcb.2022.07.003. URL http://dx.doi.org/10.1016/j.tcb.2022.07.003.

[26] P. J. Hoogerbrugge and J. M. V. A. Koelman. Simulating Microscopic Hydrodynamic Phenomena with Dissipative Particle Dynamics. *Europhysics Letters (EPL)*, 19(3):155–160, June 1992. ISSN 0295-5075, 1286-4854. doi: 10.1209/0295-5075/19/3/001. URL https://iopscience.iop.org/article/10.1209/0295-5075/19/3/001.

[27] M. D. Johnston, C. M. Edwards, W. F. Bodmer, P. K. Maini, and S. J. Chapman. Mathematical modeling of cell population dynamics in the colonic crypt and in colorectal cancer. *Proceedings of the National Academy of Sciences*, 104(10):4008–4013, Mar. 2007. ISSN 1091-6490. doi: 10.1073/pnas.0611179104. URL http://dx.doi.org/10.1073/pnas.0611179104.

[28] D. J. Jörg, Y. Kitadate, S. Yoshida, and B. D. Simons. Stem cell populations as self-renewing many-particle systems. *Annual Review of Condensed Matter Physics*, 12(1):135–153, Mar. 2021. ISSN 1947-5462. doi: 10.1146/annurev-conmatphys-041720-125707. URL http://dx.doi.org/10.1146/annurev-conmatphys-041720-125707.

[29] A. M. Klein and B. D. Simons. Universal patterns of stem cell fate in cycling adult tissues. *Development*, 138(15):3103–3111, Aug. 2011. ISSN 0950-1991. doi: 10.1242/dev.060103. URL http://dx.doi.org/10.1242/dev.060103.

[30] A. M. Klein, T. Nakagawa, R. Ichikawa, S. Yoshida, and B. D. Simons. Mouse germ line stem cells undergo rapid and stochastic turnover. *Cell Stem Cell*, 7(2):214–224, Aug. 2010. ISSN 1934-5909. doi: 10.1016/j.stem.2010.05.017. URL http://dx.doi.org/10.1016/j.stem.2010.05.017.

[31] J. C. Krämer, E. Hannezo, G. Gompper, and J. Elgeti. Mechanically-driven stem cell separation in tissues caused by proliferating daughter cells. *SciPost Physics*, 16(4), Apr. 2024. ISSN 2542-4653. doi: 10.21468/scipostphys.16.4.097. URL http://dx.doi.org/10.21468/SciPostPhys.16.4.097.

[32] D. Krueger, W. K. Spoelstra, D. J. Mastebroek, R. N. U. Kok, S. Wu, M. Nikolaev, M. Bannier-Hélaouët, N. Gjorevski, M. Lutolf, J. van Es, J. van Zon, S. J. Tans, and H. Clevers. Epithelial tension controls intestinal cell extrusion. *Science*, 389(6764), Sept. 2025. ISSN 1095-9203. doi: 10.1126/science.adr8753. URL http://dx.doi.org/10.1126/science.adr8753.

[33] J. Liu, Q. Xiao, J. Xiao, C. Niu, Y. Li, X. Zhang, Z. Zhou, G. Shu, and G. Yin. Wnt/β-catenin signalling: function, biological mechanisms, and therapeutic opportunities. *Signal Transduction and Targeted Therapy*, 7(1), Jan. 2022. ISSN 2059-3635. doi: 10.1038/s41392-021-00762-6. URL http://dx.doi.org/10.1038/s41392-021-00762-6.

[34] J. Llewellyn, A. Charrier, R. Cuciniello, E. Helfer, and R. Dono. Substrate stiffness alters layer architecture and biophysics of human induced pluripotent stem cells to modulate their differentiation potential. *iScience*, 27(8):110557, Aug. 2024. ISSN 2589-0042. doi: 10.1016/j.isci.2024.110557. URL http://dx.doi.org/10.1016/j.isci.2024.110557.

[35] G. Mascré, S. Dekoninck, B. Drogat, K. K. Youssef, S. Brohée, P. A. Sotiropoulou, B. D. Simons, and C. Blanpain. Distinct contribution of stem and progenitor cells to epidermal maintenance. *Nature*, 489(7415):257–262, Sept. 2012. ISSN 1476-4687. doi: 10.1038/nature11393. URL http://dx.doi.org/10.1038/nature11393.

[36] D. May, S. Yun, D. G. Gonzalez, S. Park, Y. Chen, E. Lathrop, B. Cai, T. Xin, H. Zhao, S. Wang, L. E. Gonzalez, K. Cockburn, and V. Greco. Live imaging reveals chromatin compaction transitions and dynamic transcriptional bursting during stem cell differentiation in vivo. *eLife*, 12, Mar. 2023. ISSN 2050-084X. doi: 10.7554/elife.83444. URL http://dx.doi.org/10.7554/eLife.83444.

[37] T. Merle, M. Cazales, T. Mangeat, R. Bouzignac, A. Proag, B. Ronsin, C. Rouvière, E. Pitot, and M. Suzanne. Compressive stress drives morphogenetic apoptosis through lateral tension and piezo. *Cell Reports*, 44(9):116161, Sept. 2025. ISSN 2211-1247. doi: 10.1016/j.celrep.2025.116161. URL http://dx.doi.org/10.1016/j.celrep.2025.116161.

[38] K. R. Mesa, K. Kawaguchi, K. Cockburn, D. Gonzalez, J. Boucher, T. Xin, A. M. Klein, and V. Greco. Homeostatic epidermal stem cell self-renewal is driven by local differentiation. *Cell Stem Cell*, 23(5):677–686.e4, Nov. 2018. ISSN 1934-5909. doi: 10.1016/j.stem.2018.09.005. URL http://dx.doi.org/10.1016/j.stem.2018.09.005.

[39] Y. A. Miroshnikova, H. Q. Le, D. Schneider, T. Thalheim, M. Rübsam, N. Bremicker, J. Polleux, N. Kamprad, M. Tarantola, I. Wang, M. Balland, C. M. Niessen, J. Galle, and S. A. Wickström. Adhesion forces and cortical tension couple cell proliferation and differentiation to drive epidermal stratification. *Nature Cell Biology*, 20(1):69–80, Dec. 2017. ISSN 1476-4679. doi: 10.1038/s41556-017-0005-z. URL http://dx.doi.org/10.1038/s41556-017-0005-z.

[40] F. Montel, M. Delarue, J. Elgeti, L. Malaquin, M. Basan, T. Risler, B. Cabane, D. Vignjevic, J. Prost, G. Cappello, and J.-F. Joanny. Stress clamp experiments on multicellular tumor spheroids. *Physical Review Letters*, 107(18), Oct. 2011. ISSN 1079-7114. doi: 10.1103/physrevlett.107.188102. URL http://dx.doi.org/10.1103/PhysRevLett.107.188102.

[41] F. Montel, M. Delarue, J. Elgeti, D. Vignjevic, G. Cappello, and J. Prost. Isotropic stress reduces cell proliferation in tumor spheroids. *New Journal of Physics*, 14(5):055008, May 2012. ISSN 1367-2630. doi: 10.1088/1367-2630/14/5/055008. URL http://dx.doi.org/10.1088/1367-2630/14/5/055008.

[42] A. Mukherjee, Y. Huang, J. Elgeti, S. Oh, J. G. Abreu, L. Ammar, A. R. Neliat, J. Schüttler, D.-D. Su, C. Dupre, N. C. Benites, X. Liu, L. Peshkin, M. Barboiu, H. Stocker, M. W. Kirschner, and M. Basan. Membrane potential mediates the cellular response to mechanical pressure. *Cell*, 189(1):143–160.e22, Jan. 2026. ISSN 0092-8674. doi: 10.1016/j.cell.2025.11.004. URL http://dx.doi.org/10.1016/j.cell.2025.11.004.

[43] I. Pagonabarraga, M. H. J. Hagen, and D. Frenkel. Self-consistent dissipative particle dynamics algorithm. *Europhysics Letters (EPL)*, 42(4):377–382, May 1998. ISSN 0295-5075, 1286-4854. doi: 10.1209/epl/i1998-00258-6. URL https://iopscience.iop.org/article/10.1209/epl/i1998-00258-6.

[44] F. Pedregosa, G. Varoquaux, A. Gramfort, V. Michel, B. Thirion, O. Grisel, M. Blondel, P. Prettenhofer, R. Weiss, V. Dubourg, J. Vanderplas, A. Passos, D. Cournapeau, M. Brucher, M. Perrot, and E. Duchesnay. Scikit-learn: Machine learning in Python. *Journal of Machine Learning Research*, 12:2825–2830, 2011.

[45] J. M. Pita, I. F. Figueiredo, M. M. Moura, V. Leite, and B. M. Cavaco. Cell cycle deregulation andtp53andrasmutations are major events in poorly differentiated and undifferentiated thyroid carcinomas. *The Journal of Clinical Endocrinology & Metabolism*, 99(3):E497–E507, Mar. 2014. ISSN 1945-7197. doi: 10.1210/jc.2013-1512. URL http://dx.doi.org/10.1210/jc.2013-1512.

[46] N. Podewitz, M. Delarue, and J. Elgeti. Tissue homeostasis: A tensile state. *EPL (Europhysics Letters)*, 109(5):58005, Mar. 2015. ISSN 1286-4854. doi: 10.1209/0295-5075/109/58005. URL http://dx.doi.org/10.1209/0295-5075/109/58005.

[47] N. Podewitz, F. Jülicher, G. Gompper, and J. Elgeti. Interface dynamics of competing tissues. *New Journal of Physics*, 18(8):083020, Aug. 2016. ISSN 1367-2630. doi: 10.1088/1367-2630/18/8/083020. URL http://dx.doi.org/10.1088/1367-2630/18/8/083020.

[48] J. Ranft, M. Basan, J. Elgeti, J.-F. Joanny, J. Prost, and F. Jülicher. Fluidization of tissues by cell division and apoptosis. *Proceedings of the National Academy of Sciences*, 107(49):20863–20868, Nov. 2010. ISSN 1091-6490. doi: 10.1073/pnas.1011086107. URL http://dx.doi.org/10.1073/pnas.1011086107.

[49] J. Ranft, M. Aliee, J. Prost, F. Jülicher, and J.-F. Joanny. Mechanically driven interface propagation in biological tissues. *New Journal of Physics*, 16(3):035002, Mar. 2014. ISSN 1367-2630. doi: 10.1088/1367-2630/16/3/035002. URL http://dx.doi.org/10.1088/1367-2630/16/3/035002.

[50] P. Rompolas, K. R. Mesa, K. Kawaguchi, S. Park, D. Gonzalez, S. Brown, J. Boucher, A. M. Klein, and V. Greco. Spatiotemporal coordination of stem cell commitment during epidermal homeostasis. *Science*, 352(6292):1471–1474, June 2016. ISSN 1095-9203. doi: 10.1126/science.aaf7012. URL http://dx.doi.org/10.1126/science.aaf7012.

[51] P. Sahu, S. Monteiro-Ferreira, S. Canato, R. M. Soares, A. Sánchez-Danés, and E. Hannezo. Mechanical control of cell fate decisions in the skin epidermis. *Nature Communications*, 16(1):8440, 2025.

[52] C. L. G. J. Scheele, E. Hannezo, M. J. Muraro, A. Zomer, N. S. M. Langedijk, A. van Oudenaarden, B. D. Simons, and J. van Rheenen. Identity and dynamics of mammary stem cells during branching morphogenesis. *Nature*, 542(7641):313–317, Jan. 2017. ISSN 1476-4687. doi: 10.1038/nature21046. URL http://dx.doi.org/10.1038/nature21046.

[53] H. Shenghui, D. Nakada, and S. J. Morrison. Mechanisms of stem cell self-renewal. *Annual Review of Cell and Developmental Biology*, 25(1):377–406, Nov. 2009. ISSN 1530-8995. doi: 10.1146/annurev.cellbio.042308.113248. URL http://dx.doi.org/10.1146/annurev.cellbio.042308.113248.

[54] S. J. Streichan, C. R. Hoerner, T. Schneidt, D. Holzer, and L. Hufnagel. Spatial constraints control cell proliferation in tissues. *Proceedings of the National Academy of Sciences*, 111(15):5586–5591, Mar. 2014. ISSN 1091-6490. doi: 10.1073/pnas.1323016111. URL http://dx.doi.org/10.1073/pnas.1323016111.

[55] S. Upadhaya, O. Krichevsky, I. Akhmetzyanova, C. M. Sawai, D. R. Fooksman, and B. Reizis. Intravital imaging reveals motility of adult hematopoietic stem cells in the bone marrow niche. *Cell Stem Cell*, 27(2):336–345.e4, Aug. 2020. ISSN 1934-5909. doi: 10.1016/j.stem.2020.06.003. URL http://dx.doi.org/10.1016/j.stem.2020.06.003.

[56] L. Valon, A. Matamoro-Vidal, A. Villars, and R. Levayer. Interfacial tension and growth both contribute to mechanical cell competition. *Current Biology*, 35(21):5372–5383.e4, Nov. 2025. ISSN 0960-9822. doi: 10.1016/j.cub.2025.09.040. URL http://dx.doi.org/10.1016/j.cub.2025.09.040.

[57] C. Villeneuve, A. Hashmi, I. Ylivinkka, E. Lawson-Keister, Y. A. Miroshnikova, C. Pérez-González, S.-M. Myllymäki, F. Bertillot, B. Yadav, T. Zhang, et al. Mechanical forces across compartments coordinate cell shape and fate transitions to generate tissue architecture. *Nature Cell Biology*, 26(2):207–218, 2024.

[58] H. Wang, M. Guo, H. Wei, and Y. Chen. Targeting p53 pathways: mechanisms, structures and advances in therapy. *Signal Transduction and Targeted Therapy*, 8(1), Mar. 2023. ISSN 2059-3635. doi: 10.1038/s41392-023-01347-1. URL http://dx.doi.org/10.1038/s41392-023-01347-1.

[59] S.-L. Xue, Q. Yang, P. Liberali, and E. Hannezo. Mechanochemical bistability of intestinal organoids enables robust morphogenesis. *Nature Physics*, pages 1–10, 2025.

[60] B. Zhang and T. Chen. Local and systemic mechanisms that control the hair follicle stem cell niche. *Nature Reviews Molecular Cell Biology*, 25(2):87–100, Oct. 2023. ISSN 1471-0080. doi: 10.1038/s41580-023-00662-3. URL http://dx.doi.org/10.1038/s41580-023-00662-3.

4 Measuring the dynamic response coefficient of cellular tissues from steady state fluctuations reveals growth induced division rate memory

Abstract

Longevity of multi-cellular systems requires finely tuned feedback to control the balance of cellular proliferation and loss. To understand the microscopic details which control this feedback in homeostasis, it is crucial to quantify the feedback with a robust, minimal invasive method. Existing methods, however, usually depend on perturbation of the system to quantify response. Not only can this change the cell physiology, but also are they difficult to conduct. We propose a novel, steady state fluctuation analysis framework to measure the dynamic response coefficient of cellular tissues. Under the minimal assumption of crowding feedback and Markovian noise, we derive a theoretical framework, which is tested against a simple stochastic simulation, an agent-based mechanical model of tissues growth, and a multi scale model of membrane potential regulated growth. These tests reveal the suitability of using fluctuations to characterize the tissue response. Furthermore, this quantification can help unravel more complex effects, like a memory effects arising from the non-equilibrium nature of growth. Our model opens new avenues to quantify growth parameters in living tissues.

4.1 Introduction

Internal energy consumption and environmental noise continuously drives biological systems out of equilibrium [26, 35]. In order to maintain a stable steady state despite the highly dynamic environment, a robust feedback mechanism is required. However, this feedback is not easily accessible and existing measurement protocols are not only complicated but often invasive. Also, in order to quantify possible changes in dynamic response to perturbations it requires a method to quantify the homeostatic response mode first. Thus, it is importance to develop methods, which are minimal invasive, ideally passive, and still provide quantitatively correct estimates of the response mode.

In thermal equilibrium, fluctuations and response to perturbation are related by the fluctuation-dissipation theorem [11, 25]. Active processes, which internally consume energy, break this relation and can cause differences between active and passive

measurement protocols [39]. Yet, already purely fluctuation based methods, which connect the amplitude of fluctuations with response, can provide insight into the dynamics [37]. In this context, correlation functions are a valuable tool to access information in fluctuating systems [22, 23, 30]. And recently many helpful methods for statistical methods of confined Random walkers have been derived [12, 27, 28]. Yet, these models are derived for ideal systems and the complexity of real world systems require additional efforts to apply them.

The response of cellular tissues is commonly studied by applying external stresses, i.e. perturbing the cells. *In-vitro* this can be done with stretching devices, revealing biomechanical properties of cells [8, 13]. To make these devices compatible with live cell imaging and realize stretching over long periods is challenging. Cyclic stretching devices aim to overcome the limitation of limited stretch duration and in addition probe the mechanoresponse to oscillatory cues, often sensed in the natural environment of cells [34]. Further, realistically engineering the *in-vivo* micro-environment poses difficulties [7]. *In-vivo* stretching has been recently introduced to overcome limitations of *in-vitro* models [3]. However, such methods require surgery, which limits their non-invasiveness.

Here, we present an extension of fluctuation-based response measurements to cellular tissues. First, we derive the population dynamics of a self-renewing cell population with density feedback on the division rate, under the assumption of stochastic apoptosis and division processes close to the homeostatic state. We find, that the resulting model can approximately be mapped on a Brownian particle confined by a harmonic potential. This system is a well studied system, e.g. for beads trapped in optical tweezer. This allows us to apply a number of statistical methods derived earlier to quantify the tissue response coefficient from steady state cell number trajectories. We illustrate this method on data generated from a coarse grained numerical solution of a stochastic ordinary differential equation describing the population dynamics with known ground truth of the response. Further, we test two agent based simulation models of increasing complexity, and compare results against perturbation protocols. From deviations between theory and simulation data, we show how our method can be used to reveal differences in the underlying microscopic mechanisms. We present how advanced theories, like a relaxing memory of the division rate caused by non-Markovian processes, can be identified and resolved within our framework.

Our novel approach to quantitatively measure the systems response relies purely on passive measurements of cell number trajectories, allowing for straightforward, non-invasive implementation.

4.2 Fluctuation response in systems with crowding feedback

Without noise, we write the evolution of a cellular system consisting of N cells of the same cell type as

$$\partial_t N = (k_d - k_a)N = \Delta k N, \tag{4.1}$$

where we denote the net bulk growth rate $\Delta k = k_d - k_a$, which describes the difference of proliferation via division with rate k_d and cell loss, e.g. through apoptosis, with rate k_a. For $\Delta k = 0$, the number of cells remains constant. This state is defined as *homeostatic state*. We also define the cell turnover rate $k_+ = (k_d + k_a)/2$. At homeostasis $k_+ = k_d = k_a$ measures the rate at which cells are replaced. However, division and loss are random events, so even for zero net growth stochastic drift can lead to over- or underpopulation, where the latter may result in extinction. Thus, some form of density-feedback is generally assumed [18, 38]. Recent research indicates that mechano-chemical coupling plays a relevant role for the details of the feedback mechanism [2, 15, 19]. Yet, minimal physics based approaches that assume a simple mechanical relation between division rate and cell density and pressure have been successfully applied to study cellular tissues [4, 29, 33]. Recent work demonstrates how density couples to pressure and membrane potential, which in turn regulates growth via the *HIPPO* pathway [31]. To lowest order around the homeostatic state, density based feedback reads as

$$\Delta k = \varkappa \frac{\rho^H - \rho}{\rho^H}, \tag{4.2}$$

with cell density $\rho = N/V$, ρ^H the homeostatic density, and $\varkappa$ the response coefficient. Combining Eq. 4.2 and Eq. 4.1 yields the logistic equation, with the general solution

$$\rho(t) = \frac{\rho^H}{1 + e^{-\varkappa(t-t_0)}}. \tag{4.3}$$

where t_0 is chosen to satisfy the boundary conditions $\rho(t=0) = \frac{\rho^H}{1+e^{\varkappa t_0}}$. It ignores however the noise, and requires that Eq. 4.2 holds for larger density variations. It is thus ill suited to reliably obtain the response coefficient.

In order to derive a method, which allows us to measure the response in or close to homeostasis, we consistently linearize around homeostasis, and include noise to benefit from a generalized fluctuation-dissipation approach. We derive noise from assuming markovian division and apoptosis, and arrive at (see SI 4.A for details)

$$\partial_t \Delta\rho = -\varkappa \Delta\rho + \sqrt{\frac{2\rho^H k_+}{V}}\eta(t) \tag{4.4}$$

with $\Delta\rho = (\rho - \rho^H)$, and $\eta(t)$ delta correlated white noise. Note that Eq. 4.4 is identical to the overdamped Langevin equation of an *equilibrium* Brownian particle confined in a harmonic potential with particle position replaced by cell number density, and the spring constant by the division feedback response coefficient $\varkappa$. Noise is not introduced by a finite temperature, but originates from cell turnover, corresponding to a cell density diffusion coefficient $D = \frac{\rho^H k_+}{V}$, which was also found in a different framework [36].

We have thus mapped this highly non-equilibrium system to an effective equi-

librium one, thus enabling the full power of equilibrium dynamics including Boltzmann distribution, the fluctuation dissipation theorem, and more dynamic quantifiers [6, 12, 27, 28] for further analysis. In the remainder of this work, we will harness this power, to provide a method of obtaining effective tissue parameters $(\rho^H, k_+, \varkappa)$ from simple measures of cell number versus time, and to provide additional dynamical quantification to better quantify tissue behavior beyond this simplistic model.

Homeostatic and mean density The *homeostatic density* ρ^H can be directly measured from mean of the cell number trajectory as

$$\rho^H \equiv \langle \rho \rangle = \frac{1}{M} \sum_{i=0}^{M-1} \rho(t_i), \tag{4.5}$$

where M depicts the number of measurement points. Because Eq. 4.4 is symmetric around the homeostatic density, the average correctly predicts the mean. If fluctuations are very large, nonlinearities can play a role (see SI 4.A), and the homeostatic density can deviate from the mean. Because noise scales with V^{-1}, this can be easily avoided by choosing larger measurement volumes. Subsequent data points are however most likely correlated, thus the standard deviation of the mean has to be calculated with care.

Mean squared shift and variance Because cell turnover rate relates to diffusion and the response coefficient to the harmonic confinement, these parameters can be obtained via the short term diffusion and variance, respectively. However, in practice measuring the *mean squared shift* (MSS) is more reliable. We define the MSS analogous to the *mean squared displacement* (MSD), frequently studied to describe dynamics of particle systems, as the MSD in cell density as a function of time, i.e.

$$MSS(\Delta t) = \langle (\Delta\rho(\Delta t))^2 \rangle = \langle (\rho(t+\Delta t) - \rho(t))^2 \rangle \tag{4.6}$$

$$= \frac{2D}{\varkappa} \left(1 - e^{-\varkappa \cdot \Delta t}\right), \tag{4.7}$$

where $\langle \cdot \rangle$ corresponds to time and/or ensemble averages (see Ref. [21] for deriving Eq. 4.7 for a Brownian particle in confinement). For small time differences, noise from cell-turnover dominates and the theory simplifies to the linear relation $\lim_{\Delta t \to 0} MSS(\Delta t) = 2D \cdot \Delta t$. With increasing time difference, feedback constrains the MSS and it reaches a plateau corresponding to twice the variance σ^2, that is $\lim_{\Delta t \to \infty} MSS(\Delta t) = 2D/\varkappa = 2\sigma^2$ (see SI Eq. 4.30). Thus, measuring the MSS, or alternatively the short time diffusion D and variance σ^2, provides us with estimates of the remaining tissue parameters: cell turnover rate $k_{+,D} = VD/\rho^H$ and response rate $\varkappa_\sigma = D/\sigma^2$.

Density Auto Correlation Function An alternative dynamic quantifier is the density fluctuation auto correlation function, given by

$$C_{\Delta\rho}(\Delta t) = \langle(\rho(t+\Delta t) - \rho^H)(\rho(t) - \rho^H)\rangle/\sigma^2 \tag{4.8}$$
$$= e^{-\varkappa\cdot\Delta t}, \tag{4.9}$$

where the relaxation time $\tau = 1/\varkappa$ is given by the response coefficient. This is equivalent to the MSS (see SI Eq. 4.30). For an infinitely long and time-invariant process, either quantity allows to determine the response rate $\varkappa$. However, for finitely long experimental trajectories, or changes in the microscopic details of cellular processes, like division memory effects, differences can arise.

Power Spectral Density Similar to the density auto correlation, the *power spectral density* (PSD), is equivalent to the other dynamic quantities presented above. Indeed, the PSD is defined as the Fourier transform of the pair correlation function, thus, directly connected to the MSS (see SI Eq. 4.26). Again, however, it can provide additional insight in case of deviations and the inverse time emphasizes different scales. Already derived for the analogous Brownian particle system [6], it is given by

$$PSD(f) = \frac{1}{T_{meas}} \left| \int_{-T_{meas}/2}^{T_{meas}/2} dt\rho(t)e^{i2\pi ft} \right|^2 \tag{4.10}$$
$$= \frac{D/2\pi^2}{f_c^2 + f^2} \tag{4.11}$$

with corner frequency $f_c = \varkappa/2\pi$, and discrete (Fourier) frequency $f = q/T_{meas}$, with $q \in \mathbb{N}$ and t_{meas} the measurement time.

Probability density By analogy to the Brownian particle in a harmonic trap, we quickly obtain the probability density to observe a certain cell-number density via the Boltzmann weights.

$$p_{eq}(\rho) = \sqrt{\frac{\varkappa}{\pi 2D}} \exp\left(-\frac{\varkappa}{2D}\left(\frac{\Delta\rho}{\rho^H}\right)^2\right) \tag{4.12}$$

I.e. the probability distribution of density fluctuations are a Gaussian, centered around the homeostatic density with width given by the variance $\sigma^2 = D/\varkappa$. This approximation is valid for sufficiently large response rate and system sizes. For reduced system size or diminished response coefficient, non-linearity becomes relevant and results in a non-Gaussian distribution (see SI 4.A for details) with increased risk of population extinction [1]. The deviation from a Gaussian can be quantified by the skewness $M_3 = \left\langle \left((\rho - \rho^H)/\sigma\right)^3 \right\rangle$ and the excess kurtosis $\tilde{M}_4 = \left\langle \left((\rho - \rho^H)/\sigma\right)^4 \right\rangle - 3$. The Boltzmann statistics adds a static analysis tool to our toolbox to complement

the other dynamic measures.

We thus arrive at a simple procedure to estimate parameters and further analyze tissue behaviour from simple cell-number measurements. In the remainder of this work, we analyze how three different models of increasing complexity behave in this framework, and how a decaying memory kernel can explain deviations.

4.3 Application to growing tissue systems

To test our theory we investigate various different systems. First, we implement stochastic process that we expect to match the stochastic ordinary differential equation (sODE) described by Eq. 4.1&4.2 and integrate the cell number trajectory numerically. For this system, all input parameters are known, and we can evaluate our measurement against the ground truth. Our second test case is data from more complex agent based simulations. We adapt the two-particle growth (2PG) model [5, 33] (see SI 4.B.2 for details) to simulate a growing cell colony in two dimensions. Intercellular mechanical interactions are modelled explicitly and implicitly control the division rate, while apoptosis is modelled in a stochastic process with fixed rate k_a. Lastly, we turn to a sophisticated mechano-electro-osmotic model (see SI 4.B.3 for details). Cells are represented by a Voronoi tessellation, taking into account more complex shape effects. In addition to mechanical forces, membrane potential and internal ion concentration are crucial components for the cell cycle dynamics. In this Voronoi cell membrane potential growth (VMPG) model, coarse grained tissue parameters are not known a priori and due to the complexity of the simulation, system sizes are limited.

4.3.1 Stochastic Model

We implement a stochastic process that closely represents our stochastic ordinary differential equation (sODE) model described by Eq. 4.1&4.2 with well defined tissue parameters. A number of N cells in a volume V evolve over time in discrete (short) time step δt. Cells are lost via a Poisson process with constant apoptosis rate $k_a = k_+(\rho^H)$, while the division rate adapts to fulfill the crowding feedback Eq. 4.2. We integrate the stochastic model for a large variety of apoptosis rates, response coefficients, homeostatic densities, and system sizes, but avoid parameters for which density fluctuations are too large $3\sigma < \rho^H$. Overall, we find that simulations coincide with our theory.

For two different response input coefficients, $\varkappa/k_a = 1$ and $\varkappa/k_a = 10$, the cell density trajectory in the steady state over long time, density probability function $p_{eq}(\rho)$, division rate response to a sudden increase in system volume by 20 % (substrate stretching), MSS, auto-correlation function $C_{\Delta\rho}$, and power spectral density are shown in Fig. 4.3.1 to illustrate the expected behavior, and demonstrate the match between simulations and theory. The analytic predictions discussed in the previous section are shown using the input parameters of the simulation. As expected, the data closely follow the analytic predictions, confirming our calculations.

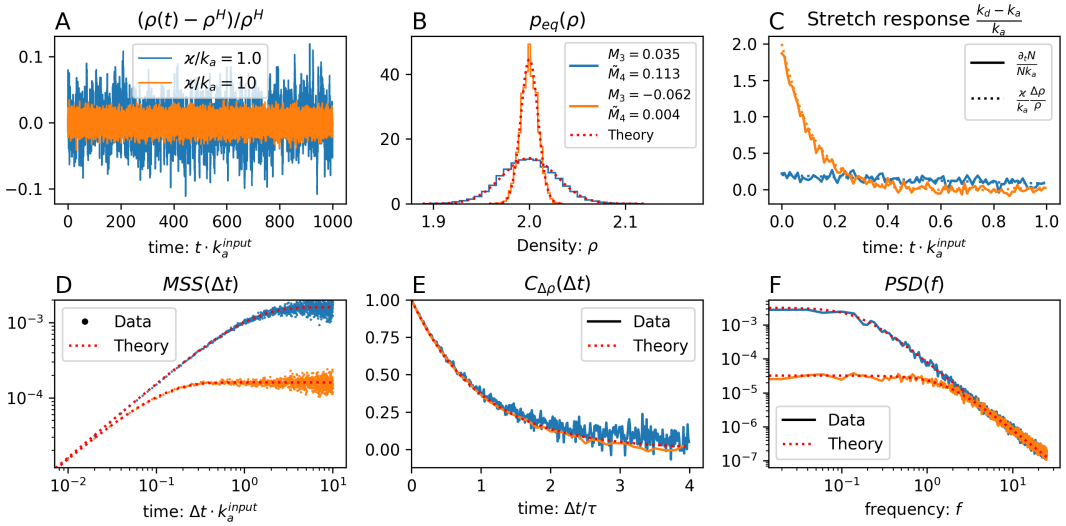

Figure 4.3.1: Analysis of stochastic model trajectories against ground truth. (A) Steady state trajectories of stochastic ODE (sODE) model for two response rates $\varkappa$. (B) Density probability density $p_{eq}(\rho)$ as function of $\Delta\rho = \rho - \rho^H$, skewness M_3 and excess kurtosis $\tilde{M}_4 = M_4 - 3$, where M_4 is the kurtosis, are given in legend. (C) Division rate, measured via Eq. 4.1 (solid lines) and Eq. 4.2 (dotted lines) following 20 % variation of cell density and averaged over 20 realizations. (D) Mean squared displacement of density as a function of time lag and (E) density fluctuation autocorrelation function over time lag rescaled by relaxation time. (D) Power spectral density as function of frequency f. For all figures, two different values of $\varkappa = [1, 10]\, k_a$ are shown in blue and orange, respectively. Simulation were performed with $N^H = 5000$ cells and for target density $\rho^H = 2$, and statistics is aggregated over 1000 generations.

Besides confirming our calculations, these simulations can be used to verify how well these quantifiers can be used to estimate tissue parameters given limited data. Naturally, tissue parameters can be estimated by fitting the described quantifiers, however limited data leads to limited accuracy. The two substantial time scales, apoptosis rate and response rate, of our system lay the data requirements down. Frame rate must be fast enough to resolve the noise contribution, i.e. result in linearity of the short term MSS. Trajectories must be long enough to cover the full decorrelation time τ and reach the plateau of the MSS. Furthermore, the number of measurements or length of measurement trajectory need to be large enough to ensure good statistics, since in particular the variance measurement is sensitive to errors in the measurement of the mean density.

4.3.2 Agent based tissue simulations with mechanical feedback–2PG

Coarse grained models with known input parameters are a valuable tool to illustrate our methodology. However, real systems come with additional layers of complexity, which may influence the behavior. In simulations of the two particle growth (2PG)

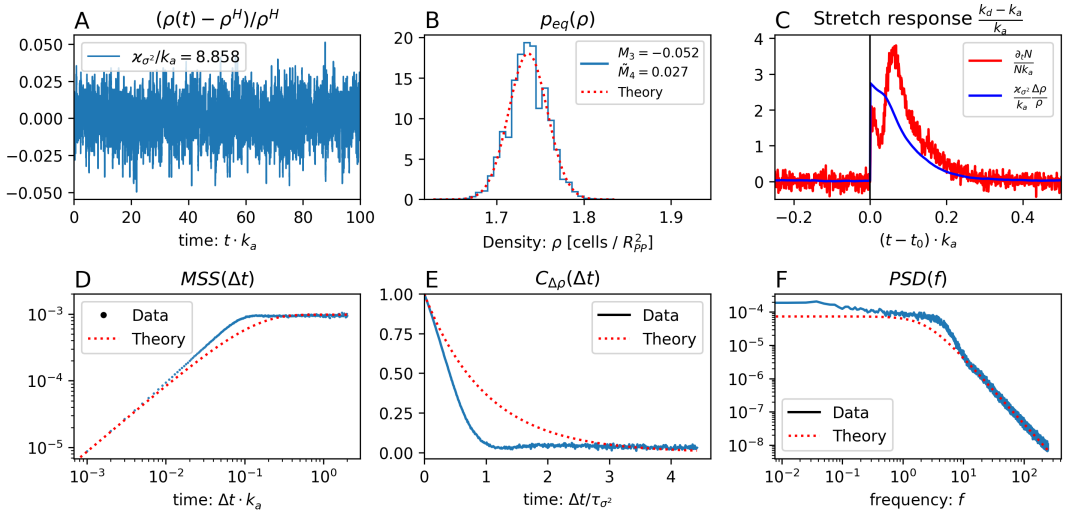

Figure 4.3.2: Fluctuation-response in agent based simulations (A-F) Same as Fig.4.3.1, but measured in the 2PG model, where $\varkappa_{\sigma^2}$ was determined by measuring the variance of density fluctuations and inserted in the same theory equations. (C) Perturbation is realized by stretching the substrate, such that cell density is reduced by $\sim 20\,\%$. Following the stretch, division rate is measured directly from the current cell number change (Eq. 4.1, red line) and as function of density variation (Eq. 4.2, blue line), result is averaged over 20 realizations. Simulations used for statistical analysis (B, D-F) ran for 4000 cell generations with a area of $(20\,R_{PP})^2$, where R_{PP} is the cell interaction radius. The resulting homeostatic cell density is $\rho^H = 1.74\,\text{cells}/R_{PP}$.

model, cells are represented by two point particles. While the apoptosis rate is set, division happens via mechanics. The two particles that represent a biological cell separate by a repulsive force and once a critical distance is reached, the cell divides. Together with mechanical interactions, including excluded volume, attraction, and dissipation, this finite growth force leads to response of the growth on the mechanical environment, resulting in division-apoptosis balance ($k_d = k_a$) at homeostasis. Yet, how cells respond exactly to density fluctuations is not known a priory. Simulations are sufficiently fast, that very long trajectories can be simulated for moderately sized systems, resulting in robust observables (see Fig 4.3.2).

Obtaining the turnover rate via the short term diffusion yields excellent agreement with the known ground truth of the set apoptosis rate k_a. The density distribution is very close to a Gaussian, and symmetric, confirmed by a skewness of $M_3 = -0.052$ and excess kurtosis $\tilde{M}_4 = 0.027$. Thus, the mean can indeed be identified as the homeostatic density. While $\varkappa_\sigma$ is well defined, verification if this estimate corresponds to the response coefficient $\varkappa$ requires more effort:

A conceptually orthogonal approach to measure the response coefficient is by external perturbation of the system. In simulations, density can be modulated by expanding or compressing volume. We utilize a constant volume growth ensemble, in which the volume is rescaled with a small, constant rate β, as well as cell positions

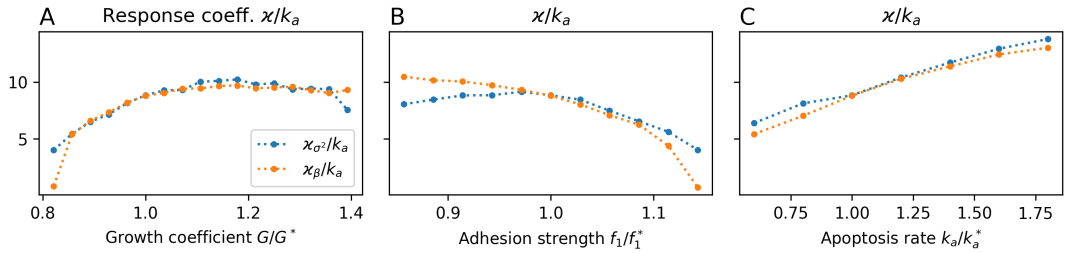

Figure 4.3.3: Comparison of fluctuation-response and perturbation response parameters. For variation of (A) cell growth coefficient G, (B) cell adhesion strength f_1, and (C) apoptosis rate k_a we measure the response coefficients $\varkappa_{\sigma^2}$ and $\varkappa_\beta$ via the variance based method and compression-expansion method, respectively. Parameters are scaled by base parameter $G^* = 28.0$, $f_1^* = 7.0$, and $k_a^* = 0.01$.

are changed to realize homogeneous density variations [33] (see SI 4.B.2 for details). Then, we measure the change in division rate and density as a function of the rescaling rate β. Fitting Eq. 4.2 to data allows us to measure the perturbation response coefficient $\varkappa_\beta$ (see SI Fig. 4.B.1). The whole procedure is numerically and analytically rather complex, highlighting the simplicity of our fluctuation based approach. Both methods (variance and perturbation) give very similar results over a range of simulation parameters as shown in Fig. 4.3.3.

Here, we have varied the growth coefficient G, which controls the active growth force of cells, intercellular adhesion strength f_1, and apoptosis rate k_a. The parameter scan hints increasing deviations, when parameters are tuned far from the base parameter set. For high k_a or f_1 or low G, tissues in simulation may end in a partially teared state, where confluency is no longer given. In the opposite extreme, cells get jammed or crystallization effects can arise, and their dynamics are again altered. For a large range of parameters, however, we find good agreement of both methods.

Again, we confirm the validity of estimating tissue parameters via the cell number and its fluctuations. While parameters can be obtained via perturbation methods, the fluctuation analysis is less intricate and non-invasive.

All dynamic quantifiers ($MSS(\Delta t)$, $C_{\Delta\rho}$, $PSD(f)$), however, suggests that indeed the particle based simulations display a more complex response. A significant bump on time scales around $0.1/k_+ \approx \varkappa/k_+$ is apparent in all quantifiers. The autocorrelation shows best how the much faster relaxation than expected causes full decorrelation at $t = \tau_\sigma$. Where the relaxation time τ_σ was found to be set by the response rate, as $\tau_\sigma = 1/\varkappa$. Importantly, the steady state fluctuations not only allow us to understand long-term response, but even reveal details of the underlying microscopic cellular model.

We speculate, that this deviation comes from a form of memory in the particle based simulations: Cell division is not a random process, but results from cells growing with a finite force against the surrounding. They divide, when a critical size is reached. Therefore, division rate increase after density is lower *after some time*! Figure 4.3.2 (C) shows the net growth rate $k = \partial_t N/N$ and the expected growth rate

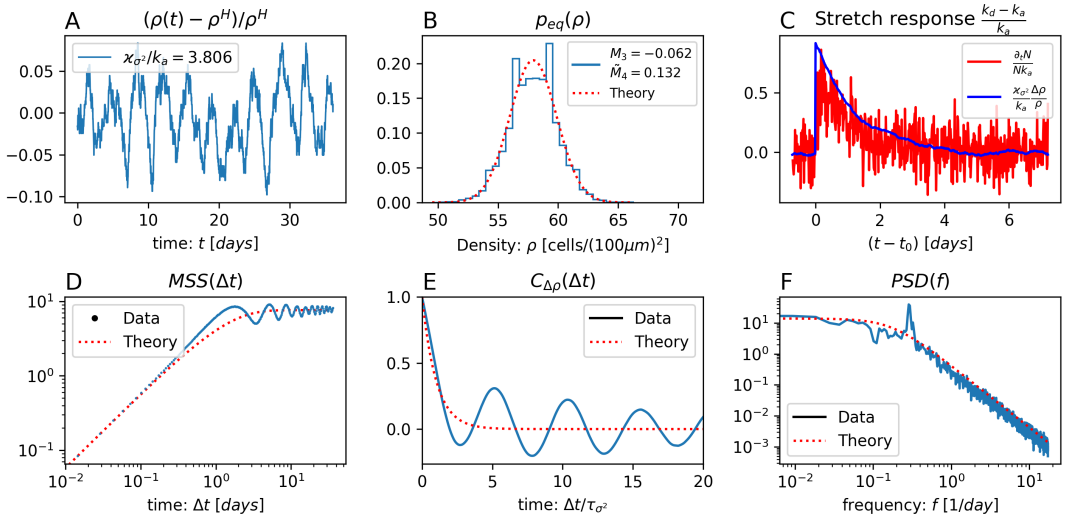

Figure 4.3.4: Membrane potential controlled cell cycle dynamics. Same as Fig. 4.3.1 but for an electro-osmotic model originally published in [31], wild type parameters. Response rate is determined from variance. The underlying adder model apparently results in some form of synchronization, which results in oscillations of the MSS and autocorrelation function and a peak at a frequency of approximately every third day in the PSD. Data of 16 independent runs, each 100 days long, is aggregated in statistical analysis. Stretch response is averaged over 32 independent realisations, system size is $(200\,\mu m)^2$.

$\varkappa_\sigma \Delta\rho/\rho$ after a 20 % stretch. Indeed, cell number does not grow to full extend immediately, but seems to show a short delay. We will study this in more detail further below.

4.3.3 Voronoi model with membrane potential dependent growth–VMPG simulations

Finally, we turn our attention to a much more detailed model calibrated to fit experimental data. We exploit cell-number trajectories generated by agent based simulations of a model published in reference [31] (see SI 4.B.3). In this model, none of the tissue parameters are imposed or known a-priori. Only the apoptosis rate can be assumed to be one in five days, if membrane potential never exceeds $-70\,mV$, which seems to be the case for the data used. Indeed, the linearity of the short term diffusion equals the base value for apoptosis. Note that the numerical cost of these simulations prevents to simulate large systems or obtain response coefficients via perturbation simulations. We still obtain reasonable statistics by aggregating data from independent runs. As for the particle based simulations, the density distribution is rather symmetric ($M_3 = -0.062$, $\tilde{M}_4 = 0.132$), so that we get a homeostatic density $\rho^H =< \rho >= 57.92\,\text{cells}/(100\,\mu m)^2$. The raw cell number trajectory already hints that the system is not just randomly fluctuating in steady state. Regular patterns indicate ongoing oscillations. We suspect that these are caused by the underlying

adder-growth model and may be enhanced by the small scale of the simulations, which can favor synchronization. This effect is investigated in more detail below.

The periodicity can be assigned to a peak at a specific frequency of roughly every fifth day in the power spectral density, matching the apoptosis rate. It is also reflected in oscillations of the MSS and autocorrelation function, which shows that oscillations are weakly damped and continue for many days. Despite the significantly different dynamics, the response of $\varkappa_{\sigma^2}/k_a = 3.806$ coefficient determined from the variance still describes the overall relaxation process well.

4.3.4 Memory in Division control

Both agent based simulation models showed differences between in their dynamic relaxation compared to our theory. Relaxation seems to be much faster than expected from the long term response rate, defined by the plateau value of the different dynamic quantifiers, i.e. the variance of fluctuations. Also, oscillations hint some synchronization of growth in the VMPG model. To better understand this difference we investigate the effect of division memory on the fluctuations.

Instead of immediately increasing the division rate in response to lower density, cells first need to grow. This (short) growth period is then followed by an excess number of divisions. To test this idea, we adapt the division rate update rule in the stochastic model. A generic form of memory is given by integrating over the past states of the system

$$k_d^m(t) - k_a = \int_{\infty}^{t} dt' \; \varkappa \frac{\rho^H - \rho(t')}{\rho^H} w_m(t'). \tag{4.13}$$

where $k_d^m(t)$ is the resulting memory division rate and $w_m(t)$ a time dependent weight function, which describes the memory process. In general $w_m(t)$ is unknown, so we assume for simplicity that the system does loose memory of the past in an exponential relaxation process. Then, the weight function is given by

$$w_m(t') = \frac{e^{-(t-t')/\tau_m}}{\tau_m} \tag{4.14}$$

with memory relaxation time τ_m. Division by τ_m ensures, that for $\tau_m \to 0$ the memory free division rate, given by Eq. 4.2, is recovered. Alternatively, this memory can be written as a dynamic equation for the effective growth rate

$$\partial_t (k_d^m(t) - k_a) = \frac{1}{\tau_m} \left(\varkappa \frac{\rho^H - \rho(t)}{\rho^H} - (k_d^m(t) - k_a) \right). \tag{4.15}$$

i.e. the growth rate relaxes on times τ_m towards the linear term of the memory free theory.

Implementing this process into the stochastic simulations, we find, that with increasing memory relaxation time τ_m the same features as observed in agent-based

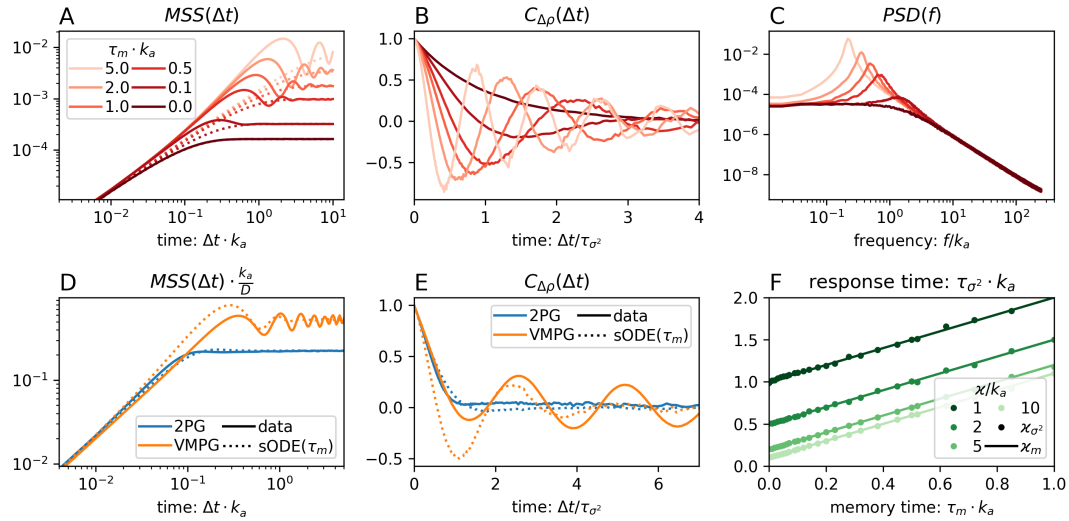

Figure 4.3.5: Division memory effects on fluctuation response. (A) MSS, (B) $C_{\Delta\rho}$, and (C) PSD for sODE system with division memory as described in Eq. 4.15. In (A), the memory free MSS for measured $\varkappa_{\sigma^2}$ (dotted line) and MSS in presence of memory (solid line) are shown in comparison. Color encodes memory relaxation time τ_m and input response rate is $\varkappa/k_a = 10$. (D) MSS, normalized by k_a/D to align curves, and (E) $C_{\Delta\rho}$ for 2PG simulations (blue) and VMPG simulations (orange). The sODE model with fitted memory time is shown as dotted lines, where $\tau_m \cdot k_a = 0.035$ and $\tau_m \cdot k_a = 0.22$ are used for the 2PG and VMPG model, respectively. For VMPG simulations, long standing oscillations are not correctly explained by exponentially decaying memory alone. Note that $\varkappa$ of sODE simulations is chosen such that resulting response rate matches $\varkappa_{\sigma^2}$ of particle based simulation. (F) Effective relaxation time $\tau_{\sigma^2} = 1/\varkappa_{\sigma^2}$ measured from sODE memory simulations (dots) as function of memory time τ_m, with input response rate $\varkappa$ encoded in color. Solid line represents response rate following from superposition of response relaxation time and memory relaxation time $\tau_{\sigma^2} = \tau_m + 1/\varkappa$.

simulations are recovered (see Fig. 4.3.5 top row). First, we investigate the effect of an increasing memory relaxation time τ_m. All other parameters of the simulation are kept identical. We find that effectively the measured response coefficient $\varkappa_{\sigma^2}$ decreases, and is described by adding up the fluctuation relaxation time and memory relaxation time, i.e.: $\tau_{\sigma^2} = 1/\varkappa_{\sigma^2} = 1/\varkappa + \tau_m$. In comparison with the memory free theory, deviations progressively build up with increasing memory time, resulting in oscillations of the mean squared shift (MSS) and density auto correlation ($C_{\Delta\rho}$) and a corresponding peak in the frequency spectrum. This is a result coming from a delayed adaption of the division rate. States late in the past continue to drive high excess divisions.

We fit this adapted theory to our agent based simulation data. The updated input response coefficient is not a free parameter, but calculated from the previously measured response coefficient and fit value of the memory relaxation time. For the 2PG model, we find that a relatively short memory time $\tau_m \cdot k_a = 0.035$ yields good agreement between the memory sODE model and growth model simulation data.

However, small differences remain. This suggests that, while a collective memory effect explains the previously observed differences well, higher order effects are adding even more complex features.

The VMPG model cannot be fitted sufficiently well by the exponentially decaying memory kernel. Even though we can recover oscillations with increasing memory times, frequency and decay rate differ from simulation results. A memory time of $\tau_m \cdot k_a = 0.22$ comes closest to describe the general trend. A more complex memory kernel function, like for example a weakly damped oscillating function, may be required to capture the long standing oscillations, which we assume are coming from synchronisation events from the underlying adder-growth model. This is beyond the scope of this work and may be subject to future studies. In the end, it seems that memory plays a key role in describing and understanding the finer details of tissue response to cell number variation.

4.4 Discussion

Biological systems are constantly driven out of equilibrium by intrinsic or environmental noise. Steady state must be restored, resulting in fluctuations of the system around the steady-state. We have shown, that these fluctuations can be very useful in quantifying the dynamic response of a noisy system. Mapping a growing, self-renewing tissue population to an analog system of a Brownian particle confined in a harmonic oscillator allowed us to derive a set of static, i.e. cell density probability density, and dynamic, i.e. mean squared shift, autocorrelation function, and power spectral density, which can together quantify the dynamic response coefficient and detect indications to non-equilibrium effects, like finite memory of the division rate. With help of cell number trajectories for a simplified, coarse grained system, where direct feedback of the division rate on the current density is implemented, we illustrate the correctness of our mapping.

In two agent based models of increasing complexity, first a mechanistic two-particle growth model and second a mechano-electro-osmotic model, we find that the variance based method to estimate the response coefficient to be robust. For the 2PG model, the variance response coefficient was compared to a response coefficient measured via compression-expansion modulations of the tissue. Over a large parameter range both methods show quantitative agreement. In addition, we find that differences between our theory and the simulation data can be resolved by a memory of the division rate. Due to finite growth periods, the division rate requires a finite time to adapt. This non-Markovian mechanism can resolve differences between two particle growth model and our theory. In the more complicated mechano-electro-osmotic model, long standing oscillations could not be fully resolved by a simple exponentially decaying memory kernel. More sophisticated division update rules are required to account for the synchronization effects, which we assume to arise due to the underlying adder-mechanism of the growth model.

Recently, other studies did show, that a combination of active and passive rheol-

ogy [39], but also three point correlation functions of passive fluctuations only [23, 30], can indicate the non-equilibrium nature of biological systems. In single cell experiment, fluctuations of the cell are probed. While a comparison between active and passive rheology may cause spurious artifacts stemming from the required external force to perturb the system, in particular passive-only methods are of interest. We did not find any additional signs of activity in the mean back relaxation (MBR) function, a three point correlation function calculated by averaging over the ratio of future and past displacements (see SI 4.B.5). As expected for Gaussian processes, which we found in all of our systems, the MBR contains no additional information beyond what is encoded in the MSS and can be expressed in terms of the latter. On the other hand, our results suggest that cellular tissues can serve as an interesting model to investigate non-equilibrium physics.

In this work, we focused on tissues with a cellular tissue consisting of a single cell type. Real tissues consist of various different cell types, which may have different dynamic response coefficient. If response coefficients vary greatly, classical perturbation measurements are unlikely to resolve all coefficients equally well. We expect the variance based measurement protocol to be suitable to obtain the different response coefficients in multi-cellular systems, when sufficiently long trajectories are recorded.

Last, microscopy of biological samples comes with additional challenges. On one hand, the same section of cells is rarely imaged repeatedly. Also, even if the exact same position is imaged, cells randomly move in or out of the image section. Both effects result in an additional noise contribution. In order to apply our method to experimental data, one has to understand how spatial noise affects cell number fluctuations. We expect that for large volumes, this surface term plays a minor role but becomes relevant for limited image sections.

Supplementary Information - Chapter 4

4.A Details on density fluctuations due to noise

In order to describe the biological, noisy nature of tissues, we assume that both, division and apoptosis are subject to stochastic noise and can be modelled by Poisson processes. Then we rewrite the change of cell numbers N in terms of Gaussian distributions $\mathcal{N}$ as

$$\begin{aligned}\Delta N &= N(t+\delta t) - N(t) \\ &= \mathcal{N}(k_d N\delta t, k_d N\delta t) - \mathcal{N}(k_a N\delta t, k_a N\delta t) \\ &= (k_d - k_a)N\delta t + \mathcal{N}(0, k_d N\delta t) - \mathcal{N}(0, k_a N\delta t) \\ &= (k_d - k_a)N\delta t + \sqrt{(k_d + k_a)N\delta t}\mathcal{N}(0,1) \\ &= \Delta k N\delta t + \sqrt{2k_+ N\delta t}\mathcal{N}(0,1)\end{aligned} \tag{4.16}$$

Note that we assume that the system is already in steady state ($\Delta k = k_d - k_a \approx 0$ and $k_+ = (k_a + k_d)/2$). Also, we do assume markovian noise with finite variance, which leads to the Gaussian distribution at large cell numbers. Inserting Eq. 4.2 after division by Volume V, gives

$$\partial_t \rho = -\varkappa \frac{\rho - \rho^H}{\rho^H}\rho + \sqrt{\frac{2k_+\rho^H}{V}}\eta(t) \tag{4.17}$$

with $\eta(t)$ describing a mean centered $\langle\eta(t)\rangle = 0$, uncorrelated $\langle\eta(t)\eta(t')\rangle = \delta(t-t')$ white noise. Note that we already made the assumption that number fluctuations are small and replaced ρ in the noise term by ρ^H. For small fluctuations $y = \frac{\rho-\rho^H}{\rho^H}$ and densities close to the homeostatic density, this can further be simplified as

$$\partial_t y = -\varkappa y\left(\frac{y}{\rho^H} + 1\right) + \sqrt{\frac{2k_+\rho^H}{V}}\eta \tag{4.18}$$

$$\approx -\varkappa y + \sqrt{\frac{2k_+\rho^H}{V}}\eta \tag{4.19}$$

Eventually, under the assumption of mechanical feedback on growth and only small fluctuations around the homeostatic state, we've derived the equivalent Langevin equation for a Brownian particle confined in a harmonic potential. This allows us to provide a number of analytic expressions as discussed in the main text and below.

Non-linear confinement potential In Eq. 4.19, we've introduced a simplified description analogue to a Brownian particle confined by a harmonic potential. To better understand this approximation, we can rewrite Eq. 4.17 as

$$\partial_t \rho = [-\partial_\rho U(\rho)] + \sqrt{\frac{2k_+\rho^H}{V}}\eta(t) \tag{4.20}$$

with (full) feedback potential

$$U(\rho) = \frac{\varkappa}{\rho^H}\left(\frac{\rho^3}{3} - \frac{\rho^2\rho^H}{2}\right). \tag{4.21}$$

Note that negative densities are not possible, and that the potential has a saddle point at $\rho = 0$ and $\rho = \rho^H$. The response rate describes the effective temperature of the tissue. Thus, faster response is equivalent to higher temperature and thus stronger coupling.

Density probability density function In equilibrium, the stationary Fokker-Planck equation

$$D\frac{d^2p(x)}{dx^2} = \frac{d}{dx}\left[-\frac{dU(x)}{dx}p(x)\right] \tag{4.22}$$

describes the probability density of a drift diffusion process and is solved by

$$p(x) = p_0 \exp\left(-\frac{U(x)}{D}\right). \tag{4.23}$$

For a harmonic potential $U(x) = \varkappa x^2/2$, the solution is the Boltzmann statistics. In case of the tissue given by

$$p_{eq}(\rho) = \sqrt{\frac{\varkappa}{2\pi D}} \exp\left(-\frac{\varkappa}{2D}\left(\rho - \rho^H\right)^2\right). \tag{4.24}$$

for the non-linearized potential, given in Eq. 4.21, can only be treated numerically. Since negative densities are not realistic, normalization condition $\int_0^\infty d\rho\ p(\rho) = 1$ converges. For a series of response rates and system sizes, we observe that the potential is close to a Gaussian for sufficiently large response rate ($\varkappa/k_a \geq 1$) and system sizes ($N^H \geq 100$). Importantly, reduction of $\varkappa$ or N^H results in a stronger skewness of the potential and deviation from the Gaussian. Also, the extinction probability, measured as $p(\rho = 0)$, increases for these cases.

Autocorrelation and Variance The power spectral density discussed in the main text represents the Fourier space representation of the fluctuation auto-correlation function $C_X(t)$, defined as

$$C_X(t) = \langle (X(t) - \mu)(X(0) - \mu)\rangle, \tag{4.25}$$

where $X(t)$ depicts the observable of our measurement and μ its mean value. Now, one can obtain the autocorrelation or PSD from each other via

$$\begin{aligned} C_X(t) &= \int_{-\infty}^{\infty} P_X(\omega) e^{i\omega t} d\omega \\ P_X(t) &= \frac{1}{2\pi} \int_{-\infty}^{\infty} C_X(\omega) e^{-i\omega t} d\omega \end{aligned} \tag{4.26}$$

with frequency $\omega = 2\pi f$.

For zero time lag, the auto-correlation equals the variance of $X(t)$

$$\sigma_X^2 \equiv Var(X) = \mathbb{E}\left((X-\mu)^2\right). \tag{4.27}$$

Inserting Eq. 4.11 in Eq. 4.26 for $t = 0$ is analytically tractable and yields

$$\begin{aligned} \sigma_\rho^2 &= C_\rho(t=0) \\ &= (2\pi) \int_{-\infty}^{\infty} \frac{(k_+ \cdot \rho_H)/(V \cdot 2\pi^2)}{\kappa^2 + \omega^2} d\omega \\ &= \frac{k_+ \rho^H}{\kappa V} \end{aligned} \tag{4.28}$$

Thus, that one can directly measure the response coefficient via the variance of fluctuations.

Equivalence of MSS and density fluctuation correlation function Here, we show that mean squared shift (MSS) of density and the "pair"-correlation $C_|\Delta\rho$ of density fluctuations are equivalent. First, we note, that the MSS and the MSS of density fluctuations are the same. We derive the relation connecting density pair correlations with density fluctuation pair correlation, as

$$\begin{aligned} C_{\Delta\rho}(\Delta) &\equiv \left\langle \left(\rho(t+\Delta) - \rho^H\right)\left(\rho(t) - \rho^H\right) \right\rangle / \sigma^2 \\ &= \left\langle \rho(t+\Delta)\rho(t) + \left(\rho^H\right)^2 - \rho^H \left(\rho(t+\Delta) + \rho(t)\right) \right\rangle / \sigma^2 \\ &= \left(\langle \rho(t+\Delta)\rho(t) \rangle + \left(\rho^H\right)^2 - \rho^H \langle (\rho(t+\Delta) + \rho(t)) \rangle \right) / \sigma^2 \\ &= \left(\langle \rho(t+\Delta)\rho(t) \rangle - \left(\rho^H\right)^2 \right) / \sigma^2 \\ &= C_\rho(\Delta)/\sigma^2 - \left(\rho^H\right)^2 / \sigma^2. \end{aligned} \tag{4.29}$$

In the last step, we introduced the density pair correlation function $C_\rho(\Delta) = \langle \rho(t+\Delta)\rho(t) \rangle$. This expression can be found to describe the MSS, when expanding the

expectation values, and allows us to show the equivalence of MSS and $C_{\Delta\rho}$, given by

$$\begin{aligned} MSS &= \left\langle (\rho(t+\Delta t) - \rho(t))^2 \right\rangle \\ &= \left\langle \left(\rho(t+\Delta t)^2 + \rho(t)^2\right) - 2\left(\rho(t+\Delta t)\rho(t)\right) \right\rangle \\ &= 2\overline{\rho^2} - 2\left\langle (\rho(t+\Delta t)\rho(t)) \right\rangle \\ &= 2\overline{\rho^2} - 2C_\rho(\Delta t) \\ &= 2\overline{\rho^2} - 2\left(\rho^H\right)^2 - 2\sigma^2 C_{\Delta\rho}(\Delta t) \\ &= 2\sigma^2(1 - C_{\Delta\rho}(\Delta)). \end{aligned} \tag{4.30}$$

Where we have used, that the variance of density fluctuations is given by

$$\begin{aligned} \sigma^2 &= \left\langle \left(\rho(t) - \rho^H\right)^2 \right\rangle \\ &= \left\langle \rho(t)^2 + \left(\rho^H\right)^2 - 2\rho(t)\rho^H \right\rangle \\ &= \left\langle \rho(t)^2 \right\rangle - \left(\rho^H\right)^2. \end{aligned} \tag{4.31}$$

Eventually, we've shown, that for known variance, one can directly measure the response coefficient via density fluctuation pair correlations. Also, the characteristic relaxation time is equivalent to the response rate $\tau = 1/\varkappa$, as one can see in the main text.

4.B Simulation details and additional results

Simulation code and data is made available upon reasonable request and stored according to good scientific practice at the Forschungszentrum Jülich. Here, we briefly introduce the three different simulation models used to test our theory in the main text.

4.B.1 sODE model

Eq. 4.1 & 4.2 are implemented to numerically solve a stochastic ODE system in `python`. At each time point of the simulation, the number of deaths and divisions are drawn from a binomial distribution, where the probability of success is given by the current division rate, or fixed apoptosis rate, multiplied by the time step Δt of the simulation. Then, the current number of cells is updated followed by an update of the division rate. These simulations do not require a simulation volume, as the update rule for the division rate can be normalized with a target cell number instead. Yet, we chose to set a volume to match the cell density of 2PG and VMPG simulations, when fitting our model, and a density of $\rho^H_{sODE} = 2$ for independent simulations.

4.B.2 Two particle growth model

The described SC model is implemented in the two-particle growth (2PG) model of Refs. [5, 33] and has been adapted in Refs. [9, 10, 16, 24] to a variety of different models.

Each cell is described by two particles, which repel each other via an active growth force

$$F_{ij}^{(G)} = \frac{G}{(r_{ij} - r_0)^2} \hat{\boldsymbol{r}}_{ij} \tag{4.32}$$

with unit vector $\hat{\boldsymbol{r}}_{ij}$, distance r_{ij} between the two particles, a constant r_0, and growth strength G.

To prevent overlap of cells, particles of different cells interact via a soft repulsive volume-exclusion force

$$\boldsymbol{F}_{ik}^{(V)} = f_0 \left(\frac{R_{PP}^5}{r_{ik}^5} - 1 \right) \hat{\boldsymbol{r}}_{ij}, \text{ for } r_{ik} < R_{PP} \tag{4.33}$$

with exclusion strength f_0 and interaction length R_{PP}, which sets the length scale of our simulations. Further, cells in contact interact via an attractive adhesion force of the form

$$\boldsymbol{F}_{ik}^{(V)} = -f_1 \hat{\boldsymbol{r}}_{ik}, \text{ for } r_{ik} < R_{PP} \tag{4.34}$$

with adhesion strength f_1. We employ a dissipative particle dynamics-type thermostat [20], with an effective temperature T, to account for energy dissipation

$$F_{ij}^{(D)} = \gamma \cdot \left(1 - \frac{dr}{rt} \right)^2 \cdot (\boldsymbol{v}_{ij} \cdot \hat{\boldsymbol{r}}_{ij}) \, \hat{\boldsymbol{r}} \tag{4.35}$$

and random fluctuations

$$F_{ij}^{(R)} = \sigma \xi \cdot \hat{\boldsymbol{r}}_{ij} \tag{4.36}$$

where γ and σ are related to fulfill the fluctuation-dissipation theorem [14]. Also, background dissipation is taken into account as

$$\boldsymbol{F}_i^B = -\gamma_b \boldsymbol{v}_i. \tag{4.37}$$

A self-consistent velocity-Verlet algorithm [32] is implemented to integrate the equations of motion, and all simulations were performed with periodic boundary conditions.

Cell division is performed, when the two particles of one cell are separated by a critical threshold R_{ct}. A new particle is randomly placed near each original particle in a distance R_d, and the two new particle pairs form the two daughter cells. Cells are stochastically removed from the simulation with a finite apoptosis rate k_a. Time is measured in terms of the inverse apoptosis rate, and referred to as "generation". The standard parameter set for our simulations are given in Tab. 4.B.1. However, not all of these simulation parameters, have a direct conversion to physical units. As

Table 4.B.1: 2PG tissue simulation parameters (standard parameter set).

Parameter	Symbol	Value
Time step	Δt	0.001
Pair potential interaction range	R_{PP}	1
Cell expansion constant	r_0	1
Division distance threshold	R_{ct}	0.8
New cell particle initial distance	R_d	10^{-5}
Growth-force strength	G	28
Mass	m	1
Intra-cell dissipation coefficient	γ_c	100
Inter-cell dissipation coefficient	γ_t	50
Background dissipation coefficient	γ_c	0.1
Apoptosis rate	k_a	0.01
Noise intensity	k_BT	0.1
Repulsive cell-cell potential coefficient	f_0	2.39566
Attractive cell-cell potential coefficient	f_1	7.0

discussed in [5] one has to chose well defined measurable quantities, such as apoptosis rate and range of the pair potential as rescaling units for inverse time and particle diameter, to allow for conversion to physical units and comparison with experiments. Simulations are performed in a two-dimensional squared area with periodic boundary conditions.

Compression expansion module In mechanical tissue simulations, the response coefficient is a priori not known, but results from the mechanical properties of cells and their local interactions. For monoclonal tissues, local configuration can be expected to play a minor role, but for more complex multi-cellular tissues this may become relevant. We compare the result for measurements of $\varkappa_{\sigma^2}$, obtained from the fluctuation response methods, and $\varkappa_\beta$, the response to volume rescaling.

The volume rescaling method is motivated by common experimental techniques. For example cell spheroids can be grown under increased pressure, by placing them in a semipermeable membrane and controlling the osmotic pressure by the dextrane concentration of the surrounding medium [29]. Also, cells grown on an elastic substrate can be tested for response to stretch or destretch of the underlying substrate. We transfer these methods to simulations, where the simulation volume is rescaled at a constant rate β. Cell center of mass positions are updated by the same factor, while cell sizes remain unchanged. The position of a cell is given by

$$\boldsymbol{r}_{new} = \beta \cdot \boldsymbol{r}_{old}^{PBC}, \tag{4.38}$$

were $\boldsymbol{r}_{old}^{PBC}$ is the position of the particle in the unit box of our simulations, ranging from $(0, L_{xy}(t))$.

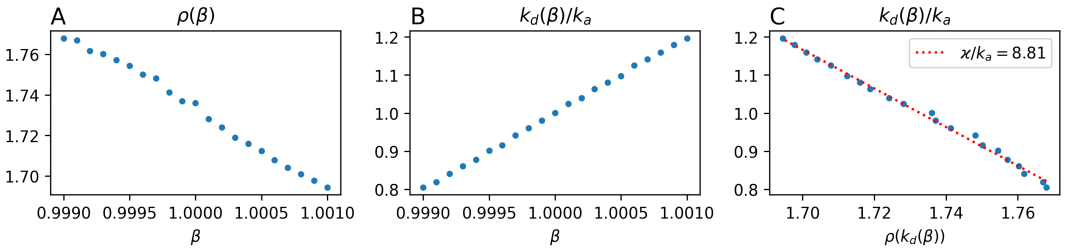

Figure 4.B.1: Perturbation-response in agent based simulations. Example how response is measured via perturbation, where β is the rescaling coefficient of volume change and (A) density and (B) division rate variation are shown as a function of rescaling. (C) Fitting Eq. 4.2 to data.

This allows to observe the response of the division rate as a consequence of reduced ($\beta > 1$) or increased ($\beta < 1$) density (see Fig. 4.B.1). While in principle this method can be applied for infinite time, large volumes come with increased computational time, which limits our experiments. Thus, data is averaged over independent rescaling runs to improve statistics. Plotting the division rate as a function of density, we find the expected linear relation, where the slope equals the response coefficient $\varkappa_\beta$ (see Fig. 4.B.1).

Although the exact value of $\varkappa$ is not known, certain model parameters allow for a physical interpretation, which can be confirmed qualitatively. The active growth force of cells is controlled by the growth coefficient G. With an increase of G one can associate a faster response to cell loss. Thus, higher value of $\varkappa$. This is confirmed by our measurements. For too small values of G, the tissue loses confluency, which in particular affects the rescaling measurement, which requires a confluent tissue even under expansion. With increasing growth coefficient, both methods reach a plateau, since fluidization gets lost and a crystal like phase is realized. This already depicts the limit of biological relevant parameters.

Since the beginning of computational modeling of cellular systems, cell adhesion is known to be a crucial factor, which drives cell sorting or tissue fluidization [17]. We find, that higher adhesion reduces the response coefficient. Tightly coupled cells can not as easily rearrange to respond to cell loss, thus response is smaller for high adhesion. Lower adhesion supports fluidization of cells, and an increase of the response coefficient.

In the mechanical model, time is measured in generations, set by the fixed apoptosis rate k_a. On the other hand, apoptosis is the relevant process, which initiates fluidization of tissues [5]. As discussed above, fluidization is relevant for quick response, and we can confirm that increasing k_a comes with an increase of $\varkappa$. Note, that the ratio $\varkappa/k_a$ stays approximately constant.

The same rescaling method is applied to the stretch-experiments, however, only for a short time with much larger scaling factor.

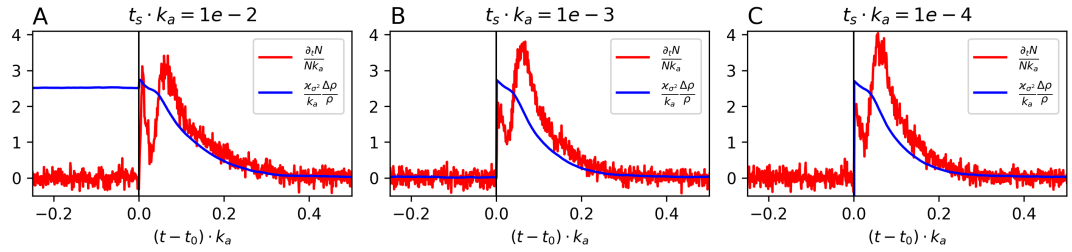

Figure 4.B.2: Stretch response rate dependence. 2PG simulations for three different stretch duration. In all simulations, 20 % stretch is realized, however, over different time intervals t_s.

4.B.3 Voronoi membrane potential growth (VMPG) model

As a more sophisticated agent based model, we adapt the simulations originally published by Mukherjee et al. [31], where a more detailed description is given. Again, simulations are performed in 2D with periodic boundary conditions. When solving the mechano-electro-osmotic model, a constant cell height is assumed, as cell height fluctuations are only expected to be small. Cells are represented by their center position, and cell shape is constructed via Voronoi triangulation. The mechano-electro-osmotic model is solved for each cell to calculate the ion-concentrations, membrane potential V and pressure P. These are then used to calculate forces on a cell from the gradient of an energy functional, given by

$$E_{cell} = P \cdot V + T \cdot (p - p_0)^2, \tag{4.39}$$

with tension coefficient T and current perimeter p and target perimeter p_0. In addition, frictional forces with the substrate $\boldsymbol{f}_{sub} = -\gamma \boldsymbol{v}$ act on cells moving with velocity $\mathbf{v}$ and friction coefficient γ. Cellular biomass degrades with a constant rate and is produced proportional to the membrane potential U, until a threshold value for the potential is reached. Cell division is implemented as an *adder*-model: A cell divides, if a constant increase in biomass is reached. This value is decided at the time of division and drawn from a Gaussian distribution. Cell death is a stochastic process with half-life time of five days, except for high potentials succeeding a value of $-70\,mV$, when the rate is doubled resulting in a half-life time of 2.5 days. All simulations parameters are chosen the same as in Ref. [31], where they were calibrated against experimental data.

Rescaling for stretch-experiments is performed instantaneous, in the same fashion as for the 2PG simulations.

4.B.4 Stretch Response

In 2PG stretch simulations, we find a small increase in the current division rate directly after applying stretch. We speculate that this peak is a result from the stretch-method implemented in simulations. Stretch is not instantaneous, but carried out over a short

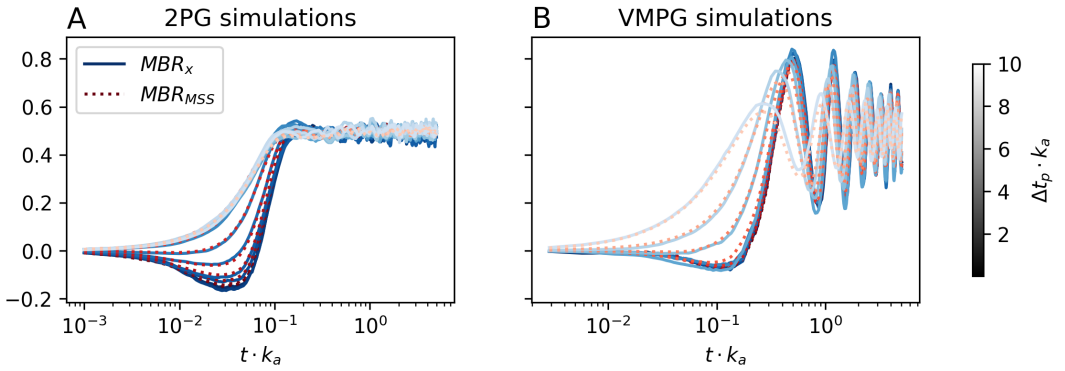

Figure 4.B.3: Mean back relaxation. Mean back relaxation function (MBR) over forward time Δt_f for color coded backward times Δt_p (dark: short displacement; bright: large displacement). Solid line is calculated directly from data by Eq. 4.40 with $l_c = 1e-5$. and dotted line via the MSS following Eq. 4.41. (A) shows data for 2PG simulations and (B) data for the VMPG simulations.

time. We test how the peak changes for different stretch times, ranging over two orders of magnitude from $t \cdot k_a = 1e-4$ (1000 integration steps) to $t \cdot k_a = 1e-2$ (10 integration steps) we perform stretch experiments, all resulting in 20 % stretch (see Fig. 4.B.2). We find, that for the slowest process, the peak is most pronounced, while no additional saturation is found for even shorter times. Note that only cell position and not cell size is rescaled during the stretch. A possible explanation is, that adhesive forces cause additional growth, which is more pronounced if cells pull on each other continuously. While here this has to be understood as an artifact of the simulation setup, real cells are expected to show physiological change when stress is applied externally. Thus, highlighting the need of non-invasive methods. In the main text figure 4.3.2, data for the intermediate stretch time is shown.

4.B.5 Mean back relaxation (MBR)

All previously discussed dynamic methods correlate the tissue population at two time points. Recently a related quantity, the mean back relaxation (MBR), has been introduced, which correlates three time points of a trajectory [23]. It is defined by the average future displacement divided by the past displacement and given by

$$MBR_x(\Delta t_f, \Delta t_p, l_c) = \left\langle \frac{x(t+\Delta t) - x(t)}{x(t) - x(t-\Delta t_p)} \theta_{l_c}(|x(t) - x(t-\Delta t_p)|) \right\rangle, \tag{4.40}$$

where Δt_f and Δt_p are the time displacements to the future and past, respectively. l_c is a cutoff value, which prevents division by zero, and θ_{l_c} a Heaviside function. An

alternative representative of the MBR can be given for Gaussian systems in the form

$$MBR_{MSS}(\Delta t_f, \Delta t_p) = \frac{1}{2}\left(1 - \frac{MSS(\Delta t_f + \Delta t_p) - MSS(\Delta t_f)}{MSS(\Delta t_p)}\right), \tag{4.41}$$

which is independent of the cutoff l_c and relates the MBR to the MSS. In general, this three point correlation function provides a condensed insight in the dynamic of the system and has been shown to be in particular helpful to probe the non-equilibrium nature of a system with passive measurements [30]. Both agent based models studied in this work do result in a Gaussian cell density distribution, thus, both methods to calculate the MBR are equivalent (see Fig. 4.B.3). Further, we do not find strong indication for broken detailed balance in the 2PG simulations, as the MBR converges to 1/2, while for the VMPG simulations, oscillations make it difficult to correctly identify the long term limit.

References

[1] B.-Q. Ai, X.-J. Wang, G.-T. Liu, and L.-G. Liu. Correlated noise in a logistic growth model. *Physical Review E*, 67(2), Feb. 2003. ISSN 1095-3787. doi: 10.1103/physreve.67.022903. URL http://dx.doi.org/10.1103/PhysRevE.67.022903.

[2] D. N. Alasaadi and R. Mayor. Mechanically guided cell fate determination in early development. *Cellular and Molecular Life Sciences*, 81(1), May 2024. ISSN 1420-9071. doi: 10.1007/s00018-024-05272-6. URL http://dx.doi.org/10.1007/s00018-024-05272-6.

[3] M. Aragona, A. Sifrim, M. Malfait, Y. Song, J. Van Herck, S. Dekoninck, S. Gargouri, G. Lapouge, B. Swedlund, C. Dubois, P. Baatsen, K. Vints, S. Han, F. Tissir, T. Voet, B. D. Simons, and C. Blanpain. Mechanisms of stretch-mediated skin expansion at single-cell resolution. *Nature*, 584(7820):268–273, July 2020. ISSN 1476-4687. doi: 10.1038/s41586-020-2555-7. URL http://dx.doi.org/10.1038/s41586-020-2555-7.

[4] M. Basan, T. Risler, J. Joanny, X. Sastre-Garau, and J. Prost. Homeostatic competition drives tumor growth and metastasis nucleation. *HFSP Journal*, 3(4):265–272, Aug. 2009. ISSN 1955-2068. doi: 10.2976/1.3086732. URL http://dx.doi.org/10.2976/1.3086732.

[5] M. Basan, J. Prost, J.-F. Joanny, and J. Elgeti. Dissipative particle dynamics simulations for biological tissues: rheology and competition. *Physical Biology*, 8(2):026014, Apr. 2011. ISSN 1478-3975. doi: 10.1088/1478-3975/8/2/026014. URL http://dx.doi.org/10.1088/1478-3975/8/2/026014.

[6] K. Berg-Sørensen and H. Flyvbjerg. Power spectrum analysis for optical tweezers. *Review of Scientific Instruments*, 75(3):594–612, Mar. 2004. ISSN 1089-7623. doi: 10.1063/1.1645654. URL http://dx.doi.org/10.1063/1.1645654.

[7] I. Bertoncello. *Optimizing the Cell Culture Microenvironment*, page 23–30. Springer New York, 2019. ISBN 9781493990863. doi: 10.1007/978-1-4939-9086-3_2. URL http://dx.doi.org/10.1007/978-1-4939-9086-3_2.

[8] B. Bighi, G. Ragazzini, A. Gallerani, A. Mescola, C. Scagliarini, C. Zannini, M. Marcuzzi, E. Olivi, C. Cavallini, R. Tassinari, M. Bianchi, L. Corsi, C. Ventura, and A. Alessandrini. Cell stretching devices integrated with live cell imaging: a powerful approach to study how cells react to mechanical cues. *Progress in Biomedical Engineering*, 7(1):012005, Dec. 2024. ISSN 2516-1091. doi: 10.1088/2516-1091/ad9699. URL http://dx.doi.org/10.1088/2516-1091/ad9699.

[9] T. Büscher, A. L. Diez, G. Gompper, and J. Elgeti. Instability and fingering of interfaces in growing tissue. *New Journal of Physics*, 22(8):083005, Aug. 2020. ISSN 1367-2630. doi: 10.1088/1367-2630/ab9e88. URL http://dx.doi.org/10.1088/1367-2630/ab9e88.

[10] T. Büscher, N. Ganai, G. Gompper, and J. Elgeti. Tissue evolution: mechanical interplay of adhesion, pressure, and heterogeneity. *New Journal of Physics*, 22(3):033048, Mar. 2020. ISSN 1367-2630. doi: 10.1088/1367-2630/ab74a5. URL http://dx.doi.org/10.1088/1367-2630/ab74a5.

[11] H. B. Callen and T. A. Welton. Irreversibility and generalized noise. *Physical Review*, 83(1):34–40, July 1951. ISSN 0031-899X. doi: 10.1103/physrev.83.34. URL http://dx.doi.org/10.1103/PhysRev.83.34.

[12] A. G. Cherstvy, S. Thapa, Y. Mardoukhi, A. V. Chechkin, and R. Metzler. Time averages and their statistical variation for the ornstein-uhlenbeck process: Role of initial particle distributions and relaxation to stationarity. *Physical Review E*, 98(2), Aug. 2018. ISSN 2470-0053. doi: 10.1103/physreve.98.022134. URL http://dx.doi.org/10.1103/PhysRevE.98.022134.

[13] I. Constantinou and E. E. Bastounis. Cell-stretching devices: advances and challenges in biomedical research and live-cell imaging. *Trends in Biotechnology*, 41(7):939–950, July 2023. ISSN 0167-7799. doi: 10.1016/j.tibtech.2022.12.009. URL http://dx.doi.org/10.1016/j.tibtech.2022.12.009.

[14] P. Español and P. Warren. Statistical Mechanics of Dissipative Particle Dynamics. *Europhysics Letters (EPL)*, 30(4):191–196, May 1995. ISSN 0295-5075, 1286-4854. doi: 10.1209/0295-5075/30/4/001. URL https://iopscience.iop.org/article/10.1209/0295-5075/30/4/001.

[15] C. Ferrai and C. Schulte. Mechanotransduction in stem cells. *European Journal of Cell Biology*, 103(2):151417, June 2024. ISSN 0171-9335. doi: 10.1016/j.ejcb.2024.151417. URL http://dx.doi.org/10.1016/j.ejcb.2024.151417.

[16] N. Ganai, T. Büscher, G. Gompper, and J. Elgeti. Mechanics of tissue competition: interfaces stabilize coexistence. *New Journal of Physics*, 21(6):063017, June 2019. ISSN 1367-2630. doi: 10.1088/1367-2630/ab2475. URL http://dx.doi.org/10.1088/1367-2630/ab2475.

[17] F. Graner and J. A. Glazier. Simulation of biological cell sorting using a two-dimensional extended potts model. *Physical Review Letters*, 69(13):2013–2016, Sept. 1992. ISSN 0031-9007. doi: 10.1103/physrevlett.69.2013. URL http://dx.doi.org/10.1103/PhysRevLett.69.2013.

[18] O. Hallatschek, S. S. Datta, K. Drescher, J. Dunkel, J. Elgeti, B. Waclaw, and N. S. Wingreen. Proliferating active matter. *Nature Reviews Physics*, 5(7):407–419, May 2023. ISSN 2522-5820. doi: 10.1038/s42254-023-00593-0. URL http://dx.doi.org/10.1038/s42254-023-00593-0.

[19] E. Hannezo and C.-P. Heisenberg. Mechanochemical feedback loops in development and disease. *Cell*, 178(1):12–25, June 2019. ISSN 0092-8674. doi: 10.1016/j.cell.2019.05.052. URL http://dx.doi.org/10.1016/j.cell.2019.05.052.

[20] P. J. Hoogerbrugge and J. M. V. A. Koelman. Simulating Microscopic Hydrodynamic Phenomena with Dissipative Particle Dynamics. *Europhysics Letters (EPL)*, 19(3):155–160, June 1992. ISSN 0295-5075, 1286-4854. doi: 10.1209/0295-5075/19/3/001. URL https://iopscience.iop.org/article/10.1209/0295-5075/19/3/001.

[21] J.-H. Jeon and R. Metzler. Inequivalence of time and ensemble averages in ergodic systems: Exponential versus power-law relaxation in confinement. *Physical Review E*, 85(2), Feb. 2012. ISSN 1550-2376. doi: 10.1103/physreve.85.021147. URL http://dx.doi.org/10.1103/PhysRevE.85.021147.

[22] T. R. Kirkpatrick and D. Belitz. Fluctuation-response relation in nonequilibrium systems and active matter. *Physical Review E*, 111(1), Jan. 2025. ISSN 2470-0053. doi: 10.1103/physreve.111.014102. URL http://dx.doi.org/10.1103/PhysRevE.111.014102.

[23] G. Knotz and M. Krüger. Mean back relaxation for position and densities. *Physical Review E*, 110(4), Oct. 2024. ISSN 2470-0053. doi: 10.1103/physreve.110.044137. URL http://dx.doi.org/10.1103/PhysRevE.110.044137.

[24] J. C. Krämer, E. Hannezo, G. Gompper, and J. Elgeti. Mechanically-driven stem cell separation in tissues caused by proliferating daughter cells. *SciPost Physics*, 16(4), Apr. 2024. ISSN 2542-4653. doi: 10.21468/scipostphys.16.4.097. URL http://dx.doi.org/10.21468/SciPostPhys.16.4.097.

[25] R. Kubo. The fluctuation-dissipation theorem. *Reports on Progress in Physics*, 29(1): 255–284, Jan. 1966. ISSN 0034-4885. doi: 10.1088/0034-4885/29/1/306. URL http://dx.doi.org/10.1088/0034-4885/29/1/306.

[26] M. C. Marchetti, J. F. Joanny, S. Ramaswamy, T. B. Liverpool, J. Prost, M. Rao, and R. A. Simha. Hydrodynamics of soft active matter. *Reviews of Modern Physics*, 85 (3):1143–1189, July 2013. ISSN 1539-0756. doi: 10.1103/revmodphys.85.1143. URL http://dx.doi.org/10.1103/RevModPhys.85.1143.

[27] P. G. Meyer and H. Kantz. Time reversal symmetry and the difference between relaxations and building-up periods. *Physical Review E*, 104(2), Aug. 2021. ISSN 2470-0053. doi: 10.1103/physreve.104.024208. URL http://dx.doi.org/10.1103/PhysRevE.104.024208.

[28] P. G. Meyer and R. Metzler. Stochastic processes in a confining harmonic potential in the presence of static and dynamic measurement noise. *New Journal of Physics*, 25 (6):063003, June 2023. ISSN 1367-2630. doi: 10.1088/1367-2630/acd94f. URL http://dx.doi.org/10.1088/1367-2630/acd94f.

[29] F. Montel, M. Delarue, J. Elgeti, L. Malaquin, M. Basan, T. Risler, B. Cabane, D. Vignjevic, J. Prost, G. Cappello, and J.-F. Joanny. Stress clamp experiments on multicellular tumor spheroids. *Physical Review Letters*, 107(18), Oct. 2011. ISSN 1079-7114. doi: 10.1103/physrevlett.107.188102. URL http://dx.doi.org/10.1103/PhysRevLett.107.188102.

[30] T. M. Muenker, G. Knotz, M. Krüger, and T. Betz. Accessing activity and viscoelastic properties of artificial and living systems from passive measurement. *Nature Materials*, 23(9):1283–1291, July 2024. ISSN 1476-4660. doi: 10.1038/s41563-024-01957-2. URL http://dx.doi.org/10.1038/s41563-024-01957-2.

[31] A. Mukherjee, Y. Huang, J. Elgeti, S. Oh, J. G. Abreu, L. Ammar, A. R. Neliat, J. Schüttler, D.-D. Su, C. Dupre, N. C. Benites, X. Liu, L. Peshkin, M. Barboiu, H. Stocker, M. W. Kirschner, and M. Basan. Membrane potential mediates the cellular response to mechanical pressure. *Cell*, 189(1):143–160.e22, Jan. 2026. ISSN 0092-8674. doi: 10.1016/j.cell.2025.11.004. URL http://dx.doi.org/10.1016/j.cell.2025.11.004.

[32] I. Pagonabarraga, M. H. J. Hagen, and D. Frenkel. Self-consistent dissipative particle dynamics algorithm. *Europhysics Letters (EPL)*, 42(4):377–382, May 1998. ISSN 0295-5075, 1286-4854. doi: 10.1209/epl/i1998-00258-6. URL https://iopscience.iop.org/article/10.1209/epl/i1998-00258-6.

[33] N. Podewitz, M. Delarue, and J. Elgeti. Tissue homeostasis: A tensile state. *EPL (Europhysics Letters)*, 109(5):58005, Mar. 2015. ISSN 1286-4854. doi: 10.1209/0295-5075/109/58005. URL http://dx.doi.org/10.1209/0295-5075/109/58005.

[34] R. Püllen, J. Konrad, B. Hoffmann, and R. Merkel. *Cell Stretcher Assay to Analyze Mechanoresponses to Cyclic Stretching*, page 91–105. Springer US, 2023. ISBN 9781071628515. doi: 10.1007/978-1-0716-2851-5_6. URL http://dx.doi.org/10.1007/978-1-0716-2851-5_6.

[35] S. Ramaswamy. The mechanics and statistics of active matter. *Annual Review of Condensed Matter Physics*, 1(1):323–345, Aug. 2010. ISSN 1947-5462. doi: 10.1146/annurev-conmatphys-070909-104101. URL http://dx.doi.org/10.1146/annurev-conmatphys-070909-104101.

[36] J. Ranft, M. Basan, J. Elgeti, J.-F. Joanny, J. Prost, and F. Jülicher. Fluidization of tissues by cell division and apoptosis. *Proceedings of the National Academy of Sciences*, 107(49):20863–20868, Nov. 2010. ISSN 1091-6490. doi: 10.1073/pnas.1011086107. URL http://dx.doi.org/10.1073/pnas.1011086107.

[37] K. Sato, Y. Ito, T. Yomo, and K. Kaneko. On the relation between fluctuation and response in biological systems. *Proceedings of the National Academy of Sciences*, 100 (24):14086–14090, Nov. 2003. ISSN 1091-6490. doi: 10.1073/pnas.2334996100. URL http://dx.doi.org/10.1073/pnas.2334996100.

[38] B. I. Shraiman. Mechanical feedback as a possible regulator of tissue growth. *Proceedings of the National Academy of Sciences*, 102(9):3318–3323, Feb. 2005. ISSN 1091-6490. doi: 10.1073/pnas.0404782102. URL http://dx.doi.org/10.1073/pnas.0404782102.

[39] H. Turlier, D. A. Fedosov, B. Audoly, T. Auth, N. S. Gov, C. Sykes, J.-F. Joanny, G. Gompper, and T. Betz. Equilibrium physics breakdown reveals the active nature of red blood cell flickering. *Nature Physics*, 12(5):513–519, Jan. 2016. ISSN 1745-2481. doi: 10.1038/nphys3621. URL http://dx.doi.org/10.1038/nphys3621.

5 Discussion and Outlook

In this thesis, we aimed to improve our understanding of how stem cell dynamics, self-organisation, and dynamic response follows from microscopic intercellular interactions and mechanical cell cycle control. Therefore, three different aspects were studied: First, how cell differentiation following the textbook picture of epithelial renewal and mechanical interactions control stem cell dynamics and structure; Second, how mechanically regulated growth with stochastic differentiation regulates tissue composition and how this alters structure; And last, how dynamic response can be quantified from steady state cell density fluctuations. In this chapter, the main findings of each result chapter are summarized and discussed. Finally, an outlook on open questions and promising future research directions is presented.

5.1 Summary

Cellular tissues must continuously balance the loss of cells due to apoptosis or delamination. Stem cells, which lie at the apex of the cell lineage hierarchy, play a pivotal role in the control of this renewal process. In the textbook picture of epithelial renewal [1], stem cells give rise to transient amplifying (TA) cells through asymmetric divisions. These TA cells undergo a limited number of symmetric divisions, thus, amplifying cell mass, before terminally differentiating into post-mitotic cells, which undergo apoptosis.

We implement this cell lineage hierarchy into an agent based, mechanical simulation model, the two particle growth (2PG) model, and find that combining the deterministic cell fate model with mechanically regulated growth results in an expected outflux of cells from the stem cell.

Stem cells and their progeny form well defined units, which are found homogeneously distributed in the tissue. Each stem cell division is amplified trough N_{TA} division cycles of the TA cells, resulting in a halo of growing TA cells in close vicinity of the generating stem cell. The generated number of cells per stem cell division allows us to determine an active area or characteristic length scale of growing cells, much larger than a single cell.

Stem cells are not found fixed in space at the center of their colony, but undergo surprisingly persistent bursts of motion leaving behind a trail of daughter cells. We quantify this motion by long simulations of single stem cells and their respective progeny. We find, that proliferating progeny propel the stem cell, resulting in superdiffusive motion. With increasing cell density in confluent tissues, the propulsion mechanism reduces but continues to exist.

Not only do transient cells exert a force on their mother stem cell, but also on cells generated by other stem cells. This results in an effective repulsive interaction between a pair of stem cells, described with help of an analogy to thermal equilibrium. We relate the pair distribution function $g(r)$ with the partition function, which allows us to derive an exponentially decaying interaction potential. Importantly, the interaction length is chosen by the characteristic length scale set by growing daughter cells and not a free parameter of the interaction potential. Only the effective temperature, which quantifies the softness of the interaction, remains a free parameter, determined by fitting to data.

In order to test the correctness of our proposed stem cell pair interactions, we implement the derived interaction potential in a system of interacting Brownian particles. We find, that this reproduces spatial structures surprisingly well, despite expected differences in their dynamics, as quantified by the relaxation in the dynamic structure factor.

These results demonstrate, that an amplifying outward flow of cells from the stem cell does establish a well defined and maintained tissue composition. Along with microscopic mechanical interactions, the outward flow and cell mass amplification result in unexpected dynamics of stem cells and an effective, long range interaction between them.

The division-differentiation scheme studied in the first result chapter comes with the limitation of a fixed stem cell population, which cannot adapt to events of unexpected stem cells loss. To amend this, symmetric replication of stem cells is required. We investigate this by adapting the division differentiation scheme and implement symmetric divisions for both the stem (S) and transient (T) cell types in our 2PG simulations. In addition, the fixed number of T cell divisions is repealed and differentiation is modeled in a stochastic process with fixed, cell type specific rates.

With these changes we arrive at a model, in which mechanical interaction result in a self-regulated tissue composition. The cell number fractions are no longer set by fixed simulation parameters, like the number of stem cells in the tissue or the number of division cycles of TA cells, but result from the mechanical properties of cells and their differentiation rates. Importantly, this is a consequence of the fact that division rates are controlled by mechanical interactions and not explicitely set. In order to better understand our simulation results and derive at a biologically relevant tissue composition, we use number balance to describe the dependence of cell number fractions on division and differentiation. The resulting phase diagram consists of stem cell rich and rare phases, as well as a stem cell depleted phase, in which T cells adopt the phenotype of stem cells. Simulations confirm the predicted phase diagram. However, the discrete simulation model reveals that for fast differentiation a tensile state results in loss of confluency through ripping, an effect not considered in our theory.

We investigate large scale structural properties in tissues, which represent biologically relevant compositions. These tissues have a small but finite stem cell population, which is slow cycling, and the main mass of differentiated cells is replenished by short

lived T cells. In contrast to the previous model, stem cells no longer repel each other strongly, since the outflux of differentiated daughter cells is changed. Yet, they form localized units, i.e. clusters, consisting of a small but finite number of cells. These clusters are reminiscent of the so called stem cell niche, a compartment consisting of stem cells. With increasing stem cell fraction, clusters naturally percolate. When stem cells are rare, large stem cell void regions can form, which are sufficiently replenished by T cells. However, as long as stem cells exist, the T cell proliferation potential remains limited, that is to say that no T cell clone persist unlimited. A closer look at the stem cell neighborhood reveals, that in contrast to previously discussed deterministic cell fate model, T cells are rare in the vicinity of stem cells. Instead, they separate from the generating stem cells. Thus, cell lineage models must be carefully evaluated when immediate descent is derived from static, spatial arrangement of cells.

Interestingly, clusters remain surprisingly stable in space over long times. The density fluctuation autocorrelation of a stem cell rare tissue decays slower than expected for a passively diffusive system, with diffusion coefficient derived from the short term diffusion of stem cells. Further, the clone evolution, quantified by the fraction of surviving stem cell clones, only approximately follows the expected decay for neutral competition. These findings indicate the subtle influence of local mechanical interactions on long term, large scale structure and dynamics.

We have seen that, in the stochastic differentiation model, tissue composition does self-regulate. This is a necessary mechanism to recover from perturbation events, like wounds. Yet, it remains unclear how such dynamic response can be quantified in a robust, non-invasive manner.

This aspect is studied in the third project of the thesis, where we introduce a novel theoretical framework to quantify the dynamic response from steady state cell density fluctuations. First, we derive an Ornstein-Uhlenbeck like equation to describe the cell number dynamics in the presence of mechanical feedback. Here, a linear feedback of the division rate on density around the homeostatic density is assumed as well as Markovian processes for division and apoptosis. The resulting population dynamics can be mapped on a Brownian particle confined by a harmonic potential. A system well studied in the context of optical tweezers, where the position of fluctuating beads is controlled by lasers. Then, we characterize the response coefficient as the rate defined by the ratio of noise induced diffusion and variance of resulting density fluctuations. A set of complementary statistical methods, including the density probability function, mean squared shift, density autocorrelation function, and power spectral density allows us to provide quantitative measurements.

Our theory is tested against three simulation models of increasing complexity. The first model is the nonlinear coarse-grained response model, closely related to the theoretical analogue. As long as systems are sufficiently large, and therefore Gaussian, and response is carried out with a rate not much slower than the apoptosis rate, we do obtain a stable cell population. In this model, theory and simulation data agree extremely well, and illustrate the data requirements of the method, i.e. sufficiently frequent sampling intervals to detect the diffusion due to apoptotic noise and long

enough to observe effects from the confinement due to mechanical feedback.

The second model we investigate is a single cell type implementation of the 2PG model. Here, the exact form of the feedback is not known but a consequence of the mechanical properties of cells. We find, that the response coefficient measured by the variance does describe our data very well. Since no ground truth is known, we utilize additional compression-expansion simulations, similar to stretch or compression experiments, to get an complementary measure of the response coefficient. Comparison of both methods shows great agreement over a large parameter range. Interestingly, we observe a difference between theory and simulation data in the correlation functions, which reveal a non-Markovian division rate feedback mechanism. Indeed, a modified version of the division rate update rule, where an exponentially decaying memory kernel takes into account past configurations, does explain the observed difference.

Last, an elaborate mechano-electro-osmotic growth model, calibrated against experimental data, was tested. Again, the overall relaxation process is described well by the steady state response coefficient. However, we observe long-lasting oscillations, most likely generated by synchronization effects in the underlying adder-model, which could not be explained by the exponentially decaying memory kernel.

These results demonstrate, that information of steady state fluctuations can be a valuable tool to quantify dynamic response in tissues. They are applicable in situations, where previously the response coefficient was not accessible and our method further can reveal additional information of the underlying microscopic mechanisms in homeostasis.

5.2 Discussion

In summary we have shown how the interplay of mechanical feedback on growth and cell differentiation can result in complex spatial structure and dynamics of stem cells. The microscopic details of the model affect the macroscopic structure and dynamics. This reveals surprising effects, which are not expected from coarse grained theory. Interestingly, even in the absence of any biochemical signaling, for example from cell-cell signaling or environmental cues, our mechanical model did reproduce the formation of an proliferating unit or stem cell niches. Note that we also did not consider detailed mechanical information, like differential adhesion, to be present, which can also be expected to favor structure formation.

Adapting thermal equilibrium analogies and mapping to classical statistical physics did support us to gain a better understand of several of these mechanisms. Even though growing tissues are active, non-equilibrium systems, these methods were able to quantify effective interactions, structure, and dynamic response. By observing differences between theory and computational experiments we were able to reveal underlying microscopic details of the mechanisms.

For each project we did introduce detailed analysis methods which help to under-

stand the spatial and temporal properties of growing tissues. Our results suggest, that in many cases these can provide additional insight beyond the information of spatial snapshots or genetic markers. While on one hand our methods can be adapted to the analysis of experimental works, on the other hand they can guide improvements in experimental techniques and data generation. Further, our computational software represents an interesting addition to effectively bridge the gap between theory and experiments. Not only does it allow to analyze data and verify theoretical predictions, it also can provide a novel perspective. Simulations can efficiently test a hypothesis and provide reliable data, which can be tested against experimental findings and theoretical predictions.

In this thesis, we did focus on a minimal modeling approach to unravel the dynamics and self-organisation of stem cells in the presence of intercellular mechanical interactions. Various organ specific mechanisms may be required to explain experimental findings. But also extensions to the minimal modeling approach, by varying the microscopic details of the model, may already result in varied structures.

For example, we have seen that purely symmetric stem cell divisions and symmetric divisions show unique stem cell niches. Our symmetric model effectively describes a ratio of 25% symmetric division, 50% asymmetric division, and 25% symmetric differentiation for the stem cell [9]. However, experiments typically report smaller fractions of symmetric events, around 10-20% in total [14], and respectively higher likelihood of asymmetric divisions. In particular during development abrupt transitions between a symmetric amplification phase and asymmetric maintenance mode are found [13]. Such differentiation modes and altered cell cycle dynamics have been studied with respect to homeostatic stability or mutational prevention [19, 21, 23], but it remains an open question how structures change between the fully asymmetric model and the purely symmetric model. Other aspects of cell fate decisions, like reversible cell fate, may also significantly contribute to cellular dynamics and organisation.

In addition, we did not excessively change the mechanical properties of cells. Only adjustments of the growth potential of cells has been taken into account to realize specific division rates and resulting tissue compositions. Cell differentiation can come with a change in cell adhesion, and differential adhesion is known to be a driver of cell sorting and tissue organisation [5, 22]. Thus, even for the same differentiation schemes studied in this work this may result in different structural and dynamical properties of the tissues.

For motile cells, a dynamic exchange of neighbors has been observed [18] and cell motility explains cluster heterogeneity in breast cancer [6]. These structural changes can result in different phases for mixtures of growing and motile matter, where changes between well mixed and phase separated states depend on the growth of cells and motility driven sorting [12]. For stem cell generated tissues, transitions between immobile and motile states can be associated with differentiation and would therefore additionally influence the observed structures in our models.

Last, we have not taken into account any form of explicit biochemical signaling. Yet, real systems are subject to its influence, and for example volumetric growth is

biochemically regulated [17], the Yes-associated protein (YAP) is known as a master regulator of mechanotransduction, susceptible to changes in the local packing fractions [7, 15], or chemotaxis controls collective motion[4]. In order to incorporate these effects, our agent based model can be coupled to such signaling fields by including reaction-diffusion models for the chemicals [11].

5.3 Outlook

An epithelial tissue is a single layer of cells in contact with a basement membrane. In this thesis, we modelled such thin films in planar 2D simulations. However, in reality, more complex topology and structure exist. Quasi-3D forms, like formation of villi and crypts or undulation of the planar epithelial sheet, are a result of mechanical cues and form due to anisotropic stress [3, 8, 9, 20]. Stratification of epithelial tissues, for example in the epidermis, requires coordinated action of cell proliferation, differentiation, delamination, and tissue-scale mechanical forces [2]. For tissues generated by stem cells, anisotropic growth results from the different growth dynamics of different cell types. This consequently leads to anisotropic stress, which is expected to result in modulation of the underlying membrane. Furthermore, a feedback of the underlying structure can be expected to affect growth. Thus, mutual feedback between growth shaping structure and structure controlling growth will determine tissue formation.

Initial studies with focus on simplified setups and geometries are required. These may include simulations to understand how cells grow in confinement or on predefined quasi-3D structures, to study the influence of geometry on growth and resulting stresses in the tissue. Further, one needs to relax the fixed planar simulation setup and allow for deformations. One way to realize this is to include a deformable membrane to our agent based simulation. A meshless membrane model poses a promising candidate [10, 16]. Here, the membrane is modeled with help of particles, which allows direct integration in the present simulation framework. First, one needs to identify a suitable parameter setup. The membrane must be tight and closed. Yet, it should allow flexible deformations. Proliferating cells on the membrane need to attach to the membrane without being excessively coupled. In particular when studying stratification, the number of cells will increase strongly, which may require additional optimizations of the simulation code to restore performance.

It remains to be seen, how specific structures and stem cell organization result from the underlying growth and differentiation mechanism and how surface modulation is guided by mechanical forces. Growth dynamics and adhesion can be assumed to shape the structure formation, and result for example in wrinkling or formation of buds. However, how structure formation mutually interacts with feedback on growth is still unclear. Such a framework can also be expected to explain stratification, i.e. formation of a multi-layered epithelium, which may naturally emerge for specific conditions.

In chapter 4 we have introduced a novel method to measure the dynamic response of the cell division rate from cell number fluctuations of the steady state. Our results

demonstrate that this method did work well on *in-silico* trajectories. While differences between theory and 2PG growth simulations were very well explained by an exponentially decaying memory kernel, this did not explain the long standing oscillations in the VMPG model. It remains to be seen, if other division rate update rules could be suited to resolve this discrepancy, but also, if the synchronization effect is simply linked to simulation artifacts or limited tissue size. In systems different from tissues, like bacteria, yeast, or amoebae different forms of growth control are present, which can result in other forms of nonlinear memory [24], and it remains to be seen if they are distinguishable by our model.

Further efforts must be taken to see how our method translates to *in-vitro* or *in-vivo* experimental data. The application to real world data may come with additional challenges. For example, the duration of experiments may be much more limited than in simulations. Culturing cells requires extreme care, and generating data *in-vitro* can only be done for limited duration. Cells may modulate the extracellular matrix, which in turn affects cell growth, causing complex memory effects. Also, microscopy only records an image section and the selection of the image section, or the motion of cells at the boundaries can be additional sources of fluctuations.

In order to understand how these additional effects influence the correctness of our measurement protocol, one may need to further investigate their contribution to the system noise. For example, we speculate that cell motion at the boundary of a frame may be negligible for sufficiently large image sections. Spatial variability, when imaging different regions of an *in-vitro* cell culture, can result in overestimates of the actual response coefficient. Extension of our theory and validation remains to be done.

Eventually, the variance based response measurement is a promising method to reveal changes in the dynamic response of cells to perturbations. In our simulations, cell growth and division have been sensitive to mechanical feedback, however, no additional mechanisms are implemented to account for exceptional perturbations. Real cells may adapt differently in response to these events compared to homeostatic fluctuations. While traditional approaches, like cell or substrate stretching experiments, only access the dynamic response for different levels of perturbations, our new approach allows to quantify the difference in comparison with the base homeostatic response. If cells adapt differently, this opens up follow-up question, like how this difference in response is related to their fate.

In the context of this thesis, the natural extension to the fluctuation response method is to apply it to more complex systems, like stem cell generated tissues. While a thorough implementation and analysis requires much more details, we want to discuss some preliminary data (see Fig. 5.3.1) and point out interesting aspects for future work.

First, we select the stem cell rare tissue studied in detail in chapter 3. To realize longer trajectories, we rerun the system with reduced simulation area of $L_{xy} = (50\,R_{PP})^2$. Data is aggregated from four independent simulations and in each simulations 3000 D cell generations after equilibration are realized. Beside the original

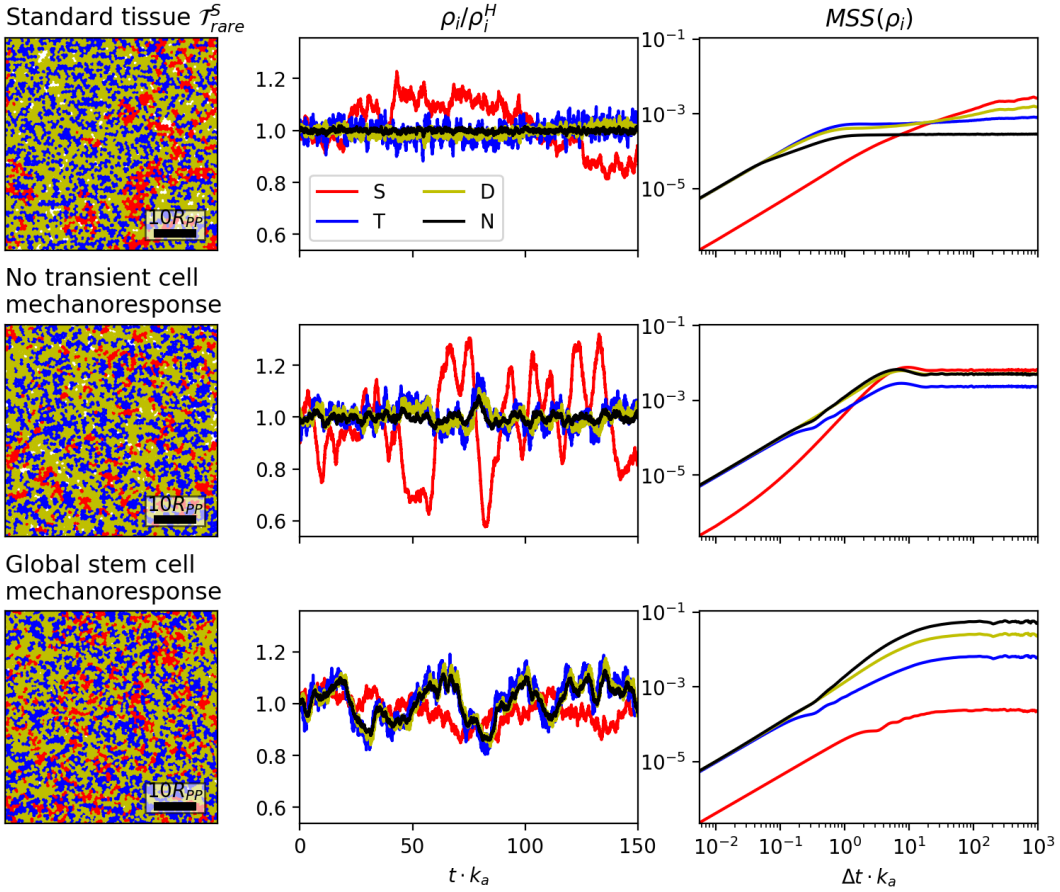

Figure 5.3.1: Mechanoresponse in stem cell generated tissues. Preliminary fluctuation response analysis for the standard tissue $\mathcal{T}^S_{rare}$ from chapter 3 (top row), a model with vanishing T cell response (middle row), and only global stem cell number feedback (bottom row). For each model, a snapshot (left column) is shown, where stem (red), transient (blue), and differentiated (yellow) cells are color coded. The same color coding is applied to a part of the cell number trajectory (center column), normalized by the homeostatic density of each cell type, where the black line represents total density. MSS is calculated for cell density data (right column). For each tissue, four independent runs of 3000 D cell generations after equilibration are averaged.

model, we set up two different simulation models with varied mechanoresponse mechanism. Note that in general mechanoresponse can also be modulated by tuning the mechanical properties of cells. However, our results for the parameter sweep performed in chapter 4 suggest, that this only results in changes in the same order of magnitude as the apoptosis, or differentiation, rate.

Here, the usual growth mechanism, in which an active growth force and intercellular interactions result in density feedback, is replaced by switching from an active growth force to a deterministically growing spring. The two particles of a cell are tightly

coupled to the growing rest length of the spring. To avoid synchronization, stochastic noise is added to the spring growth dynamics. This renders cells insusceptible to local mechanical feedback. First, we exchange the growth mechanism only for transient (T) cells. The growth rate of the spring is chosen to realize the same division rate as in the original simulations. Stem cells still follow the usual mechanism and continue to locally sense cell density and adjust their cell cycle due to mechanical feedback. In a second setup, also stem cells are made insusceptible to local mechanical feedback, as described above. To avoid neutral drift, we globally couple the stem cell number to the homeostatic stem cell density in the original simulations. Again, aiming to realize the same cell number fractions and division rates. This coupling is realized via a dynamic update of the rest length growth rate for stem cells.

Before discussing the fluctuation dynamics, we want to point out a fascinating effect following the changes in the response mode. Tissue snapshots reveal, that stem cell voids, which had been observed for stem cell rare tissues earlier, no longer exist, if only stem cells are sensitive to local feedback. Also, stem cell clusters seem to break up, and the stem cell distribution is more homogeneous. This can be explained by the fact, that in order to globally balance cell loss, stem cells must be much more evenly distributed, if T cells are not mechanoresponsive. On the other hand, in some tumor cell lines, it was reported that cells loose mechanoresponse by crowding feedback. Then, this could lead to spreading and metastasis. It is still to be clarified how this effect can be quantified in detail, taken into account the spatio-temporal dynamics of stem cells, and which argumentation can be drawn from these results.

The shown section of the cell density trajectories, where current density is normalized by the homeostatic density of each individual cell type, reveal that indeed each model has slightly different fluctuation dynamics. This is quantified by the mean squared shift (MSS), introduced in chapter 4. As we have seen, other correlation functions are connected to the MSS but may contribute to a better understanding. For the sake of simplicity, here, we limit the analysis to a single quantifier. In all models, the total cell density reaches a plateau, however, the relaxation time and magnitude differ. This is associated with a change in the tissue response coefficient but also shows the total density fluctuation in the system. The original model is found most stable with the weakest fluctuation amplitude. Further reducing mechanoresponse does result in larger fluctuations.

At this point, we want to explain why response coefficients are not given quantitatively. While in principle the formula for the response coefficient derived in chapter 4 could be used, it is unclear how to apply it correctly. In this model, in addition to the apoptosis rate, two more rates, the stem cell differentiation rate and T cell differentiation rate, are present. Also, for T cells, the division and differentiation rate are no longer identical. Cell density can also be defined in different ways, for example via cell fractions or by cell type density. Before quantifying the response coefficient, one should carefully decide how to calculate it correctly.

When looking more closely at the stem cell MSS, we see that fluctuations vary strongly between all three models. The model with global feedback seems to have the most stable stem cell population. However, this is a consequence of the chosen

global coupling coefficient, a simulation parameter, which can be explored in more detail. Surprisingly, the original model does not reach a clearly visible plateau, even after long times. Although we carefully checked for signs of aging or coarsening, this raises the question if long term remodeling of the tissue is happening. Also the other two cell types seem to continue to modulate over long times, i.e. thousands of cell generations. It is of importance to note that for the chosen parameters, the time scale is in the order of many years for real organisms. Also, stem cells do not deplete during the whole simulation.

Our analysis only takes global cell numbers into account. However, it may be of importance to advance our methods to provide deeper insights into the spatio-temporal dynamics and response. As snapshots suggest, not only the total cell number, but also the distribution of cells is relevant for renewal of the tissue.

It will be interesting to see how it turns out.

References

[1] B. Alberts, A. Johnson, J. Lewis, M. Raff, K. Roberts, and P. Walter. Epidermis and Its Renewal by Stem Cells. *Molecular Biology of the Cell. 4th edition*, 2002. URL https://www.ncbi.nlm.nih.gov/books/NBK26865/. Publisher: Garland Science.

[2] S. Azote epse Hassikpezi, R. S. Negi, N. A. Chen, and M. L. Manning. A predictive model for coupling cell division orientation to tissue mechanics during epithelial morphogenesis. *bioRxiv*, 2026. doi: 10.64898/2026.04.17.719304. URL https://www.biorxiv.org/content/early/2026/04/21/2026.04.17.719304.

[3] M. Ben Amar and F. Jia. Anisotropic growth shapes intestinal tissues during embryogenesis. *Proceedings of the National Academy of Sciences*, 110(26):10525–10530, June 2013. ISSN 1091-6490. doi: 10.1073/pnas.1217391110. URL http://dx.doi.org/10.1073/pnas.1217391110.

[4] G. Briozzo, G. J. Sibona, and F. Peruani. Collective behavior based on agent-environment interactions, 2026. URL https://arxiv.org/abs/2601.10046.

[5] R. A. Foty and M. S. Steinberg. The differential adhesion hypothesis: a direct evaluation. *Developmental Biology*, 278(1):255–263, Feb. 2005. ISSN 0012-1606. doi: 10.1016/j.ydbio.2004.11.012. URL http://dx.doi.org/10.1016/j.ydbio.2004.11.012.

[6] P. Gottheil, S. Bhattacharyya, K. Lettl, P. Friedrich, K. Roth, S. Rivera-Moreno, M. Merkel, B. Aktas, I. Sauer, A. Daneshgar, J. Wieland, H. Kubitschke, A.-S. Wegscheider, J. M. Yeomans, and J. A. Käs. Self organisation of invasive breast cancer driven by the interplay of active and passive nematic dynamics, 2024. URL https://arxiv.org/abs/2412.01285.

[7] V. Grudtsyna, V. S. Swaminathan, and A. Doostmohammadi. Packing-driven mechanotransduction: local crowding overrides adhesion and stiffness cues for yap activation in cellular collectives. *Journal of the Royal Society Interface*, 22(233), Dec. 2025. ISSN 1742-5662. doi: 10.1098/rsif.2025.0490. URL http://dx.doi.org/10.1098/rsif.2025.0490.

[8] E. Hannezo, J. Prost, and J.-F. Joanny. Theory of epithelial sheet morphology in three dimensions. *Proceedings of the National Academy of Sciences*, 111(1):27–32, Dec. 2013. ISSN 1091-6490. doi: 10.1073/pnas.1312076111. URL http://dx.doi.org/10.1073/pnas.1312076111.

[9] E. Hannezo, J. Prost, and J.-F. Joanny. Growth, homeostatic regulation and stem cell dynamics in tissues. *Journal of The Royal Society Interface*, 11(93):20130895, Apr. 2014. ISSN 1742-5662. doi: 10.1098/rsif.2013.0895. URL http://dx.doi.org/10.1098/rsif.2013.0895.

[10] R. Hornung. *Simulation of Growing Cell Sheets*. PhD thesis, Universität zu Köln, 2019. URL http://kups.ub.uni-koeln.de/10340/.

[11] R. Hornung, A. Grünberger, C. Westerwalbesloh, D. Kohlheyer, G. Gompper, and J. Elgeti. Quantitative modelling of nutrient-limited growth of bacterial colonies in microfluidic cultivation. *Journal of The Royal Society Interface*, 15(139):20170713, Feb. 2018. ISSN 1742-5662. doi: 10.1098/rsif.2017.0713. URL http://dx.doi.org/10.1098/rsif.2017.0713.

[12] L. Hupe, J. M. Materska, D. Zwicker, R. Golestanian, B. Waclaw, and P. Bittihn. Phase separation in a mixture of proliferating and motile active matter. *Physical Review Research*, 8(2), Apr. 2026. ISSN 2643-1564. doi: 10.1103/9pns-h5ll. URL http://dx.doi.org/10.1103/9pns-h5ll.

[13] S. Itzkovitz, I. C. Blat, T. Jacks, H. Clevers, and A. van Oudenaarden. Optimality in the development of intestinal crypts. *Cell*, 148(3):608–619, Feb. 2012. ISSN 0092-8674. doi: 10.1016/j.cell.2011.12.025. URL http://dx.doi.org/10.1016/j.cell.2011.12.025.

[14] P. H. Jones, B. D. Simons, and F. M. Watt. Sic transit gloria: Farewell to the epidermal transit amplifying cell? *Cell Stem Cell*, 1(4):371–381, Oct. 2007. ISSN 1934-5909. doi: 10.1016/j.stem.2007.09.014. URL http://dx.doi.org/10.1016/j.stem.2007.09.014.

[15] A. Mukherjee, Y. Huang, J. Elgeti, S. Oh, J. G. Abreu, L. Ammar, A. R. Neliat, J. Schüttler, D.-D. Su, C. Dupre, N. C. Benites, X. Liu, L. Peshkin, M. Barboiu, H. Stocker, M. W. Kirschner, and M. Basan. Membrane potential mediates the cellular response to mechanical pressure. *Cell*, 189(1):143–160.e22, Jan. 2026. ISSN 0092-8674. doi: 10.1016/j.cell.2025.11.004. URL http://dx.doi.org/10.1016/j.cell.2025.11.004.

[16] H. Noguchi and J. Elgeti. Growth and shrinkage of tissue sheets on substrates: buds, buckles, and pores. *New Journal of Physics*, 26(10):103027, Oct. 2024. ISSN 1367-2630. doi: 10.1088/1367-2630/ad86e8. URL http://dx.doi.org/10.1088/1367-2630/ad86e8.

[17] N. Olaranont, C. Wei, J. Lowengrub, and M. Wu. Chemomechanical regulation of growing tissues from a thermodynamically-consistent framework and its application to tumor spheroid growth. *Journal of Mathematical Biology*, 91(3), Sept. 2025. ISSN 1432-1416. doi: 10.1007/s00285-025-02257-2. URL http://dx.doi.org/10.1007/s00285-025-02257-2.

[18] A. Ruppel, V. Misiak, S. Arzash, D. S. Herrador, G. Cappello, T. Boudou, L. Manning, F. Fagotto, and M. Balland. Morphogenesis-on-chip: A minimal in vitro assay for cell intercalation highlights the importance of interfacial tension and migratory forces. *bioRxiv*, 2025. ISSN 2692-8205. doi: 10.1101/2025.06.30.662274. URL https://www.biorxiv.org/content/early/2025/07/03/2025.06.30.662274.

[19] L. Shahriyari and N. L. Komarova. Symmetric vs. asymmetric stem cell divisions: An adaptation against cancer? *PLoS ONE*, 8(10):e76195, Oct. 2013. ISSN 1932-6203. doi: 10.1371/journal.pone.0076195. URL http://dx.doi.org/10.1371/journal.pone.0076195.

[20] A. E. Shyer, T. Tallinen, N. L. Nerurkar, Z. Wei, E. S. Gil, D. L. Kaplan, C. J. Tabin, and L. Mahadevan. Villification: How the gut gets its villi. *Science*, 342(6155):212–218, Oct. 2013. ISSN 1095-9203. doi: 10.1126/science.1238842. URL http://dx.doi.org/10.1126/science.1238842.

[21] B. D. Simons and O. Karin. Cell cycle criticality as a mechanism for robust cell population control. *bioRxiv*, 2025. doi: 10.1101/2025.06.12.659375. URL https://www.biorxiv.org/content/early/2025/06/17/2025.06.12.659375.

[22] S. A. Wickström and C. M. Niessen. Cell adhesion and mechanics as drivers of tissue organization and differentiation: local cues for large scale organization. *Current Opinion in Cell Biology*, 54:89–97, Oct. 2018. ISSN 0955-0674. doi: 10.1016/j.ceb.2018.05.003. URL http://dx.doi.org/10.1016/j.ceb.2018.05.003.

[23] J. Yang, M. V. Plikus, and N. L. Komarova. The role of symmetric stem cell divisions in tissue homeostasis. *PLOS Computational Biology*, 11(12):e1004629, Dec. 2015. ISSN 1553-7358. doi: 10.1371/journal.pcbi.1004629. URL http://dx.doi.org/10.1371/journal.pcbi.1004629.

[24] S. Zhang, C. Fei, and J. Dunkel. Nonlinear memory in cell-division dynamics across species. *Proceedings of the National Academy of Sciences*, 122(36), Sept. 2025. ISSN 1091-6490. doi: 10.1073/pnas.2417416122. URL http://dx.doi.org/10.1073/pnas.2417416122.

6 Eidesstattliche Erklärung — Declaration for the doctoral thesis

Hiermit versichere ich an Eides statt, dass ich die vorliegende Dissertation selbstständig und ohne die Benutzung anderer als der angegebenen Hilfsmittel und Literatur angefertigt habe. Alle Stellen, die wörtlich oder sinngemäß aus veröffentlichten und nicht veröffentlichten Werken dem Wortlaut oder dem Sinn nach entnommen wurden, sind als solche kenntlich gemacht. Ich versichere an Eides statt, dass diese Dissertation noch keiner anderen Fakultät oder Universität zur Prüfung vorgelegen hat; dass sie – abgesehen von unten angegebenen Teilpublikationen und eingebundenen Artikeln und Manuskripten – noch nicht veröffentlicht worden ist sowie, dass ich eine Veröffentlichung der Dissertation vor Abschluss des Prüfungsverfahrens der Promotion nicht vornehmen werde. Die Bestimmungen der Promotionsordnung der Mathematisch-Naturwissenschaftlichen Fakultät der Universität zu Köln sind mir bekannt. Darüber hinaus erkläre ich hiermit, dass ich die Ordnung zur Sicherung guter wissenschaftlicher Praxis und zum Umgang mit wissenschaftlichem Fehlverhalten der Universität zu Köln gelesen und sie bei der Durchführung der der Dissertation zugrundeliegenden Arbeiten und der schriftlich oder elektronisch verfassten Dissertation beachtet habe, und verpflichte mich hiermit, die dort genannten Vorgaben bei allen wissenschaftlichen Tätigkeiten zu beachten und umzusetzen.

Die Primärdaten, Analysen und Versuchsprotokolle, die dieser Dissertation zugrunde liegen, sind im Datenspeicher der Forschungsgruppe archiviert, in der die Arbeit durchgeführt wurde. Sofern sie nicht auf öffentlichen wissenschaftlichen Datenservern – wie in der Dissertation angegeben – zugänglich sind, bleiben sie dort in Übereinstimmung mit den geltenden gesetzlichen Bestimmungen gespeichert.

*(*unofficial translation) I hereby declare that I have prepared the present dissertation independently and without using any aids or literature other than those indicated. All passages that have been taken verbatim or in substance from published or unpublished works, in wording or in meaning, are identified as such. I declare under oath that this dissertation has not previously been submitted to any other faculty or university for examination; that it — apart from the publications and embedded articles and manuscripts listed below — has not yet been published, and that I will not publish the dissertation before the conclusion of the doctoral examination procedure. I am aware of the terms of the doctoral degree regulations of the Faculty of Mathematics and Natural Sciences of the University of Cologne. Furthermore, I hereby declare that I have read the regulations on ensuring good scientific practice and on dealing with scientific misconduct of the University of Cologne, and that I have complied

with them in carrying out the work underlying this dissertation and in preparing this dissertation in written or electronic form, and I hereby undertake to observe and implement the rules set out therein in all my scientific activities.

The primary data, analyses, and experimental protocols underlying this dissertation are archived in the data storage of the research group, where the work was conducted. Unless they are accessible on public scientific data servers, as stated in the dissertation, they will remain stored there in compliance with applicable legal requirements.

Partial publications of the thesis / Teilpublikationen:

1. Krämer, J. C., Hannezo, E., Gompper, G., & Elgeti, J. (2024). Mechanically-driven stem cell separation in tissues caused by proliferating daughter cells. *SciPost Physics, 16(4).* `https://doi.org/10.21468/scipostphys.16.4.097`

2. Krämer, J. C., Hannezo, E., & Elgeti, J. (2026). Mechanics and fate stochasticity shape stem cell distribution in tissues. *submitted to eLife & published as bioRxiv–preprint.* `https://doi.org/10.64898/2026.06.10.731353`

Ort, Datum

Johannes Caspar Krämer

7 Declaration of individual contributions

In addition to the formal declaration of independence given above, here a more technical declaration of contribution to the individual parts is given.

General For all three result chapters, I adapted the simulation source code and performed simulations using high performance compute infrastructure of the research center Jülich and CLAIX. Furthermore, I developed all other simulation software used in this thesis, except for the original version of the two particle growth (2PG) model and the vertex membrane potential growth (VMPG) model. All simulation data was analyzed and visualized by me using software developed by me with `python` and its publicly available modules, e. g. `numpy`, `matplotlib`, or `pandas`.

In all projects, I wrote the initial draft of the manuscript. I did contribute in writing and editing of the manuscripts in collaboration with the co-authors.

Artificial intelligence (AI) software was not used to generate new text. During the writing process, AI was used in part to improve grammar and language. All corrections by AI were thoroughly checked and not copied blindfolded. AI was explicitely not used for literature research or citation management. Figure 1.9 was generated with AI tools and excessive, iterative prompting.

The thesis was supervised by Jens Elgeti.

Below, for each manuscript included in the thesis, a detailed declaration of individual contributions is given.

Article 1: Krämer, J. C., Hannezo, E., Gompper, G., & Elgeti, J. (2024). Mechanically-driven stem cell separation in tissues caused by proliferating daughter cells. *SciPost Physics, 16(4).* `https://doi.org/10.21468/scipostphys.16.4.097`

- **Corresponding chapter:** 2
- Status: published
- Conceptualization & Methodology: Jens Elgeti
- Software: (2PG) provided by Jens Elgeti and adapted by Johannes Krämer, (BP) developed by Johannes Krämer.
- Formal Analysis, Investigation, Data Curation & Visualization: Johannes Krämer
- Validation: Jens Elgeti, Edouard Hannezo, Gerhard Gompper
- Writing - Original Draft & Editing & Review: Johannes Krämer, Jens Elgeti, Edouard Hannezo, Gerhard Gompper
- Supervision: Jens Elgeti

Article 2: Krämer, J. C., Hannezo, E., & Elgeti, J. (2026). Mechanics and fate stochasticity shape stem cell distribution in tissues. *submitted to eLife & published as bioRxiv–preprint.* `https://doi.org/10.64898/2026.06.10.731353`

- **Corresponding chapter:** 3
- Status: submitted manuscript, published as bioRxiv–preprint.
- Conceptualization & Methodology: Jens Elgeti & Johannes Krämer
- Software: Adapted by Johannes Krämer
- Formal Analysis, Investigation, Data Curation & Visualization: Johannes Krämer
- Validation: Jens Elgeti & Edouard Hannezo
- Writing - Original Draft & Editing: Johannes Krämer, Jens Elgeti, Edouard Hannezo
- Supervision: Jens Elgeti

Article 3: Krämer, J. C. & Elgeti, J. (in preperation). Fluctuation-based measurement of tissue response reveals growth memory effects.

- **Corresponding chapter:** 4
- Status: manuscript in preparation for submission
- Conceptualization & Methodology: Jens Elgeti & Johannes Krämer
- Software: Jens Elgeti provided VMPG model, Johannes Krämer adapted VMPG and 2PG model.
- Formal Analysis, Investigation, Data Curation & Visualization: Johannes Krämer
- Validation: Jens Elgeti
- Writing - Original Draft: Johannes Krämer, Jens Elgeti
- Supervision: Jens Elgeti

8 Acknowledgments

This work would not be possible without the continued support of my supervisor Jens Elgeti, who allowed me to learn about so many facets of how to do good science and research and shared many helpful tricks of the trade with me. During the extended time of my doctorate, we experienced ups and downs, but eventually only your support did allow me to continue to work on my thesis and most importantly: get it done.

Further, I want to thank Edouard Hannezo for fruitful discussions, being an unlimited source of stem cell biology knowledge, and not stopping to untangle my nested sentences in manuscripts to let them flow nicely. I thank Prof. Gerhard Gompper, who allowed me to start my doctorate at his institute and provide feedback to my work. I want to thank Prof. Joachim Krug for accepting to review my thesis and Prof. Tobias Bollenbach to chair my examination committee.

At the institute, I want to thank Maike Kleinen to handle every bit of bureaucracy with ease, Marisol Ripoll for providing seedlings and helping me to grow my office plants, and Gerrit Vliegenthart for discussing difficult headwind situations during bike rides (and of course thanks to all three for having a sympathetic ear for my moaning about the doctorate). Thanks to all other doctoral researchers and colleagues, who I was allowed to get to know during my time at the research center Jülich and in particular in the *theory of living matter* group. I appreciate the short (and not so short) coffee chats and shared walks around the campus.

A doctorate comes with many challenges. Beside the complexity of scientific work, structural problems in academia can lead to substantial mental health problems, in particular with regards to mental stresses, anxiety, and even depressive syndromes[1]. While I hope, that the results of my scientific work will at some point help to make the world slightly better or healthier, the more I hope that my efforts on the "side quest" to reduce such structural problems in academia will have great impact and helps future generations of doctoral researchers to work in a healthy, supportive, and enjoyable environment! I am forever grateful for all the amazing people I met as part of the Helmholtz Juniors, a community that welcomed me with a warm and kind atmosphere, and those amazing friends I was allowed to make in this group.

Finally, I want to appreciate my family and friends, but also mourn the losses. Life is about more than just academic pursuits, and I am grateful to everyone who spent time with me and regularly pulled me out of my (academic) Ivory Tower. Spending quality time with wonderful people brings me genuine joy and creates beautiful memories—and that is an invaluable source of energy for me.

[1] Helmholtz Juniors – HeJu Survey Group (2023) *N^2 Survey 2021 – Helmholtz report*, https://www.helmholtz.de/assets/helmholtz_gemeinschaft/Bilder/HelmholtzJuniors/N__Survey_2021_-_Helmholtz_report/HeJus_Helmholtz_Report_2021.pdf.